NASA TECHNICAL TRANSLATION

NASA TT F-581

NASA TT F-581
C. 1

SOLAR ACTIVITY

Collection of Articles, No. 3

E. R. Mustel', E. I. Mogilevskiy, and I. A. Zhulin, Editors
Nauka Press, Moscow, 1968

NATIONAL AERONAUTICS AND SPACE ADMINISTRATION • WASHINGTON, D. C. • JULY 1969

SOLAR ACTIVITY

Collection of Articles, No. 3

E. R. Mustel', E. I. Mogilevskiy, and I. A. Zhulin, Editors

Translation of "Solnechnaya Aktivnost'.
Sbornik Statey. No. 3"
Nauka Press, Moscow, 1968

NATIONAL AERONAUTICS AND SPACE ADMINISTRATION

For sale by the Clearinghouse for Federal Scientific and Technical Information
Springfield, Virginia 22151 – CFSTI price $3.00

Annotation

These are original studies concerning actual contemporary problems in the investigation of the physical nature of solar activity and the problem of the link between solar and geophysical phenomena. /4

Many of the articles treat an investigation of the magnetic fields in sunspots, solar perturbances and the chromosphere, a theoretical and experimental basis for the method of magnetic measurements, etc. The information in the calculation tables of a large number of solar spectrum lines observed in the far shortwave spectral range are of particular interest, since they determine the state of ionization in the Earth's ionosphere.

This collection is of interest to specialists in the field of solar physics and the physics of the Sun and the Earth, for astrophysicists, geophysicists and for doctoral students and students of the upper classes specializing in this field.

68 illustrations, 19 tables, 242 references

TABLE OF CONTENTS

Annotation.....iii

E.I. Mogilevsky. Forceless Structure of Magnetic Fields in the Atmosphere of Active Solar Regions and Problems of the Generation of Geoeffective Corpuscular Streams.....1

I.A. Zhulin, B.A. Ioshpa, E.I. Mogilevsky, V.N. Obridko. Simultaneous Measurement of Magnetic Fields on Two Levels in the Sun's Atmosphere.....39

B.A. Ioshpa. Measurement of Magnetic Fields in Prominences and the Structure of the Magnetic Field in the Region of Chromospheric Filaments.....51

V.N. Obridko. Magnetic-Field Radiation-Scattering Matrix Derived With Allowance for the Phase Couplings of the Upper-Level Wave Function.....77

V.N. Obridko. Applicability of the Existing Theories of the Formation of Spectral Lines in a Magnetic Field for Quantitative Interpretation of Solar Magnetograph Readings.....86

M.A. Livshits. Facula Structure.....95

S.O. Obashev. The Area Variation Curve and the Lifetime of Chromospheric Flares.....107

S.O. Obashev. Total Energy of Chromospheric Flares.....118

S.O. Obashev. Energy Classification of Chromospheric Flares....122

N.S. Shiloya. Contours of the Mg I b_1 - b_4 and Sr II 4216 and 4078 Å Lines in the Chromosphere.....125

R.A. Guliaev. Helium Ionization and the Excitation of Orthohelium in the Solar Atmosphere.....130

M. Yu. Zeldina. Shape of the Contours of the Hα Line in Prominences.....147

P.N. Polupan. Spectral Photometry of the Chromospheric Flare of July 12, 1961.....157

V.F. Chistiakov. The Synchronism of Active Fluctuations of the Old and New Cycles in the Intermediate Epoch.....173

NATIONAL AERONAUTICS AND SPACE ADMINISTRATION

TECHNICAL TRANSLATION EVALUATION

Budget Bureau No. 104-R037
Approval Expires: Sept. 30, 1969

TO: THE USERS OF THIS TRANSLATION →

NASA TTF NO. 581

MAINTAINING THE QUALITY OF NASA TRANSLATIONS REQUIRES A CONTINUOUS EVALUATION PROGRAM. PLEASE COMPLETE AND MAIL THIS FORM TO AID IN THE EVALUATION OF THE USEFULNESS AND QUALITY OF THE TRANSLATING SERVICE.

THIS PUBLICATION *(Check one or more)*

- ☐ FURNISHED VALUABLE NEW DATA OR A NEW APPROACH TO RESEARCH.
- ☐ VERIFIED INFORMATION AVAILABLE FROM OTHER SOURCES.
- ☐ FURNISHED INTERESTING BACKGROUND INFORMATION.
- ☐ OTHER *(Explain)*: _____

FOLD LINE FOLD LINE

TRANSLATION TEXT *(Check one)*

- ☐ IS TECHNICALLY ACCURATE.
- ☐ IS SUFFICIENTLY ACCURATE FOR OUR PURPOSE.
- ☐ IS SATISFACTORY, BUT CONTAINS MINOR ERRORS.
- ☐ IS UNSATISFACTORY BECAUSE OF *(Check one or more)*:
  - ☐ POOR TERMINOLOGY.
  - ☐ NUMERICAL INACCURACIES.
  - ☐ INCOMPLETE TRANSLATION.
  - ☐ ILLEGIBLE SYMBOLS, TABULATIONS, OR CURVES.
  - ☐ OTHER *(Explain)*: _____

FOLD LINE FOLD LINE

REMARKS

FROM

DATE

NOTE: REMOVE THIS SHEET FROM THE PUBLICATION, FOLD AS INDICATED, STAPLE OR TAPE, AND MAIL. NO POSTAGE NECESSARY.

NASA Form 1332 AUG 66

GPO 915-777

CUT ALONG THIS LINE

CUT ALONG THIS LINE

FORCELESS STRUCTURE OF MAGNETIC FIELDS IN THE ATMOSPHERE OF ACTIVE SOLAR REGIONS AND PROBLEMS OF THE GENERATION OF GEOEFFECTIVE CORPUSCULAR STREAMS.

E.I. Mogilevskiy

ABSTRACT: The results of a number of studies conducted for the purpose of determining the nature of the magnetic fields of solar active regions in connection with problems concerning the generation of geoeffective corpuscular streams are presented. The probable forceless structure of the magnetic fields in the chromosphere and in the corona is discussed. Two types of magnetic fields in the chromosphere are analyzed, including those associated with the photosphere and those which are isolated and have their own forceless structure. The conditions which must correspond to the formation and emission of geoeffective corpuscular streams from the active regions are analyzed. A semiquantitative scheme proposed for the generation of discrete plasmoids from the active regions is found to satisfy the conditional requirements.

Introduction

Comparisons of the numerous phenomena of solar activity with /5* the global characteristics of geophysical phenomena have shown that the magnetic fields on the Sun determine both the development of the solar activity and the conditions for regeneration and outflow of geoeffective corpuscular radiation and radio emission. The magnetic fields cause the energetics and kinematic characteristics of solar phenomena and the dynamics of corpuscular streams in interplanetary space and the space around the Earth. As observations have shown, the density of magnetic energy in active regions of the solar atmosphere, in a substantial part of solar corpuscular streams (in a system of coordinates linked with the stream), and in the Earth's magnetosphere exceeds the density of total intrinsic energy of the plasma under investigation. This means that the magnetic fields are determined by the phase and change of the currents which cause them, while the plasma in the effective range of the magnetic field follows up the changes in the magnetic fields. In the case under investigation, it is not so such the intensity

---

* Numbers in the margin indicate pagination in the foreign text.

of the magnetic field which is essential, but its macroscopic characteristics-general structure and configuration of the entire magnetic field, geometry of the magnetic surfaces and lines of force. As will be shown below, this characteristic property of the media under investigation determines the particular properties of their magnetic fields-in quasi-equilibrious systems they necessarily become forceless, i.e., the relationship [rotH,H] = 0 does not hold for them. The measurements of the distribution of the magnetic vector in active regions on the Sun have required the designing and construction of a complex solar tower with a spectral photoelectric complex magnetograph. They have cleared up some problems of the nature of the magnetic fields in active regions of the chromosphere, which are probably very close to a forceless structure, and certain problems in the mechanism for the generation of geoeffective corpuscular streams. The measurements of the magnetic fields and plasma in interplanetary space and the space around the Earth which were carried out recently with the aid of space rockets and automatic stations have permitted us to study the nature of solar corpuscular streams and certain aspects of their interaction with the Earth's magnetosphere by direct experiments. Finally, a combination of the many years of geophysical studies on geomagnetic and ionospheric perturbability, variations in cosmic rays, and auroras (particularly the global observations during the IGY period and the subsequent years) can be used for testing and validifying the general scheme of the link between solar and geophysical phenomena. /6

The results of this series, which I carried out independently or together with coworkers at the IZMIRAN (Institute of Terrestial Magnetism, the Ionosphere and Radio Wave Propagation of the Academy of Sciences, USSR) for the purpose of determining the nature of magnetic fields of active solar regions in connection with the problems of regeneration of geoeffective corpuscular streams, are presented briefly below.

1. Measurement of the Magnetic Fields on the Sun

Measurements connected with weak local magnetic fields in active solar regions according to the Zeeman effect require large solar telescopes with spectrographs which have high spectral resolution. Thus, in order to measure magnetic field of roughly 10 Oe on the level of the photosphere (along the line FeI, λ 5250,2Å), we must determine a separation value on the order of $4 \cdot 10^{-4}$ Å between Zeeman components, while the half-width of the measured line is on the order of 10^{-1} Å. Such fine measurements are possible if we use the so-called modulation photoelectric magnetograph. Even in 1952-1954, the first solar magnetograph was constructed and tested on a small horizontal telescope [1-2]. This was the first spectro-photoelectric device in the Soviet Union with allowed recording not only the magnetic fields of small sun spots, but also weak (about 40 Oe) magnetic fields in Faculae.[1] Later (from 1957), the workers at the

1 Survey of studies on measurement of magnetic fields on the Sun can be found in work [2].

Crimean Astrophysical Observatory perfected the method of measuring the magnetic fields on their solar tower with the aid of a magnetograph, and they obtained rich and original observational materials, Of particular interest are the series of studies in which chromospheric flares are examined as the result of rearrangements of magnetic fields of active centers. In 1960, promising investigations of the magnetic field were begun at the Main Astronomical Observatory (Pulkova) by a group of workers (L.I. Kotlyar, G.F. Zyal'shin, G.Ya. Zasil'yeva) under the leadership of V.A. Krat. Recently, photoelectric measurements of local magnetic fields were started at the Siberian Institute of Terrestrial Magnetism, the Ionosphere and Radio Wave Propagation (Irkutsk). Further development of the studies at the IZMIRAN (Institute of Terrestrial Magnetism, the Ionosphere and Radio Wave Propagation of the Academy of Sciences, USSR) required investigations for the optimal electronic scheme of the magnetograph [3] and the designing of a solar tower and spectrograph suitable for this purpose [4,5]. A number of improvements were introduced during the designing and subsequent use of the solar tower at the IZMIRAN. The large scale dual tubule-monolith of the telescope with an input aperature covered by a high-precision plane-parallel glass yielded excellent images and allowed observations even under terrestrial conditions (as the result of the high stability of temperature stratification of the air in the telescope obtained in this case). The optical view from the high-quality H_α-filter ($\Delta\lambda$ = 0.5 Å) and movie-film recorder, which used the light reflected from the mirror sidepieces of the spectral slit in the spectrograph, allowed determining, practically continuously and with the precision needed in these studies, to what sites in the active region the measured magnetic fields referred. The use of two independent spectral chambers for one collinator of the spectrograph made it possible to construct two simultaneously-operating magnetographs and to measure the magnetic field at two levels in the active region (photosphere and chromosphere). The solar magnetograph of a longitudinal field vector which was developed at IZMIRAN [6-8] has a number of principal characteristics which distinguish it, for example, from the American design [9]. First of all, the magnetograph operates with one output slit and one photomultiplier, while both arms of the effective spectral line enter in sequence at this slit during continuous oscillation of the plane-parallel plates. This design, which keeps the advantages of the /7
American one (excepting the instrumental polarization), has a number of preferences: a low spectral magnitude can be used, where the quality of the spectrum is higher and there are no difficulties in balancing the two photomultipliers. The nonlinearity of the signal-intensity ratio is preserved in using two photomultipliers. The latter is very essential, since it is practically impossible to measure the Doppler frequency at the same time as the magnetic field in structures with two photomultiplers, according to the investigations of A.E. Severniy and S.I. Gophsyuk [10]. A dual signal modulation is made in the magnetosphere by the IZMIRAN: at high frequency (500 Hz) the signal of the magnetic field is isolated with the aid of an electro-optical ammonium dihydrogen phosphate

crystal, while at low frequency (9 Hz) there is a signal which is used for guiding the lines on the output spectral slit and for continuous recording of the Doppler frequency. The simultaneous and continous recording of the average light flux in the spectral line permits calculations of the magnitude of the magnetic field at different sites on the Sun (considering the changes in the transmissivity) as well as indirect solutions to other problems (for example, the relationship between the brightness and the magnitude of the field at different sites in a floccula, etc.).

The studies of the IZMIRAN workers B.A. Ioshpa and V.N. Obridko, who developed the method of measuring all the elements of a magnetic vector, were a significant advance in the methods used for investigating magnetic fields on the Sun [11-14]. They succeeded in developing an original method, constructing the corresponding apparatus, and conducting a series of observations, which confirmed the satisfactoriness of the method proposed.[2] Its principal advantage is that the Stokes parameters, by which all the components of the total-field vector are subsequently calculated on an electronic computer, are measured simultaneously, while measurements in a total-vector magnetograph, e.g., that of the Crimean Observatory [15], required at first three and then two subsequent measurements of the field at one and the same point on the Sun.

The longitudinal field vector magnetograph in the apparatus of IZMIRAN permitted recording the magnetic field at the level of the photosphere with sensitivity on the order of 1-3 Oe for resolution over the disc of about 3", while the sensitivity for measurements at the level of the chromosphere (at a height on the order of $2 \cdot 10^8$ cm) was one order lower. The total-vector magnetograph had a lower sensitivity (on the order of 50-70 Oe), although the sensitivity could be increased by a large factor by selecting the optimal operational regime of the modulator, for example, or by a selection of the corresponding photomultiplier, etc.

Investigations of the local magnetic fields on the Sun have been carried out with the aid of this complex device since the

---

[2] We should mention that the solar photoelectric magnetograph for a total vector was the first device of this kind. The methods used for measuring a total vector with a magnetograph were first proposed and executed at the Crimean Astrophysical Observatory [15], and somewhat later at IZMIRAN. A similar magnetograph was developed at the Siberian IZMIR (Irkutsk). A total-vector magnetograph was also recently constructed at the Main Astronomical Observatory (Pulkovo), where investigations of the magnetic fields on the Sun have been carried out successfully for a number of years.

end of 1961: the magnetic fields of protuberances and filaments have been measured, as have sunspots and the structure of magnetic fields in the chromosphere of active regions on the Sun.

Despite the definite advances in the development of methods for direct measurements of local magnetic fields on the Sun, they have recently been found to be insufficient in order to investigate the structure of the magnetic fields of an active region, or problems of regeneration of a geoeffective corpuscular stream. Data on the magnitude and structure of the magnetic field and active regions of the solar corona are very important and necessary. The following can be considered in this respect to be promising types of field measurements: (a) according to spectral coronal lines, with the aid of a most powerful Lyot coronograph; (b) according /8
to the radio-astronomical measurements of polarized properties of radiation bursts, particularly narrowband ones of the first type, which apparently have the nature of laser radiation [16].

The successive recording of magnetic fields in this same region at the level of the photosphere and chromosphere along the H_β line which were carried out in 1961-1962 [17] showed that, as a rule, there is correspondence (in magnitude and sign of polarity) in the magnetic fields in the photosphere and the chromosphere. The relatively large value for the magnitude of the magnetic field in the chromosphere (particularly over spots) which was established earlier [18] was thus confirmed. However, there have been detected magnetic "mounds" in the chromosphere ($H \approx 100$-150 Oe) under which there was practically no magnetic field in the photosphere.[3] An investigation of the structure of the magnetic field led to the assumption that in this case we have an isolated forceless magnetic field. It was assumed in the calculations that there was an axisymmetrical forceless field.

The idea of the forceless nature of magnetic fields in the solar atmosphere had been discussed earlier [20] in connection with the problem of the penetration of local magnetic fields into the solar corona. In using the so-called principle of dynamic possibility of motion in a compressed fluid for the chromospheric coronal plasma [21], it was shown that the presence of a forceless magnetic field is a necessary condition for the possibility of movement in the solar atmosphere. Significant observational materials on the distribution of the total magnetic vector in a number of active regions of the photosphere were obtained in 1963. This allowed researchers to conduct more detailed investigations of the preliminary proposition, of the forceless structure of magnetic fields in active regions of the solar chromosphere.

---

[3] The idea that the so-called chromospheric patches could exist was investigated even in 1958 by V.Ye. Stepanov and N.N. Petrova [19].

The principal results of these observations amount to the following.

1. The magnetic fields of sunspots and of the facular-floccular field, in which they are developed, have in many ways a different history and rate of development, and can be examined independently to some extent. Therefore, the structures of the magnetic field in the chromosphere over a facula differ from those over sunspots. This result has also been obtained from an analysis of regular observations which were carried out in 1957-1958 at the Mount Wilson Observatory (USA) [22].

2. As a rule, the magnetic fields in the chromosphere over faculae corresponds in magnetude and sign to the photospheric fields (for the longitudinal component) [23]. A comparison of maps of chromospheric magnetic fields and Doppler frequencies (see, for example, Fig. 1) showed that there is a simple dependence of the following type between the field vector H and the velocity vector v (particularly in "magnetic mounds"):

$$\mathbf{H} \simeq \beta' \mathbf{v}, \tag{1}$$

where β' is a parameter which depends on the coordinates.

This also follows from a comparison of the records of the magnetic field and velocity along individual crossovers (Fig. 2). An investigation of a large number of such records showed that the polarity of the field and the sign of the velocity vector coincide roughly for 75-80% of the cases. Such an experimental dependence permits us to conclude that the magnetic field of an active region in the chromosphere is primarily forceless. Actually, let us have an equation for this field as such:

$$\frac{\partial \mathbf{h}}{\partial t} = \mathbf{rot}\left[\mathbf{v},\ \mathbf{h}\right] + \frac{c^2}{4\pi\sigma}\nabla^2\mathbf{h} \tag{2}$$

(here $h = H(4\pi\rho)^{-1/2}$, ρ is the density of the plasma), and the equation of motion is

$$\frac{\partial \mathbf{v}}{\partial t} + (\mathbf{v},\ \mathrm{grad})\,\mathbf{v} - \frac{1}{4\pi\rho}\left[\mathrm{rot}\ \mathbf{h},\ \mathbf{h}\right] = -\mathbf{grad}\left(\frac{P}{\rho} + X\right), \tag{3}$$

where P is the gas pressure and X is the gravitational potential. We should examine this problem for the quasi-stationary case on the condition that

$$\mathbf{h} = \beta\mathbf{v}. \tag{4}$$

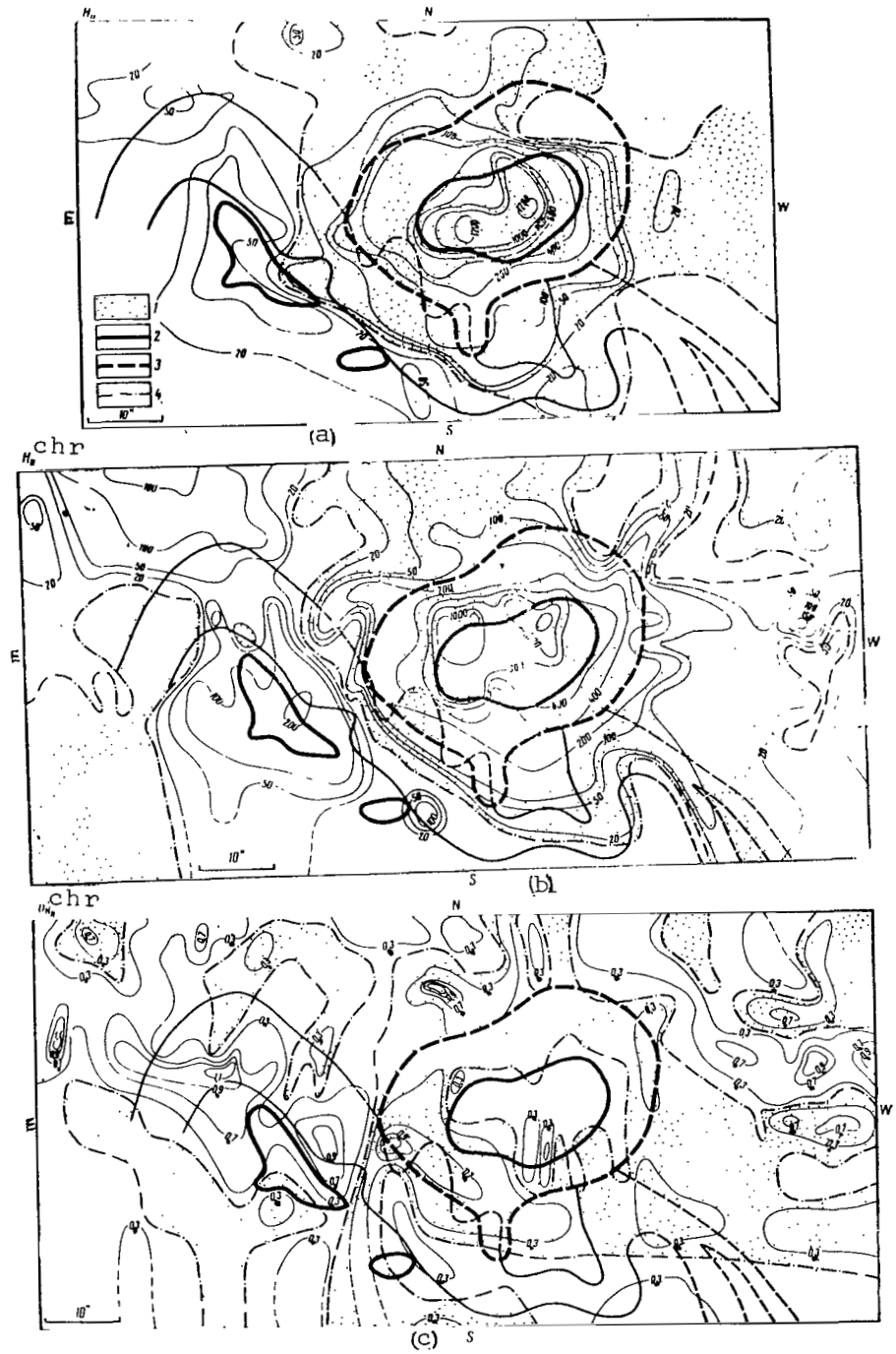

Fig. 1. Example of Maps of the Longitudinal Component of Magnetic Fields in the Photosphere (a) Chromosphere (b) and of the Radial Velocity in the Chromosphere (c) in One of the Active Regions for August 4, 1963. Isolines of the Magnetic Field Expressed in Oersteds, Radial Velocity in km/sec. (1) Direction of the Vector Towards the Observer; (2) Boundaries of the Core of Sunspots; (3) Boundaries of the Half-Shade of the Spots; (4) Boundary of the Zero Values for Field or Velocity Vectors.

Here $\beta = \beta' (4\pi\rho)^{1/2}$. Taking the operator rot of (3), and introducing the vector A = (v,grad) v for div A = 0, we obtain the following for the condition in (4): /10

$$(\mathbf{h},\ \mathrm{grad})\,\beta\mathbf{h} = \frac{\mathbf{A}}{\beta}. \qquad (5)$$

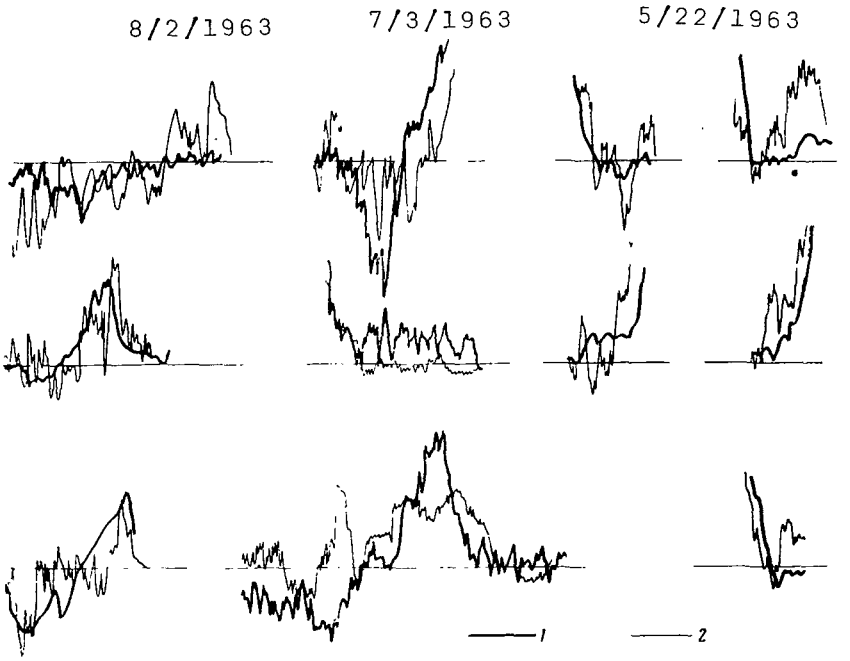

Fig. 2. Examples of Records of the Magnetic Field (1) and Radial Velocity (2) in the Chromosphere Along Isolated Cross-overs in Active Regions.

We can find a solution for the two-dimensional axisymmetrical case in (5), which would correspond to the case of a forceless field, i.e., [rot h,h] = 0. For this, it is easily seen that it is sufficient for the parameter β to satisfy the following relationship:

$$\beta = \frac{a}{|h|}\exp\left(-\frac{\lambda^2}{2}r\right), \qquad (6)$$

where a and λ^2 are constants. The expression in (6) was tested according to the magnetic charts of a field of the chromosphere for regions of chromospheric mounds where the radial field components velocities were predominant. The satisfactory agreement between (6) and observations is illustrated in Fig. 3. This shows that the necessary condition responsible for the forceless structure of a field in the chromosphere can be fulfilled there. A

similar conclusion can be obtained in fulfilling the condition of (4), if we also introduce the condition of "dynamic possibility of movements" [21, 24]. In our case this is reduced to the following expression: /11

$$\mathrm{rot}\,[\mathrm{rot}\ \mathbf{v},\ \mathbf{v}] = 0, \tag{7}$$

This corresponds to the condition of non-conservativeness of body forces. The latter can be obtained independently from an examination of a map of the magnetic field in the chromosphere (at a height of about $2 \cdot 10^8$ cm), which is determined according to the photospheric fields by a solution to the Neumann problem [25]. A comparison of the calculated magnetic field at a given height to the observed magnetic field on the H_β line shows that the field in the chromosphere is non-potential.

3. Measurements of the total field vector along the photospheric lines, which were carried out in 1963, as well as of $H_{||}$ in the chromosphere along the H_β line allow a proper investigation of the magnetic field over a sunspot. Measurements of the total field vector in the sunspot at the level of the photosphere showed that, even in the middle of the core of the sunspot, the longitudinal components of the magnetic field have high values. It was shown in [14] that, if the modulus of the sunspot field can even approximate the fields of the equivalent dipole submerged below the photosphere, then the distribution of the field vector component is clearly contradictory to this approximation. Therefore, it was of special interest to examine the sunspot field as part of a field of a forceless toroid [25].

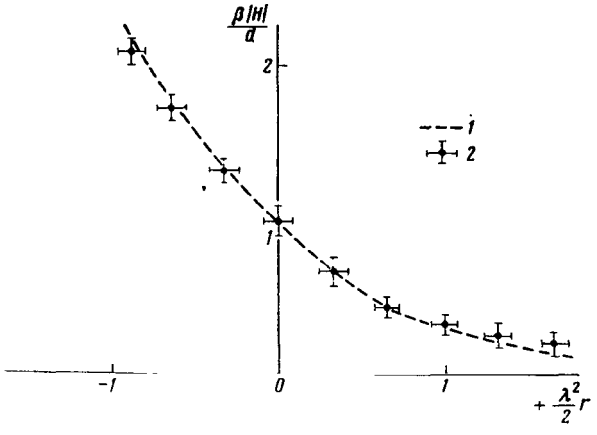

Fig. 3. Dependence of the Parameter $\beta\,|H|\,/a$ on the Relative Distance r from the Center of a Magnetic Mound in the Chromosphere. (1) Theoretical Dependence; (2) Average Measured Values (with root-mean-square deviation) for 25 Magnetic Mounds Inside Spots According to Observations on May 29, July 7, and August 2-4, 1963; β, in Units of $5 \cdot 10^2$ cm/sec times Oe; H, in 10^2 Oe; λ^2/r in units of 10^{-9} sec; r in units of 10^{-9} cm.

Calculations of the field distribution for a forceless toroidal magnetic tube with small curvature were conducted in relation to the condition that the current was taken in an approximation of the longitudinal conductivity, i.e.,

$$\operatorname{rot} \mathbf{H} = \mathbf{j} = \sigma_{\parallel} \frac{\mathbf{H}(\mathbf{E}, \mathbf{H})}{H^2}. \qquad (8)$$

The results of numerical integration of the field distribution of such a problem were taken from [26] and used for tabulating the distribution of the magnetic field components of the sunspots at the level of the photosphere and chromosphere.

Figure 4 shows a comparison of the field distributions calculated according to [26] and observations for two specific cases (spots observed on May 7 and 21, 1963). It can be seen from the figure that there is satisfactory agreement with the observed distribution of the field components in the chromosphere [25,27]. However, such an agreement is obtained only in certain sectors of the sunspot.[4] In order to clear up the question on whether or not the magnetic fields of sunspots should be examined as a *unit* having a forceless component, or whether the sunspot fields represents non-commutating isolated forceless magnetic fields, we calculated the circulations of the magnetic fields through closed, quasi-concentric contours for a number of sunspots. It is easily seen [25,27] that, in the case of a forceless magnetic field of the type

$$\operatorname{rot} \mathbf{H} = \alpha(\mathbf{r}, \vartheta)\mathbf{H}, \qquad (9)$$

where α (r, ϑ) is an arbitrary function of the coordinates, the difference in circulations through two neighboring, closed contours related to magnetic fluxes of the longitudinal component should determine the average values of the parameter α (r, ϑ) in the zone under investigation. The values of the vertical current and the parameter α (r, ϑ) which were obtained from observations are shown in Figure 5. A quasi-vortical distribution of "lines" of vertical currents with an abrupt change in the sign of the current vector was obtained earlier in [29]. In this respect, the results of the calculations shown in Figure 5 repeat and confirm the studies of A.B. Severniy. They show that the field of the sunspot and its vicinity are clearly not potential. It follows from Figure 5 that the distribution of the parameter α (r, ϑ)

[4] Studies by A.B. Severniy [18], G.B. Kuklin and V.Ye. Stepenov [28] show that the distribution of the total magnetic field vector observed in a sunspot at the level of the photosphere can be approximated by a unit forceless magnetic field only for individual simple sunspots and only during isolated periods of their developments.

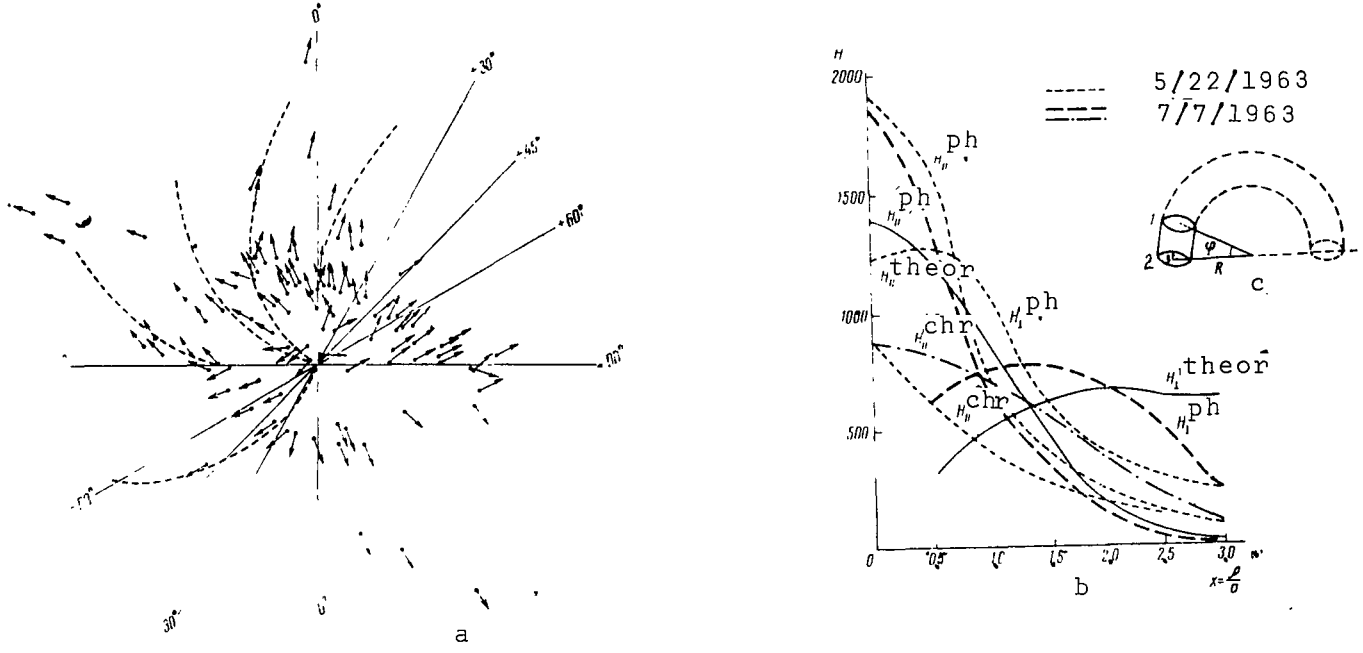

Fig. 4. Comparison of the Distribution of Elements of the Magnetic Fields Calculated for a Forceless Magnetic Toroid According to [26], and Observed Values of $H_{\parallel}$ and $H_{\perp}$ at the Level of the Photosphere and $H_{\parallel}$ at the Level of the Chromosphere. (a) Distribution of the Azimuths of the Magnetic Vector at the Level of the Photosphere in a Spot on May 22, 1963, The Sector from +30°to -30° Corresponds to the Range of Averaging of the Measured Values for the Elements of the Fields $H_{\parallel}^{ph}$ and $H_{\perp}^{ph}$; (b) $H_{\parallel}^{theor}$ and $H_{\perp}^{theor}$ are Calculated Curves for a Forceless Magnetic Toroid According to [25]; $H_{\parallel}^{ph}$ and $H_{\perp}^{ph}$ are the Values for the Longitudinal and Perpendicular Components of the Fields, Respectively, in the Photosphere, and $H_{\parallel}^{chr}$ According to Observations in the Line of the Chromosphere; (c) Scheme of a Toroidal Tube. (1) Level of the Chromosphere; (2) Level of the Photosphere.

within the range of the sunspot changes not only its value but also its sign. /13 However, it follows from the general properties of forceless magnetic fields for $\alpha \neq$ const (see below) that forceless magnetic fields with parameters differing in sign belong to different classes of forceless fields which are never put together. Therefore, the magnetic fields of sunspots can be examined, not as a single toroidal tube of flow, but as a field of "osculating", forceless, "enclosed", and probably, deformed toroids. This sunspot can yield a qualitative explanation for the distribution of the total field vector in a sunspot at the level of the photosphere, and it makes a substantial extension of the sunspot field into the chromosphere and corona possible ($H_{\parallel}$ components). The predominance of the toroidal components of the field at the level of the photosphere brings about a screw dislocation of the field components $H_{\parallel}$ going into the chromosphere and corona. The runoff of the chromospheric plasma along the field (Evershed effect, looped and active protuberances) favors the preservation of the magnetic tube ($H_{\parallel}$) of a sunspot all the way to the altitudes of the corona. This makes it possible to explain qualitatively the high value of the magnetic flux observed in the chromosphere, as well as the possibility that there may be a magnetic field over the spot in the corona which is greater in magnitude (up to $3\text{-}5\cdot10^2$ Oe). It is well known that the latter follows from radioastronomical observations [30], and that it has important significance in analyzing the problem of the generation of a geoeffective corpuscular stream. The model of a sunspot as a forceless field of contiguous and contorted toroids can be considered merely one possible model. The construction of a model of a sunspot field requires further investigations concerning the distribution of the magnetic vectors at several levels over a sunspot, as well as the so-called fine structure of the sunspot field. [18]. We should also mention that the development of a forceless structure in a field of the chromosphere(is as in laboratorial plasma) the result of local convection of screw dislocation [26, 31].

4. Chromospheric magnetic "mounds" ($H \lesssim 10^2$ Oe) which are not linked with the photospheric fields are often observed in the vicinity of the neutral line of the longitudinal field [17,25]. The distribution of the total magnetic vector in these regions at the level of the photosphere, where the field is on the order of zero (or sometimes even another sign), indicates the "confinement" of the magnetic fields of the "chromospheric mounds" (Fig. 6). In order to show that magnetic lines of force of the photosphere do not pass through such chromospheric magnetic "mounds", we compared the photometric brightness of H_α - flocculae to the intensity of the magnetic field at a given site in the chromosphere. According to the hypothesis of S.B. Pikel'ner [32], the brightness of a floccula reaches a maximum at a certain value of the field H_{max}. An initial increase in the brightness in the floccula is due to a decrease (as an effect of the fields) of the turbulent vicosity. At $H > H_{max}$, the magnetic field begins to suppress the convective energy transfer, and this should bring about a decrease

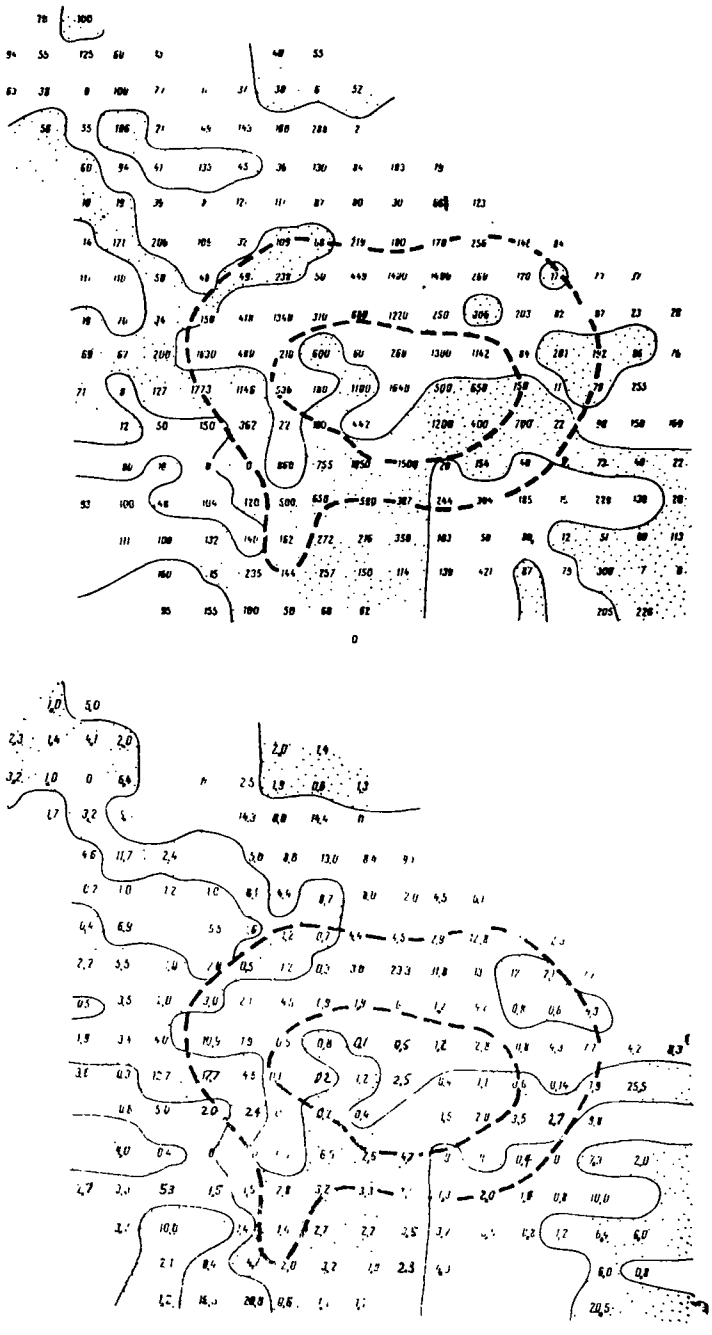

Fig. 5. Distribution of Calculated Vertical Currents (a) and the Parameter α (b) in the Region of a Spot (Contour Outlined by the Dashed Line) According to Observations of the Total Field Vector on August 4, 1963 at the Level of the Photosphere. The Vectors of the Currents Directed Toward the Observer are Designated by the Points (or the Positive Values of the Parameter α).

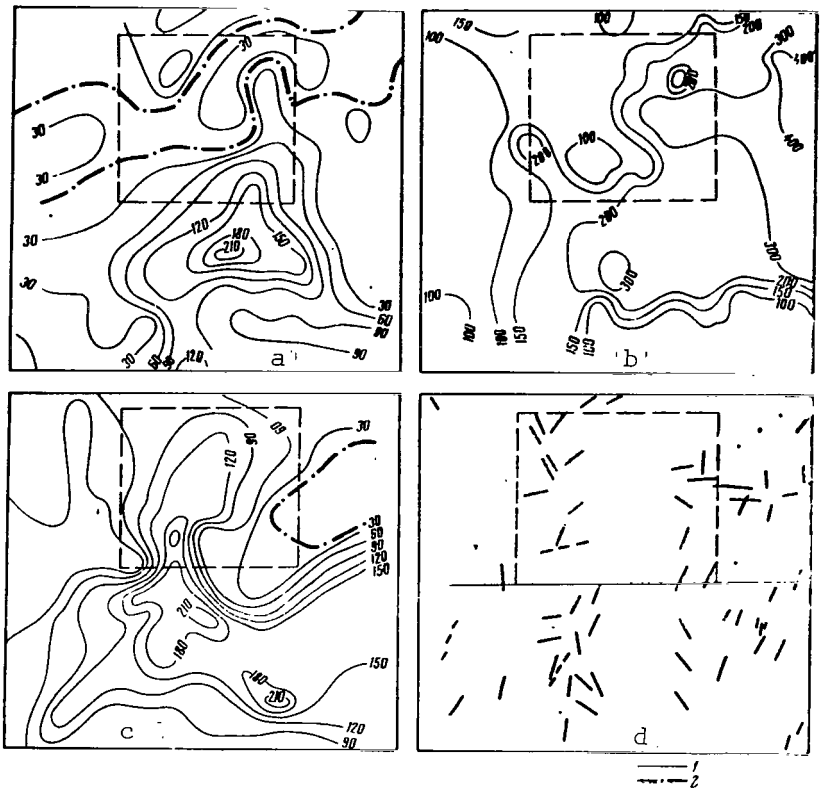

Fig. 6. Example of an "Isolated" Magnetic Mound in the Chromosphere (Outlined by the Dashed Square) According to Observations on August 3, 1963. Distribution: (a) Components $H_{\parallel}$ in the Photosphere; (b) Total Vector in the Photosphere; (c) Components $H_{\parallel}^{chr}$ in the Chromosphere; (d) Azimuth of Magnetic Plane in the Photosphere; (1) Isolines of the Fields; (2) Lines of Sign Change of the Fields for the Component $H_{\parallel}$ in the Photosphere.

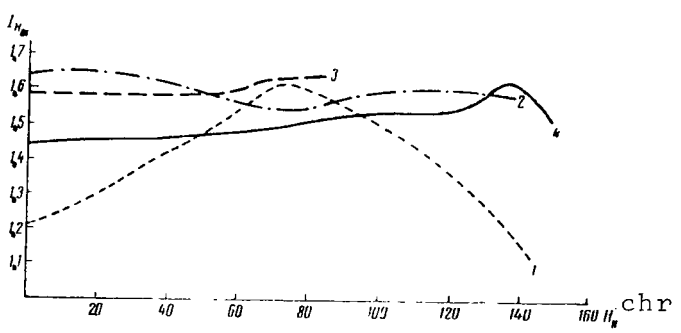

Fig. 7. Dependence of the Relative Brightness of a H_{α} - Floccula on the Value of the Magnetic Field in the Chromosphere ($H_{\parallel}^{chr}$)

According to Observations on May 22, and July 3, 1963. Curve 1 is the Average for a Number of Regular (Linked with the Photosphere) Chromospheric "Mounds" of the Magnetic Field; Curves 2, 3 and 4 are for Chromospheric Magnetic "Mounds" not Linked with the Photospheric Field.

in the brightness with an increase of the field. This dependence, /16 which was obtained earlier by Z.Ye. Stepanov and N.N. Petrova [19][5] was also the general rule found in our observations (Fig. 7). This indicates the continuous extension of the magnetic field from the photosphere to the chromosphere, which channels the energy transfer from the photosphere to the chromosphere [33]. However, this dependence is abruptly broken in "isolated magnetic fields" in the chromosphere (Fig. 7, Curves 2-4). Although the magnetic field inside a mound continues to grow at certain sites to 150-200 Oe, the brightness of a H_α -floccula remains almost unchanged in this case. In these regions, the magnetic lines of force which are enclosed in the chromosphere itself outline a plasma cloud with the inherent magnetic fields. Detailed comparisons of the records of Doppler frequencies and the field have shown that, in contrast to the regular proportionality between the field and the frequency ($H = \beta v$), there is observed a change in the sign of the frequency at these sites in the range of the maximum of the magnetic fields of the chromospheric mounds.

The symmetry of the pictures for distribution of the fields and frequency can be explained by the assumption that the fields in the magnetic chromospheric "mounds" represent a field of an horizontally arranged toroid. We can find from the condition of equilibrium of the field of a forceless toroid (H_{nt}) that

$$H_{nt} = \frac{\pi r^2}{H_{ex} r}, \tag{10}$$

where H_{ex} is the external (in relation to the forceless toroid) magnetic field of the neighboring active region; the latter determines the stable equilibrium of the toroid; r is the smaller radius of the circular toroid. The time the "isolated" forceless magnetic fields exist in the chromosphere was found to be on the order of 1-2 days. The presence of "isolated" plasmoids with an inherent forceless magnetic field not linked with the neighboring fields in active regions of the chromosphere is of particular interest in solving the problem concerning the generation of geoeffective corpuscular streams.

2. Forceless Magnetic Fields

The idea of forceless magnetic fields in a magnetized plasma was introduced in 1954 by Lundquist and studied in detail by Chandrasekar, Volterra, Lyust and Shlyuter, Alfven, Kaplan and other authors, particularly for the case when the parameter α = const in the ratio rot H = αH. It is now used for interpreting

[5] In contrast to [19], the brightness of an H_α -floccula was compared in our study to the magnetic fields in the chromosphere itself.

magnetic fields, for example, for branches of the Galaxy and Crab Nebulae, as well as for analyzing the magnetic fields of laboratory plasma [29,31,34-36]. It was shown in the works of these authors that the forceless magnetic field in an isolated plasma corresponds to a minimum energy, i.e., it is stable and thermodynamically preferable. For a given possible flow in the plasma, the forceless configuration of the magnetic field corresponds to the least value of the magnetic field and minimum dissipation. The magnetic field remains forceless during any temporary changes if the initial field had been forceless. We should mention that a number of the general properties of forceless magnetic fields follows from helical movements of the Gromeko-Belteram type [37], which had been studied extensively at the end of the last century in hydrodynamics. The latter refers to a movement for which the Lamb vector $L = [\mathrm{rot}\ x, \dot{x}] = 0$, where x is the coordinate and $\dot{x}$ is the velocity. The analogy between such a hydrodynamic movement and a forceless magnetic field /17 in a plasma is not merely of a formal nature. In a number of studies, an analogy has been shown between hydrodynamic movements and magneto-hydrodynamic phenomena [38].

The axisymmetric magnetic fields can be represented by a system of orthogonal poloidal (H_p) and toroidal (H_t) fields and the corresponding toroidal ($j_r = \mathrm{rot}\ H_p$) and poloidal ($j_p = \mathrm{rot}\ H_t$) currents. For a forceless magnetic field, there is equilibrium between the integral energies of the poloidal and toroidal fields. These and other general properties of forceless fields were obtained mainly for the case when the parameter $\alpha = \mathrm{rot}\ H/H = \mathrm{const}$. It then follows from a determination of the forceless fields that $\nabla^2 H + \alpha^2 H = 0$. This means that there is a scalar function which satisfies the equation $\nabla^2 \psi + \alpha^2 \psi = 0$, since the toroidal components of the fields $H_t = \mathrm{rot}(a\psi)$, while the poloidal components $H_p = 1/\alpha\ \mathrm{rot}\ H_t$. A solution for ψ is found in the form of complex series comprising a combination of the Bessel and Legendre functions [34,36].

An analysis of the stability of a symmetrical forceless field at $\alpha = \mathrm{const}$ showed [39] that convective instability takes place during a time interval determined by the following relationship:

$$t_0 = 3 \cdot 10^{-9} l_0 n^{1/2} H^{-1} \mathrm{sec}, \tag{11}$$

where l_0 is the characteristic dimension of the region with a forceless magnetic field H and with plasma concentration equal to n. It can be seen from (11) that a forceless magnetic field can exist for a very long period of time for the high values of l_0 usually found in cosmic scale and for relatively small values of n and H, even in the most disadvantageous case ($\alpha = \mathrm{const}$).

The forceless magnetic field is stable in relation to unidimensional and two-dimensional disturbances and, when disintegration

results from attenuation of currents, it preserves its forceless character.

It was clear from the moment the concept of forceless magnetic fields was introduced that such a structure of the field should be found most often in space objects. However, the best direct measurements of magnetic fields in space objects being conducted at the present permit determinations of the magnitude and certain integral characteristics of the field, while it is necessary to know the distribution of the field *vector* throughout the entire space being examined in order to study the forceless nature of the field. In this sense the magnetic fields on the Sun can be considered the most convenient objects for investigation, since the completeness of information on the spatial distribution of the magnetic field in active regions (even at the present) is rather great and comparable, for example, to what is known of the distribution of the magnetic field in magnetized laboratory plasmas. In contrast to the latter, the time for stability of forceless magnetic fields [for example, in active regions of the chromosphere and corona even in a disadvantageous case (α = const) according to (11)] is evaluated as 10^5 - 10^6 sec, which is a large factor higher than the time that magnetized laboratory plasmas exist. On the other hand, the possibility of measuring a large number of characteristic parameters in laboratory experiments which are often not measured in solar phenomena makes the laboratory experiments irreplaceable in investigations of a number of properties of forceless magnetic fields (for example, the processes of formation in a rarified plasma of a forceless magnetic field, etc.). Therefore, certain laboratory experiments with plasma can be very useful in obtaining some characteristic parameters of phenomena in the magnetized solar plasma (usually nonlinear, and almost unsolvable problems) [31, 40, 41].

Let us examine the properties of forceless magnetic fields and the case where $\alpha \neq$ const in somewhat more detail. As was shown above, such a more general case takes place in the solar atmosphere and in the interplanetary medium. The problem of the distribution of the magnetic field is reduced in this case [42] to a solution for a system of vector equations; /18

$$\operatorname{rot} \mathbf{H} = \alpha \mathbf{H}, \qquad (12)$$

$$(\operatorname{grad} \alpha, \ \mathbf{H}) = 0.$$

The boundary surface of the plasma under investigation should satisfy the conditions of a magnetic surface. In this respect, the problem is reduced to a solution of a nonlinear elliptical equation. A solution to the latter is sought in the form of a series, the numbers of which are a combination of Legendre polynomials and Bessel functions of a half-integral order of a real argument. A numerical solution can be obtained on an electronic computer if we give a specific model of the plasma and boundary conditions. Expressions for the field components $H\phi$, H_r and H_z can be obtained

from a general solution. Since the field H decreases as r^{-1}, then as $\alpha\ r \to \infty$ the integral of the field energy will disperse over the entire volume V if $V \to \infty$. This means that forceless magnetic fields cannot exist over the entire volume: there can be only boundary regions with a forceless magnetic field, at the limit of which the magnetic field is forceful, i.e., the current j = rot H and the field H are not parallel. There could be a case where the "source" of the field is forceful in the boundary volume, while it is forceless over the remaining space occupied by the plasma. In our case, such a model can be used for the forceless magnetic field in the chromosphere and the corona of an active region, while the"forceful" source is found below the photosphere. For "isolated" chromospheric forceless fields, the "forceful" source can be found, for example, in the boundary "skin" layer. Considering this position, it would follow to speak of a "quasiforceless" magnetic field for solar phenomena. Because of the limitedness of information (for example, in the case of analyzing the structure of a magnetic field in the corpuscular stream according to sounding measurements on a rocket [27, 43]), it is often useful to use integral or certain local properties of forceless magnetic fields in order to establish the structure of the fields. For an isolated, limited, magnetized plasma, we find from the virial theorem [38] (in addition to the above-mentioned equilibrium of integral energies for toroidal and poloidal field components) that volumetric energy $\mathscr{E}_V = \int_V e_V d\tau$ of the field is equal to three times the energy of the surface field $\mathscr{E}_S = \oint_S e_S dS$, while in the case of the presence of boundary currents,

$$\mathscr{E}_V = 9\mathscr{E}_S. \tag{13}$$

For a cylindrical forceless field, the following integral relationship is obtained:

$$\ln \frac{H_{\varphi,0}}{H_\varphi} + \frac{H_z^2 - H_{z,0}}{H^2} = r^2, \tag{14}$$

where r is the radius of the cylinder. As mentioned above, these relationships were used for testing the forceless nature of fields, for example, in a sunspot, when the average value of the parameter α was calculated. Certain general characteristics of the forceless magnetic fields can be obtained from the variation principle, if we introduce the functional L, which is determined from the relationship

$$\tilde{L} = H_z^2 + H_r^2 - H_\varphi^2. \tag{15}$$

The equations for the field components can be obtained from the condition $\delta (rL) = 0$ for an arbitrary (variable) parameter α.

Different classes (non-commutative) of forceless magnetic fields ($\alpha > 0$; $\alpha < 0$) are obtained for a selected system of coordinates, depending on the sign for the second variation of the functional L ($\gtrless 0$). Thus, forceless fields with $\alpha < 0$ are stable, while the expression determining the stability in this case is similar to the condition of convective stability for a magnetized plasma (Sideman condition). /19

An indication that an isolated plasma (particularly of cosmic scales) with an arbitrary set of initial currents in the field systems tends toward a forceless field and current configuration is of particular interest. The term "isolated" should be understood as the absence (or smallness) of external force fields and currents, or as the case when the external fields and currents are forceless. There could also be a case when part of the external field and current has force in relation to the object under investigation, while the evolution of the fields and currents in an isolated region is not significant and is not determined by the external force part. It is possible that the latter case is often realized under conditions of stellar and solar atmospheres, etc. Any field which is complex in its field and current configuration can "spread" into elementary and interconnected orthogonal toroidal and poloidal force fields (currents), for which the following relationships are valid:

$$\mathbf{j}_{\tau}^{i} = \operatorname{rot} \mathbf{h}_{p}^{i}; \quad \mathbf{j}_{p}^{i} = \operatorname{rot} \mathbf{h}_{\tau}^{i}. \tag{16}$$

Naturally, such a formal expansion of a complex function into orthogonal components is permissable for continuous differential functions, and corresponds to the situation where arbitrary currents (fields) in the plasma are represented by orthogonal "force" components. Let the function f (q,p,t) characterize the distribution of the elementary currents (fields) under investigation. We can now write out the following "kinetic equations" for the toroidal (poloidal) elements:

$$\frac{\partial f_{\tau}}{\partial t} + \frac{\partial (v f_{\tau})}{\partial q} + \frac{\partial}{\partial v}(\mathbf{F}_{\tau p}^{i} f_{\tau}) = 0, \tag{17}$$

$$\frac{\partial f_{p}}{\partial t} + \frac{\partial (v f_{p})}{\partial q} + \frac{\partial}{\partial v}(\mathbf{F}_{p\tau}^{i} f_{p}) = 0, \tag{18}$$

where v = q, while q and p are the generalized coordinate and impulse (or energy) of an "elementary" current plasma toroids. The source of the interaction between elementary currents is

$$\mathbf{F}_{\tau p}^{i} = \mathbf{F}_{p\tau}^{i} = \frac{1}{c}\left[\mathbf{j}_{\tau}^{i}, \mathbf{h}_{i}\right] + \mathbf{F}, \tag{19}$$

where j_t^i is an elementary current and h_i is the summary effective field of all the elementary fields acting on the currents j_t^i at the point q, while F is a force of nonelectromagnetic nature. In the plasma of the solar atmosphere of the interplanetary medium, the magnetosphere and, probably, in the plasma of a large number of objects in space, the value F can be disregarded when compared to the first term in (19). For our principally qualitative analysis, we can assume that the fields of elementary currents are approximated by the field of linear elements, so that

$$\mathbf{h}_i = \sum_i \frac{2}{cq}(\mathbf{j}_\tau^i,\ \mathbf{j}_p^i) \approx \frac{2}{cq_{\tau p}}(\mathbf{I}_\tau + \mathbf{I}_p). \tag{20}$$

Then

$$\mathbf{F}_{\tau p}^i = \frac{2}{c^2 q_{\tau p}}\left[\mathbf{j}_\tau(\mathbf{I}_\tau + \mathbf{I}_p)\right] = \frac{2}{c^2 q_{\tau p}}\mathbf{j}_\tau \mathbf{I}_p. \tag{21}$$

Considering (21) (the force F_{pt}^i is obtained in a similar way) systems (17) and (18) are rewritten in the following way: /20

$$\frac{\partial f_\tau}{\partial t} + \frac{\partial (v f_\tau)}{\partial q} + \frac{\partial}{\partial v}\left(\frac{2}{c^2 q_{\tau p}}\mathbf{j}_\tau \mathbf{I}_p f_\tau\right) = 0, \tag{22}$$

$$\frac{\partial f_p}{\partial t} + \frac{\partial (v f_p)}{\partial q} + \frac{\partial}{\partial v}\left(\frac{2}{c^2 q_{pr}}\mathbf{j}_p \mathbf{I}_\tau f_p\right) = 0. \tag{23}$$

In these equations we took into account only the electromagnetic interaction of the elementary currents with a self-consistent field, and we disregarded the "collision term". This not only simplifies the problem to a great extent but also corresponds to the conditions of a rarefied magnetized plasma, which is found most often in space objects. In correspondence with Boltzmann's H-theorem, we should consider that f_t and f_p are Maxwell functions in the stationary case. The possibility of using a statistical formalism in our case is determined by the fact that, having taken only electromagnetic forces for a mobile plasma, we can examine rather frequent interactions with a self-consistent magnetic field for "divided elementary" currents.

Then, having integrated systems (22) and (23) by all velocity values, we can obtain the following after obvious conversions:

$$\frac{\partial N_\tau}{\partial t} + \operatorname{div}(N_\tau, \mathbf{v}_\tau) = 0, \tag{24}$$

$$\frac{\partial N_p}{\partial t} + \operatorname{div}(N_p, \mathbf{v}_p) = 0, \tag{25}$$

where

$$N_т = \int_v f_т dv, \quad N_p = \int_v f_p dv.$$

Having introduced $N = N_t + N_p$; $v = v_t + v_p$, we find that

$$\frac{\partial N}{\partial t} + \operatorname{div}(N\mathbf{v}) = 0. \tag{26}$$

Since there can be only changes of the type $T \rightleftarrows P$ in the process of current interaction, the total number of "elementary" currents $N = \text{const}$. Consequently, we find the following for the state of equilibrium:

$$V\mathbf{v} = \text{const}. \tag{27}$$

Having added and subtracted Equations (22) and (23) in order after integration by velocities, and having considered (24 and (25), we obtain

$$\frac{\partial}{\partial v}[\operatorname{rot}\mathbf{H}_т, \mathbf{H}_p] = 0, \tag{28}$$

$$\frac{\partial}{\partial v}[\operatorname{rot}\mathbf{H}_p, \mathbf{H}_т] = 0. \tag{29}$$

In the determination

$$\mathbf{H} = \mathbf{H}_p + \mathbf{H}_т; \ (\operatorname{rot}\mathbf{H}_т, \operatorname{rot}\mathbf{H}_p) = 0; \ (\mathbf{H}_p, \mathbf{H}_т) = 0. \tag{30}$$

Then, considering that $[\operatorname{rot}\mathbf{H}_т, \mathbf{H}_p] = (\mathbf{H}_т\nabla)\mathbf{H}_p$; $[\operatorname{rot}\mathbf{H}_p, \mathbf{H}_т] = (\mathbf{H}_p\nabla)\mathbf{H}_т$, we find from (28)-(30) that

$$[\operatorname{rot}\mathbf{H}, \mathbf{H}] = 0. \tag{31}$$

Consequently, for the above-mentioned propositions, the isolated system with currents becomes forceless in the state of equilibrium (or dynamic equilibrium).

We will limit ourselves to this important conclusion which follows from a statistical examination of the kinetic equation for a system of elementary currents in a bounded plasma. We should mention that an analysis of the kinetic equations presented permits us to obtain, for example, an integral equation for the energies of the poloidal and toroidal fields in a forceless field. Having multiplied equations (22) and (23) by the energy density

/21

of the poloidal and toroidal fields respectively, and having integrated them by the velocities on the assumption that the distribution functions f_t and f_p are Maxwellian, we can obtain the time equations for the energy balance, which allows us to evaluate the time for relaxation and disintegration of the magnetic fields. Using the kinetic investigation, we can obtain an idea of the nature of evolution of the forceless fields, considering the boundary conditions. As shown above, there is a certain relationship between the surface energy $\mathscr{E}_S$ (in the presence of the boundary forces) and the intrinsic volumetric energy $\mathscr{E}_V$:

$$\int_{(V)} \varepsilon_V dV = 9 \int_{(S)} \varepsilon_S dS. \tag{32}$$

It is clear from these statistical presentations that the elementary force currents are not compensated for a simple, connected boundary surface[6], and, after summation, gives that surface force current (or equivalent external magnetic field) which should guarantee stability of the internal forceless fields. If (32) is not fulfilled, then there can be (as a result of the instability) an expansion of the plasma region with the forceless fields (or its fractionation) until a more rapid decrease of the volumetric energy (than for $\mathscr{E}_S$) leads to restoration of the state of equilibrium in (32). The interaction of magnetized plasmoids with other magnetic fields, for which (32) is broken (as the result of a decrease in $\mathscr{E}_S$) brings about a subsequent expansion (fractionation) of the plasmoid, so that in time we again find the state of equilibrium in (32) for which force fields and currents restrain the internal forceless fields. A similar evolution can occur rather frequently; for example, it takes place for isolated magnetized plasmoids which are discrete components of corpuscular streams.

3. Generation of Corpuscular Streams

The problem of how the generation of corpuscular streams takes place in an active region on the Sun has not yet been studied sufficiently in experiments or in theory. It is often assumed that the generation and outflow of a corpuscular stream takes place in the form of a brief outburst phenomenon, which is observed at a certain depth below the photosphere. This is hardly probable, even for the case of the outburst of a plasma in a chromospheric flare. The problem of the propagation of an outburst (shock waves or system of shock waves) through the convective zone and the stellar atmosphere has been solved by many authors [44,45] for a homogeneous or nonhomogeneous isothermal atmosphere (Brinkley-Kirkwood method).

---

[6] The external analogy with surface phenomena, e.g. in diamagnetism, is relevant here.

It was found that weak waves[7] go out rapidly, while a short impulse disintegrates in time. Consequently, the geoeffective emission under investigation cannot be the result of outburst processes at great depths (on the order of the thickness of the convective process). The relatively long duration for the generation of the corpuscular stream, (judging by geomagnetic data, it is no less than several hours) makes the assumption concerning the outburst of a corpuscular geoeffective stream from the solar atmosphere in the flare-up region very improbable. We should mention that, according to numerous statistical data, the predominant number of geomagnetic disturbances is not linked with flares. The complex set of phenomena in chromospheric flares (generation of cosmic rays, hard ultraviolet, x-ray, and radio-wave emissions, etc.) is often "superimposed" over the phenomena of the regular generation of corpuscular streams, thus changing them substantially. Flares (particularly high-intensity ones) can be made for a time by a more powerful corpuscular stream, can change the structure of the magnetic field of the stream, and in certain cases can "prevent" the outflow of a plasma stream by means of the changing magnetic field [46]. This probably can explain the results of many statistical investigations which showed that even large flares accompanied by the radiation outburst of Type IV (which is characteristic of high activity) often do not cause geomagnetic storms [47]. The outburst mechanism is thereby unsuitable for explaining the regular corpuscular emission of an active region (in the so-called M-regions), which sometimes takes place continuously during the course of ten and more revolutions of the Sun, according to geophysical data. /22

For a hydrodynamic model of the corpuscular emission of the *active regions*, E.N. Parker [48] met a number of difficulties in a theoretical [49] and, particularly, in an experimental explanation for the prolonged process of generation of a corpuscular stream. The high temperature ($T > 2 \cdot 10^6$ K) which is required in Parker's hypothesis[8] exists for a relatively short time, for example during a flare-up, while during the remaining time the temperature of the active region in the corona $T \lesssim 10^6$ [50,51]. This is particularly noticeable during the years of minimum solar activity, when the non-disturbed thermal "S_a-component" of radio emission "disappears" (in the absence of spots), and high-temperature emission lines of

---

[7] The system of strong waves which brings about a discharge in the external atmosphere of a star obviously does not relate to the problem we are examining.

[8] Obviously, this does negate the model which is used for explaining the general, relatively weak corpuscular emission, and which is determined by the expansion of the corona to all sides. This so-called quiet solar wind is not linked with the active regions on the Sun.

the corona are observed very rarely, even in active regions. At the same time, the corpuscular streams (judging by geomagnetic disturbances) exist continuously and for a long period of time, despite the clear signs of the relatively low temperature of the corona. It is characteristic that the total energy of the geomagnetic disturbances during the years of minimum solar activity is proportional to the intensity of the corpuscular emission of active regions, a factor of 1.5-2 less than what is observed during the years of high activity. The total energy of prolonged geomagnetic disturbances often exceeds that of storms which are brief but have great amplitude during the maximum years. Moreover, the "high-temperature" bypothesis of corpuscular emission has not been developed at all for an active region where powerful, bounded magnetic fields usually act (in the chromosphere, to several hundreds of oersteds; in the corona, to tens of oersteds), thereby preventing a simple hydrodynamic investigation similar to that by Parker for disturbed and active regions of the Sun.

The combination of the properties of geomagnetic disturbances as well as the principal characteristics of active regions on the Sun determine the following conditions which must be satisfied by the mechanism for the generation of corpuscular streams.

1. The duration of corpuscular emissions should be comparable to the time an active region exists. The latter is equal to the time a magnetic field in an active region exists, which time is known to greatly exceed the time that individual phenomena of solar activity exist. In the corresponding development of groups of spots, there can be observed a temporary "prohibiting" of the outflow of corpuscular streams [46,52]. However the process of generation can then be renewed.

2. The forces which effect plasmoids ejected from an active region should act for a relatively long period, in any case until the decelerating effect of the magnetic field in an active region is weakened. If a plasmoid (sphere of radius r) is ejected in the radial direction from an active region of size l_a with magnetic moments of m_a*[9], then the work which must be expended for its removal (against the forces of magnetic deceleration) is equal to the following: /23

$$W_{\text{м}} = \frac{m_a^2 r^3}{4 l_a^6}(1 + 3\cos^2\vartheta), \tag{33}$$

[9] For the sake of simplification, we are considering the field of an active region to be a dipole field, in the same way as the dipole fields of a plasmoid, which necessarily must be formed in its movement in the magnetic fields of an active region. The magnetic moment of the plasmoid in this respect is equal to $m_p = \frac{r^2}{2}(1 - p^{-3})\left(-\frac{m_a}{l_a^3} + \frac{3(\mathbf{m_a R})\mathbf{R}}{R^5}\right.$ [53]. In our case, at $p \to \infty$ (removal of the plasmoids), $|R| \approx l_a$, we obtain $m_p \Big| \approx -\frac{m_a r^3}{l_a^3}$.

where ϑ is the polar angle. We have the following for the removal of a plasmoid in equatorial plane of an active region:

$$W_{\text{м}} = \frac{m_a^2 r^3}{l_a^6} = H_0^2 r^3, \tag{34}$$

where $H_0 = m_a l_a^{-3}$.

It follows from (34) that at $H_0 \approx 10\text{-}10^2$ Oe, $r \approx 2\text{-}5 \cdot 10^9$ cm, and W_M is always greater than the kinetic energy of the plasmoid ejected from a coronal region where there is no magnetic field. Thus, the greatest obstacle to the emergence of a plasmoid is the ever-present quasi-dipole magnetic field of an active region. The effectiveness of the action of the magnetic field in an active region practically ceases at a distance of $\gtrsim 5\text{-}8R_\odot$, if the velocity of the plasmoid at this distance reaches $v \gtrsim 3 \cdot 10^7$ cm/sec. The movements should be accelerated before this (although the magnitude of the acceleration can decrease substantially with distance), so that the velocity of the movement of the plasmoid in the upper chromosphere and the inner corona can still be low ($v \gtrsim 20\text{-}30$ km/sec.). This agrees with the observations of contours of coronal lines, radar observations of the Sun, etc.

3. It follows from (34) that the characteristic dimensions of a plasmoid (r) cannot be greater than or equal to the size of the active region. On the other hand, if the plasmoid were small (for example, $r \lesssim 10^8$ cm), its integral and kinetic energy would be insufficient to cause a geomagnetic storm during an encounter with the magnetosphere. Moreover, for such dimensions even large (about 10 Oe) magnetic fields could not guarantee its stability during movement through an extended solar atmosphere. The optimal dimensions of a geoeffective plasmoid are evaluated as $2\text{-}5 \cdot 10^9$ cm (if the dimensions of the active region $l_a \approx 2 \cdot 10^{10}$ cm). In this case (at $n \approx 10^8$ cm^{-3}, $v \approx 5 \cdot 10^7$ cm/sec, $H_0 \approx 10$ Oe),

$$\frac{W_{\text{м}}}{W_{\text{к}}} = \frac{H_0^2}{4\pi \langle \rho \rangle v^2} \gtrsim 10^2 \div 10. \tag{35}$$

Consequently, as a rule the integral energy of closed currents in a plasmoid which are formed during its release from a magnetic field in an active region is substantially greater than the integral energy and radial movement of a plasmoid. If we assume that the energy of a plasmoid does not exceed (it would be better to consider it 1-2 orders less than) the energy of a chromospheric flare (about 10^{31} erg) then for the given parameters $W_M \lesssim 10^{30}$ erg, W_K /24
$\approx 10^{28}\text{-}10^{29}$ erg. This very substantial *integral* property of the corpuscular stream[10], i.e., $W_M > WK$, which is obtained from simple

[10] We should mention that in a nonhomogeneous plasmoid and beyond
(cont'd on next page)

and almost indisputable concepts, should be considered in discussing the problem of the structure and energy of a geoeffective corpuscular stream and its interaction with the Earth's magnetosphere.

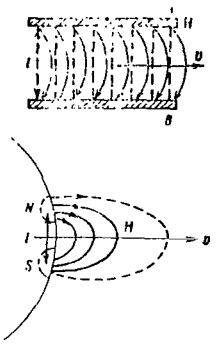

Fig. 8. Scheme of "Hartmann's Problem" and the Corresponding Model of Continuous Elongation of the "Magnetic Tongue" in an Active Region.

It is easy to see that if there were continuous extension of the magnetic fields in an active region together with the outgoing plasma (this is permissable in the hypothesis of an extending "magnetic tongue" made by Gold, et al.), then the solid corpuscular stream, even at a distance of several radii of the Sun, would "increase" the magnetic moment of the active region by a factor of two, while the "drift" of a continuous magnetized plasma stream to the Earth's orbit would require an energy greatly exceeding the permissible value (greater than 10^{39} ergs). The simple "elongation" of the magnetic field in an active region which was postulated in Gold's hypothesis, and which met obvious objections, forced the authors to make an additional assumption on the "breaking" of solid lines from the Sun, when the "magnetic tongue" reached at least the Earth's orbit. Without even mentioning the artificialness of such an assumption, it is easy to see from the general concepts of a magnetohydrodynamic flow that the breaking off and tubulization of a flow of magnetized plasma arises in the vicinity of the Sun. This conclusion follows from [54], and can be confirmed in addition by using the results of [55] on the stability of the flow of magnetized plasma stream across a magnetic field (Hartmann's problem). It is seen from Fig. 8 that the ejection of a solid plasma stream from an active region can be modeled to some extent by Hartmann's problem, where the "fixing" points of the boundary lines of force (A and B) corresponds, for example, to sunspots in an active region. For a rather high rate of flow, i.e., if the kinetic energy of the flow is much greater than the magnetic one, then, according to [55], a convective instability necessarily arises in the range of points A and B. The increment of the increase of this instability is determined by the following expression:

$$\frac{1}{\tau} = \frac{v_A}{l} \ln A, \tag{36}$$

where v_A is the Alfven velocity, l is the characteristic size of

---

footnote 10 cont'd
its boundaries the *local* relationships between the magnetic and kinetic energies can be either $\mathcal{E}_M > \mathcal{E}_K$, or $\mathcal{E}_K > \mathcal{E}_M$. Obviously, this depends on the structure of the field and the distribution of the plasma.

the magnetic dipole (H_0) in an active region, and ln A is the periodic term depending on H_0, l and the pressure gradient in the direction of the movement. The average value of ln A is on the order of 1. It follows from this that an instability arises during the time $t \approx l/v_A$. In our case, $l \approx 10^{10}$ cm v_A 10^7-10^8 cm/sec, $t \approx 10^2 - 10^3$ sec. In this time the leading edge of the extended magnetic "bubble" goes to a distance of $\lesssim 10^{11}$ cm. Thus, the extention of the lines of force of the magnetic field (on the condition that the kinetic energy of the radial movement of the plasma is much greater than the magnetic energy) is possible only to a distance of 2-3 $R_\odot$. Further, because of the development of the instability, the lines of force close on each other at some sites, while the transverse field is intensified at other sites. This /25 brings about the formation of plasma bunches with closed magnetic fields which are capable of freely moving in space.

If we consider that the magnetic lines of force are "frozen" in the corpuscular stream and "fastened" to the Sun, then it is usually considered an obvious condition for the existence of the stream that the kinetic energy for radial movement should greatly exceed the energy of the magnetic field. This energy ratio can be arbitrary for "separated" magnetized plasmoids. In this respect, there could be a case where the energy of the magnetic fields of the plasmoids greatly exceeds the kinetic energy for radial movement. Only a number of discrete plasmoids with "inherent" magnetic fields "separated" from the field of an active region can be released from that region. The formation of this "inherent" field can take place relatively slowly ($\gtrsim 10^3$ sec) during the process of acceleration of the plasmoid movement through the entire atmosphere ($\gtrsim 8R_\odot$) of the active region [27,51].

4. The forces acting in the ejection of a solar plasmoid should encompass the entire plasmoid as a whole. For the size of plasmoid under investigation ($r \simeq 5 \cdot 10^9$ cm), the body forces play a substantial role, while such forces as, for example, the viscosity can be disregarded. The possibility of a combination of accelerated thermal particles "wearing" through the solar atmosphere is also excluded, since a prolonged, total radial movement of the entire chromospheric-coronal plasma would be observed as the result of interactions with the solar atmosphere (ionization and other losses). It is well known that this is not observed in an active region.

The principal conditions enumerated above can be satisfied by a magnetoelectric field, whereas it is obvious that only the actions of changing magnetic fields in active regions can be responsible for the generation of a geoeffective stream. Since the energy density of magnetic fields in active regions in the chromosphere and corona prevails over the total intrinsic energy of the plasma, the appearance of nonstationary electric fields can be the result only of disturbances of magnetic fields arriving in the photosphere where hydrodynamic forces predominate. The movements of spots in

a group, their large-scale, vortical distribution, and the structural elements of an active region at the level of the chromosphere [56-58] indicate that, as a rule, a quasi-cyclonic vortex motion is noticed in inactive regions. This hydrodynamic movement in the greater part (or all) of an active region is determined by subphotospheric forces. It is observed all the time when an active region exists, although its intensity changes in dependence on the phase of development of the active region.

We will assume that the primary cause determining the energy of the corpuscular streams is this long-existing quasi-cyclonic motion of the matter in the active region. The predominant radial components of the magnetic fields in an active region of the chromosphere transfers these motions toward the upper chromosphere and corona in the form of slow torsional vibrations. In the active region of the chromosphere and corona, there is increased pressure and gas (plasma) discharge along the lines of force, i.e., the active region can be examined as an anti-cyclone region. The appearance of a screw instability arises at certain critical values of the parameter equal to $4\pi\sigma_{\parallel} E r H_{\parallel}^{-1}$ [31]. Here $\sigma_{\parallel}$ is the longitudinal conductivity, E is the longitudinal electric field arising in the torsion[11], r is the characteristic size of the total or local vortex, and $H_{\parallel}$ is the vertical magnetic field in the chromosphere (corona). For a cylindrical anticyclone ($v_r = 0$, $v_\phi = \omega r$, $v_z = 0$, where ω is the constant angle of velocity), the time equation for the magnetic field h gives the following: /26

$$\frac{\partial \mathbf{h}}{\partial t} = -\omega \frac{\partial \mathbf{h}}{\partial \vartheta} + \nu_M \nabla \mathbf{h}, \tag{37}$$

where ν_M is the magnetic viscosity.

As shown above, the condition for dynamic possibility of the movement under investigation is rot[rot h,h] = 0[12], which indicates the forceless nature of the fields.

Taking a solution for h in the form of

$$\mathbf{h} = \mathbf{h}_0 \exp(inv - kt), \tag{38}$$

---

[11] The torsion of the lines of force is determined by the relationship between the magnetic fluxes through the side and end walls of a magnetized cylinder.

[12] The problem of a magnetohydrodynamic cyclone in the general case is examined in [24].

we obtain the dispersion equation, i.e.,

$$\frac{in\omega - k}{\nu_M} = \gamma^2. \tag{39}$$

The equation for h_0 is

$$\nabla \mathbf{h}_0 - \alpha^2 \mathbf{h}_0 = 0. \tag{40}$$

Its solution is the following:

$$\mathbf{h}_0 = \operatorname{rot}(r\psi) - \frac{1}{\gamma} \operatorname{rot}\operatorname{rot}(r\psi), \tag{41}$$

where the scalar ψ is a solution to the equation

$$\nabla \psi - \gamma^2 \psi = 0. \tag{42}$$

For $\psi = R(r)Z(z)$, we obtain

$$\frac{1}{r}\frac{d}{dr}\left(r\frac{dR}{dr}\right) - \gamma^2 R = 0, \tag{43}$$

$$\frac{d^2Z}{dz^2} = \gamma^2 Z. \tag{44}$$

The solution for (43) is found in Bessel functions of zero order of minimum argument (i γr). After the corresponding substitutions, we can obtain the expression for the field (h) in the form of a selection of torsional vibrations. In a similar way we can obtain the solution to the equation of motion of the plasma for the case of helical symmetry. The solution for the field h is represented graphically. There is a substantial increase in the amplitude of the vibrations within the distance r, and modulation of the amplitude with the altitude. For a further analysis, only this qualitative result is important.

The generation of a plasmoid with an inherent magnetic field (not linked with the field of the active region) is considered as the result of extension with subsequent breaking of the field and the plasma at the boundary of the chromospheric (coronal) regions with a forceless magnetic field with different (in sign) parameters. Convective stability at this boundary arises as the result of the above-examined torsional vibrations coming continuously from the active photospheric (subphotospheric) regions. We should mention

that detailed investigations of the fine structure of magnetic fields in active regions which were conducted by A.B. Severniy [29] showed that, in the photosphere and probably in the chromosphere and corona, the magnetic fields are divided into relatively small-scale "plaits" which, when joined, form a large-scale hierarchy of structural formations. In this case we are speaking of the scales of structural formations of fields which are roughly one order less than the scale of the active region. It is assumed that, in each of the regions under investigation, the parameter α in the relationship /27

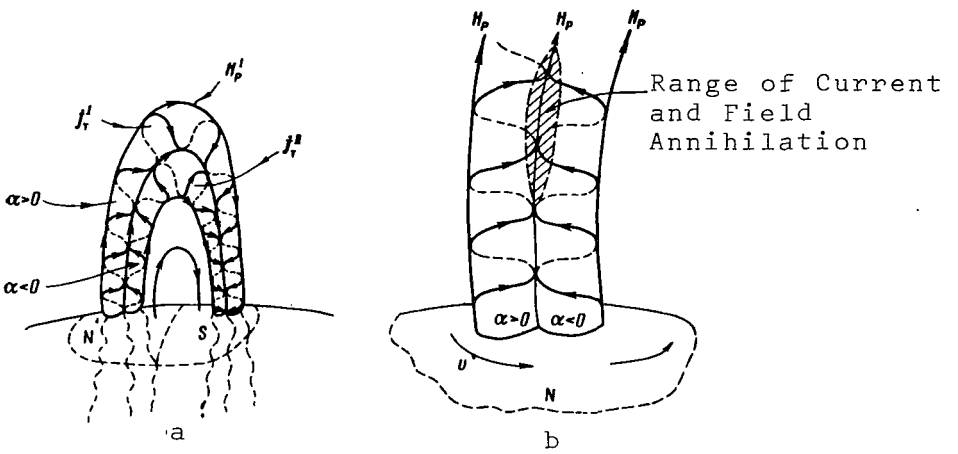

Fig. 9. Schemes of Two Continuous Forceless Tubes of a Magnetic Fields in an Active Region. (a) With Different Parameters α; (b) Scheme of the Propagation From the Photosphere to the Corona of a Screw Dislocation Along Continuous Forceless Magnetic Tubes of the Active Region.

rot h = α h depends on the coordinates, but has the opposite sign. This means that, in keeping the sign of the field vector, the currents in these continuous regions are directed along the fields or against the fields. The different signs of the parameter α can be realized in the helical symmetry in the direction opposite to the "winding" of the lines of force of the field in these regions (Fig. 9).

As was shown above, the hydrodynamic quasi-cyclonic movements at the level of the photosphere can propagate along the fields in the form of screw dislocations which disorder the state of equilibrium of the boundary of regions with different values of the parameter α. For the cylindrical case the state of equilibrium of the fields H (r) and the velocity v of the plasma are determined by the current functions ψ and ψ_0, so that [59]

$$d\psi = J(r)\,rdr, \quad d\psi_0 = J_0(r)\,rdr, \tag{45}$$

where

$$J = aH_z - \frac{H_\varphi}{r};\ J_0 = av_z - \frac{v_\varphi}{r}.$$

In our case, it follows from (4) in correspondence with the observations of $v \simeq \beta H$ (see above § 1) that

$$\frac{d\psi}{d\psi_0} = \beta(r) = \frac{raH_z - H_\varphi}{rav_z - v_\varphi}. \tag{46}$$

The components of the current density at each of the regions with different values of α are now the following:

$$j_\varphi = \mp \frac{dH_z}{dr},\ j_z = \pm \frac{1}{r}\frac{d}{dr}(rH_\varphi). \tag{47}$$

Thus, in the propagation of a helical wave, the magnetic field beyond the boundaries of each of the regions under investigation also has helical surfaces corresponding to the sign of the parameter α. In the range of the skin layer (covered zone in an instability of the boundary of regions with different values of α) /28 of this external screw dislocation, there is an addition of the opposite currents, and "annihilation" of the field (see Fig. 9,b). An investigation of the "annihilation" of a magnetic field as the energy source of a chromospheric flare was carried out in [60,61]. It was shown in [18,62] that a chromospheric flare arising in the vicinity of the so-called neutral line is linked with a substantial rearrangement and simplification of the structure of the magnetic

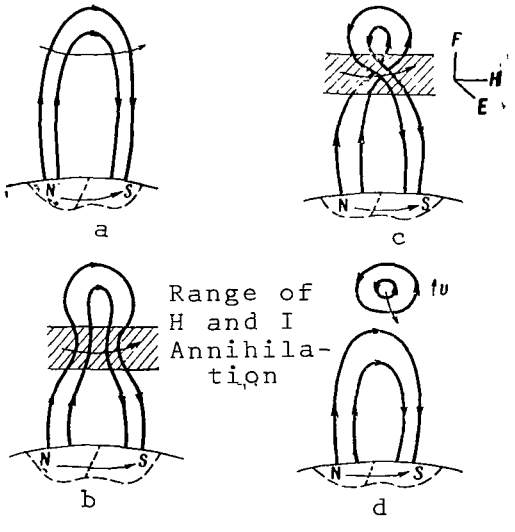

Fig. 10. Scheme of the Generation (Breakoff) of a Geoeffective Plasmoid for Propagation along a Mag-Tube of an Active Region of Torsional Vibrations from the Photosphere to the Corona. (a) First Phase; (b) Second Phase, in which There is Partial Annihilation of the Field and Currents in the Region of the Maximum; (c) Third Phase of the Development of a Screw Dislocation (Appearance of "Criss-Crossing" and Nonlinear Process of Plasma and Field Compression, Appearance of Nonstationary Electrodynamic field (E); (d) Fourth Phase, "Breakoff" of the Plasmoid Field with the Formation of an Inherent Closed Magnetic Field.

fields in the active region. The energy of the flare, according to these concepts, is ultimately the result of the "annihilation" of the magnetic fields and the limited volume of the active region.

The scheme examined here is reminiscent of the models of the development of chromospheric flares made by T. Gold and F. Hayle [63], where the annihilation of twisted forceless magnetic fields in the chromosphere was investigated. However, the difference here is not only quantitative (time for the flare $\lesssim 10^2$ sec, time for the outbreak of the plasmoid $\gtrsim 10^3 - 10^4$ sec), but also qualitative. We are speaking of the process of continuous superposition of external disturbances in the region of the skin layer (in the form of screw dislocations), bringing about the outbreak and subsequent ejection of plasma bunches with the formation of an inherent forceless magnetic field in them. In the chromosphere, the range of the skin layer of external screw dislocations is on the order of $\lesssim 10^8$ cm (for a period of a hydrodynamic screw dislocation at the level of the photosphere of about $10^4 - 10^5$ sec). Therefore, the range of the "separation" of the field in the chromosphere is on the order of the size of the thin structure of the magnetic fields at this level (about $10^7 - 10^8$ cm). This can probably explain the fact that the "isolated" forceless fields in the chromosphere which were examined above have a characteristic size of about 10^8 cm. In the upper chromosphere and the lower corona, the thickness of the skin layer of the disturbance becomes (as a result of the drop in ν_M) 1-2 orders greater, so that the "separation" of the field can take place in a region whose characteristic dimensions are equal to $10^9 - 10^{10}$ cm, which corresponds to the above-presented dimensions of a corpuscular stream in the vicinity of the solar surface. The energy which is expended in the "annihilation" of the field in the range of the screw dislocation of forceless fields with different (in sign) values of the parameter α can serve as the cause for the primary movements of a plasmoid, as well as other phenomena accompanying the generation of the corpuscular stream (particularly) if the process occurs during a flare, i.e., in a short time). A general scheme for the generation of magnetized plasmoid is illustrated in Fig. 10. The presence of general rotation (Fig. 10a) at the level of the photosphere, which is transferred to the region of the corona along the magnetic tube of force, brings about instability and convergence and subsequent "criss-crossing" of part of the tube of force. In the region of the "criss-crossing", there is not only annihilation of the fields and currents, but also non-stationary "neutral" points developed there (Fig. 10 b and c). In this region, the plasma is unstable, and there is an ultimate separation of the lines of force of this field, a release of the energy contributing to the initial movements of the plasmoid, and extension (regeneration) of the preliminary configuration of the magnetic tubes in the active region as a result of the nonlinear effects in the range of the "neutral" points (Fig. 10d). /29

At the moment of the breakoff of the magnetic lines of force,

(i.e., generation of the current whose fields "intersect" the lines of force), the movement of the plasma "lags" behind the movement of the lines of force of the field, i.e., the conditions of frozeness of the field are disordered. As a result of this, there appears a nonstationary electric field which determines (together with a magnetic field) the nature of the drifting movement of the plasmoid which had broken out. Obviously, the process of generation can occur continuously in the presence of a continuous rotation in the active region. The above-described scheme is still only qualitative, and cannot be calculated because of the particularly nonlinear nature of the phenomena under investigation. It can be examined as a possible variation of the generation of magnetized plasmoids when the changing magnetic fields of active regions play a determinant role. It is also necessary to mention that this process of generation of a corpuscular stream has much in common with the continuous generation of plasma toroids with forceless magnetic fields, which can be obtained in laboratory experiments with the so-called conical theta-pinch [41]. It is characteristic that the generation of such plasmoids occurs continuously with the preservation (for a given initial direction of the external field) of the polarity of the field in the plasma toroids. It is possible that similar laboratory experiments could explain certain basic problems in the generation of magnetized plasmoids, since a theoretical solution to such a nonlinear problem is extremely complicated.

In an active region on the Sun, where the general distribution and polarity of the field are stable, the generation of geoeffective plasma bunches with "separated" inherent magnetic fields can also occur continuously within a period on the order of the period of the helical waves of the disturbance (about 10^4 - 10^5 sec). As was shown above, a field in an isolated magnetized plasmoid necessarily tends to become, and does become, forceless. The time for the conversion of the "separated" magnetic field in the plasmoid into a forceless magnetic field can be evaluated if we investigate the problem concerning the change in the magnetic fields, considering the strong anisotropic conductivity of a rarified magnetized plasma. In this case, using the results of [19], we have the following:

$$\frac{\partial \mathbf{h}}{\partial t} = \operatorname{rot}[\mathbf{vh}] + \nu_M \left\{ \nabla \mathbf{h} - \operatorname{rot}\left((1 - 2\beta' F) \frac{[\mathbf{h}, \operatorname{rot} \mathbf{h}]}{k' h} \right) + \frac{\beta' F^2}{k_e k' h^2} [\mathbf{h}, [\mathbf{h}, \operatorname{rot} \mathbf{h}]] \right\}, \quad (48)$$

where ν_M is the magnetic viscosity, while the parameters k, β' and F are evaluated for the chromosphere as follows: $\beta' \approx 5 \cdot 10^{-3}$; $F \approx 1$; $k' \approx 10^{-3}$; $k_e \approx 2 \cdot 10^{-5}$. In the chromosphere and the corona, the Joule losses are insignificant and the changes in the structure of the field which are caused by the anisotropic conductivity take place relatively rapidly. Thus, for $l \approx 10^8$ cm, $h \approx 10^2$ Oe (for the chromosphere), the time for the "change-over" of the current along the field is found to be on the order of $\lesssim 10$ sec. In the corona ($h \approx 10$ Oe, $l \approx 10^9$ cm) this time increases roughly by 1.5.

Thus, the magnetic fields in a plasmoid which is limited in size become forceless rather rapidly (if they were not forceless before this). The nature of the further movement of a separated magnetized plasmoid is determined to a great extent by the interaction of the /30
slowly-changing quasi-dipole magnetic field of an active region with the tangential component of the forceless field of the plasmoid going beyond the limits of the plasma toroids. In certain cases (when the Hall current over an active range is directed towards the solar surface), the magnetized toroid may decelerate and not go beyond the boundaries of the corona. Such cases can arise, for example, in a "disadvantageous" development of the magnetic field of a group of sunspots in an active region [46, 52]. When there is no "electromagnetic deceleration" on the part of the changing magnetic field in an active region, the plasma toroid with forceless magnetic field moves in the radial direction from the Sun with an acceleration which decreases as $\sim R^{-2\cdot 6}$, where R is the distance from the horizontally-arranged magnetic dipole of the active region. In this case, as in the problem of the hydrodynamic expansion of the corona of Parker [48], a threshold velocity exceeding the Alfven velocity will be reached at a distance of $R \gtrsim 5R_\odot$ in this region of the corona ($\lesssim 5\cdot 10^7$ cm/sec).

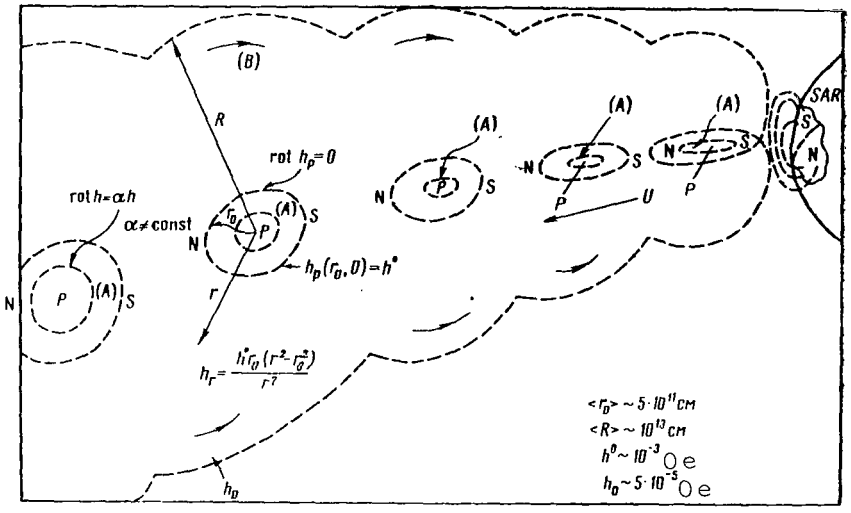

Fig. 11. General Scheme of a Geoeffective Corpuscular Stream Consisting of a Sequence of Magnetized Forceless Plasma Toroids (M-Elements), Region (A).
Direction of the Fields in the External Region (B) Corresponds to the "Polarity" of the M-Elements.

A further movement of the plasmoid with the field is determined by the interaction of the neighboring plasmoids ("chains" of the corpuscular stream) and the effect of the co-moving interplanetary medium ("quiet solar winds"). The general appearance of such a chain of discrete magnetized plasmoids coming in a radial direction from the active region on the Sun is represented in Fig. 11. If

during the process of generation and outflow of the plasma with the field there were a chromospheric flare with generation of cosmic rays, then the latter (particularly the high-energy particles) could go directly to the Earth, having been channeled by the external magnetic field in the sequence of the plasmoids (range (B) in Fig. 11). It is also possible that the plasmoid fields of solar cosmic rays could be captured by a magnetic trap, in which case they would reach the Earth after 1-2 days. Such a scheme for the movement of solar cosmic rays [64] follows from the scheme examined in [52].

This analysis of the possible scheme for the generation and outflow of plasma elements of geoeffective streams with a forceless magnetic field (we will call them conditionally the "M-elements") cannot be examined as a solution to the problem of the generation of corpuscular geoeffective streams. This complicated problem requires substantial expansion of our knowledge on the magnetic fields of the chromosphere and particularly the corona, as well as investigations of the nature of radiation outbursts and other solar phenomena accompanying the generation and outflow of corpuscular streams. However, this scheme can explain a number of the characteristic properties and the discrete structure of a corpuscular stream, and it corresponds to the principal conditions which should be satisfied, as shown above, for any mechanism of the generation of geoeffective streams in active regions of the Sun. /31

Unfortunately, we have as yet found no source of information which could show directly and unambiguously the location and nature of the mechanism for the generation of corpuscular streams. The dynamic phenomena observed in the chromosphere and corona (movements of plasma clouds in the corona, eruptive protuberances, structure of the corona in active regions, etc., non-stationary phenomena in x-ray, ultra-violet and radio-wave ranges) have yet to permit us to establish a direct correspondence between the phenomena observed in active regions of generation of corpuscular streams. The combination of a number of phenomena in active regions (radiation outbursts, movements and structural characteristics of the corona, etc.,) best characterize the phenomena which accompany the generation of corpuscular streams during chromospheric flares. Even radiation outbursts of type IV which often appear in rather powerful solar flares, have a far from unambiguous link with a geomagnetic disturbance (corpuscular streams). If we can link the generation and outflow of corpuscular streams with the phenomena of large solar flares (with certain probability), we still cannot do this for the more frequently encountered cases of recurrent geomagnetic disturbances (long-existing corpuscular streams). We can only say the following.

1. The prolonged generation of corpuscular streams is not accompanied by such rapid changes in the magnetic fields for which there would appear in sufficient quantity "epithermal" electrons responsible for radiation outbursts, increased radio-wave emission,

or x-ray emission.

2. At the present, we still cannot establish which phenomena on the Sun accompany the generation of corpuscular streams. Therefore, it is clear how essential in this problem is information on corpuscular streams obtained from geophysical data and direct measurements with the aid of artificial Earth satellites and space rockets, as well as on the magnetic fields and plasma in the interplanetary medium and the space around the Earth.

We should mention that, within the range of astrophysical and radio-astronomical observations, attempts at direct detection of corpuscular streams of active regions can be promising if the information relates to phenomena of the corona ($r > 1.2R_\odot$), where the region of the corpuscular stream differs from that of the stationary plasma of an active region. Radar detection of the corona by the method of radio transmission using a number of radiation sources [30], and systematic polarimetric and spectroscopic observations of the corona in active regions may aid in explaining the nature of the process of generation and outflow of corpuscular streams from an active region. The studies connected with optical and radio-astronomical determinations of the vector and structure of magnetic fields in the upper chromosphere and the corona are of particular interest for the problem under investigation.

REFERENCES

1. Mogilevskiy, E.I., Ye.A. Veller and B.M. Val'd-Perlov: Doklady Akad. Nauk S.S.S.R., Vol. 45, No. 5, p. 957, 1956.
2. Mogilevskiy, E.I., I.A. Zhulin and B.A. Ioshpa: Geomagnetizm i Aeronomiya, Vol. 2, No. 4, p. 585, 1963.
3. Mogilevskiy, E.I., I.D. Gits and B.S. Ioshpa: Izv. VUZ, Radiofizika, Vol. 3, No. 1, p. 67, 1960.
4. Zhulin, I.Z., B.Z. Ioshpa and E.I. Mogilevskiy: Sb.: Solnechnaya aktivnost' (Collection: Solar Avtivity), No. 2. "Nauka", 1965.
5. Mogilevskiy, E.I., I.A. Zhulin and B.A. Ioshpa: Author's Report No. 168475, Priority March 23, 1963.
6. Ioshpa, B.A. and E.I. Mogilevskiy: Sb.: Solnechnaya aktivnost' (Collection: Solar Activity), No. 2. "Nauka", 1965.
7. Zhulin, I.A. and E.I. Mogilevskiy: Sb.: Solnechnaya aktivnost' (Collection: Solar Activity), No. 2. "Nauka", 1965.
8. Ioshpa, B.A., E.I. Mogilevskiy and J.A. Zhulin: Proc. Sympos. Solar Magnet. Fields. Rome, Sept. 1964.
9. Babcock, H.W.: Astrophys. J., Vol. 118, p. 387, 1953.
10. Severnyy, A.B. and S.I. Gepasyuk. Solnechnyye Dannyye, No. 12, p. 43, 1964.
11. Ioshpa, B.A. and V.N. Obridko: Geomagnetizm i Aeronomiya, Vol. 4, p. 17, 1964.
12. Ioshpa, B.A. and V.N. Obridko: Sb.: Solnechnaya aktivnost' (Collection: Solar Activity), No. 2. "Nauka", 1965.
13. Ioshpa, B.A.: Candidate Dissertation, IZMIRAN, 1965.
14. Obridko, V.N.: Candidate Dissertation, IZMIRAN, 1965.

15. Stepanov, V.Ye. and A.B. Severnyy: Izv. Krymskoy Astrofiz. Obs., No. 28, p. 166, 1962.
16. Mogilevskiy, E.I.: Report at KISO Conference, October, 1963; Baku; Geomagnetizm i Aeronomiya, No. 6, 1966.
17. Ioshpa, B.A., E.I. Mogilevskiy and V.N. Obridko: Space Res. IV. Amsterdam, No. 789.
18. Severnyy, A.B.: Astron. Zhur., Vol. 42, p. 217, 1965.
19. Stepanov, V.Ye. and N.N. Petrova: Izv. Krymskoy Astrofiz. Obs., No. 21, p. 152, 1959.
20. Mogilevskiy, E.I.: Geomagnetizm i Aeronomiya, Vol. 1, No. 2, p. 153, 1961.
21. Fridman, A.A.: Opyt gidrodinamiki szhimayemoy zhidkosti (Experiment on the Hydrodynamics of a Compressible Fluid). "Gostekhizdat" 1934.
22. Zhulin, I.A. and E.I. Mogilevskiy: Geomagnetizm i Aeronomiya, Vol. 5, No. 6, p. 1092, 1965.
23. Severnyy, A.B., and V. Bumba: Observatory, Vol. 78, p. 33, 1958.
24. Khantadze, A.G.: Geomagnetizm i Aeronomiya, Vol. 5, p. 167, 1965.
25. Mogilevskiy, E.I. and B.D. Shelting: Proc. Symp. Solar Magnetic Fields (Sept., 1964). Florence, 1966.
26. Kadomtsev, B.B.: Sb.: Voprosy teorii plazmy (Problems of the Plasma Theory), No. 2. "Gosatomizdat", 1963.
27. Mogilevskiy, E.I.: Preprint of a Report at the International Symposium on Solar and Stellar Links. Moscow, June, 1964.
28. Kuklin, G.V. and V.Ye. Stepanov: Solnechnyye dannyye, No. 1, p. 55, 1963.
29. Severnyy, A.B.: Izv. Krymskoy Astrofiz. Obs., No. 33, 1965.
30. Zheleznyakov, V.V.: Radioizlucheniye Solntsa i planet (Radio Emission of the Sun and Planets). "Nauka", 1964.
31. Kadomtsev, B.A.: Yadernyy Sintez, No. 3, p. 269, 1962.
32. Pikel'ner, S.B.: Osnovy kosmicheskoy elektrodinamiki (Principles of Cosmic Electrodynamics). "Fizmatgiz", 1961.
33. Leighton, R.B.: Astrophys. J., 1962, Vol. 135, p. 474, 1964, Vol. 140, p. 1547, 1965.
34. Woltjer, L.: Bull. Astron. Inst. Netherl., Vol. 14, p. 39; 1958, Astrophys. J., Vol. 128, p. 384, 1958, Proc. Nat. Acad. Sci. USA, Vol. 45, p. 769, 1959.
35. Alfven, H.: Astrophys. J., Vol. 133, p. 1049, 1961.
36. Chandrasekhar, S., and P.C. Kendall: Astrophys. J., Vol. 126, p. 457, 1957.
37. Truesdell, C.: The kinematics of vorticity. Indiana Univ. Publ., Sci. Ser., N 19, 1954.
38. Shafranov, V.D.: Sb.: Voprosy teorii plazmy (Collection: Problems of the Plasma Theory), No. 2. "Gosatomizdat", 1963.
39. Veslamber, D., and D.K. Callebant: Phys. Rev., Vol. 128, p. 2016, 1962.
40. Babichev, A.P. et al.: Yadernyy sintez, No. 2, p. 635, 1962.
41. Wells, D.R.: Phys. Fluids, Vol. 7, p. 826, 1964.
42. Lebedev, A.N.: Zhur. Teoret. Fiz., Vol. 34, p. 812, 1964.
43. Mogilevskiy, E.I.: Geomagnetizm i Aeronomiya, Vol. 4, No. 2, p. 213, 1964.

44. Brinkley, S.R., and I.G. Kirkwood: Phys. Rev., Vol. 71, p. 606, 1947.
45. Bhatnager, M.S., and R.S. Kushwaha: Ann. Astrophys., Vol. 24, p. 21, 1961.
46. Mogilevskiy, E.I.: Trudy NIIZM, No. 6 (16). "Gidrometeoizdat", 1951.
47. Mustel', E.R. and N.B. Yegorova: Sb.: Solnechnaya aktivnost' (Collection: Solar Activity), No. 1, 1961; No. 2. "Nauka", 1965.
48. Parker, E.N.: Dynamicheskiye protsessy v mezhplanetnoy srede (Dynamic Processes in Interplanetary Space). "Mir", 1965.
49. Deych, A.: Sb.: Kosmicheskaya gazodinamika (Collection: Space Gas Dynamics). "Mir", 1963.
50. Shklovskiy, I.S.: Fizika solnechnoy korony (Physics of the Solar Corona). "Fizmatgiz", 1962.
51. Mogilevskiy, E.I.: Geomagnetizm i Aeronomiya, Vol. 2, No. 6, p. 1041, 1962.
52. Mogilevskiy, E.I.: Izv. Akad. Nauk S.S.S.R., ser. fiz., No. 12, p. 95, 1965.
53. Uus, U.: Publikatsiya Tartuskoy Astron. Obs., No. 34, p. 359, 1964.
54. Dokuchayev, V.P.: Astron. Zhur., Vol. 39, p. 1098, 1962.
55. Tverskoy, B.A.: Doklady Akad. Nauk S.S.S.R., Vol. 143, No. 2, p. 301, 1962.
56. Bumba, W., and R. Howard: Astrophys. J., Vol. 141, p. 1502, 1965.
57. Krat, V.A.: Izv. GAO, Vol. 21, No. 162, p. 11, 1958; Vol. 22, No. 170, p. 2, 1962.
58. Tsap, T.T.: Izv. Krymskoy Astrofiz. Obs., Vol. 31, p. 200, 1964.
59. Solov'yev, L.S.: Sb.: Voprosy teorii i plazmy (Collection: Problems of Theories and Plasmas), No. 3. "Gosatomizdat", 1963.
60. Parker, E.N.: Astrophys. J., Vol. 138, p. 310, 1963.
61. Papchec, H.E.: Magnetic field annihilation. Preprint, 1964.
62. Severnyy, A.B.: Astron. Zhur., Vol. 38, p. 402, 1961; Vol. 39, p. 961, 1962; Vol. 39, p. 990, 1962; Izv. Krymskoy Astrofiz. Obs., Vol. 30, p. 161, 1963.
63. Gold, T., and F. Hayle: Monthly Notices Roy. Astron. Soc., Vol. 120, p. 89, 1960.
64. Charakhch'yan, A.N. et al.: Zhur. Eksp. i Teoret. Fiz., Vol. 41, p. 735, 1960.

SIMULTANEOUS MEASUREMENT OF MAGNETIC FIELDS AT TWO LEVELS IN THE SOLAR ATMOSPHERE

I.A. Zhulin, B.A. Ioshpa, E.I. Mogilevskiy and V.N. Obridko

ABSTRACT: Simultaneous measurements of the magnetic fields in the photosphere and chromosphere using a two-channel solar magnetograph are described. The instrument features the simultaneous operation of two magnetographs on one spectrograph sent by a solar tower telescope. One magnetograph uses the photospheric Fe I line (5250.2 Å), while the other uses the chromospheric H_β line (4861 Å). The possibility of using both wings of the H_β line is analyzed, and the existence of other magnetosensitive chromospheric lines is examined. Results are given in terms of magnetic field patterns in the chromosphere and photosphere according to measurements in the Fe I, H_β, Ba II (4554 Å) lines.

1. One of the most important problems in the physics of the /34* Sun at the present is the investigation of the spatial (three-dimensional) structure of the magnetic field in the photosphere and chromosphere. The progress of investigations in this direction determines the achievements of studies on solar-terrestrial links, the physical nature of phenomena of the solar activity responsible for the generation and outflow of geoeffective solar corpuscular streams. *Simultaneous* observations of magnetic fields and rates of movements of the matter of two levels (photosphere and middle chromosphere, lower and middle chromosphere, etc.) which can aid in clarifying some problems of this transfer of changes in the magnetic field from the photosphere to the upper layers of this Sun's atmosphere are particularly important. Up to the present, the measurements of magnetic fields in the photosphere and chromosphere were not conducted simultaneously, but in sequence (Crimean Astrophysical Observatory, Main Astronomical Observatory, and IZMIRAN). At the same time, the advantages of simultaneous observations are indisputable. They can aid in solving the problem regarding the correspondence and gradients of the magnetic field at different points of an active region. In this case, errors connected with non-coincidence of observation sites or with possible rearrangement of the field are

* Numbers in the margin indicate pagination in the foreign text.

excluded. The latter is particularly important for magnetic fields in the chromosphere, where a magnetic field is frozen because of the conductivity, and the corresponding changes in the field should be observed during rather rapid and substantial dislocations of the chromospheric substance.

Simultaneous measurements of the magnetic fields in the photosphere and chromosphere were begun in the summer of 1964 by IZMIRAN (Institute of Terrestrial Magnetism, the Ionosphere and Radiowave Propagation of the Academy of Sciences, USSR) [1].[1] A two-channel solar magnetograph [3] in which two magnetographs operated simultaneously on one spectrograph fed by a solar tower telescope [4] was used for this. One of these mag tographs used the photospheric Fe I line (λ 5250.2 Å), and the other used the chromospheric H_β line (λ 4861 Å).

2. Simultaneous measurements of the magnetic field at two levels in the solar atmosphere are linked with the necessity of selecting the corresponding pairs of spectral lines. The greatest difficulties in this case are caused by selection of the chromospheric lines (the heights of formation of lines of the metals are too small, the presence of the lens is characteristic of a number of broad lines, etc.). The greater part of measurements of the fields in the chromosphere was carried out according to the H_β line formed /35
at altitudes of 1500-2000 km [5-8]. At the same time, it was recently found [2, 9] that the use of both wings of the line is connected with definite errors, since blending lines of a photospheric origin are detected in the blue wing of the line. However, the specific degree to which the blends affect the measurements depends on a number of factors: width and distribution in the wings of the line of output slits of the magnetograph, relationships between the real values of the intensity of photospheric and chromospheric fields, and also radial velocities in the photosphere and chromosphere. In regards to this, it was of definite interest to investigate the distributions along the contour of the lines of Zeeman circular polarization in H_β with the purpose of evaluating the possiblity of using this line in order to measure the magnetic fields in the chromosphere [10]. It was particularly important to carry out these measurements at a spot where the photospheric field was particularly strong, while the blending lines were most clearly announced, as was mentioned in [2, 9].

The measurements of the polarization in the H_β line were carried out on one of the channels of the magnetograph of the IZMIRAN [11] on October 4-5, 1965 in a group consisting of two large spots at the western part of the solar disk (group No. 63 according to the numeration of the State Administrative Council of the Main Astrophysical Observatory). In this respect, the revolving plate was

[1] Simultaneous measurements in the photosphere and chromosphere were also begun at the Crimean Astrophysical Observatory (summer of 1965) [2].

stopped and the system of feedback compensation was disconnected (see [11]). The magnetograph was converted here into a polarimeter, and it recorded the intensity of the circularly-polarized components of incident radiation. The profile of the line and the distribution of polarization on it were recorded with the aid of a special device in the spectrograph (see [4]) which allowed moving the output slit of the spectrograph together with the photomultiplier of the relatively immovable spectrum uniformly at the necessary rate. It took 3-5 min to record a segment of the spectrum with width of about 2 Å. During this time, a selected segment of the shadow of a spot was kept at the input slit by careful guiding. Possible dislocations were controlled with the aid of a monochromatic guide [4]. Before the beginning of the measurements, compensation was made for instrumental polarization along the undisturbed segment of the Sun with the aid of regular plane-parallel plates arranged in front of the slits of the spectrograph.

Figure 1 shows distributions of polarization in H_β. The first two records (curves a and b) refer to an eastern spot while the last one (curves c) refers to a western spot. The signs of the magnetic field and, correspondingly, the signs of polarization at both spots were mutually opposing. The lined segments correspond to the effective segments used in the IZMIRAN magnetograph for work with the H_β line ($\Delta\lambda_1$ = 0.075 Å, $\Delta\lambda_2$ = 0.225 Å). The width of the output slit in the record of polarization was 0.048 Å. It can be seen that the blue wing of H_β is actually disturbed by two blendings. Obviously, these are weak Fe I (λ 4860.98 Å) and Cr I (λ 14861.205 Å) lines. There is only one separated blend of Cr I (λ 4861.842 Å) in the red wing.[2] V. Bumba [13] noted that there is a weak blend in the blue H_β at a distance of 0.2 Å from the center; this blend intensifies at the spot. This was apparently assumed to be the Cr I (λ 4861.205 Å) line. However, this line was located at a distance of 0.13 Å from the H_β center on our records. The Lande factor for this line, compared to the division of the Fe I (λ 5250 Å) line for the same spot, had a value of ~1.0-1.2. The effective segment in the red wing was practically undisturbed. The effective segment in the blue wing was disturbed both with a far iron line and a chromium line closer to the center. It was easy to evaluate the magnitude of the relative error introduced by these blends in the measurements with the aide of both wings of the line. We will designate the signal coming through the right-hand effective segment (in the red wing) by the letter R, and that coming through the left-hand segment by the letter L. When there was no magnetic field in the photosphere, the effective signal of the magnetograph was proportional to 2R; when there were blends, it was proportional to L + R. Thus, the value of the relative error was equal to $\delta = (R - L)/2R$, where R and L are proportional to the segments lying in Fig. 1. For the first of the records shown in Fig. 1, the /36

[2] The lines were identified according to the tables in [12].

value $\delta \approx 5\%$, and for the second $\sim 10\%$, and for the third, $\sim 2\%$.

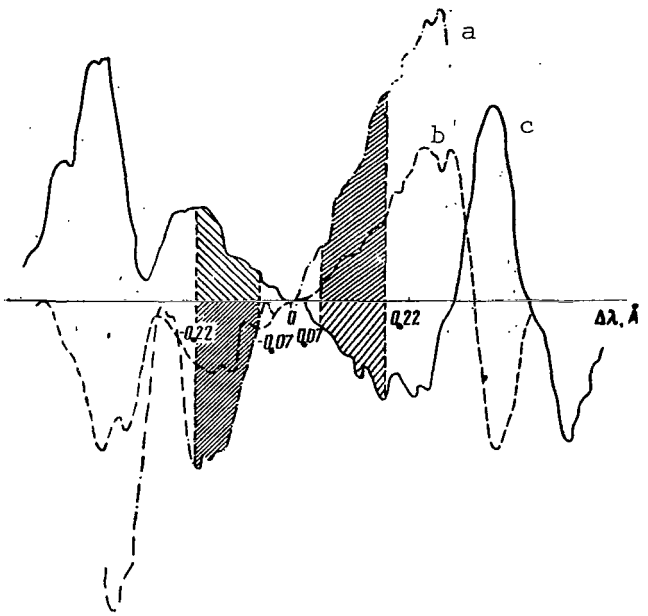

Fig. 1. Distribution Along the Contour of the H_β Line of the Zeeman Circular Polarization. The Numbers Along the Abscissa Axis Correspond to Distances From the Center of the H_β Line.

A number of recordings of H_β polarization were carried out for an effective width of the output slit of ($\Delta\lambda_1$ = 0.075 Å, $\Delta\lambda_2$ = 0.225 Å) for the control. The effect of weak central blending was almost unnoticeable on these records. After such recordings, the regular measurement of the field at the same points on the spot was carried out along both wings of the H_β line. In this regard, the half-sum of the average ordinates of the lined segments (R and L) coincided well with the deviation for the regular measurement of the field.

The measurements carried out (Fig.1) related to the shade of a spot with very high field intensity both in the photosphere and in the chromosphere (2000-2500 Oe).

We can examine the change in the relative error linked with the blending lines for different possible relationships between the magnetic fields in the photosphere and chromosphere. We will assume that the relative radial velocity at the levels of H_β formation and the blending lines is equal to zero. We now find the following:

(1) $H_{chr} \approx H_{phot}$ (the fields in the photosphere and chromosphere are comparable). It is to this case that our measurements relate. As seen from Fig.1, the error is small for very large fields, and

$\delta \approx 5$-10%. Thus, the error ΔH_{chr} corresponding to H_{phot}/n (where $n \approx 10$-20) is introduced into the signal of the chromospheric field.

The relative small value of the error can be explained, first of all, by the fact that the blend closest to the Hβ center is located close to the middle of the effective segment of the output slit; therefore, if the σ-components of the blend do not go beyond /37 the limits of the effective segment, the value of the useful signal is not distorted (Fig. 1, Curve b). Second of all, the value of the polarization signal from each wing of the blend is relatively small, and therefore even for withdrawal of one of the wings of the blend beyond the limits of the slit for a very high value of the field (or high relative velocity in the chromosphere and photosphere) brings about a change in the measured value of H_{chr} by a value of $\leq 0.05\ H_{phot}$ (Fig. 1, Curve a). On the other hand, the center of the second, more intensive blend is far from the outer edge of the output slit, at a distance of 0.13 Å, and, consequently, this blend can cause a substantial change in the field signal only for very large fields in the photosphere (several thousands of oersteds) and high relative velocities ($\gtrsim 5$ km/sec). In the case represented in Curve b, the distortion of a signal roughly by 10% is due to a decrease in the signal from the left-hand wing of the line, mainly because of the effect of the second blending.

The relative value of the ghost signal linked with the blendings decreases with a decrease in the values of the fields in the photosphere and chromosphere when the condition of $H_{chr} \approx H_{phot}$ is preserved, since the "red" σ-components of the Fe I (λ 4860.98 Å) line withdraw from the effective segment and begin to give a ghost signal, while the σ-components of the Cr I (λ 4861.205 Å) line are found inside the effective segments and their effect is reciprocally compensated.

During a decrease of H_{chr}, the useful signal decreases according to a law which is close to linear. Therefore, the relative error should become even less than that obtained above ($\lesssim 5\%$) with a decrease in the field intensity both in the photosphere and in the chromosphere. Errors of such a value are not substantial in interpreting measurements of the fields in the chromosphere, since calibration of the indices of the solar magnetograph usually has an uncertainty of 10-20%.

(2) For $H_{phot} \ll H_{chr}$, the relative error is obviously still less than in case 1, since the value of the "ghost" signal linked with photospheric blendings decreases much more rapidly than does the value of the useful signal. In particular, for $H_{phot} \approx 0$ and $H_{chr} \neq 0$ ("chromospheric magnetic mount"), the error is obviously equal to zero.[3]

---

3 We are disregarding here the errors linked with the asymmetry of the Hβ line introduced by the blend of λ 4861.205 Å, in view of the low intensity of this blend.

(3) For $H_{chr} << H_{phot}$, the errors can obviously be greater. As seen from Fig. 1, the "ghost" signal is one order less than the useful signal for comparable fields in the photosphere and chromosphere with intensity of several thousands of oersteds. Let us now assume that the field in the photosphere does not change (and consequently the value of the "ghost" signal also does not change), while the field in the chromosphere decreases. In this case, the useful signal also decreases roughly according to a linear law, while the useful signal is comparable to the "ghost" one at $H_{chr} \approx 0.1\ H_{phot}$, i.e., the relative error is about 100%. Thus, the measurements in which fields of several thousands of oersteds are observed at the level of the photosphere while those of several hundreds of oersteds are observed in the chromosphere (according to measurements using both H_β wings) are substantially distorted. The "chromospheric" signal obtained in such measurements can be connected with the effect of the blending lines, and does not correspond to the real field in the chromosphere.

However, the error is not as strongly pronounced if H_{phot} is less than several hundreds of oersteds while the condition of $H_{chr} << H_{phot}$ is preserved (case of the field of an active region far from the spots). In this case, the error introduced into the determination of H_{chr}, which corresponds roughly to $10^{-2}\ H_{phot}$, is reduced practically to the value determined by the sensitivity of the magnetograph in measurements of H_β (~10 Oe).

The relative radial velocities can change the picture under investigation to some extent. A dislocation of the intensive blend Fe I (λ 4860.98 Å) toward the H_β center can introduce the greatest error here. It can be seen from the distributions obtained (see Fig. 1) that the relative error can exceed 20% for a relative velocity of $\gtrsim$ 5 km/sec at $H_{phot} \approx H_{chr} \approx 2000$ Oe. In the case of $H_{chr} << H_{phot}$, this error can be even higher. /38

Having thus ended our discussion on the possibilities of using both wings of the H_β line for measurements of the magnetic field in the chromosphere, we can again confirm the conclusion that we derived in [14] concerning the legitimacy of measurements of the magnetic fields and radial velocities in the chromosphere (in any case in an active region inside sun spots) carried out with the aid of the two-modulation solar magnetograph of the IZMIRAN along the H_β line, although the quantitative side of this problem requires further clarification and more complete investigation.

3. Together with the investigation of the possibilities of using both wings of the H_β line, the IZMIRAN also carried out a study investigating other chromospheric magneto-sensitive spectral lines which were not compliacted by blends and asymmetry of the line. The line of Ba II (λ 4554 Å) can be included in such lines [15]. The effective level for summation of the center of this Fraunhofer line (lower limit) is about 600 km, and the Lande factor

is g $\approx$1.17. Figure 2 shows three subsequent sections of an active region with a sunspot; they were obtained on Sept. 6, 1965 in the Ba II (1), H_β (2) and Fe I (3) lines, respectively (the measurements were carried out with the aid of one channel of the magnetograph).

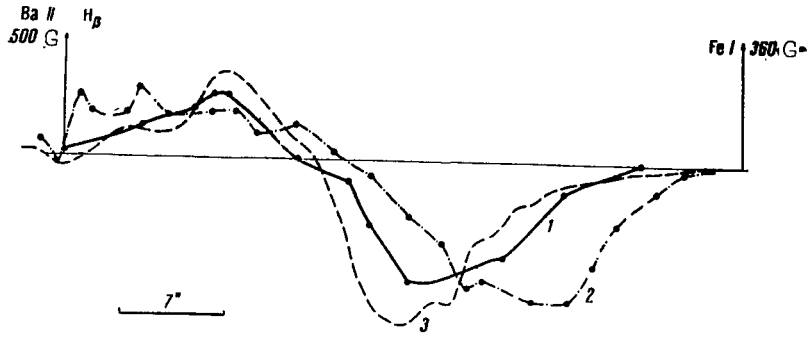

Fig. 2. Distribution of the Magnetic Field Along Three Successive Sections (Position of the Sections Shown in Fig. 3) of an Active Region According to Measurements on the Ba II, H_β and FeI Lines on September 6, 1965.

The relative position of the sections, which was determined with t the aid of a monochromatic guide (see [4]), is shown in Fig. 3.

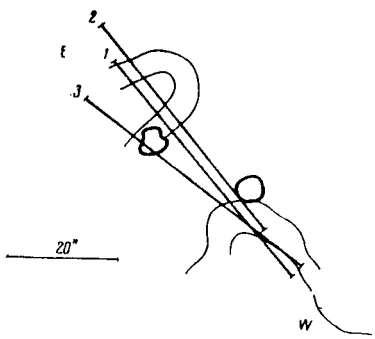

Fig. 3. Distribution of Three Successive Sections (Straight Lines 1, 2 and 3) in an Active Region with Spots (Solid Lines) and Filaments (Thin Lines).

4. Figures 4 and 5 show maps of the magnetic fields in the photosphere and chromosphere of the Sun (components along the line of sight) which were obtained on July 9 and 11, 1965 according to measurements on a two-channel magnetograph using the Fe I (λ 5250.2 Å) line (photosphere), as well as the H_β line (λ 4861 Å) (chromosphere, altitude of about 2000 km).

For measurements in the second spectral order of the spectrograph grid (dispersion $\sim$ 0.8 Å/mm), the widths of the output slits were $\sim$ 0.06 Å (first channel, Fe I line) and $\sim$0.15 Å (second channel, H_β line), respectively. The amplitudes of line oscillation were 0.7 and 0.15 Å, respectively, from the zero position. The sensitivity of the recording for resolution roughly of 3" x 3" was about 1 Oe for the photosphere and about 10 Oe for the chromosphere.

A preliminary analysis of the maps confirms the conclusions

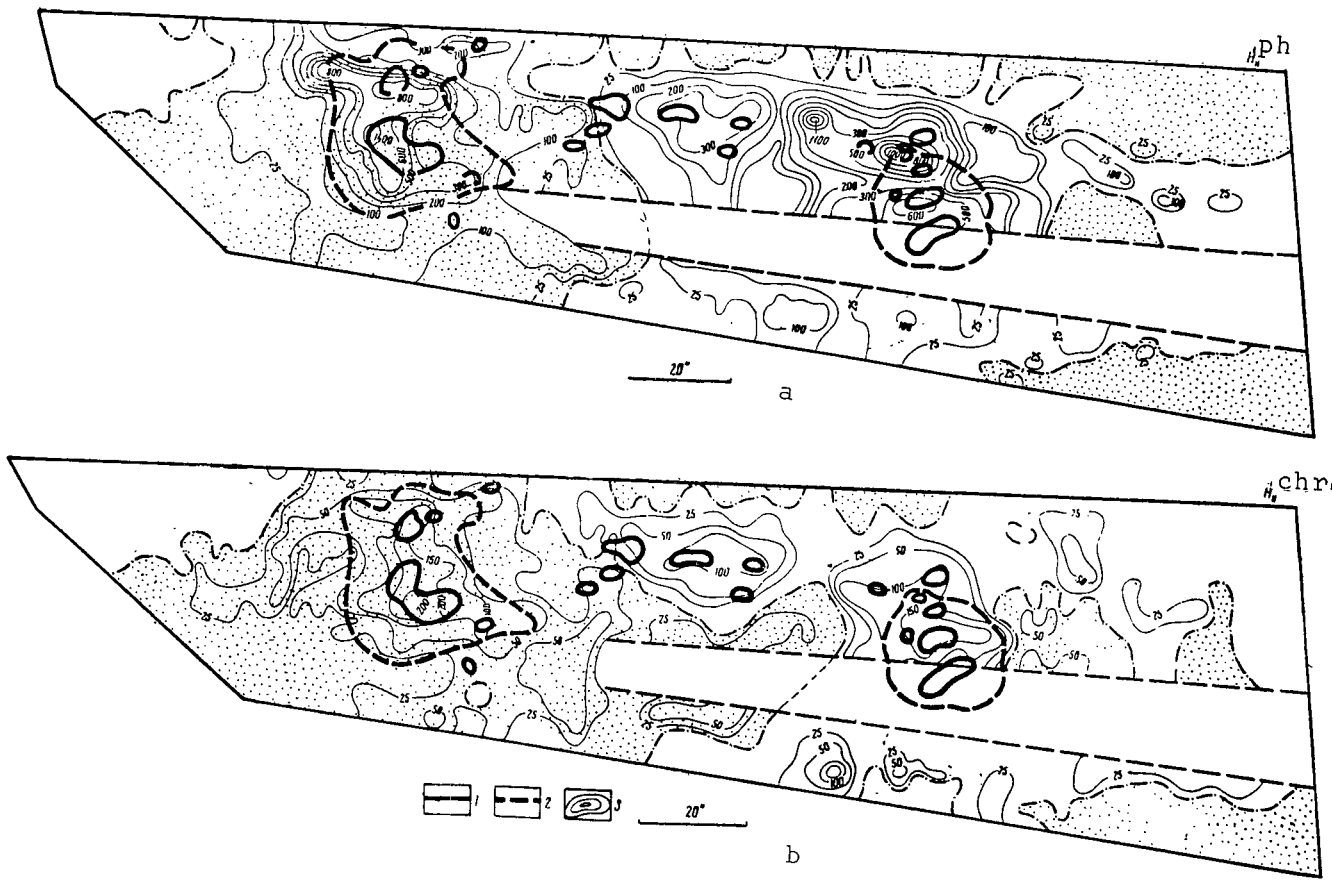

Fig. 4. Maps of the Magnetic Fields in the Photosphere and Chromosphere on July 9, 1965. (a) Line Fe I, λ 5250.2 Å ; (b) Line Hβ, λ 4861 Å. (1,2) Shadows and Half-Shadows of Spots, Respectively; (3) Northern Polarity of the Magnetic Fields. The Numbers on the Isolines Refer to the Value of the Fields in Oersteds.

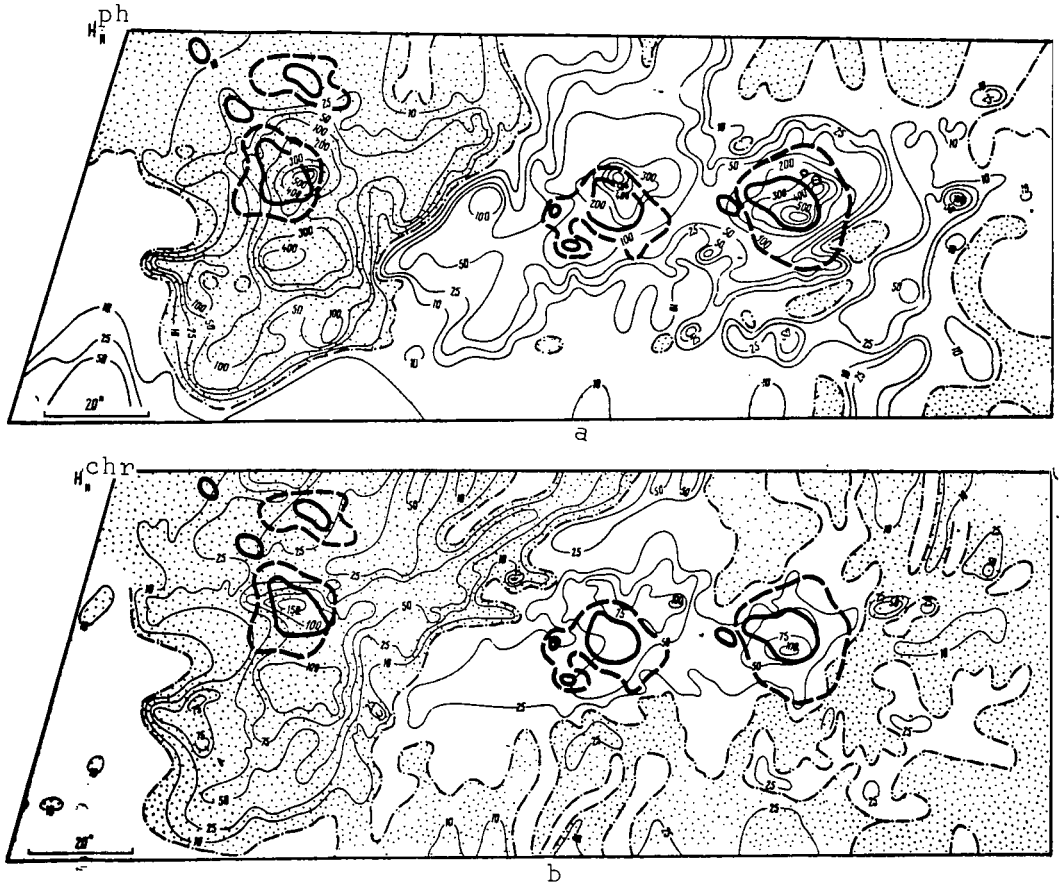

Fig. 5. Maps of the Magnetic Fields in the Photosphere and Chromosphere for July 11, 1965. Designations the same as in Fig. 4.

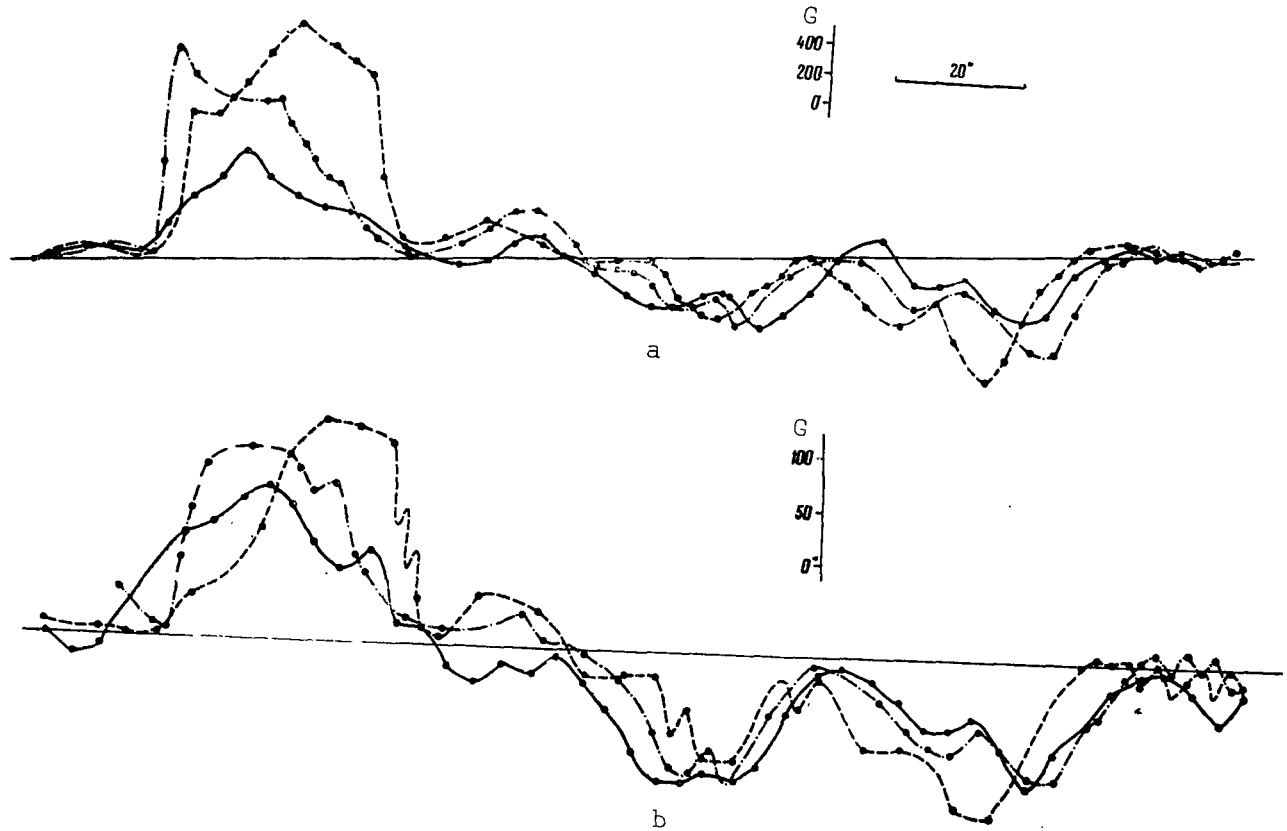

Fig. 6. Three Successive Sections of an Active Region According to Simultaneous Measurements on the Fe I (a) and H_β (b) Lines on July 9, 1965.

A preliminary analysis of the maps confirms the conclusions obtained previously by successive measurements [6, 7, 16, 17] concerning the general qualitative similarity of field distributions in the photosphere and chromosphere. It is agreed that there is polarity of the field at both levels, that the greater values in the photosphere correspond to greater values of the field in the chromosphere, etc.[4] At the same time, as regards the data of measurements with dual magnetographs, we can speak with certainty of the reality of existence of several differences in the field distributions at different levels. There are definite sites in the chromosphere where the magnetic field is rather strong, although the value of the field in the photosphere is small. A similar result was obtained earlier [6,7], but in successive measurements at two levels. In this regard, the reality of the differences in the fields of the photosphere and chromosphere in these studies required assumptions concerning the lack of changes in the field during both measurements. It is also seen from the maps shown in Figs. 4 and 5 that a change in the fields with the course of time does not take place simultaneously at both levels. Thus, the distance from the magnetic center in the region of the tailing spot to the center of the shadow of this spot begins to change (increase) first in the photosphere. Certain changes in the field structure, its simplification and even polarity variation at isolated regions with the transition from July 9 to 11 are possibly linked with the flare of scale-number 1+ which took place in this region on July 10 (data of the Observatory of Anacapri, Italy).

Figure 6 shows three successive sections (from the 13th to 16th) of the region under investigation according to simultaneous measurements on two lines on July 9, 1965. An analysis of such repeated and paired sections permits as, on the one hand, to discuss the changes in the field with time, since the measurements for each section took several minutes; the possible noncoincidence of the repeated sections practically did not exceed 2-3" of an arc for our guiding method used at IZMIRAN [4]. On the other hand, the simultaneity of the measurements for the two levels in the solar atmosphere permitted us to clarify the correspondences (or differences) in the magnetic fields in the photosphere and chromosphere of the Sun.

Unfortunately, the concurrence of a number of disadvantageous circumstances (poor meteorological conditions, minimum of the cycle of solar activity, etc.) has still not permitted us to obtain a rather large amount of maps of the magnetic fields at two levels in the solar atmosphere, which could yield the possibility of deriving more definite conclusions concerning the spatial structure of the magnetic fields, exchanges with time, etc. The first results

[4] This has also been indicated in the above-presented measurements of the field at three levels in the solar atmosphere (Fig. 2).

presented here are more an illustration of the possibilities of a double magnetograph, and they permit us to discuss that set of problems which can be solved with the aid of an apparatus of such a type. We can hope that similar observations of the magnetic field and rates of movement of the matter simultaneously for two levels in the atmosphere will yield new data on the dynamics of the fields of active regions on the Sun.

The authors would like to express their appreciation to E.D. Shel'ting for his aid in carrying out certain measurements, and also to O.I. Vasil'yeva for her aid in analyzing the data obtained.

REFERENCES

1. Zhulin, I.A.: Solnechnyye Dannyye, 1965, No. 11, p. 48, 1966.
2. Severnyy, A.B.: Report at the Plenum Commission on the Study of the Sun. Kislovodsk, October, 1965.
3. Zhulin, I.A. and E.I. Mogilevskiy: Sb.: Solnechnaya aktivnost' (Collection: Solar Activity), No. 2. "Nauka", 1965.
4. Mogilevskiy, E.I., I.A. Zhulin and B.A. Ioshpa: Sb.: Solnechnaya aktivnost' (Collection: Solar Activity), No. 2. "Nauka", 1965.
5. Severnyy, A.B.: Space Sci. Rev., No. 3, 1964.
6. Ioshpa, B.A., E.I. Mogilevskiy, and V.N. Obridko: Space Res., IV. Amsterdam, No. 789, 1964.
7. Mogilevskiy, E.I., and B.D. Shelting: Proc. Sympos. Solar Magnet. Fields. Rome, Sept. 1964.
8. Vyal'shin, G.F. and V.A. Krat: Izv. GAO, Vol. 24, No. 178, Rep. 2, p. 26, 1965.
9. Stepanov, V.Ye.: Report at the Plenum Commission on the Study of the Sun. Kislovodsk, October, 1965.
10. Ioshpa, B.A. and V.N. Obridko: Solnechnyye dannyye, No. 5, p. 68, 1966.
11. Ioshpa, B.A. and E.I. Mogilevskiy: Sb.: Solnechnaya aktivnost' (Collection: Solar Activity), No. 2. "Nauka", 1965.
12. Moore, C.E.: Multiplet table of astrophysical interest, pt. I, II. Contribs. Princeton Observ., N 2, 1945.
13. Bumba, V.: Izv. Krymskoy Astrofiz. Obs., Vol. 23, p. 212, 1965.
14. Zhulin, I.A., B.A. Ioshpa, E.I. Mogilevskiy and V.N. Obridko: Report at the Plenum Commission on the Study of the Sun. Kislovodsk, October, 1965; Materials of a Report on the Method of Measuring Magnetic Fields on the Sun. Krymskaya Astrofiz. Obs., October, 1965.
15. Shilova, N.S. and V.N. Obridko: Solnechnyye Dannyye, No. 8, p. 73, 1966.
16. Severnyy, A.B.: Izv. Krymskoy Astrofiz. Obs., Vol. 24, p. 281, 1960.
17. Stepanov, V.Ye.: Izv. Krymskoy Astrofiz. Obs., Vol. 23, p. 291, 1960.

MEASUREMENT OF MAGNETIC FIELDS IN PROMINENCES AND THE STRUCTURE OF THE MAGNETIC FIELD IN THE REGION OF CHROMOSPHERIC FILAMENTS

B.A. Ioshpa

ABSTRACT: Results of measurements of the magnetic fields in solar prominences are given, and the structure of the magnetic fields in areas of the solar disk having chromospheric filaments are investigated. The studies were conducted during the period from 1961 to 1963, using H_β line. Results are tabulated for 12 prominences, and show the existence of magnetic fields up to several gauss. In rare cases, considerable fields ($\sim$ 100 gauss) were observed in prominences which had no apparent connection with the active region on the disk. A hypothesis is suggested for the existence of two field systems in the region of chromospheric filaments. One system consists of an outer field lying at the top of the arched filament structure and perpendicular to the filaments, while the other system consists of an inner field directed along the filaments.

One of the problems in the physics of the Sun which has been least studied up to the present is the nature of solar protuberances. /44* Cinematographic studies of protuberances in radial H_α lines show the surprising complexity and variety of movements in them [1]. In many cases, the form of the trajectories of individual points in a protuberance and their development indicate their close relationship with magnetic fields [2]. It is also obvious that the existence of a prominence in itself during the course of a long period of time is possible only when there is a magnetic field. Evaluations of the magnitude of the magnetic field in quiet protuberances derived from equilibrium in the magnetic and kinetic energies have given a value for the internal field in them on the order of several gauss [3]. In more detailed investigations of the curvature of trajectories for points and bunches in isolated active protuberances, the magnetic field was evaluated as several hundreds of gauss [4]. The difficulties in this type of evaluation are linked with our incomplete knowledge of the mechanism for the movements and the characteristic parameters of the prominences, which leads to indefiniteness in quantitative evaluations of the field.

* Numbers in the margin indicate pagination in the foreign text.

The first attempts at determining the fields according to the effect of polarization in the H_α and D_3 radiation lines did not result in reliable results, because of the difficulty in separating the effects of the field from effects linked with the process of scattering [5-7]. Further, measurements of the polarization were carried out by Newkirk [8] along the D_3 lines and by Bruckner [9] along the Ca II K-line. Their measurements showed that the effect of polarization was more strongly pronounced in active protuberances than in quiet ones; however, the field was not evaluated. The first successful measurements of the magnetic field in prominences were carried out in 1960 along the H_β line with the aid of the magnetograph of the Crimean Astrophysical Observatory [10, 11]. The measurements showed that there is a relatively large magnetic field (100-250 gauss) in active prominences. In some cases, there were also observed substantial (25-100 gauss) fields in quiet protuberances. The report in [12] discusses a determination of the field in a loop-shaped prominence linked with an active group, according to polarization on the H_α line. The field at the apex of the arc was evaluated as 45-60 gauss.

A solution to the problem concerning the connection of the magnetic fields with the structure of the dynamics of prominences can be found only in complex investigations of both the magnetic fields and the protuberances themselves, as well as the structure of the magnetic region in the disk over the filaments. The first information on the connection of the magnetic field with the position of filaments on the disk was obtained in [13]. The measurements showed that the filaments are most often arranged along the boundary of the division of magnetic polarity (along the neutral line). These observations were confirmed by V.Ye. Stepanov [14], who showed, however, that a filament sometimes intersects the neutral line. Such a configuration of the magnetic field below a prominence in the photosphere caused the authors of [15] to think /45
that calm filaments lie at the top of the arched structure of the magnetic fields, where quasi-horizontal magnetic lines of force are perpendicular to the line where the filament is located and support the substance of the prominences against the force of gravity. In order to study the link between the structure of solar prominences and the magnetic fields, measurements of the longitudinal components of the magnetic field and prominences were carried out during the course of 1961-1963 with the aid of the magnetograph of the longitudinal vector at the IZMIRAN (Institute of Terrestrial Magnetism, the Ionosphere and Radio Wave Propagation of the Academy of Sciences, USSR) [16,17]. Some preliminary results of these measurements were published in [16,18]. Together with measurements of the magnetic fields in the prominences, we also investigated the magnetic structure of the region on the disk in the range where the filaments were located. The materials of the observations of fields in such regions were obtained in 1962 (measurements of the longitudinal components) and in 1963 (measurements of the total vector).

Method of Measuring the Magnetic Field in Prominences

The H_β line in the second order of the diffraction grid of the spectrograph were investigated for the measurements. The width of the output split of the spectrograph for the measurements in 1961 was equal to 0.15 mm, which corresponded to 0.12 Å. The span of oscillations of the plate was such that segments of the line which were removed from the center by 0.1 Å were incident at the middle of the slit. In 1962 and 1963, the width of the output slit of the spectrograph was greater ($\sim$0.2 Å), and the span of the plate oscillations was also increased, so that the line wings removed from the center of the line by 0.15 Å were incident at the middle of the output slit of the spectrograph. The height of the input slit was usually 1-1.5 mm, which corresponded to 10-16" for a diameter of the image of the Sun of 170 mm. Before the beginning of the observation, we surveyed the edge of the Sun on the H_α line with the aid of a monochromatic guide. The design of the guide used in 1961 was described in [16]. For the observations in 1962-1963, the guiding system was improved, so that we could make more reliable divisions [19]. The plane of the input slit of the photographs was inclined so that the normal to the input slit made a small angle ($\sim 3°$) with the optical axis; the beam reflected from the mirror surface of the sidepieces of the slit fell on the mirror and was directed toward the filter. The image and the H_α light was examined in a microscope and photographed. Thus, the images of a section of the Sun and the input slit were seen simultaneously.

The calibration for measurements of the field in the prominences was carried out either along the absorption line on an undisturbed segment of the solar disk or, if the protuberance was relatively stable, along the emission line in the protuberance [16,17]. The calculations for the calibration factor in the standardization carried out with the aid of the absorption line are given in [16]. For an identical nature of the form of the contour for the H_β line in absorbtion and emission and identical half-width of the contours, the calibration expression had the following form:

$$\left(\frac{I_\omega}{I_=}\right)^H = \alpha\left(\frac{I_\omega}{I_=}\right)^K \frac{1-r_\lambda}{r_\lambda}\frac{\Delta\lambda_H}{\Delta\lambda_v}, \qquad (1)$$

where $(I_\omega / I_=)^{H,K}$ is the ratio between the variable and constant signals for measurements of the fields and calibration, respectively, r_λ is the depth of contour of the line, α is the coefficient of proportionality depending on the amplification, $\Delta\lambda_V$ is the shift of the line in the calibration, and $\Delta\lambda_H$ is the division of the line when there is a magnetic field [11], i.e.,

$$\Delta\lambda_H = 1{,}65\cdot 10^{-5} H.$$

The calibration expression in (1) differs from that derived for measurements of the field according to the absorption line [17] by a factor of $(1-r_\lambda)/r_\lambda$. It is easy to see that the factor $(\Delta\lambda_D^{пр}/\Delta\lambda_D^{эр})^2$ is introduced into (1) for a Gaussian form of the line contour at different Doppler half-widths. The absorbtion line can be represented in the following way for the position of the slit we selected: $I = I_0[1 - r_0 e^{-(\Delta\lambda/\Delta\lambda_D)^2}]$, where $\Delta\lambda_D = 0.64$ Å. The average value of $\Delta\lambda_D$ for the prominences was assumed to be equal to 0.46 Å [20]. Equation (1) then took the following form: /46

$$\left(\frac{I_\omega}{I_=}\right)^H \approx 0{,}5\,\alpha\left(\frac{I_\omega}{I_=}\right)^K \frac{1-r_\lambda}{r_\lambda}\,\frac{\Delta\lambda_H}{\Delta\lambda_v}.$$

The deviation of the real values of $\Delta\lambda_D$ from that for the prominences (see, for example, [21]) could bring about an error in calibration

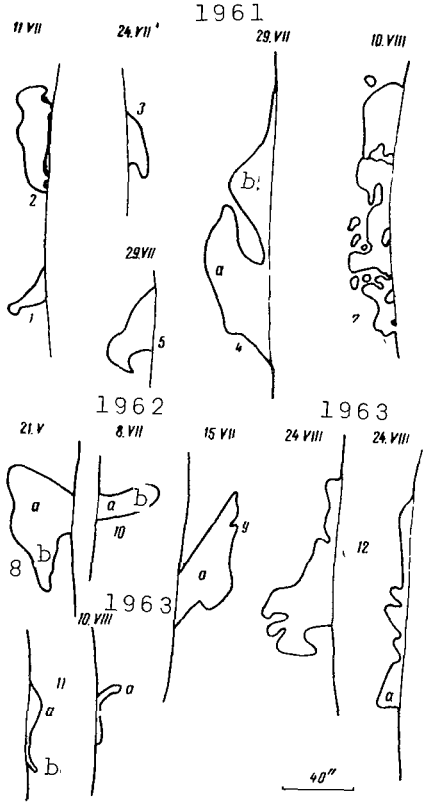

Fig. 1. External Appearance of Prominences in which Field was Measured (see Table). Sketches of Protuberances: (1-5) According to Data of the Chromospheric Studies Service of the IZMIRAN, Scale of 40''; (7) According to the Bulletin "Solnechnyye dannyye" (Solar Data), Scale of 80''; (8-12) According to Photographs of H_α From the Guided Tower Solar Tower Telescope. Scales for (8-10), 30''; Scales* for (11, 12), 40''.

up to ~ 40%. In order to use the calibration expression, it is necessary to know the value of the remanent intensity r_λ in the absorbtion line at the same site of the contour where the slit is located. Even small changes in r_λ can bring about an error in the calibration. Therefore, if the prominence were rather stable, we would carry out graduations directly along the emission line of the prominence by the regular method. The errors linked with the assumptions concerning the half-width of the emission and

absorption lines were thereby excluded. In this case, the calibration expression had the same form as that for measurements along the absorption line.

Measurement Results

The first measurement of the magnetic field of prominences was carried out by us on July 11, 1961. On that day we measured fields in two prominences at the eastern edge of the disk. In prominence 1 (see the table), which had the form of a bright protrusion (Fig.1), we measured a field of 100-150 gauss. In prominence 2, a field was not detected. Both protuberances were apparently linked with a filament which enveloped a unipolar active region from the east, and which went out on the disk on July 10. The sign of the field in the protuberance corresponds to the sign of the fields at the spot of an active group. Prominence 1 corresponds to the lower part of this filament, and is very unstable. During the following days, this part of the filament on the disk was seen to be broken off from the main body of the filaments, and it sometimes disappeared completely. The second protuberance corresponds to the middle part of the filament, and is rather stable.

TABLE

/47

Number Prominence	Date and Time of Observation	Coordinates	Field Magnitude, gauss	Comments
1	July 11, 1961 t ~ 0900	E, $\varphi = +4°$	100	Quiet filament enveloped an active region from the east; the field component directed perpendicular to the line of the filament was measured
2	July 11, 1961 t ~ 0900	W, $\varphi = 15°$	Not Detected	Same
3	July 24, 1961 t ~ 0700-0900	W, $\varphi = 25°$	100—150	Prominence corresponded to the northern part of the same filament as Protuberances Nos. 1 and 2.
4	July 29, 1961 t ~ 1300	E, $\varphi = 10°$	180	Not connected with active regions. The field component along the line of the filament was measured.
5	July 29, 1961 t ~ 1400	E, $\varphi = -22°$	150	Outburst from region of the spot
6	August 7, 1961 t ~ 0900	E, $\varphi = +12°$	500	Active prominence not linked with an active group on the disk; the component along the filament line was measured.

TABLE

Number of Prominence	Date and Time of Observation	Coordinates	Field Magnitude, Gauss	Comments
7	August 10, 1961 t ~ 0900	E, $\varphi = -27°$	100	Active prominence linked with an active group on the disk.
8	May 21, 1962 t ~ 0800	E, $\varphi = 15°$	150—200	Active prominence not linked with an active group; the field component along the filament was measured.
9	July 15, 1962 t ~ 0900	W, $\varphi = 25°$	60	Prominence not linked with an active region on the disk; the field component along the filament was measured.
10	August 8, 1962 t ~ 1300	W, $\varphi = 20°$	150	Prominence not linked with an active region on the disk; the field component along the filament was measured.
11	August 10, 1963 t ~ 1200 - 1400	W, $\varphi = 13°$	100—150	Active group approached the edge; the field component perpendicular to the filament was measured.
12	August 24, 1963 t ~ 1400 - 1500	E, $\varphi = 12°$	100—200	Active prominence linked with an active group on the disk

On July 24, 1961, we measured the field in prominence 3 at the western edge of the disk. The protuberance had the form of a bright protrusion. The value of the fields was roughly equal to 100-150 gauss. The field on the disk on the H_β line below the protuberance was of the same sign (which corresponds to a change in the sign of the field signal during transition from the emission line to the absorption line). We could not measure the value of the fields on the disk, since the recorder of the constant component of the signal went off scale. The protuberance under investigation corresponded to the northern part of the same filaments as that of the protuberances whose fields were measured on July 11.

On July 29, 1961, we measured the fields in two prominences. The maximum field in part a of the interacting prominence 4 corresponded to a value of 180 gauss, while the field in part b did not exceed the noise level (50 gauss). An active regions whose flocculae approached the base of the prominence, was found near that protuberance

on the disk.

The field in prominence 5 was equal to 150-200 gauss. During the following days it was observed on the disk in the form of a small, unstable filament which sometimes disappeared completely. This protuberance was not linked with any active formation.

On August 7, 1961, we measured the field in a bright eruptive outburst at the eastern edge of the Sun. The outburst was preceded by a flare of scale-number 1 on the linb, beginning at 0909, several minutes before the appearance of the protuberance. A field of several hundreds of gauss was observed in the number of sites of the protuberance. A figure of this protuberance and the results of measurements are shown in detail in [18].

On August 10, 1961, we measured the field in prominence 7 at the eastern edge (see Fig. 1). The fields in isolated regions reached a value of about 100 gauss. The protuberance was very active, and substantial changes in form were observed. It was not linked with any active group on the disk. Further, the prominence was observed on the disk as a very unstable filament; and active protuber- /48
ance was again seen during the withdrawal of the filaments toward the western edge.

On May 21, 1962, we measured the magnetic field in the active prominence 8 at the eastern edge of the disk. The maximum field in the protuberance (in region a) was roughly equal to 150-200 gauss. The field in other parts of the prominence was less, and it is possible that the sign even changed (in region b). However, the deviation of this signal in this region did not exceed the level of noises to a great extent; therefore, this result cannot be considered reliable. The protuberance was linked with an active group which came out on May 20 from the edge of the Sun. During the following days, there were frequent flares in the group. During the same day of May 21, 1962, we measured the longitudinal field in the active region at λ 5250 Å. Figure 2 shows a map of the longitudinal field in this region.

The field in the prominence (in region a) was of the same sign as in the region on the disk below the protuberance. At the same time, we can see from an examination of the map that the field is somewhat greater at the base of the protuberance in the photosphere than at different sites at the edge (see the course of the isogauss of 25 G). However, the value of the field below the protuberances of the photosphere itself (about 30-40 G) was several orders less than that of the field in the protuberance at an altitude of 15,000 km.

On July 15, 1962, we measured the field in prominence 9 at the western edge of the disk. The prominence was active, and an outburst was observed at this site at the edge of the Sun a short time

before the measurements, according to the data of the AFR-2 service. However, this protuberance was not connected with any active region.

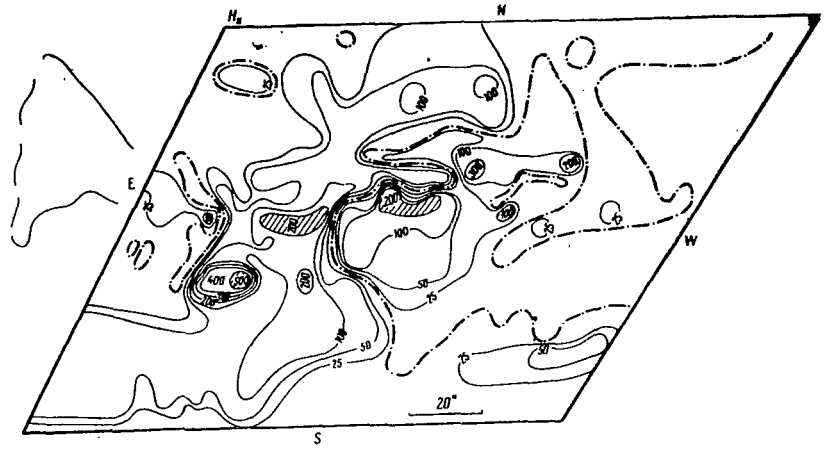

Fig. 2. Map of the Longitudinal Component of the Magnetic Field in the Photosphere (λ 5250.2 Å) in Group No. 70 for May 21, 1962 [23]. The Dashed-Dot Line Represents the Neutral Line of the Longitudinal Field. The Numbers Show the Field Intensity, Gauss.

The measurements showed that the field in region a of the protuberance was about 60 gauss. However, there is no complete certainty in this results, since the signals were small and the amount of data was insufficient.

On August 8, 1962, we measured the field in a prominence at the western edge of the Sun. The altitude of the prominence was 30,00 km. The protuberance was seen earlier in the projection on the disk in the form of an unstable filament which sometimes disappeared. The magnetic field did not decrease smoothly with the altitude of the prominence: in region a, the magnetic field had a value of about 200 gauss, then decreased to 40-70 gauss (in one of the sections the sign of the field even changed), and then increased to about 150 gauss (in region b). Such a change in the field with altitude can be linked either with a real change in the value of this field or with a change in the direction of the field along the protuberance, since only the longitudinal field component was recorded. This prominence was not connected with any active group. /49

On August 10, 1963, we measured the field in the active prominence 11 at the western edge of the disk. During this day, an active region with spots approached the edge; this was observed in the total vector during the period from July 30 to August 7. The field in the prominence was measured twice: the first measurement began at 1515, and the second at 1720. Bright projections whose form changed were seen at the edge of the disk in the first measurement. In projection a, the field had a value of about 150 gauss (the sign corresponds to the sign of this field in a large spot), and a residue

corresponding to a field of another sign was recorded in projection b. However, the value of the residue was close to the noise level. The appearance of the edge changed somewhat in two hours. In region a, there was observed a field of the same kind and roughly the same magnitude (100-150 gauss) as in the first measurement.

On August 24, 1963, we measured a field in an active prominence at the eastern edge of the disk. The loop-shaped protuberance was connected with an active group coming out on the disk on August 25. An outburst was observed at that site of the limb a short time before the beginning of the observation, according to the data of the chromospheric investigating service at IZMIRAN. High radial velocities were observed in the prominence (on the order of several tens of kilometers). On August 26, flares were seen in the group. Measurements showed that the field was about 200 gauss in the central part of the protuberance. The field on the disk had the opposite sign. The measurements were repeated after 30 minutes, and the appearance of the protuberance changed substantially during this time. A residue corresponding to a lesser field (about 100 gauss) of another sign was fixed in region a. During the transition to measurements on the disk, the sign of this field did not change.

We have presented above only those measurements for which the magnetic field was recorded rather reliably. There were many cases not included in the table, where the field in the protuberance was lower than the measureable limit (about 40-60 gauss, depending on the brightness of the protuberance, the constant time of the measurement). They were mainly quiet prominences, the movements in which had a chaotic nature (protuberances of the first class according to the classification of A.B. Severeiny [1]). They were often seen on the disk as a curtain or fencing. Such protuberances corresponded to individual segments of large quiet filaments which extended almost along the meridian.

The results obtained allow us to draw some preliminary conclusions relative to the link between the structure of the prominences and the magnetic fields. The measurements showed the existence of substantial magnetic fields in the prominences which were connected with an active region on the disk. Such fields (on the order of several hundreds of gauss) were observed, as a rule, in active protuberances located in the vicinity of the center of activity of the group.

We sometimes measured a field from 50 to 200 gauss in prominences which were seen on the disk as quiet filaments enveloping an active region, (for instance, Prominences 1, 3, and 4). The fields in the protuberances of such a type were usually less than the measured value. In those cases when we measured the field on the disk directly below the protuberance on the H_β line or on the Fe I line (5250 Å), it had the same sign as the field in the protuberance, if it were relatively stable. The appearance of an active prominence at a given site on the disk was possibly linked

with the structure of the magnetic field on the disk. This is indicated, for example, in a comparison of the course of an isoline of intensity 25 gauss in Fig. 2 for Prominence 7 of May 21, 1962. However, the magnitude of the magnetic field in the protuberance was usually several times greater than the magnitude of the fields on the disk below them. In some cases, the field on disk for measurements along the H_β line was much lower than the noise level (less than 10-15 gauss). It is characteristic that the magnetic field in the protuberances usually did not decrease smoothly with an increase in the altitude, while there was a maximum at a certain /50 altitude over the disk. Naturally, the fields in the protuberance must be determined, not only according to the fields directly below the protuberance, but also according to the distribution of the fields in the active region with which it is connected. If we assume that the field has a potential character over the entire region all the way to the altitude at which the protuberance is observed, we can solve the Neumann problem with the boundary condition-distribution of the magnetic field in an active region in the photosphere, which known from observations. However, this assumption is rather crude, since the fields in the chromosphere and corona over an active region probably has a nature close to a forceless one, but it can be used for evaluating the magnitude of the fields. N. Malkin [22] used a problem close to this one in calculating the course of the intensity of terrestrial magnetism along the altitude, using measurements of the normal components of the fields at the Earth's surface. The solution is written out in the following way:

$$X_p = \frac{1}{2\pi}\iint Z_\mu \frac{X-\xi}{r^3}\,d\sigma,$$
$$Y_p = \frac{1}{2\pi}\iint Z_\mu \frac{Y-\eta}{r^3}\,d\sigma,$$
$$Z_p = \frac{Z}{2\pi}\iint Z_\mu \frac{d\sigma}{r^3},$$

where X_p, Y_p, Z_p are field components at a definite altitude, and Z_μ designates the values of the normal component of the fields at the base. We used the method developed in [22] in order to determine the field of a filament in active group No. 78 [23] observed on August 4, 1963 in the vicinity of the central meridan. Figure 2 shows a map of the longitudinal component of the field in this group. Figure 3 gives the schematic appearance of the filament, for which the values of the perpendicular field component $H_\perp$ were plotted (only the values X_p and Y_p were calculated in relation to altitudes of 10,000 and 20,000 km. The values of the calculated field at individual points at an altitude of 10,000 km were close in order of magnitude to the fields determined in measurements at roughly the same altitude (considering the indefiniteness of calibration by $\sim$ 40%) as in the prominence on August 10, 1963, which appeared at the site of this filament.

Thus, in the case when strong internal movements are not observed in a prominence, we can consider that the field in it is determined mainly by the structure of the field of the active region. In the protuberances characterized by a rapid changing in form and high radial velocities, the structure of the field is determined, in all probability, not only by the external fields of the active region, but also to a great extent by the dynamics of the prominence itself (Prominences 6,12).

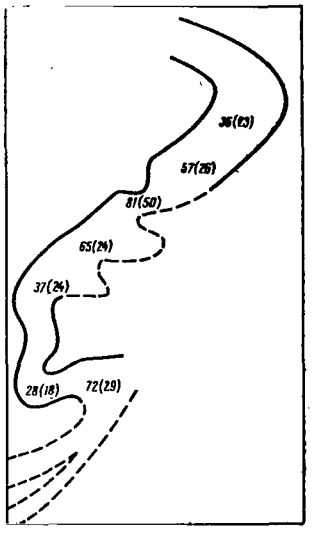

Fig. 3. Results of a Calculation of the Magnetic Fields in t the Region of a Filament According to the Neumann Problem. The First Number Corresponds to an Altitude of 10,000 km, the Numbers in Parentheses to 20,000 km.

In some cases, we observed a field (60-150 gauss) and prominences which were not connected with any active region on the disk (Prominences 5, 7, 9 and 10). In all these cases, the protuberance had the appearance of a bright protrusion on the disk. In the projection on the disk, the prominence represented a filament lying almost parallel to the equator. Therefore, the field component measured was directed, obviously, along the filaments. It is possible that in this case we measured the internal field in the protuberance. In quiet prominences which /51 were not connected with an active group and which were located along the meridian, we detected no fields.

Investigation of the Structure of the Magnetic Field In the Photosphere and Chromosphere In A Region Where Filaments Are Located

In 1962 and 1963, we carried out a number of observations of the magnetic field of active regions in a range occupied by filaments. Let us examine some results of these measurements. Figure 4 shows maps for the longitudinal component of the magnetic field for three active regions. These maps were constructed according to the materials of observations in 1962. The measurements were carried out for λ 5250 Å, and in some cases for H_β. The maps shown in Fig. 4 refer to group No. 71 [23] which came out on the eastern edge of the disk on May 21, 1962. The maps for λ 5250 Å on May 26 and 29 are also shown in this figure. The region was also observed on May 27; however, the small amount of sections obtained did not allow us to construct a map for this date. Flares often occured in this group; in particular, a flare of scale-number 1 took place on May 27.

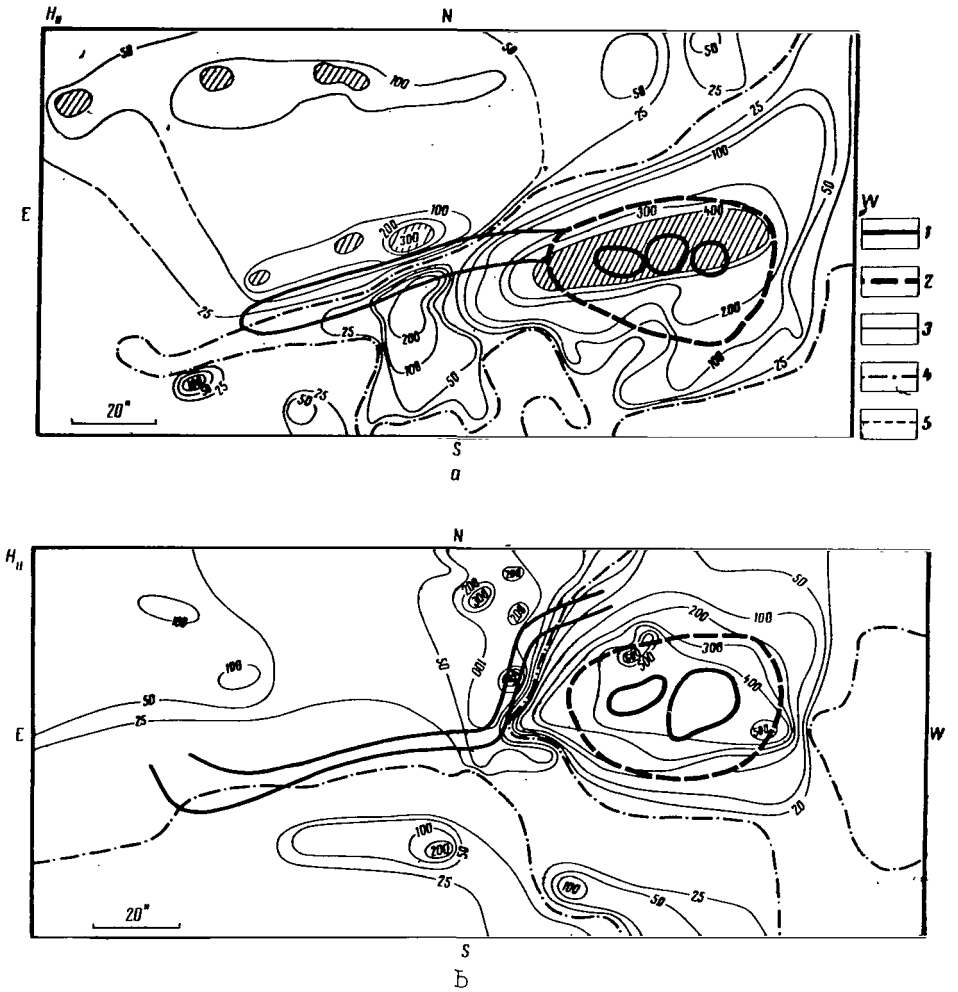

Fig. 4. Maps of the Longitudinal Component of the Magnetic Field in Group No. 71 [23].
(a) May 26, 1962, λ 5250 Å; (b) May 29, 1962, λ 5250 Å. Chromospheric Details Plotted on the Map Directly According to Guided Photographs. (1) Contour of Spots; (2) Half-Shadow: (3) Filament; (4) Zero Line of the Longitudinal Field; (5) Unreliability in Drawing the Gaussian Isolines, Due to Lack of Data.

/52

Fig. 5 (a) shows a magnetic chart for Hβ on July 4, 1962 for group No. 93 [23], which came out on the eastern edge on June 24, 1962. The group was very complex, and it consisted of two large spots of different polarities and a large number of small spots. Flares often took place in this region. On July 6, during its withdrawal toward the western edge, there was observed a limb flare and an eruptive protuberance. On July 21, this region again came out on the eastern edge of the disk, (group No. 78,[23]). The structure of the group changed radically. We observed this

group on July 22 (H_β, July 23 (H_β), July 27 (λ 5250 Å) and July 31 (H_β and λ 5250 Å).

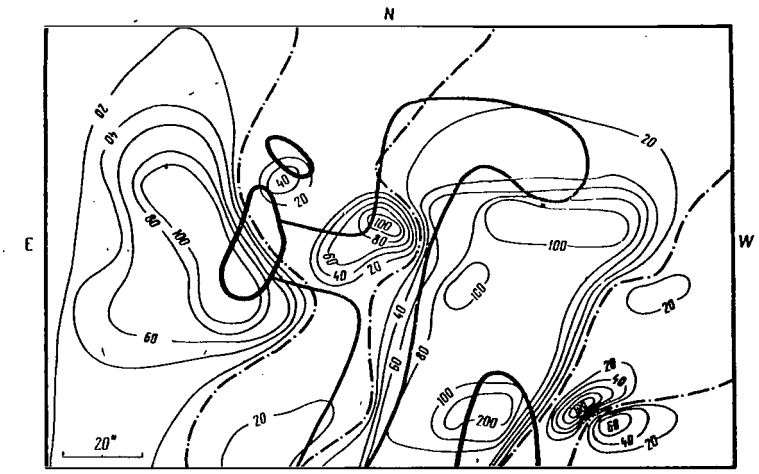

a

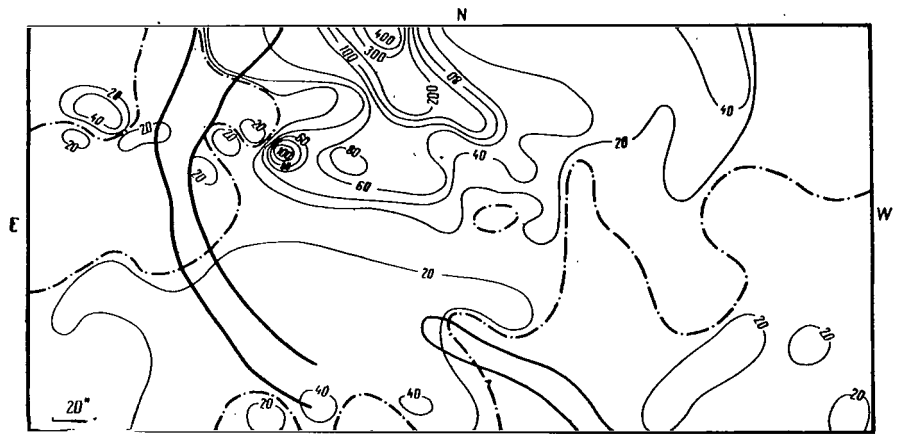

b

Fig. 5. Maps of the Longitudinal Component of the Magnetic Field in the Chromosphere (H_β).
(a) Group No. 93 [23], July 4, 1962, λ 4861 Å; (b) Same Region, Group No. 78 [23], July 23, 1962. Designations Same as in Figure 4.

Figures 5(b) and 6 show maps of this region for July 23 and 27, 1962. Figure 7 (a and c) shows maps of the longitudinal components of the field at λ 5250 Å and H_β for group No. 78 in [23] on August 1-4, 1963. The measurements of the longitudinal component at λ 5250 Å were carried out according to the total-vector scheme.

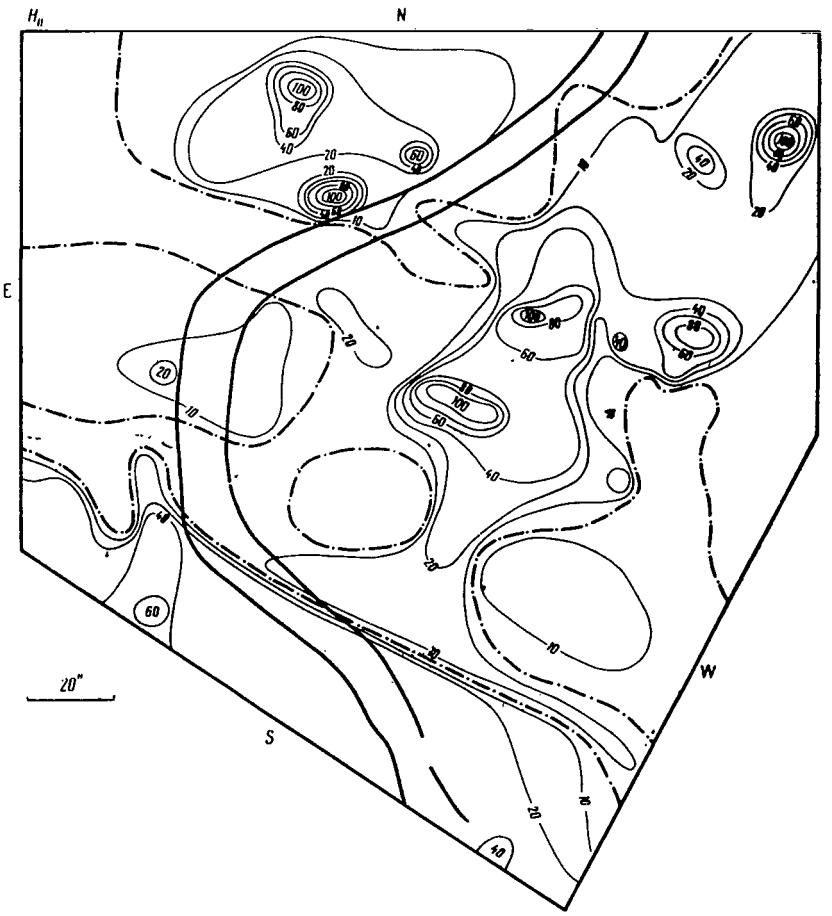

Fig. 6. Map of the Longitudinal Component of the Magnetic Field in the Photosphere on July 27, 1962. Group No. 78 [23], λ 5250 Å. Designations same as in Figure 4.

For the measurements in the photosphere, the width of the output slit of the spectograph was 0.06 Å, and the middle of the slit was a distance from the center of the line equal to 0.07 Å. The width of the output slit for measurements along H_β corresponded to about 0.15 Å, and the middle of the slit was a distance of about 0.15 Å from the center of the line.[1] The effective altitude of the region of the photosphere in which the measurements of the field were carried out along the H_β wing corresponded roughly to 1500-200 km. Measurements were carried out from a height of the slits corresponding to 3". The spatial allowance in each section was

[1] For a discussion of the errors linked with possible blending of the Hβ line, see also the article by I.A. Zhulin, B.A. Joshpa, E.I. Mogilevskiy and V.N. Obridko in this Collection.

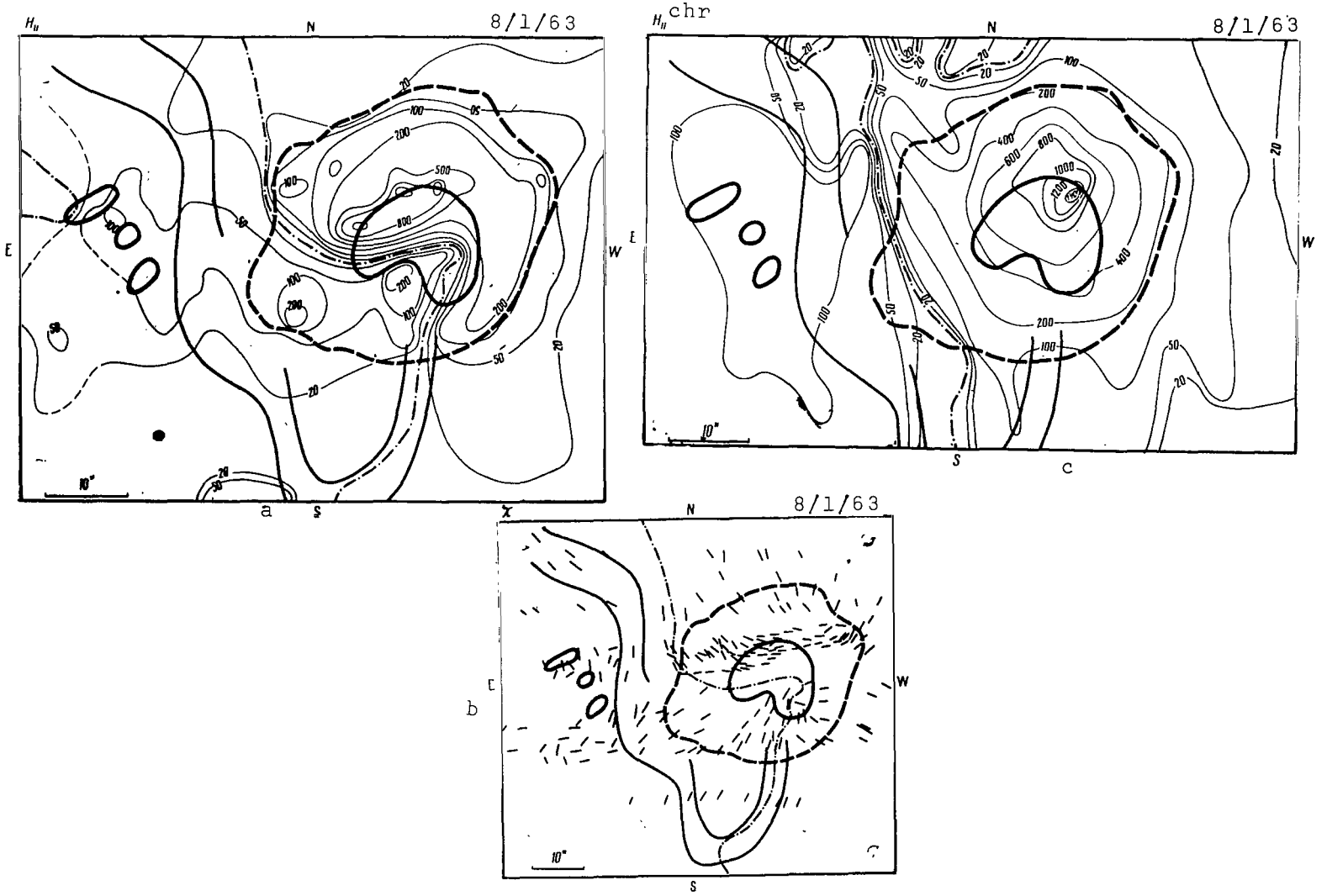

Fig. 7. Maps of the Longitudinal Component (a) and Azimuth of the Transverse Component (b) of the Magnetic Field in the Photosphere and the Longitudinal Component of the Magnetic Field in the Chromosphere (C) in Group No. 78 [23], August 1-4, 1963. Designations Same as in Figure 4.

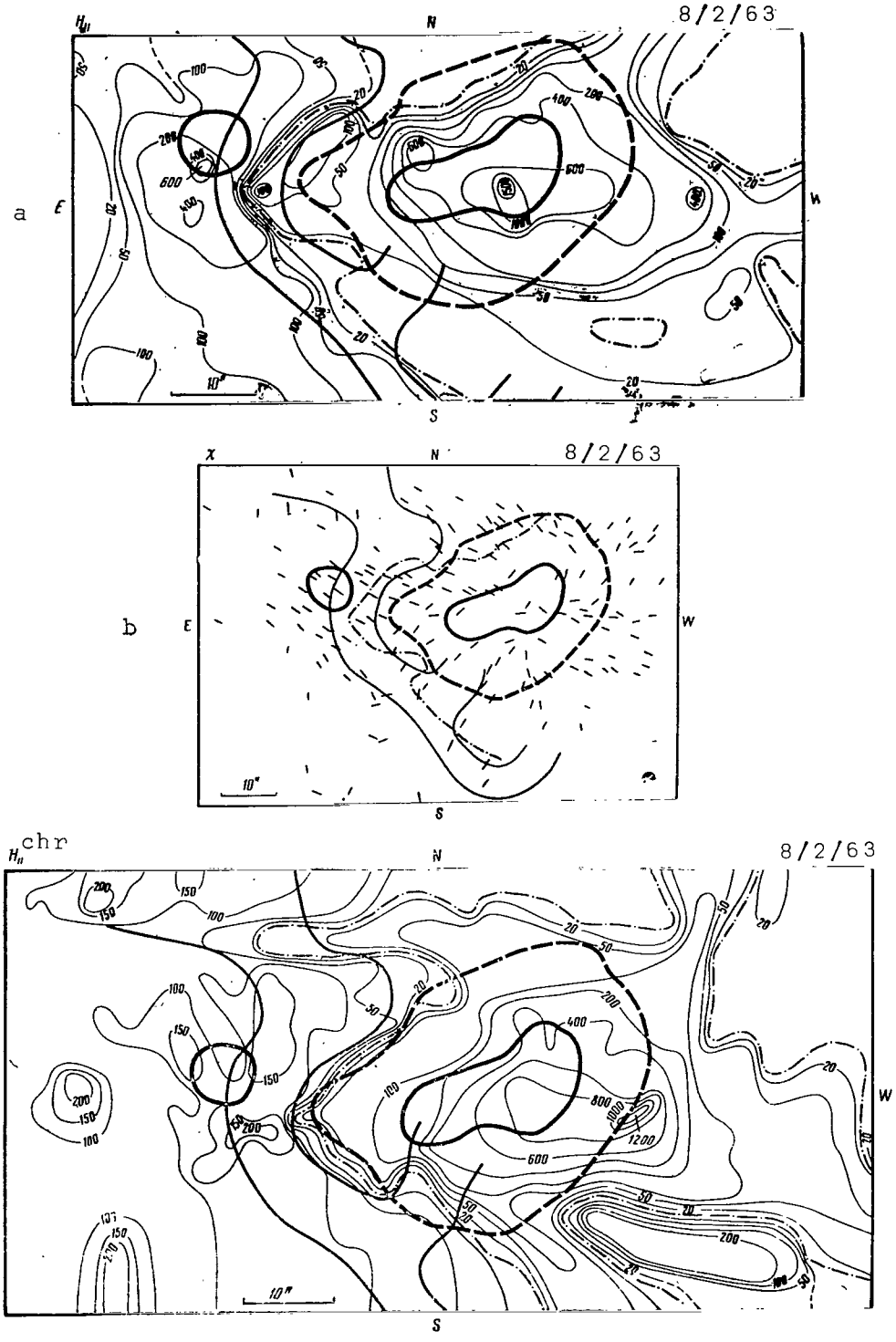

Fig. 7 (cont'd)

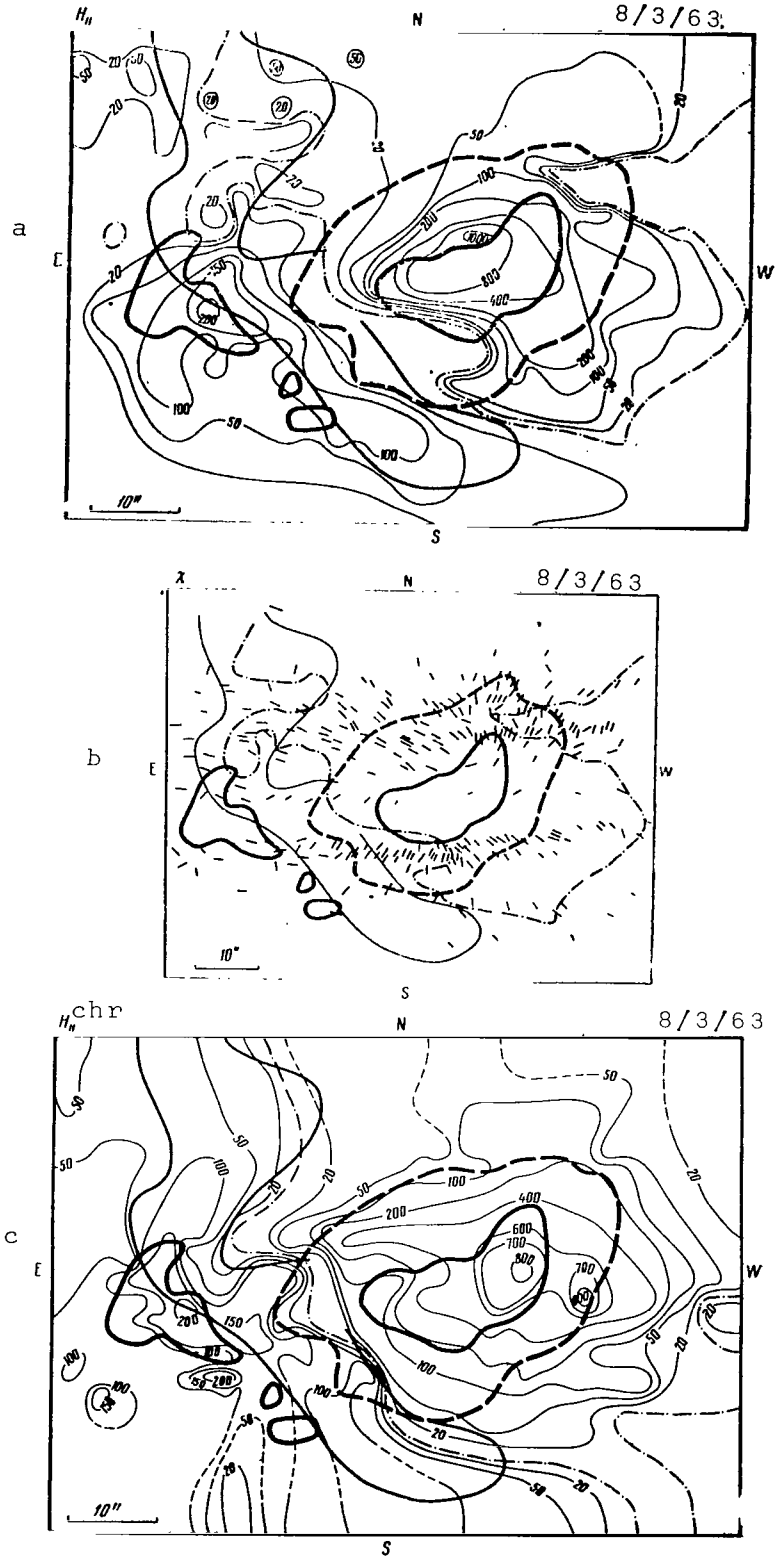

Fig. 7 (cont'd)

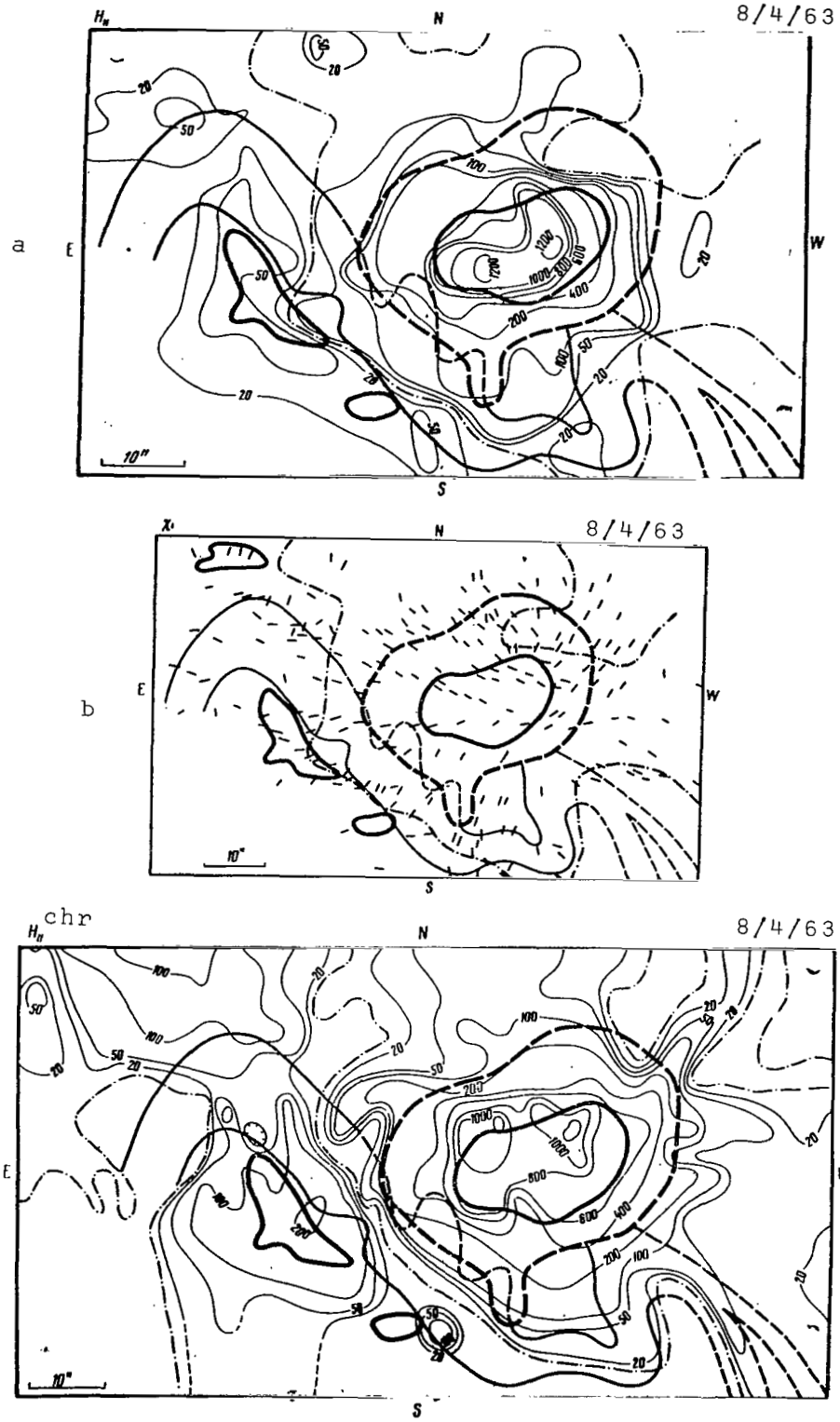

Fig. 7 (cont'd)

about .3" x 3", considering the effect of shaking. The contours of the spot and half-shadows were plotted on the maps with the aid of enlarged photographs obtained on the AFR-2 telescope. Therefore, the structure of the magnetic field was closely connected only to the chromospheric details, while the photospheric details were plotted with uncertainty on the order of 3-4". /58

It can be seen from an investigation of the maps presented that the distribution of the filaments corresponds mainly to the neutral line of the longitudinal field both in the photosphere and in the chromosphere. However, the neutral lines in a number of cases could be a substantial distance away from the filaments, while it sometimes intersected it. Thus, in that range where a filament approached a spot and apparently flowed into it, the filament usually intersected the neutral line and passed over a region of a strong field gradient of one polarity (see, for example, the map for May 26, 1962). V.Ye. Stepanov [14] first noted the fact that a filament in the vicinity of a strong magnetic field can intersect the isogauss lines of the longitudinal fields. The authors of [24] confirmed this conclusion; however, they suggested that the filaments nevertheless could lie on the neutral line of the magnetic field at the level of the chromosphere. Our observations show that this is not so. For example, it is seen on the map obtained for H_β on July 4, 1962 that the flow from the middle part of the filament is directed towards the spot across the neutral line of the field. The northern end of this filament also goes into the region of a strong magnetic field of one polarity. It is interesting to note that, on August 1, 1963, a filament approaching the spot from the south went along the neutral line of the photospheric field, while it intersected the isolines of the chromospheric fields. At the same time, an investigation of the maps of the longitudinal fields in the photosphere and chromosphere for August 1-4, 1964 showed the greater stability of the position of the neutral lines of the longitudinal component in the chromosphere corresponding roughly to the line where the filament is located (excluding the parts going into the region of the strong fields). Meanwhile, the neutral line of the longitudinal field in the photosphere showed rather great oscillations from day to day. The presence of the oscillational movement of the zero line of the longitudinal field had been noted previously by G.V. Kuklin [25], who explained this phenomenon in terms of the oscillational movement of the axis of a sunspot. We must point out that the maps in the photosphere and chromosphere for the same day were obtained not simultaneously, but in sequence, within an interval of several hours; it is possible that a certain difference in the field structures could also be linked with this.

In some cases, the neutral line intersects the line where the filament is located, even in the region of a relatively small field. On the map for July 27, 1962, (Fig. 6), it can be seen that the filament intersects the neutral line twice, both times

at the sites of the greatest bends of the filament. The field often has identical polarity at the ends of the filaments, along both sides of it (see, for example, the maps for July 23, 1962 and May 29, 1962) (Fig. 4 and 5). It is possible that the substance of the filament moves downward at just these sites.

Figure 7 (b) also shows maps of the azimuth of the transverse magnetic field (χ) for group No. 79 of August 1-4, 1963; the values of the transverse magnetic field $H_\perp$ for August 4 are also shown (Fig. 8).

A comparison of the values $H_\parallel$ and $H_\perp$ for August 4 (during this day the group passed through the central meridian) shows that the field is close to horizontal below the region where the filament is located. The longitudinal fields below the filament does not exceed values of several tens of gauss, while the transverse field has an average value of about 200-300 gauss. At isolated points, the value of the transverse field below the filament is less, and it exceeds the noise level only a little (80-100 gauss). At such points the value of the azimuth for the projection of the magnetic vector on the pictured plane is determined unreliably in each unit measurement; however, the coincidence of the direction of the azimuths for a number of sections gives a rather reliable average picture.

It can be seen from an investigation of the maps that the average, most massive part of the filament is located primarily across the magnetic lines of force, in the same part where the filament is extended on the spot, intersecting the neutral line of the field, and the direction of the filament is close to the direction of the lines of force. The orientation of this part of the filament coincides with the orientation of the thin chromo- /59

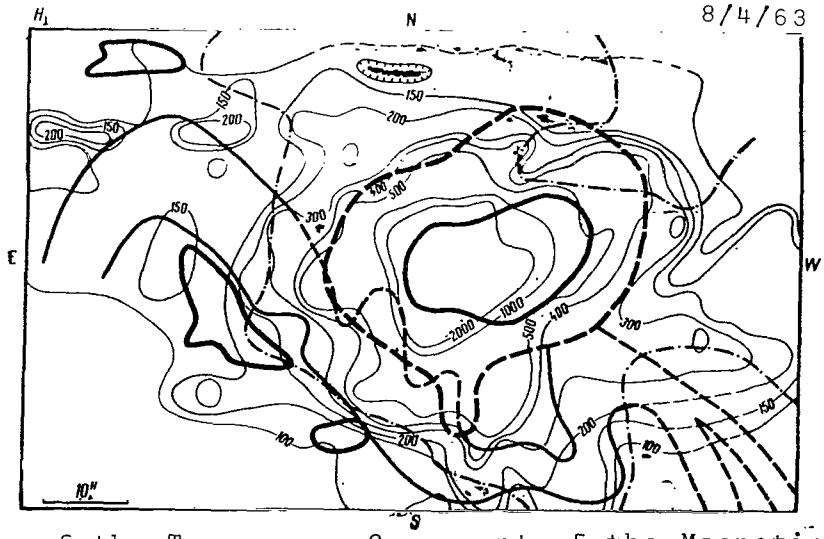

Fig. 8. Map of the Transverse Component of the Magnetic Field in the Photosphere for Group No. 78, August 4, 1963. Designations same as in Figure 4.

spheric structure, visible in H_α as dark filaments (one of such filaments is depicted in Figs. 7 and 8 and pointed out by the dashed line). Such filaments usually pass along a region of one polarity, often intersecting a line of equal intensity of the longitudinal field [24]. As was shown in [26], they are mainly oriented along the direction of the transverse magnetic fields.

The data for the region of the northeast end of the filament are not very reliable because of the small value of the fields. However, the primary direction of the lines of force here is also obviously that along the line where the filaments are located (see the maps for August 1 and 2, 1963.

On August 29, 1963, we carried out total-vector measurements of the magnetic field in the region where a quiet filament surrounded by a bright floccula was located (coordinates of the filaments: ϕ changes from -10 to -15°, $l \approx +65°$). Figures 9 (a and b) show two maps of the azimuths (angle χ) of the transverse field in this region; they were obtained in sequence, with an interval of about 1.5 hours. Unfortunately, this region was already greatly removed from the central meridian. According to the data of the solar service, there was seen a small spot in this region during the preceding dates, but disappeared after passing through the central meridian on August 24. As can be seen from the figure, the filament is extended almost along the meridian. Since the values of the fields in the surrounding filament of the floccula were much less than the values measured in the region of the spots, the observation was carried out with a larger time constant than usual ($\tau \approx 6$ sec), while the height of the spectrograph slit was increased to about 6". This permitted us to improve the signal-noise ratio roughly by 3-4, compared to regular observations, and to thereby increase the sensitivity in determining the transverse field, roughly by a factor of 2 (to 40 gauss). The points on the maps for χ show the same sites in the region under investigation where the value of the transverse field was less than the noise level or where χ was determined unreliably. It can be seen from Figure 9 that the filament lies mainly along the direction of the transverse magnetic field (excluding individual points). A consideration of the effect of projection, which is generally substantial for $l \sim 65°$, was not carried out in this case. Such a consideration could not bring about substantial changes in the structure of the transverse field in this case, since the direction of the magnetic fields on the maps for August 29 was close to the meridional. A comparison of the values $H_\parallel$ and $H_\perp$ shows that the field is mainly transverse in this region (γ differs from 90° at most of the points by no more than $\pm$ 20°). This also follows from the very appearance of the map of χ: if there were a substantial $H_\parallel$ due to the projection, the azimuth of the transverse field would make a substantial angle with the meridian. The position of the filament corresponds on the whole to the neutral line of the longitudinal fields. Thus, we can conclude that the filament under investigation lies over the region of a rather great

/60

(50-200 gauss) photospheric transverse field along the direction of the lines of force of this field. Several of the sections which are presented in the region where this filaments are located on August 21, 1963 (Fig. 9,c) obviously confirm this conclusion. On

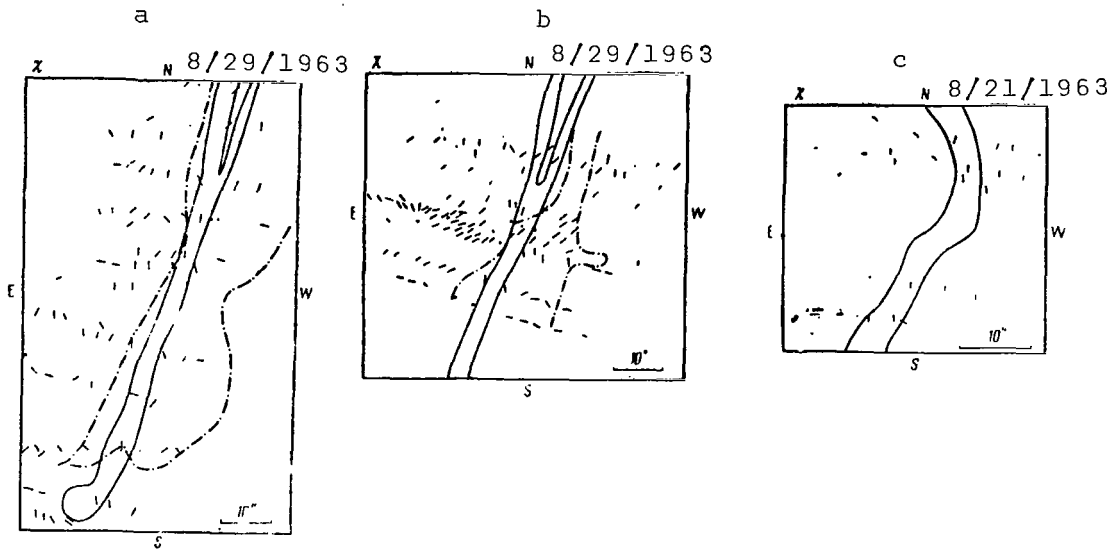

Fig. 9. Maps of the Azimuths of the Transverse Component of the Magnetic Field in the Photosphere for a Filament with Coordinates of $\phi = -(10\text{-}15°)$, $\lambda = 290°$, August 21 and 29, 1963. Designations Same as in Figure 4. The Points show Indefinitenesses in the Position of the Azimuths.

August 29, 1963, we also studied the structure of the field in the region of another quiet filament lying roughly at the same latitude in the northern hemisphere, and also extended along the meridian (ϕ changes from +5 to +15°, $l \approx 70°$). The filament was also surrounded by a bright floccula. The observation conditions were the same as in the measurements of the field in the region of the first filament.

Figure 10 a shows a map of angles of χ obtained from observations, and Figure 10b shows the same map, corrected for the projection.

At the point where the azimuth of the magnetic field is close to the direction of the parallel, the correction for projection was carried out very uncertainly, since, if the azimuth were directed precisely along the parallel, then, after considering the projection it would remain unchanged; for small deviations from the parallel, a substantial component can appear along the meridian in the correction. Moreover, in order that the correction for projection would be unambiguous, we had to know the real direction

of the transfer fields, and it had to be determined with accuracy up to 180°. On August 29, we measured only the value of the transverse field in the region of the filaments, while on August 27 and 28 we measured only the longitudinal components of the fields in λ 5250 Å in this region according to the regular scheme of the longitudinal-vector magnetograph. During these days they lay rather thinly on the boundary of polarity. In order to avoid ambiguity, we assumed that the longitudinal vector had the same direction during the passage of the filament through the central meridian. For all the indefinitenesses linked both with the small value of the field at a number of points and with observations far from the central meridian, we can see from the map that the direction of the transverse field at most of the points was close to the line where the filament was located after the correction, or else it made a small angle with this line (excluding some points on the filaments). /61

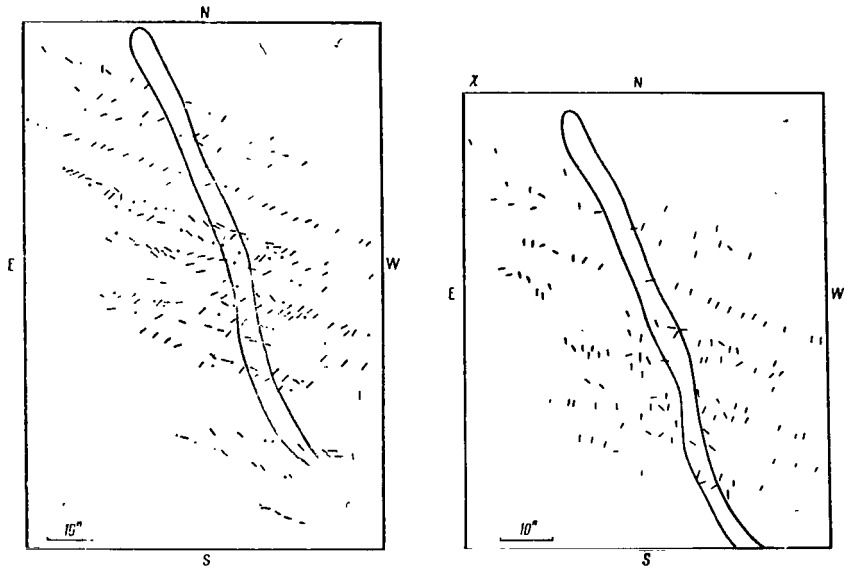

Fig. 10. Map of the Azimuths of the Transverse Component of the Magnetic Field in the Photosphere for a Filament with Coordinates of ϕ = +(5-13°); λ = 296°, August 29, 1963. (a) Map not Corrected for Projection; (b) Map Corrected for Projection. Designations Same as in Figure 4.

The field in the region was rather nonhomogeneous: sections relative to a large (100-200 gauss) field followed sections where the field was lower than the measurable limit (40-50 gauss).

The materials which have been obtained to the present are insufficient in order to draw any categorical conclusions relative to the link between the structure of the magnetic field in the photosphere and the location of the filament; the same holds for

the results for a group No. 74, which was observed on August 1-4, 1963, and for regions where quiet filaments were located, the field in which was measured on August 29, since it seems that there was a certain contradiction here. At the present, there have been no reports in the literature on any measurements of the total vector in the region of filaments.

Despite the preliminary nature of the data, certain facts can be extracted:

1) The presence of a substantial field in a number of prominences which are not linked with an active group, which field is directed along the major axis of the filament,'

2) The primary location of the filament is along the line of division of opposite polarity,'

3) The structure of the field in the photosphere below the region where the filament is located for group No. 74 (Fig. 7) (the principal part of the filament lies across the lines of force of the transverse field, while the filament is extended along the field at sites where the substance of the filament drops towards a spot) can permit us to construct an effective hypothesis concerning the existence of two systems of fields: an external field transverse to the line where the filament is located, in the tops of the arched structure of which it is located, and in internal fields, is directed along the filaments. /62

For observations in the field in the photosphere and the lower chromosphere below the filament, we see an external field which has an arched structure. Where the filament approaches the photosphere, we can see a field close to that of the filament, and it is directed along the latter. The external field, according to [15], supports the substance of the protuberance against the forces of gravity. The internal field at the end of a filament which is "fixed" through the field of the photosphere brings about the high stability of the filament in relation to disturbances caused by the force of gravity. If there is no internal field or this field is weak, then an instability can develop in the following way: there appears a small depression, and the substance flows along the weak internal fields to its bottom, accumulates there and drops downward, repelling the lines of force of the supporting field. Without an internal field, the prominence would develop at isolated parts. The internal field should be rather strong, so that a substantial curvature of the filament in the vertical plane is not permitted, except for, perhaps, isolated segments in which there appear flows which link the protuberance with the photosphere. In order to estimate the value of the field which is necessary for stability, let us compare the tensile strength of the magnetic lines of force which arises during a bending of the filament $f_м \sim \frac{H^2}{4\pi R_{кр}}$, to the force of gravity which causes this bending, ρg, where R_{cr}

is the radius of curvature of the lines of force. Let the disturbance have the form $y = A \sin 2\pi\chi/\lambda$; λ is the characteristic size of the disturbance--we will assume that it is close to the thickness of the filament ($\lambda \sim 10^9$ cm). If the magnitude of the disturbance $A \ll \lambda$, then $\frac{1}{R_{кг}} \approx \frac{4\pi^2 A}{\lambda}$; for a value of A which is one order less than λ, $R_{kr} \sim \lambda/4$. Thus, the field necessary for preventing such bends should be $H \sim \sqrt{\pi\lambda\rho g} \sim 10$ gauss. We assumed in the evaluations that the density of the prominence $n \sim 3 \cdot 10^{11}$, since the density can become several orders greater than the average one during the flow of the substance. Consequently, it is sufficient that the internal field be approximately 10 gauss for stability in the above sense.

Obviously, the field exceeds this value only in certain quiet prominences, which agrees with the fact that the field in quiet prominences is measured in rather rare cases (for measurement sensitivity of ~ 40 gauss). The prominence apparently comes from small dark filaments of the fine structure seen in H_α. The filaments are distributed along the fields, whereas there are no arches below them [26]. This confirms what we said concerning the internal fields of a protuberance. The filaments have the same internal field, which is directed along them, but, as their length and mass are small, the presence of supporting arches is not necessary, since the regidity of the internal field is sufficient. In long and massive filaments, one single internal field is not sufficient, since the entire line of force would descend towards the photosphere without support on the part of the arches. We mentioned cases above (observations for August 29, 1963) when the field of the photosphere was directed almost along the filament. Since the polarity of the field component longitudinal to the line of sight differed along both sides of the filament, the arches apparently also existed in this case, but they could be inclined, for example, so that the "props" had a substantial projection along the direction of the filament.

The observational data obtained to the present are insufficient in order to draw more definite conclusions. Supplementary materials /63 on measurements of magnetic fields and prominences and the structure of the field below them are necessary for this.

The author would like to express his gratitude to B.N. Obridko and E.I. Mogilevskiy for their aid in observing and discussing the results. I consider it my privilege to also express my deep gratitude to S.B. Pikel'ner for his discussions of the results.

REFERENCES

1. Severnyy, A.B. and V.L. Khokhlova: Izv. Krymskoy Astrofiz. Obs., Vol. 10, p. 9, 1953.
2. Klechek, I.: Byull. Astr. Instit. Chekhoslovakii, Vol. 14, No. 3, p. 86, 1963.

3. Idlis, G.M., M.G. Karimov, A.B. Delone and S.O. Obashev: Doklady Akad. Nauk S.S.S.R., Vol. 102, p. 707, 1955.
4. Kleczek, I.: Astron. J., Vol. 67, No. 5, p. 275, 1962.
5. Lyot, B.: L'Astronomie, Vol. 51, p. 217, 1937.
6. Thiessen, G.: Observatory, Vol. 71, No. 863, 1951.
7. Zanstra, H.: Monthly Notices Roy. Astron. Soc., Vol. 110, No. 5, p. 491, 1950.
8. Newkirk, G.: Publ. Astron. Soc. Pacif., Vol. 70, p. 185, 1958.
9. Brückner, G.: Z. Astrophys., Vol. 58, p. 461, 1963.
10. Zirin, H. and A.B. Severny: Observatory, Vol. 81, No. 923, p. 155, 1961.
11. Zirin, G.: Astron. Zhur., Vol. 38, p. 861, 1961.
12. Hyder, G.L.: Astrophys. J., Vol. 140, p. 817, 1964.
13. Babcock, H.W. and H.D. Babcock: Astrophys. J., Vol. 121, p. 349, 1955.
14. Stepanov, V.Ye.: Izv. Krymskoy Astrofiz. Obs., Vol. 20, p. 52, 1959.
15. Kippenchann, R. and A. Schlüter: Z. Astrophys., Vol. 43, p. 36, 1957.
16. Ioshpa, B.A.: Geomagnetizm i Aeronomiya, Vol. 2, p. 172, 1962.
17. Ioshpa, B.A. and E.I. Mogilevskiy: Sb.: Solnechnaya aktivnost' (Collection: Solar Activity), No. 2. "Nauka", 1965, p. 118.
18. Ioshpa, B.A.: Geomagnetizm i Aeronomiya, Vol. 3, p. 1125, 1963.
19. Zhulin, I. A., B.A. Ioshpa and E.I. Mogilevskiy: Sb.: Solnechnaya aktivnost' (Collection: Solar Activity), No. 2, "Nauka", 1965, p. 108.
20. Kurs astrofiziki i zvezdnoy astronomii (Course of Astrophysics and Stellar Astronomy), ed. A.A. Mikhaylov, Vol. III, Chap. V.
21. Shi-khuey, E.: Izv. Krymskoy Astrofiz. Obs., Vol. 15, p. 180, 1961.
22. Malkin, N.: Trudy GGO, Vol. 1, No. 3, Rep. 1, 24, 1934.
23. Solnechnyye dannyye (Data on the Sun), 1961-1963.
24. Howard, R. and J. Harvey: Astrophys. J., Vol. 139, p. 1335, 1964.
25. Kuklin, G.V.: Solnechnyye dannyye, No. 8, p. 45, 1964.
26. Tsap, T.T.: Izv. Krymskoy Astrofiz. Obs., Vol. 31, p. 200, 1964.

MAGNETIC-FIELD RADIATION-SCATTERING MATRIX DERIVED WITH ALLOWANCE FOR THE PHASE COUPLINGS OF THE UPPER-LEVEL WAVE FUNCTION.

V.N. Obridko

ABSTRACT: The paper presents a calculation of the matrix of resonance scattering when there is an outer magnetic field, with allowance for phase coupling of upper-level wave functions for lines with $j_h = 0$ and $j_b = 1$. The problem of the limit transition $H \to 0$ is discussed.

The equation for transfer of polarized radiation in a noniso- /64*
tropic medium can be written out in the following way:

$$\mu \frac{dS_i}{\partial \tau} = (1 + \eta_{ik}) S_k - (1 - \varepsilon) \int D_{ik}(\mu, \mu') S_k(\mu') \frac{d\omega'}{4\pi} - (1 - \varepsilon\eta_{ik}) B_\nu. \quad (1)$$

Here the vector S_i is composed of Stokes parameters which are determined in the following way:

$$I = \overline{\xi_1^2 + \xi_2^2}, \quad U = 2\overline{\xi_1 \xi_2 \cos(\varepsilon_1 - \varepsilon_2)},$$
$$Q = \overline{\xi_1^2 - \xi_2^2}, \quad V = 2\overline{\xi_1 \xi_2 \sin(\varepsilon_1 - \varepsilon_2)}, \quad (2)$$

where ξ_1, ξ_2 is the amplitude of oscillations of the electric vector in the direction of the axis of an arbitrarily selected system of coordinates, and ε_1 and ε_2 are phases of these oscillations.

Other determinations of the Stokes parameters are possible. In these cases, the general appearance of (1) is preserved, while the particular forms of the matrices for absorption η_{ik} and scattering D_{ik} change.

The absorption matrix η_{ik} for the parameters we used was presented in [1]. Independent of this study, V.Ye. Stepanov introduced the absorption matrix [2] for a certain generalized Stokes parameters $I_\pm$ in which the matrix is diagonalized. In [3-5], it was shown that the absorption matrices in the systems of Unno and Stepanov are equivalent when the effects of anamolous dispersions are disregarded, and therefore a more general expression considering these effects was given.

---

* Numbers in the margin indicate pagination in the foreign text.

As regards the scattering matrix D_{ik}, the matter is somewhat more complicated. W. Unno [1] did not consider scattering at all. Z.Ye. Stepanov [2] solved the transfer equation by assuming that the absorption matrix and the scattering matrix coincide, which is a rather crule assumption. Subsequently, more precise expressions for the scattering matrices were introdeced in [6,7] for certain partial transitions in the system assumed for the parameters. However, the parameters $I_{\pm}$ do not involve the desired simplification for a precise calculation of the scattering, since the matrix D_{ik} was not diaganalized simultaneously with η_{ik}.

As was shown in [8], the transitions from various upper-level substates resulting in resonance scattering cannot be considered to be independent. For a precise conclusion, we must consider the phase couplings of residual components of the transitions. A scattering matrix which did not consider phase couplings was derived in [9] by the method of Stepanov. Within the framework of the classical theory, this corresponds to the assumption that the oscillators linked with the atom have a vanishingly small amount of inertia, while the external field is strong. In the quantum sense this corresponds to the assumption that the upper state in the magnetic field is divided by more than the width of the sublevel. We will give a more precise expression for the scattering matrix below, with allowance for the phase couplings. /65

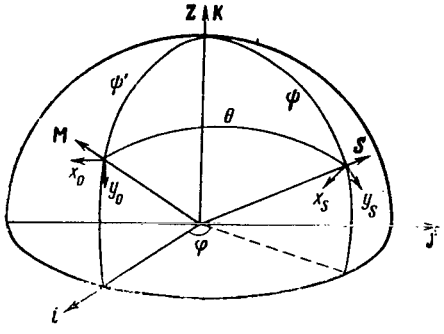

Deriving the Scattering Matrix, Considering Phase Couplings.

In the scattering of resonance radiation, we are treating transitions from the principal state A_k to the excited one B_n and back to the principal one A_p. In this case, it is necessary to consider that different sequences of transitions corresponding to the same initial state are not independent. In other words, the wave functions corresponding to different substates of B_n have relative phases connected with the phase of the wave function A_k. The theory considering these connections when there is no magnetic field, which was developed by Hamilton [8], is the one we will use here.

The coordinate system we used is depicted on the figure. The directions for excited and scattered radiations are designated by the vectors M and S, respectively. The axis Z is directed along the magnetic field.

In order to alleviate the transformation, it is convenient to use the following complex representations for the amplitude of oscillations of arbitrarily polarized light:

$$\xi_0 = E_1 x_0 + E_2 y_0.$$

The comlex values E_1 and E_2 consider the phase difference of two mutually perpendicular oscillations parallel to x_0 and y_0. The Stokes parameters are now written out in the following way:

$$\begin{aligned} I &= \overline{E_1 E_1^* + E_2 E_2^*}, \qquad U = 2\overline{\mathrm{Re}\,(E_1 E_2^*)}, \\ Q &= \overline{E_1 E_1^* - E_2 E_2^*}, \qquad V = 2\,\overline{\mathrm{Im}\,(E_1 E_2^*)}. \end{aligned} \tag{3}$$

Here the symbols Re and Im signify the operations of taking out the real or imaginary part of the expressions for which they stand. This representation of the Stokes parameters is equivalent to (1).

D. Hamilton showed that scattered radiation can be represented as the radiation of independent dipoles with the moments N_{kp}:

$$\mathbf{N}_{kp} = \sum_n (\xi_0 \mathbf{P}'_{kn})\, \mathbf{P}''_{np}. \tag{4}$$

Here the sum is extended over all possible upper-level substates, and P'_{kn} and P''_{np} are the matrix elements of the electric dipole moment of the radiating system for the transitions of $A_k B_n$ and $B_n A_p$, respectively. The Stokes parameters for scattered radiations are then obtained by means of summation of the Stokes parameters of individual dipoles over all possible values of k and p: /66

$$\begin{aligned} I &= \Sigma\,(\mathbf{N}_{kp}\mathbf{x}_s)\,(\mathbf{N}_{kp}\mathbf{x}_s)^* + \Sigma\,(\mathbf{N}_{kp}\mathbf{y}_s)\,(\mathbf{N}_{kp}\mathbf{y}_s)^*, \\ Q &= \Sigma\,(\mathbf{N}_{kp}\mathbf{x}_s)\,(\mathbf{N}_{kp}\mathbf{x}_s)^* - \Sigma\,(\mathbf{N}_{kp}\mathbf{y}_s)\,(\mathbf{N}_{kp}\mathbf{y}_s)^*, \\ U &= 2\Sigma\mathrm{Re}\,[(\mathbf{N}_{kp}\mathbf{x}_s)\,(\mathbf{N}_{kp}\mathbf{y}_s)^*], \\ V &= 2\Sigma\mathrm{Im}\,[(\mathbf{N}_{kp}\mathbf{x}_s)\,(\mathbf{N}_{kp}\mathbf{y}_s)^*]. \end{aligned} \tag{5}$$

The matrix elements of the electric dipoles can be written in the following way:

$$\begin{aligned} \mathbf{P}'_{kn} &= \sqrt{g_{kn}}\,\mathbf{T}_{n-k}, \\ \mathbf{P}''_{np} &= \sqrt{G_{np}}\,\mathbf{T}_{p-n}, \end{aligned} \tag{6}$$

where

$$\begin{aligned} \mathbf{T}_{\pm 1} &\equiv \frac{1}{\sqrt{2}}(\mathbf{i} \pm i\mathbf{j}), \\ \mathbf{T}_0 &\equiv \mathbf{k}. \end{aligned} \tag{7}$$

The systems of coordinates (x_0y_0) and (x_sy_s) are expressed in terms of the principal basis vectors (i, j, k) in the following way:

$$\begin{aligned}\mathbf{x}_0 &= -\mathbf{j},\\ \mathbf{y}_0 &= \cos\psi'\mathbf{i} - \sin\psi'\mathbf{k},\\ \mathbf{x}_s &= \sin\varphi\mathbf{i} - \cos\varphi\mathbf{j},\\ \mathbf{y}_s &= \cos\psi\cos\varphi\mathbf{i} + \sin\varphi\cos\psi\mathbf{j} - \sin\psi\mathbf{k}.\end{aligned} \tag{8}$$

Let us examine a derivation of the scattering matrix for the line λ5250 Å ($j_n = 0$, $j_b = 1$). For this line, the initial state A_k and the ultimate one A_p coincide, and there is a single dipole $N_{kp} = N_\infty$, while the sum in the expression in (5) contains only one term apiece:

$$\begin{aligned}\mathbf{N}_{00} = \frac{1}{\sqrt{2}}\sqrt{g_{01}}(E_2\cos\psi' + iE_1)\sqrt{G_{10}}\mathbf{T}_1 +\\ + \frac{1}{\sqrt{2}}\sqrt{g_{0,-1}}\sqrt{G_{-1,0}}(E_2\cos\psi' - iE_1)\mathbf{T}_{-1} - E_2\sqrt{g_{00}}\sqrt{G_{00}}\sin\psi'\mathbf{T}_0.\end{aligned} \tag{9}$$

For our line, $g_{10} = k_l$, $g_{-1.0} = k_r$, $g_{00} = k_p$, $G_{01} = A_lk_l$, $G_{-1.0} = A_rk_r$, $G_{00} = A_pk_p$, where the factors A_l, A_r and A_p are introduced for calibrations. Moreover, we should mention that the coordinate system we selected (8) differed by $\pi/2$ from that used in [9]. Considering this reversal, we can find the following, using (5)-(9);

$$\begin{aligned}I^s = I\Bigg[\frac{A_lk_l^2 + A_rk_r^2}{8}(1+\cos^2\psi)(1+\cos^2\psi') +\\ + \frac{\sqrt{A_lA_rk_lk_r}}{4}\sin^2\psi\sin^2\psi'\cos 2\varphi + \frac{A_pk_p^2}{8}\sin^2\psi\sin^2\psi' -\\ - \frac{\sqrt{A_p}k_p(\sqrt{A_l}k_l + \sqrt{A_r}k_r)}{16}\sin 2\psi\sin 2\psi'\Bigg] +\\ + Q\Bigg[-\frac{A_lk_l^2 + A_rk_r^2}{8}(1+\cos^2\psi)\sin^2\psi' -\\ - \frac{\sqrt{A_lA_rk_lk_r}}{4}\sin^2\psi(1+\cos^2\psi')\cos 2\varphi + \frac{A_pk_p^2}{8}\sin^2\psi\sin^2\psi' -\\ - \frac{\sqrt{A_p}k_p(\sqrt{A_l}k_l + \sqrt{A_r}k_r)}{16}\sin 2\psi\sin 2\psi'\Bigg] +\\ + U\Bigg[-\frac{\sqrt{A_lA_rk_lk_r}}{2}\cos\psi'\sin^2\psi\sin 2\varphi -\\ - \frac{\sqrt{A_p}k_p(\sqrt{A_l}k_l + \sqrt{A_r}k_r)}{8}\sin\psi'\sin 2\psi\sin\varphi\Bigg] +\\ + V\Bigg[\frac{A_rk_r^2 - A_lk_l^2}{4}\cos\psi'(1+\cos^2\psi) +\\ + \frac{\sqrt{A_p}k_p(\sqrt{A_l}k_l - \sqrt{A_r}k_r)}{8}\sin\psi'\sin 2\psi\cos\varphi\Bigg].\end{aligned} \tag{10}$$

Let radiation with arbitrary polarization, determined by the parameters I, Q and V, enter on the scattering layer at a certain angle ψ'. The absorption intensity is now written out in the following way: /67

$$I^n = I\left[\frac{k_l + k_r}{4}(1 + \cos^2\psi') + \frac{k_p}{2}\sin^2\psi'\right] + \\ + Q\left(\frac{k_p}{2} - \frac{k_l + k_r}{4}\right)\sin^2\psi' + V\frac{k_r - k_l}{2}\cos\psi'. \qquad (11)$$

This absorbed energy is completely expended for radiation in all directions in the case of pure scattering. Having integrated (11) over all solid angles, we can obtain the value for the scattered energy $\int I^s d\omega$, which should be equal to the absorbed energy I^n:

$$\int I^s d\omega = \frac{8\pi}{3}\left\{I\left[\frac{A_l k_l^2 + A_r k_r^2}{4}(1 + \cos^2\psi') + \frac{A_p k_p^2}{8}\sin^2\psi'\right] + \right. \\ \left. + Q\left(\frac{A_p k_p^2}{8} - \frac{A_l k_l^2 + A_r k_r^2}{4}\right)\sin^2\psi' + V\frac{A_r k_r^2 - A_l k_l^2}{2}\cos\psi'\right\}. \qquad (12)$$

Having equalized (11) and (12) and noted that this equation should be fulfilled for any values of I, Q and V, we find that $A_l = \frac{3}{8\pi k_l}$, $A_r = \frac{3}{8\pi k_r}$, $A_p = \frac{3}{8\pi}\frac{4}{k_p}$. We can now write out the Stokes parameters for scattered radiation in terms of the parameters for excited radiation:

$$I^s = \frac{3}{8\pi}\left\{I\left[\frac{k_l + k_r}{8}(1 + \cos^2\psi)(1 + \cos^2\psi') + \frac{\sqrt{k_l k_r}}{4}\sin^2\psi\sin^2\psi'\cos 2\varphi + \right.\right. \\ \left. + \frac{k_p}{2}\sin^2\psi\sin^2\psi' - \frac{\sqrt{k_p}(\sqrt{k_l} + \sqrt{k_r})}{8}\sin 2\psi\sin 2\psi'\right] + \\ + Q\left[-\frac{k_l + k_r}{8}(1 + \cos^2\psi)\sin^2\psi' - \frac{\sqrt{k_l k_r}}{4}\sin^2\psi(1 + \cos^2\psi')\cos 2\varphi + \right. \\ \left. + \frac{k_p}{2}\sin^2\psi'\sin^2\psi - \frac{\sqrt{k_p}(\sqrt{k_l} + \sqrt{k_r})}{8}\sin 2\psi\sin 2\psi'\right] + \\ + U\left[-\frac{\sqrt{k_l k_r}}{2}\cos\psi'\sin^2\psi\sin 2\varphi - \frac{\sqrt{k_p}(\sqrt{k_l} + \sqrt{k_r})}{4}\sin\psi'\sin\varphi\sin 2\psi\right] + \\ \left. + V\left[\frac{k_r - k_l}{4}\cos\psi'(1 + \cos^2\psi) + \frac{\sqrt{k_p}(\sqrt{k_l} - \sqrt{k_r})}{4}\sin\psi'\cos\varphi\sin 2\psi\right]\right\};$$

$$Q^s = \frac{3}{8\pi}\left\{I\left[-\frac{k_l + k_r}{8}(1 + \cos^2\psi')\sin^2\psi - \frac{\sqrt{k_l k_r}}{4}\sin^2\psi'(1 + \cos^2\psi)\cos 2\varphi + \right.\right. \\ \left. + \frac{k_p}{2}\sin^2\psi\sin^2\psi' - \frac{\sqrt{k_p}(\sqrt{k_l} + \sqrt{k_r})}{8}\sin 2\psi\sin 2\psi'\right] + \\ + Q\left[\frac{k_l + k_r}{8}\sin^2\psi\sin^2\psi' + \frac{\sqrt{k_l k_r}}{4}(1 + \cos^2\psi)(1 + \cos^2\psi')\cos 2\varphi + \right.$$

$$+\frac{k_p}{2}\sin^2\psi\sin^2\psi' - \frac{\sqrt{k_p}(\sqrt{k_l}+\sqrt{k_r})}{8}\sin 2\psi\sin 2\psi'\Big] +$$
$$+U\Big[\frac{\sqrt{k_l k_r}}{2}\cos\psi'(1+\cos^2\psi)\sin 2\varphi - \frac{\sqrt{k_p}(\sqrt{k_l}+\sqrt{k_r})}{4}\sin\psi'\sin 2\psi\sin\varphi\Big] +$$
$$+V\Big[-\frac{k_r-k_l}{4}\cos\psi'\sin^2\psi + \frac{\sqrt{k_p}(\sqrt{k_l}-\sqrt{k_r})}{4}\sin\psi'\cos\varphi\sin 2\psi\Big]\Big\}; \quad (13)$$

$$U^s = \frac{3}{8\pi}\Big\{I\Big[\frac{\sqrt{k_l k_r}}{8}\cos\psi\sin^2\psi'\sin 2\varphi + \frac{\sqrt{k_p}(\sqrt{k_l}+\sqrt{k_r})}{4}\sin\psi\sin 2\psi'\sin\varphi\Big] +$$
$$+Q\Big[-\frac{\sqrt{k_l k_r}}{2}\cos\psi(1+\cos^2\psi')\sin 2\varphi + \frac{\sqrt{k_p}(\sqrt{k_l}+\sqrt{k_r})}{4}\sin\psi\sin 2\psi'\sin\varphi\Big] +$$
$$+U\Big[\sqrt{k_l k_r}\cos 2\varphi\cos\psi'\cos\psi - \frac{\sqrt{k_p}(\sqrt{k_l}+\sqrt{k_r})}{2}\cos\varphi\sin\psi'\sin\psi\Big] +$$
$$+V\Big[\frac{\sqrt{k_p}(\sqrt{k_r}-\sqrt{k_l})}{2}\sin\psi'\sin\psi\sin\varphi\Big]\Big\}; \quad (13)$$

$$V^s = \frac{3}{8\pi}\Big\{I\Big[\frac{k_r-k_l}{4}(1+\cos^2\psi')\cos\psi + \frac{\sqrt{k_p}(\sqrt{k_l}-\sqrt{k_r})}{4}\sin 2\psi'\sin\psi\cos\varphi\Big] +$$
$$+Q\Big[-\frac{k_r-k_l}{4}\sin^2\psi'\cos\psi + \frac{\sqrt{k_p}(\sqrt{k_l}-\sqrt{k_r})}{4}\sin\psi\sin 2\psi'\cos\varphi\Big] -$$
$$-U\frac{\sqrt{k_p}(\sqrt{k_r}-\sqrt{k_l})}{2}\sin\psi\sin\psi'\sin\varphi + V\Big[\frac{k_l+k_r}{2}\cos\psi'\cos\psi +$$
$$+\frac{\sqrt{k_p}(\sqrt{k_l}+\sqrt{k_r})}{2}\cos\varphi\sin\psi'\sin\psi\Big]\Big\}. \quad (13)$$

We will present the scattering matrix for this line for the sake of comparison. We obtained it in [9] without a consideration of the phase couplings between components.

$$I^s = \frac{3}{8\pi}\Big\{I\Big[\frac{k_l+k_r}{8}(1+\cos^2\psi)(1+\cos^2\psi') + \frac{k_p}{2}\sin^2\psi\sin^2\psi'\Big] +$$
$$+Q\Big[-\frac{k_l+k_r}{8}(1+\cos^2\psi)(\sin^2\psi') + \frac{k_p}{2}\sin^2\psi\sin^2\psi'\Big] +$$
$$+V\Big[\frac{k_r-k_l}{4}\cos\psi'(1+\cos^2\psi)\Big]\Big\};$$

$$Q^s = \frac{3}{8\pi}\Big\{I\Big[-\frac{k_l+k_r}{8}(1+\cos^2\psi')\sin^2\psi + \frac{k_p}{2}\sin^2\psi\sin^2\psi'\Big] + \quad (14)$$
$$+Q\Big[\frac{k_l+k_r}{8}\sin^2\psi'\sin^2\psi + \frac{k_p}{2}\sin^2\psi\sin^2\psi'\Big] +$$
$$+V\Big[-\frac{k_r-k_l}{4}\cos\psi'\sin^2\psi\Big]\Big\};$$
$$U^s = 0;$$
$$V^s = \frac{3}{8\pi}\Big[\frac{k_r-k_l}{4}(1+\cos^2\psi')\cos\psi I - \frac{k_r-k_l}{4}\cos\psi\sin^2\psi' Q +$$
$$+\frac{k_r+k_l}{2}\cos\psi'\cos\psi\Big].$$

Having compared these two matrices, we should note that there are terms in (13) which consider the "interaction" of isolated substates. These terms are more substantial for weak fields. We could show directly by calculation that the differences in the matrices of (13) and (14) are insignificant for the line Fe I (5250 Å) even for fields of ~ 300-500 Oe. At H $\lesssim$100 Oe, the matrices are vary greatly for certain combinations of the angles ψ, ψ' and ϕ. Since /69
in the equation of transfer in (1) the scattering matrix is integrated over all solid angles, the differences probably will not be very great. A solution to the equation of transfer which makes allowances for the matrix in (13) presents very great difficulties because of the complexity of the latter. Nevertheless, a knowledge of the matrix derived with allowance for phase couplings has great significance for the theory of formation of the lines, since only in this way can the correctness of the simplified method usually used in the scattering matrix be explained, and only in this way can the errors linked with this method be evaluated. In particular, V.N. Rachkovskiy [10] showed that a consideration of the phase couplings for the transition $j_H = 1$, $j_b = 0$ does not change the appearance of the scattering matrix.

In conclusion, let us discuss the problem concerning the transition $H \to 0$. The matrix in (13), which was derived with allowance for the phase couplings of the upper-state wave functions in the case of no magnetic fields, converts directly into the matrix of Rayleigh scattering, which agrees with the conclusion obtained in [8]. Assuming that $H = 0$ ($k_p = k_1 = k_r = k$), and turning to the system of coordinates used in [8] ($\phi = 0$, $\psi' = 0, \psi = \theta$), we can obtain the matrix of Rayleigh scattering from (13).

For a quantum-mechanical examination which does not make allowances for phase coupling, a direct transition to the case of no outer magnetic field is impossible without supplementary assumptions. According to Bohr-Heisenberg principle of spectroscopic stability, the polarization of radiation of an atom when there is no outer field is the same as when there is an outer field which does not effect the symmetery of the system. If we now assume that the principal of spectroscopic stability can be applied in individual cases for resonance scattering in three independent fluxes of radiation incident in a group of atoms, we can carry out the limit transition $H \to 0$ for the matrix in (14), also. Let us examine the incident, arbitrarily-polarized light with vector of polarization as such:[1]

$$S = (I, Q, 0, V).$$

[1] The parameter U, as above, is equal to zero because of the selection of the system of coordinates along the axis of the ellipse of polarization.

Let us expand the incident light into three independent fluxes: linearly-polarized, circularly-polarized and non-polarized radiation:

$$S = S_1 + S_2 + S_3,$$

where

$$\begin{aligned} S_1 &= (I, Q, 0, 0), \\ S_2 &= (I_2, 0, 0, V), \\ S_3 &= (I_3, 0, 0, 0). \end{aligned} \qquad (15)$$

Here

$$I_1 = \sqrt{\overline{Q^2}}; \quad I_2 = \sqrt{\overline{V^2}}; \; I_3 = I - I_1 - I_2.$$

It is obvious that, in excitation by circularly-polarized and non-polarized radiation, the axis of symmetery is the direction of the incident beam, while in excitation by linearly-polarized light, the axis of symmetery is the direction of the exciting electric vector. Having applied the matrix in (14) and the principal of spectrocopic stability individually for each of the independent fluxes in (15), having converted to the system of coordinates in which the Rayleigh scattering matrix was written, and having turned again to the Stokes parameters I, Q, U, V for the total flux, we can obtain the angular matrix of Rayleigh scattering after rather simple transformations [11].

REFERENCES

1. Unno, W.: Publ. Aston. Soc. Japan, Vol. 8, p. 108, 1956.
2. Stepanov, V.Ye.: Izv. Krymskoy Astrofiz. Obs., Vol. 19, p. 20, 1958.
3. Rachkovskiy, D.N.: Izv. Krymskoy Astrofiz. Obs., Vol. 25, p. 277, 1961.
4. Rachkovskiy, D.N.: Izv. Krymskoy Astrofiz. Obs., Vol. 26, p. 63, 1961.
5. Rachkovskiy, D.N.: Izv. Krymskoy Astrofiz. Obs., Vol. 27, p. 148, 1962.
6. Stepanov, V.Ye.: Izv. Krymskoy Astrofiz. Obs., Vol. 27, p. 140, 1962.
7. Rachkovskiy, D.N.: Izv. Krymskoy Astrofiz. Obs., Vol. 29, p. 97, 1963.
8. Hamilton, D.R.: Astrophys. J., Vol. 106, p. 457, 1947.
9. Obridko, V.N.: Astron. Zhur., Vol. 42, p. 102, 1965.
10. Rachkovskiy, D.N.: Dissertation. Leningrad, 1964.
11. Obridko, V.N.: Dissertation. Moscow, 1965.

APPLICABILITY OF THE EXISTING THEORIES OF THE FORMATION OF SPECTRAL LINES IN A MAGNETIC FIELD FOR QUANTITATIVE INTERPRETATION OF SOLAR MAGNETOGRAPH READINGS

V.N. Obridko

ABSTRACT: The authors investigate certain problems in the theory of the formation of the Fe II spectral lines (5250 Å), which is generally used in photoelectric observations of the magnetic field in active solar regions. The applicability of various theories to the calibration of magnetograph readings is evaluated, and the dependence of the obtained values of magnetic field components on the assumptions of the particular theory is examined. The theories considered include that of Unno (1956), which proposes an intrinsic-absorption mechanism of emission, and that of Stepanov (1958), which assumes a simplified scattering scheme and discontinuous absorption. It is shown that, within the limits of accuracy of the currently available magnetographs, both theories yield corresponding results and may be used equally for calibration.

The construction of the photoelectric method of observing the /71* total vector of the magnetic field in active solar regions [1-3] has brought forth increased interest in the theory of the formation of spectral absorption lines and magneto-active stellar and solar atmospheres. It has been found that, until the rather complex problem of empirical calibration is finally solved, a quantitative interpretation of magnetograph readings can be obtained only with the aid of the corresponding theory of line formation.

However, the use of the theory of line formation in which some or other proposition relative to the mechanisms of excitation and a model for the photosphere of the Sun are necessarily made in analyzing magnetograph readings can result in a systematic error. We are therefore confronted with the following question: How greatly do the values obtained for various magnetic field components depend on the assumption of the particular theory? In this study, we will not touch upon these methods of observation and analysis themselves, since they have been examined rather thoroughly [1-4]. Rather, we will examine certain problems in the theories of the formation of the Fe I spectral line (5250 Å), which is usually used in photoelectric observations, and we will discuss the applicability of these

* Numbers in the margin indicate pagination in the foreign text.

theories to calibration of the magnetograph readings. As will be seen below, all the theories give corresponding results, within the limits of accuracy of the readings from currently available magnetographs, and they can be used equally for calibration of the magnetographs.

At the present, either the theory of Unno [3] or that of Stepanov [6-9] is used for graduation of magnetograph readings. Unno's theory, which was used in [2,3] for reading the signal of the magnetograph, is rather simple and convenient for practical purposes. However, it is generally suitable only for the lines which are formed as a result of real absorption. The line Fe I (5250 Å) is usually used in measurements of the total vector. Scattering plays a substantial role in this line. Therefore, Unno's theory, generally speaking, is not applicable for this line. However, it is well known that a consideration of the scattering in calculating a line profile without a magnetic field mainly affects the central parts of the line, and it hardly changes the wings beyond the limits of the purely Doppler nucleus. Therefore, we could expect that a consideration of the scattering hardly affects calculations of the magnetograph signal for the arrangement of the slits in the wing of the line ($\Delta\lambda_1 = 0.9\ \Delta\lambda_D$, $\Delta\lambda_2 = 2.5\ \Delta\lambda_D$) (which will be confirmed in the future).

Stepanov's theory, which was used in interpreting the signals /72 from the magnetograph of the Crimean Astrophysical Observatory [1,4], takes both absorption and scattering into account. In view of the complexity of the problem, V.Ye. Stepanov introduced a number of simplyfying assumptions so that the theory he constructed was applicable for lines with any type of division. Nevertheless, the ultimate expressions for the parameters of polarization of the outgoing emission were more complicated than in Unno's theory, and it was somewhat more time-consuming to interpret the magnetograph readings. The difference between the original assumptions in Unno's and Stepanov's theories is rather great (Table 1).

TABLE 1

Author	Emission Mechanism	Model	Solution Method	Absorption Coefficient
W. Unno	Real Absorption	Miln-Eddington	Analytical	Doppler
V.Ye. Stepanov	Simplified Scattering and Discontinuous Absorption	Minart	Numerical integration according to the Method of Teberg-Harris	Doppler + Attenuation (a = 0.02)

This comparison is all the more interesting when we consider the comparison in [4] between results obtained on the basis of Stepanov's theory and values of H measured directly according to the splitting of the line on the magnetic field of the Sun. The agreement is generally rather good. However, it was found that the calculated values of H (we mean the second interval of the value, H > 1700 Oe) were 10-20% greater than those directly observed.

Let us consider how the curves for f(H) and ϕ(H) in [1] correspond with the curve in [2,3], since the solutions in [1,7] relate to the half-intensity of the continuous spectrum.

The passage of light was examined in [1] in terms of polarization optics for the case of two independent fluxes:

$$x_+ = \xi_0 \cos\beta \sin\omega t, \quad x_- = -\eta_0 \sin\beta \sin\omega t,$$
$$y_+ = \xi_0 \sin\beta \cos\omega t, \quad y_- = \eta_0 \cos\beta \cos\omega t.$$

It is easy to see that

$$I = \xi_0^2 + \eta_0^2, \qquad Q = (\xi_0^2 - \eta_0^2)\cos 2\beta,$$
$$V = (\xi_0^2 - \eta_0^2)\sin 2\beta, \quad U = 0.$$

Here the Stokes parameters I,Q,V and U were recorded for the total emission, and they corresponded completely to the parameters we used in [2,3].

Using the formulas of (23)-(28) in [1], we find that

$$\cos\psi f^c(H) = \int_{v_1}^{v_2} \frac{(r_+ - r_-)(s_1 - s_2)\cos\psi\, dv}{\sqrt{\frac{1}{4}(2s_0 - s_1 - s_2)^2 \sin^4\psi + (s_1 - s_2)^2 \cos^2\psi}} =$$
$$= \int_{v_1}^{v_2} (r_+ - r_-)\sin 2\beta\, dv = \frac{2}{I_0}\int_{v_1}^{v_2} (\xi_0^2 - \eta_0^2)\sin 2\beta\, dv =$$
$$= \frac{2}{I_0}\int_{v_1}^{v_2} Q\, dv \approx -2\cos\psi f_1^c(H).$$

The latter equality is approximative, since in calculating the calibration functions $f_1(H)$ and $f_2(H)$ [1], we divided the measured Stokes parameters by the intensity of the line $I = \int_{v_1}^{v_2} (1 - r_1)dv$, /73

[1] For a definition and calculation of the functions $f_1(H)$ and $f_2(H)$, see [2,3,10], and for the functions $f^c(H)$ and $\phi^c(H)$ see [1,4].

and not be the intensity of the continuous spectrum I_0. This division has great physical meaning, since it is this relationship which determines the degree of polarization of the line radiation. However, both relationships practically coincide for the slits we selected, since

$$\int_{\nu_1}^{\nu_2}(1-r_I)\,d\nu \approx I_0$$

with accuracy up to 10%. In a similar way,

$$\sin^2\psi\varphi(H) \approx -2\sin^2\psi f_2^c(H).$$

Thus

$$|f_1^c(H)| = \frac{1}{2}f(H),$$
$$|f_2^c(H)| = \frac{1}{2}\varphi(H).$$

The difference of a factor of 2, which was obtained from the fact that the curves in [1] were plotted to the half-intensity of the continuous spectrum, does not have significance, since it is automatically taken into accound in calibration.

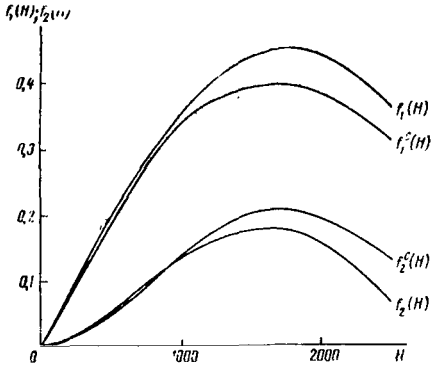

Fig. 1. Comparison of the Functions $f_1(H)$ and $f_2(H)$ Calculated According to Unno's Theory to the Corresponding Function $f_1^c(H)$ and $f_2^c(H)$ Calculated According to Stepanov's Theory.

The curves for $|f_1^c(H)|$, $|f_2^c(H)|$, $f_1(H)$ and $f_2(H)$ are shown together in Fig. 1. It can be seen that there is a certain difference between both systems. In addition to the reasons named above, which arise as a result of the difference in theories (a disregard of the attenuation can have a particularly great effect for high values of H), two more circumstances can affect a discrepancy in the curves:

(1) In calculating the functions, we should have taken into account the possibility of a change in I independent of H, despite the small value of this change, while in [1], the curves related to a constant value of I_0;

(2) We considered that for large fields $f_1(H,\psi)$ and $f_2(H,\psi)$ depend more greatly on ψ, and we took the average value (see [3, 10]), while in [1] f(H) was calculated for $\psi = 0$, and $\phi(H)$ was calculated for $\psi = 90°$.

In order to find the effect of this discrepancy, we carried out a complete analysis of a number of observations according to both theories. The results obtained are illustrated in Table 2, where H_u and ψ_u are parameters calculated according to Unno's theory, and H_c and ψ_c are calculated according to Stepanov's theory.

It can be seen that there is a certain systematic difference which exists between both groups of values for H and ψ. However, this difference does not exceed the errors in the observation up to H $\sim$ 1700 Oe. For H > 1700 Oc, H_c is roughly 10% greater than H_u. The values of ψ_u for H > 1700 Oe, 30° $\leq \psi \leq$ 60° are roughly 5° greater than ψ_c.

TABLE 2

/74

H_u, Oe	H_c, Oe	$H_u - H_c$, Oe	ψ_u	ψ_c	$\psi_u - \psi_c$	H_u, Oe	H_c, Oe	$H_u - H_c$, Oe	ψ_u	ψ_c	$\psi_u - \psi_c$
220	237	—17	55°	58°	—3°	1200	1100	100	59	58	1
320	330	—10	35	41	—6	1300	1260	40	31	30	1
410	400	10	50	52	—2	1700	1500	200	34	27	7
670	652	18	38	38	0	1700	1900	—200	34	26	8
770	748	22	45	47	—2	1700	1300	400	65	61	4
880	832	48	52	51	11	1700	2100	—400	65	60	5
900	866	34	38	38	0	2000	2300	—300	63	58	5
920	880	40	82	81	1	2120	2200	— 80	35	27	8
1070	1040	30	33	34	—1	2200	2400	—200	61	55	6
1070	1000	70	57	55	2	2230	2500	—270	83	81	2
1100	1080	20	19	17	2						

Thus, despite the great differences in the original assumptions, the discrepancy in the results is rather small, which indicates a weak dependence of the results obtained on the theory assumed.

A.B. Severnyy [11,12] made an extremely interesting attempt at calibrating a total-vector magnetograph without using any theory for line formation[2]. The calibration curves he obtained differ greatly from those presented in Fig. 1. Since, as will be shown

[2] I would like to express my deep appreciation to A.B. Severnyy, who sent me the studies before they were published.

below, the different theories for formation of the lines in a homogeneous magnetic field yield results which are similar to those presented in Fig. 1, this difference could possibly be linked with a great discontinuity in the fields and in the active region or with depolarization of the emission.

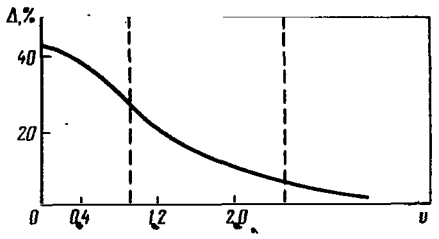

Fig. 2. Difference of Parameter Q for a Line with Split Upper Level on Unno's Solution ($v = \Delta\lambda/\Delta\lambda_D$).

However, the equations of V.Ye. Stepanov [7] did not take the scattering into account very precisely. A scattering matrix for a line with a type of splitting similar to that of Fe I (5250 Å) was derived more precisely by Stepanov's method in [9,13], and a solution to the system of equations in a continuous magnetic field was obtained for the model of Miln-Eddington by Chandrasekar's method [14]. A comparison of the solution of [14] to that of Unno for H = 1000 Oe is shown in Fig. 2. The value Δ which shows the percentage of the difference in the Stoke's parameter Q and the solutions in [14] or Unno's solutions is shown here:

$$\Delta = \frac{Q_{[14]} - Q_{[5]}}{Q_{[14]}} \%.$$

It can be seen from the figure that Unno's solution in the vicinity of the line center deviates substantially from that obtained in [14]. However, the difference is less in the wings. The closeness of the profiles obtained according to Unno's theory and those calculated in [14] is preserved, naturally, only in the neighborhood of the center of the disk. This solution tends toward zero in approaching the edge, while that obtained in [14] changes little. /75
We should mention that, in photoelectric measurements, the emissions from a rather wide segment of the line wing entered on the output slit of the magnetograph (the boundaries of the slit we used are designated in Fig. 2 by the dashed line). Therefore, those segments of the wing of the line in which the value of Δ is small yields a great contribution because of integration over a wide slit. It is easy to find that at H = 1000 Oe, the signal calculated according to the formulas presented in [14] is greater than the signal obtained according to Unno's solution, by 10% in all.

Thus, considering the weak dependence of the solution obtained in [14] on μ, we can use Unno's solution for $\mu = 1$ in interpreting observations of the total vector in the latter part of the solar disk, as was done in [2,3]. In this case, the errors are obviously small.

A solution to the equations of transfer which makes allowance

for scattering was also obtained for lines with other types of schemes ($j_n = 1$, $j_b = 0$) [10,15]. For the sake of a comparison,

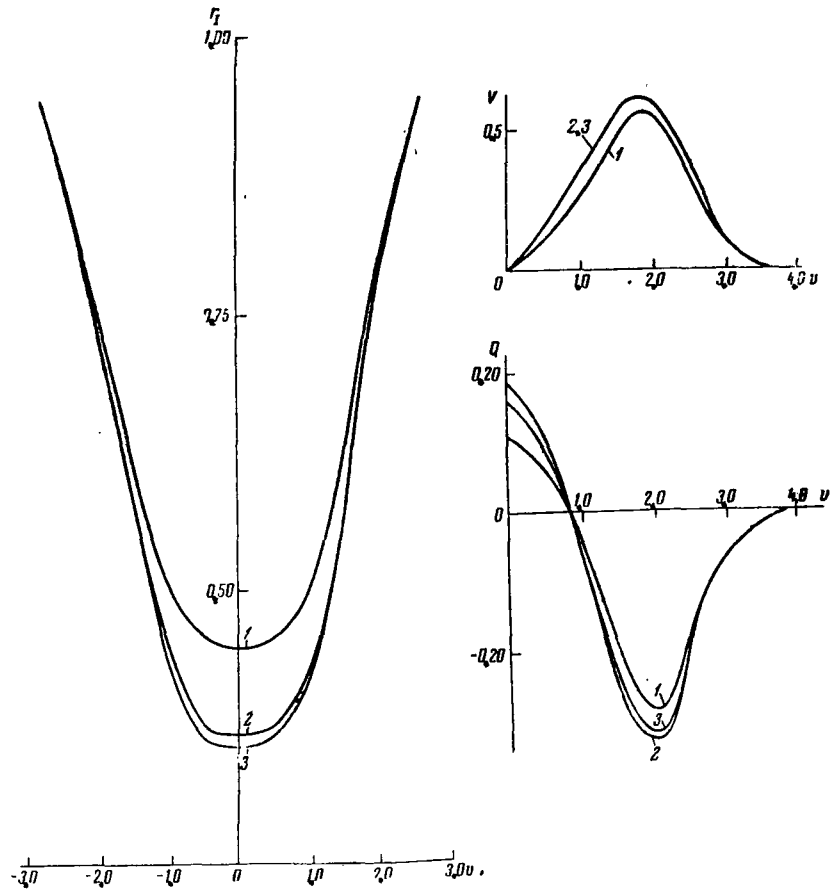

Fig. 3. Comparison of Stoke's Parameters R_I(a), V(b) and Q(c) for Unno's Solution (1), for a Line With a Split Upper (2) or Lower (3) Level ($v = \Delta\lambda/\Delta\lambda_D$).

we calculated the Stokes parameters for the lines formed as a result of real absorption (Unno's solution), a line with a split upper lever [14] and a line with a split lower lever [10,15]. Figure 3 shows a profile of the line r_I and the dependence of Q(v) and V(v) for three cases (H = 1000 Oe, $\cos\psi = 0.58$).

As can be seen from Fig. 3, the profile of the r_I line does not depend on the theory used for scattering, and it coincides for both types of splitting. The deviation from Unno's solution is greatest at the center, and it decreases rather rapidly towards the wings. Even for v = 0.8, we can consider that Unno's solution practically coincides with that which considers the scattering.

The Stokes parameters Q and V for both solutions which take

the scattering into accound are very close.

Figure 4 shows the values of

$$\Delta_Q = \frac{Q_1 - Q_0}{Q_1}; \quad \Delta_V = \frac{V_1 - V_0}{V_1},$$

where the subscripts 1 and 0 signify that the upper or lower lever, respectively, is divided. The solutions differ only by a small percentage in the range where $0.9 \leq v \leq 2.5$. Thus, it is found that, within the limits of accuracy of our investigation (Chandrasekar's approximation), the parameters for line polarization depend weakly on the scattering model.

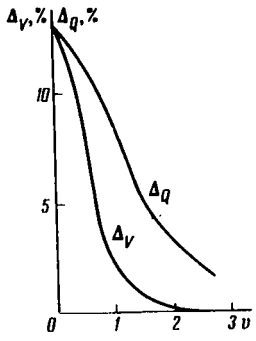

Fig. 4. Difference Between Solutions for Lines with Split Upper and Lower Levels. The Value Δ_V Shows the Difference in the Parameter V, and the Value Δ_Q Shows the Difference in the Parameter Q.

We can show that this result (closeness of the solutions for both very simple types of splitting in the wing of the line) are also preserved for a precise solution. The equations of transfer for both types of splitting differ only in the type of scattering matrix. For observations in the wing of the line ($v \sim 1.7$) and not-too-small fields ($v_H \sim 1.0$), the matrices coincide and the systems of transfer equations for both types of splitting are identical. The closeness of the solutions is even more precise when the values of v and v_H are greater, i.e., when the slit is further in the wing of the line and when the magnetic division of the line is greater.

D.N. Rachakovskiy [16] also found that a solution which makes allowance for scattering for a line with a split lower level, Stepanov's solution and Unno's solution are identically applicable for calibrations of magnetograph readings in observations in the central part of the disk ($1.0 \geq \mu \geq 0.7$) in a proper selection of the slits in the wing of the line.

Thus, a comparison of Unno's solution [5], Stepanov's solution [6,7] and more precise solutions for lines with split upper [13,14] and split lower levels [15,16,10] shows that, within the limits of accuracy for the observations, all these theories can be used for a quantitative interpretation of the total-vector readings from the currently available magnetographs. However, we should mention again that all these theories do not take into account the possible discontinuity in the fields and the polarization of the emission; moreover, the total or partial rearrangement of atoms along the Zeeman sublevels which is due to collisions is not taken into account in the comparison. The problem of the causes

for the differences between theoretical and empirical calibrations by A.B. Severniy [11,12] also remains open.

REFERENCES

1. Stepanov, V.Ye. and A.B. Severnyy: Izv. Krymskoy Astrofiz. Obs., Vol. 28, p. 166, 1962.
2. Joshpa, B.A. and V.N. Obridko: Geomagnetizm i Aeronomiya, Vol. 4, p. 17, 1964.
3. Joshpa, B.A. and V.N. Obridko: Sb.: Solnechnaya aktivnost' (Collection: Solar Activity), No. 2. "Nauka", 1965.
4. Stepanov, V.Ye. and S.I. Gopasyuk: Izv. Krymskoy Astrofiz. Obs., Vol. 28, p. 194, 1962.
5. Unno, W.: Publ. Astron. Soc. Japan, Vol. 8, p. 108, 1956.
6. Stepanov, V.Ye.: Izv. Krymskoy Astrofiz. Obs., Vol. 18, p. 136, 1958.
7. Stepanov, V.Ye.: Izv. Krymskoy Astrofiz. Obs., Vol. 19, p. 20, 1958.
8. Stepanov, V.Ye.: Izv. Krymskoy Astrofiz. Obs., Vol. 24, p. 293, 1960.
9. Stepanov, V.Ye.: Izv. Krymskoy Astrofiz. Obs., Vol. 27, p. 140, 1962.
10. Obridko, V.N.: Dissertation. Moscow, 1965.
11. Severnyy, A.B.: Izv. Krymskoy Astrofiz. Obs., Vol. 33, p. 34, 1965.
12. Severnyy, A.B.: Izv. Krymskoy Astrofiz. Obs., Vol. 36, p. 22, 1967.
13. Obridko, V.N.: Astron. Zhur., Vol. 42, p. 102, 1965.
14. Obridko, V.N.: Astron. Zhur., Vol. 42, p. 502, 1965.
15. Rachkovskiy, D.N.: Izv. Krymskoy Astrofiz. Obs., Vol. 29, p. 97, 1963.
16. Rachkovskiy, D.N.: Izv. Krymskoy Astrofiz. Obs., Vol. 33, p. 111, 1965.

FACULA STRUCTURE

M. A. Livshits

ABSTRACT: The values obtained for facula contrast (the ratio of the facula emission intensity to that of the undisturbed chromoshpere) are compared to those obtained by photoheliograms and by spectral observations. The classical measurements of Richardson (1933) were repeated by using modern photographs of the photosphere in the blue region of the spectrum for the same values of θ (the angle between the normal to the surface and the line of sight. A comparison of the results with those obtained by spectral measurements confirmed the accuracy of the values for the facula contrast. The obtained dependence of the contrast on the angle θ is used to construct a model of the facula with the aid of a numerical method. It is shown that the integral emission of the facula filaments exceeds that of the photosphere by 2-3%.

The emission in a continuous spectrum is the basic source of /78* information on the undisturbed photosphere as well as on its active regions - the photospheric facula. There is often observed a relationship between the facula emission intensity and that of the undisturbed photosphere, the so-called facula contrast. The temperature and pressure distribution in the facula is derived from the dependence of the contrast at a given wavelength on the position of the facula on the disk of the Sun ($\gamma(\theta) = I_{fac}(\theta)/I_{ph}(\theta)$, where θ is the angle between the normal to the surface and the line of sight).

The contrast of faculae are measured according to direct photographs of the solar photosphere and by the spectral method. The advantage of the first method is seen in the fact that the entire facula is visible on a photoheliogram. For sufficient resolution, we can select the characteristic detail of the facula on the photograph and measure its contrast. However, in observations in a wide spectral region it is always unclear to what extent the measured values are distorted by the effect of the absorption lines. This necessitates measurements according to selected spectra in this region which are free of absorption lines.

The segment of the image of the photosphere which is cut off by the input slit of the spectragraph is studied in the spectral

* Numbers in the margin indicate pagination in the foreign text.

method. A selection of this segment, which is carried out directly during the observation, often amounts to a search for and obtainment of the spectrum of the brightest details of a facula. Moreover, it is difficult to discuss to what degree the photosphere next to the facula - that background in relation to which the facula is studied is disturbed according to the spectrum of an aciive region. These two factors bring about a lesser reliability in the data obtained by this method.

Some spectral observations [1,2] confirm the "classic" measurements of R.S. Richardson [3], which were carried out according to the photoheliograms of the Mount Wilson Observatory in 1925-1929 (λ_{eff} = 4330 and 5780 Å), and others result in greatly higher values for the contrast [4, 5]. In this study, we are repeating the classic measurements by using modern photographs of the photosphere for the blue part of the spectrum and for the range of values of θ used [3], where the same results were obtained. The values of the contrasts γ decrease at the edge of the disk for $\sin\theta > 0.95$, which was first mentioned in [6].

Obviously, our comparison with the results of spectral observations shows that it is these values which characterize the emission intensity of facula filaments. The dependence of $\gamma(\theta)$ obtained is used for constructing a model of a facula by a numerical method (the previous method, or a presentation of the observations in the form of a polynomial [7, 2], is used as a first approximation). In the solution obtained, there is rapid equalizing of the conditions in the facula and the photosphere above the level τ = 0.3 as a direct result of the decrease in the facula contrast at the edge of the disk; at $\tau \to 0$, the temperature $\Delta T = T_{fac} - T_{ph}$ is several tens of degrees. /79

Determination of Facula Contrast According to Photoheliograms

In studying the faculae, we used four photoheliograms of the Ussuriysk Astronimal Station which were presented to us by V.S. Chistyakov. The photospheric photographs were obtained on an AFR-3 standard chromospheric telescope with exposure of about 1/100 sec. The diameter of the image of the Sun was 74 mm. We used non-sensitized Agfa printing plates without light filters. The investigations showed that the effective wavelength $\lambda_{eff} \approx 4350$ Å and the penetration band width was on the order of 600 Å. The value of λ_{eff} was also confirmed by the fact that the decrease in intensity measured according to the photoheliograms under investigation during the transfer from the center to the edge coincided with the rim darkening for λ = 4400 Å ($\pm$ 150 Å). The calibration of the plates was reliable, since the center of the Sun was imprinted on each of them with two exposures through a 9-stage reducer, together with the image of the photosphere. The clear visibility of the single-second granulation and structural details of the half-shadow of these spots indicated the high resolution of the photoheliograms obtained at the

Ussuriysk Station.

The contrasts of 40 individual filaments of the faculae were measured on an MF-2 microphotometer. The slit of the microphotometer varied for individual sections, but it was always rather large, since it was the filaments of the facula which were measured, and not individual bright granules in them. The results obtained are given in Fig. 1. and below (values for cos θ = 1.0 and 0.1, results of certain extrapolation).

$\cos\theta$	1,0	0,9	0,8	0,7	0,6	0,5	0,4	0,33	0,3	0,2	0,1
$(\gamma-1)$, % . . .	3	3	4	6	9	12	16	17,5	17	12	8

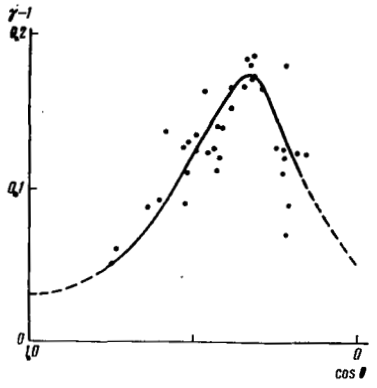

Fig. 1. Contrast of Facula Filaments. Dependence of $(I_{fac} - I_{ph})/I_{ph}$ on cos θ.

The following circumstance was of note. Two plates, one of which was exposed one day after the other, were analyzed. The same facula filaments were measured on both plates, although they had changed their position on the solar disk to some extent. It was found that the contrast of the corresponding filaments seemed to move along a line similar to the curve in Fig. 1.

The results obtained agree well with Richardson's observations [3]. Moreover, they supplement them to a great extent, since a decrease of I_{fac}/I_{ph} around the edge of the solar disk (for cos θ < 0.3) was clearly seen according to our measurements (see also [6]).

The measured values are the ratios between the intensities of the filaments and the backgrounds between them, which can differ somewhat from those of the undisturbed photosphere. Naturally, it is insufficient to have four photoheliograms with a small image of the Sun in order to investigate this difference in detail. However, since the ratio of the emission intensity of the background between the filaments to that of the undisturbed photosphere was measured directly in the photometric sections, we will present the average values for all four plates: /80

cos	0,1	0,2	0,3	>0,3
Relative exceeding of the background between filaments over the photosphere, %	9	5	2,5	<2
Accuracy, %	±2	±1	±1	—

The intensification of the brightness of the background between

filaments observed at the very edge of the disk can be explained, for example, by the fact that the entire active region is somewhat above the undisturbed photosphere. A less probable explanation is that, in measurements with cos θ = 0.1-0.2, the emission of very small, insoluble filaments was mistaken for the emission of the background between filaments to a great extent. A further investigation of the background between filaments is very interesting. However, the brightness intensification obtained in this study will not be considered. High reliability of the values obtained for γ is excluded precisely because of the simplicity of the method. Qualitatively, the nature of the dependence $\gamma(\theta)$ follows from the investigation of the photoheliograms we carried out for roughly 10 years (materials of the Sun Investigation Surface of IZMIRAN). For an example and for a clarification of the quantitative characteristics, we measured four of the best photographs we had at our disposal. The relative measurements guaranteed sufficient precision, and the possible errors resulting from the effect of scattered light or shaking of the image could not change the value $(\gamma-1)$ substantially, for example, by a factor of 1.5. This conclusion follows from the evaluation which took into account rather large dimensions, rather small differences in brightnesses (the saattered light was affected for observations of spots, for a difference in brightness of a factor of 2-3) and exposures of $\lesssim$ 0.01 sec.

Another aspect of the question is whether or not the values of $\gamma(\theta)$ reflect the real relationship of the emission intensities at a fixed wavelength of a continuous spectrum, and whether or not those objects to which these values were plotted actually exist on the Sun. In other words, we must find whether or not the measured values are greatly distorted due to the effect of the absorption lines, and to what extent the physical difference of faculae themselves and their granulation structure are substantial. In a transition from the photosphere to a facula, the absorption lines (excluding H and K Ca^+ and Hα) change insignigicantly and the energy in the lines is a small percentage of the flux of continuous emission. Therefore, we can assume a priori that the effect of the absorption lines is not substantial for the relative measurements.

Facula fields, which sometimes cover rather large areas of the solar surface, consist of individual filaments. The brightness of these filaments depends on the developmental phase of the corresponding center of activity. Directly before the arrival of spots, near developing spots, and in flare-up activity of a group of spots, a facula is anomolously bright. On the other hand, the process of aging of an activity center, which lasts up to one year, is linked with a gradual extinction of the facula. The evolution of the facula itself in combination with the difference in observational conditions also can explain the fluctuations in the measured values. However, the stable phase of the developed facula lasts for a rather long time, and this permits us to isolate and measure the contrast of a "typical" filament. In the vicinity of the minimum activity on the solar surface, there is rather large number of weak faculae,

and therefore the curve in Fig. 1 is an envelope of the values of γ for these formations. The facula filaments with $\gamma_{4300} > 1.20$ are found rather rarely and, as a rule, are connected with extremely high activity in the region. I measured two spectra of a facula at the edge of the disk (No. 7, 8 B [2]) with $\gamma_{4200} = 1.20 - 1.25$. However, a further comparison showed that at the moment the spectra of the faculae were obtained in this region there was an intensive /81 emission of the yellow coronal line; a number of weak flares took place. It should be mentioned that the spectrum of such "anomolous" faculae shows a significant increase of γ with a decrease in the wavelength (up to $\gamma = 1.30 - 1.35$ for $\lambda = 3400$ Å).

For the best resolution, the faculae filaments can be divided into a number of bright granules. The shape of the filament is usually preserved for several days. However, the granules in them change rapidly. Naturally, we could attempt even now to construct models for facular granules and the space between them individually. However, the insufficient amount of observational data makes sucha procedure extremely unreliable. Moreover, the "average" law of darkening of the solar disk towards the edge and the "average" model of the photosphere will be used subsequently; theyare essentially unknown for hot and cold regions separately. A study is carried out by way of a comparison with these laws, which already contain an averaging over elements of different temperatures. The discontinuity of facula filaments is only somewhat greater than the discontinuity of the undisturbed photosphere. Therefore, it would be intelligent to limit ourselves to an investigation of the filament on the whole. In the observations, it is necessary to consider the difference in structural elements, since the increase in the brightness of individual facular granules is roughly twice greater than the values of γ-1 for the filaments (for the granules, according to V.A. Krat [8], $\gamma_{max} = 1.30 - 1.40$).

The spectral observations I carried out in 1960 [2] for several filaments of faculae merely indicate that at $\cos\theta = 0.4 - 0.5$ the contrast $\gamma \approx 1.13$ for $\gamma = 4200$ Å. This agrees with the results obtained according to the photoheliograms. V. D. Kuz'minykh [4, 5] reduced a large number of spectral determinations to maximum values of γ (for $\cos\theta = 0.5$) from 1.26 in the green to 1.36 in the blue part of the spectrum. According to [4, 5], a facula in the center of the disk is roughly 10% brighter than the photosphere. Obviously, such values are characteristic of bright facula granules. One observation from an aerostat [9], which led to very high values of $\gamma > 1.60$ at the very edge of the disk ($\cos\theta < 0.17$) and which was extrapolated in an arbitrary manner over the entire disk, was also disregarded in this study. If even the photometric investigation in the unique experiment was carried out correctly, then the values for the contrast relate to individual granules with dimensions of < 1". It was shown in our study [10] that the upper limit to values for the contrast in filaments of a facula is determined by the possible oscillations of the solar constant during an 11-year cycle.

Thus, there are no serious reasons why we should consider that the brightness of the facula filament obtained according to direct photographs of the Sun are greatly lowered. Using Fig. 1 and the spectral data in [2], it is easy to show [10] that the integral emission flux of a facula filament exceeds that of the photosphere by roughly 3%. This value is sensitive to the brightness of faculae near the center of the disk: for strict "invisibility" of faculae at the center $\gamma(1) = 1.00$, it decreases by as much as 2% $\pi F_{\odot}$. The values in the region of the maximum contrast and at the edge of the disk have a greater effect on the structure of the facula.

Constructing a Model of a Facula

The values obtained above characterize the emission of a facula coming at different angles relative to the normal to its surface. The temperature distribution related to the depths could be derived from such data by the optic method.

It is well known that, when Kirchoff's law is fulfilled, the intensity of the outgoing emission is determined as

$$I_\lambda(0, \mu) = \int_0^\infty B_\lambda(T) e^{-\tau_\lambda/\mu} \frac{d\tau_\lambda}{\mu}, \qquad (1)$$

where $B_\lambda(T)$ is the Planck function of the emission and $\mu = \cos\theta$. /82
When $I_\lambda(0, \mu)$ and the absorption coefficient κ_λ determined by τ_λ are known, (1) can be considered as an integral equation relative to $B_\lambda(T)$. It is expedient not to solve this equation separately for the facula and the photosphere, but rather to use a different method, since, first of all, the physical conditions in the facula and photosphere differ insignificantly ($\Delta T_{max}/T \sim 0.05$) and, second of all, our observations of the facula contrasts were essentially relative ones. Therefore, it is natural to draw conclusions concerning the difference in conditions in the facula and photosphere from them.

If we write out Equations of the type in (1) for the facula and the photosphere, and take their difference, then an integral equation of the same type is obtained as a result:

$$\widetilde{\Delta I} = \frac{I_{\lambda\mathrm{fac}} - I_{\lambda\mathrm{ph}}}{I_\lambda(0, 1)} = \alpha(\gamma - 1) = \frac{1}{I_\lambda(0, 1)} \int_0^\infty (B_{\lambda\mathrm{fac}} - B_{\lambda\mathrm{ph}}) e^{-\tau_\lambda/\mu} \frac{d\tau_\lambda}{\mu} = \int_0^\infty \widetilde{\Delta B} e^{-\tau_\lambda/\mu} \frac{d\tau_\lambda}{\mu}. \qquad (2)$$

It can be seen that $\widetilde{\Delta I}$ is a derivative of the opacity of the solar disk toward the edge α for the observed contrast of the faculae $(\gamma-1)$.

A solution to (2) is found by way of representing the observed

values of $\widetilde{\Delta I}$ in the following way in first approximation:

$$\widetilde{\Delta I} = a + b\mu + 2c\mu^2 + 6d\mu^3. \qquad (3)$$

This form of $\widetilde{\Delta I}$ corresponds to the following solution:

$$\widetilde{\Delta B} = a + b\tau + c\tau^2 + d\tau^3. \qquad (4)$$

A solution to (2) is then reduced to the problem of finding the coefficients a, b, c and d according to the method of least squares. However, the coefficient a is indefinite, since α and γ are unknown for the solar disk itself ($\mu < 0.15$). The value of a and b are estimated by assuming, for example, that $\Delta T(0) \approx 100°$.

We composed and solved a system of 14 equations with 3 unknowns b, c, and d and obtained the following solution to the system:

$$b = 0{,}329,$$
$$c = -0{,}260,$$
$$d = 0{,}0334.$$

However, the representation of $\widetilde{\Delta I}$ in the form of a polynomial of the third power is possible only with very high errors, such as those in [2]. This also follows from a comparison of the observed values of $\widetilde{\Delta I}$ and the representation in the form of the polynomial (Fig. 2). Therefore, the solution

$$\widetilde{\Delta B} = \frac{B_{\text{fac}}(\tau) - B_{\odot}(\tau)}{I(0,1)} = 0{,}013 + 0{,}329\tau - 0{,}260\tau^2 + 0{,}0334\tau^3 \qquad (5)$$

was used only as a first approximation. Subsequently, the function $\widetilde{\Delta B}$ was changed somewhat, and was substituted into the right-hand part of (2), and the corresponding integrals were compared to the values of $\widetilde{\Delta I}$. The value of $\widetilde{\Delta B} = \Delta B/I(0.1)$ which was obtained as a result is shown in Fig. 3. The values of ΔI which were calculated with the aid of this solution agree well with those observed (see Fig. 2), whereas the discrepancy in the vicinity of the center of the disk ($\cos\theta = 1.0$) should not be given particular significance. If the subsequent observation confirms the value for the contrast at the center of the disk as equal to 1.03, then it is necessary to /83 investigate the temperature distribution in deep layers of the facula ($\tau > 4$) in greater detail.

The characteristic feature of the solution obtained is the abrupt decrease in ΔB during the transition to $\tau \lesssim 0.3$. This drop in ΔB is determined by the decrease in the contrasts of the faculae at the edge of the disk for $\cos\theta < 0.33$.[1]

[1] Since the model of the photosphere has still not been used, this conclusion does not depend on tis selections.

Physically speaking, this means that the region of highest temperatures in a facula, compared to the photosphere, is not above the

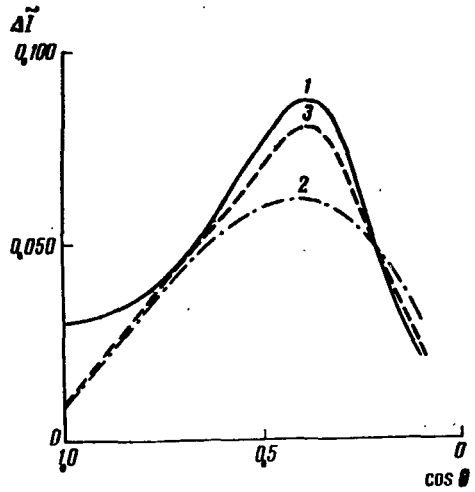

Fig. 2. Comparison of Observed Values of $\widetilde{\Delta I}$ (1) to Their Representation in the Form of a Polynomial of the Third Power (2) and to those Calculated According to the Precise Solution (3).

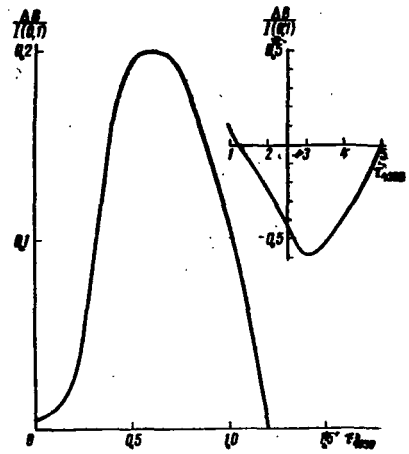

Fig. 3. Dependence of the $\widetilde{\Delta B} = \dfrac{B_{fac}(\tau) - B_{ph}(\tau)}{I\ (0.1)}$ on the Optical Thickness τ.

level τ = .3.

In calculating the model for a facula, let us use, in addition to $\widetilde{\Delta B}$, the values of I_λ (0.1) according to [11], the absorption coefficient according to Vitense [12] and the model of the undisturbed photosphere in [13].

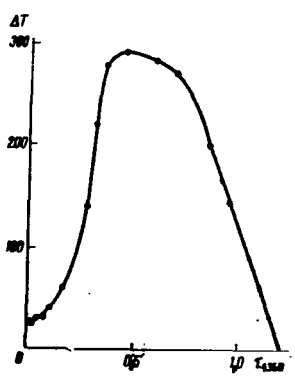

Fig. 4. Difference in Temperatures $\Delta T = T_{fac}(\tau) - T_{ph}(\tau)$.

The calculated temperature differences $\Delta T(\tau) = T_{fac}(\tau) - T_{ph}(\tau)$ are shown in Fig. 4. In the range where $0.35 < \tau < 0.7$, the exceeding of the temperature of the facula over that of the photosphere is somewhat less than 300°. For small optical thicknesses, the temperature of the facula differs by several tens of degrees in all. This fact agrees well with the observations of the lines of the CO molecule in the facula presented in [14]. It was found that the equivalent width W of the CO lines in the facula was 10% less than that in the undisturbed photosphere. The obtained value limits the maximum heating of the surface layers of the facula to several tens of degrees. The region with $\tau > 1.2$, which is not shown in Fig. 4, is characterized by the following values:

τ_{4350} . .	1,6	3	5
ΔT . . .	—100°	—400°	0°

The dependence ΔT (τ) in combination with the known structure of the undisturbed photosphere permits us to calculate a model of the facula in full. The electron pressure is taken according to the tables by Rosa in [15]. At levels with the same optical thickness in the facula and photosphere, the gas pressure is found to be identical, just as in [7]; the heights of these levels differ only insignificantly. This is understandable, since the absorption coefficient changes very insignificantly at these levels during a transition from the facula to the photosphere (the effect on κ_λ, for example, in the upper layers of the increase of T is compensated by the increase of P_e). We should mention that it was assumed in the calculations that the zero-points of the heights in the facula and the photosphere coincide. The appearance of the active lower chromosphere shows that the facula is obviously above the undisturbed photosphere and that the shift of the zero-points is comparable to the photospheric scale of the heights. However, this difference is not significant in this study. The model obtained is presented in the tables. /84

TABLE

τ_{5000}	$\bar{\tau}$	$\log P_g$	T_{ph}	ΔT	T_{fac}	$\log P_e$		h,km	
						ph	fac	ph	fac
0.010	0.013	4.00	4430	25	4455	0.03	0.05	41	39
0.024	0.025	4.20	4600	25	4625	0.27	0.28	83	81
0.056	0.050	4.40	4840	30	4870	0.58	0.60	126	122
0.087	0.076	4.50	5000	30	5030	0.70	0.72	149	145
0.12	0.11	4.60	5160	40	5200	0.77	0.79	172	168
0.18	0.17	4.70	5370	60	5430	0.96	0.98	197	193
0.30	0.30	4.80	5680	140	5820	1.21	1.31	222	215
0.40	0.41	4.85	5910	290	6200	1.32	1.48	236	227
0.50	0.52	4.90	6140	280	6420	1.54	1.71	250	238
1.02	1.08	5.00	6760	145	6905	2.09	2.15	280	265
1.74	1.89	5.05	7380	-100	7280	2.47	2.40	296	284
3.2	4.3	5.10	8100	-400	7700	2.83	2.62	314	309
6.8	8.7		8450		8450			333	328
10.0	12.5		8550		8550			342	337

We should note immediately the limits to applicability of the results obtained. The model of a facula filament presented in the table was derived from observations in only one (blue) region of the spectrum. This model can satisfy the observations of the facula in other spectral regions only approximately. Let us evaluate to what degree it is necessary to obtain a model such that it describes observations at all wavelengths in a roughly identical manner. For this purpose, we will calculate the difference in the outgoing integral fluxes of emission of the facula and the undisturbed photosphere, using the temperature distribution in them (see Table). The difference in fluxes at the level $\bar{\tau} = 0$ is given by the follow-

ing formula:

$$\Delta F(0) = \int_0^\infty \Delta B(t)\, Ei_2(t)\, dt, \qquad (6)$$

where $\Delta B(t) = (\sigma/\pi)(T_{fac}^4 - T_{ph}^4)$, σ is the Stefan-Boltzmann constant, and the Euler function Ei_2 is expressed in terms of the exponential integral function Ei, as $Ei_2(t) = e^{-t} - tEi(t)$. The integral in (6) was calculated numerically, whereas the peculiarities of the Euler function at the point t = 0 could be disregarded by assuming that $\Delta B = 0$ at $\bar{\tau} = t \to 0$. We should mention that the evaluation is presented within the framework of the theory of radial energy transfer and that the selection of the model for the photosphere is essential for it, since $\Delta B \propto T^3 \Delta T \approx T_{ph}^3 (T_{fac} - T_{ph})$.

It was found as a result of the calculations that $\Delta F(0) \approx 1.7 \cdot 10^9$ erg/cm^2·sec·stere, or more than 8% of the photospheric flux. It was shown above that, according to our observations, the outgoing integral flux of facula emission exceeds the photospheric flux by no more than 3%. The discrepancy between the value obtained according to the model and that observed can be explained in two ways. First of all, the observations of the facula contrast, in the blue part of the spectrum always are reduced to a model with greater expanse of the region in which $T_{fac} > T_{ph}$ [2,7]. Secondly, the values for the temperatures are relatively high in the model we used for the photosphere. The value calculated according to (6) coincides with that observed if we use the following model for the facula within the framework of the same structure of the photosphere: $T_{fac} = T_{ph}$ at $\bar{\tau} = 1.0$, and not 1.3; around $\bar{\tau} = 0.3$, max $\Delta T = 200°$, and in the range of high values of $\bar{\tau}$, it is possible that $\Delta T = -200°$ and $-600°$ at $\bar{\tau} = 1.9$ and 4, respectively. If we use the model of the undisturbed photosphere presented in [16], the difference in the facula models obtained according to measurements of the facula contrast and from a comparison of the integral emission fluxes will be much less. On the whole, the evaluation presented indicates the nature of the change from the model previously obtained for a facula filament, and it aids us in explaining the observations of different spectral regions. /85

The investigation of the vibrational and supergranulation movements which was carried out recently again emphasized the link between phenomena in the solar atmosphere and processes at two "upper levels" (or in two scales) of the convective zone. This connection underlies the hypothesis presented by S. B. Pikel'ner [17] concerning the intensification of convection as a mechanism for the formation of active regions. According to [17], a weak magnetic field of a facula decreases the mean free path and velocity of turbulence pulsations. Since under the conditions of solar convection the friction between fluxes is determined by the turbulent viscosity, it decreases. As a result of this, the rate of convection increases. The decrease of the temperature gradient caused by intensification

of large-scale movements involving a substantial amount of energy can be explained qualitatively in terms of the facula.

The conclusions obtained above can serve as an indirect confirmation of the opinions presented in [17]. Actually, a direct result of the decrease in the facula contrast at $\cos\theta \lesssim 0.33$ is the fact that the layer of increased temperature does not go out beyond the surface, and $\tau = 0.3$ (this is assumed in [17] for weaker polar faculae). The solar granules also do not go above the level of $\tau = 0.3$, which is the result of worsening of visibility of the granulation $\cos\theta \lesssim 0.3$. This coincidence, in combination with the division of individual filaments of a facula into a number of granules, is an indirect indication of the link between these two phenomena.

The convective energy transfer predominates in the subphotospheric layers and, as elementary estimations show [2], this can be noted in the photosphere. The increase of V_{conv} by 30-50% can guarantee the necessary change in ΔT for the appearance of a facula. The arrival of an excess flux in the plane-parallel atmosphere cannot cause intensification of the convection (this was shown by C. B. Pikel'ner). However, it was shown in [10] that this value is small, 2-3% $\pi F_{\odot}$. Such an increase of energy can be expected, for example, as a result of flow through the boundary of a filament (horizontal transfer). We should also mention that the increase in the flow of acoustic disturbances which is necessary for keeping higher layers of active regions is explained in [17]. However, these completely circumstantial concepts still do not solve the problem concerning the validity of the hypothesis. A direct investigation of the movements in deep layers of the active and undisturbed photosphere is necessary.

REFERENCES

1. Ambartsumyan, V.A. and N.A. Kozyrev: Tisrk. Pulkovskoy Obs., No. 2, 1932.
2. Livshits, M.A.: Astron. Zhur., Vol. 40, p. 39, 1963.
3. Richardson, R.S.: Astrophys. J., Vol. 78, p. 359, 1933.
4. Kuz'minykh, V.D.: Astron. Zhur., Vol. 39, p. 965, 1962.
5. Kuz'minykh, V.D.: Candidate's Dissertation. State Astronomical Institute imeni P.K. Shternberg, 1963.
6. Waldmeier, M.: Z. Astrophys., Vol. 26, p. 147, 1949.
7. Reichel, M.: Z. Astrophys., Vol. 33, p. 79, 1953.
8. Krat, V.A.: Izv. GAO, No. 152, p. 1, 1954; No. 170, p. 2, 1962.
9. Rogerson, J.B.: Astrophys. J., Vol. 134, p. 331, 1961.
10. Livshits, M.A.: Sb.: Solnechnaya aktivnost' (Collection: Solar Activity), No. 2. "Nauka", 1965.
11. Sitnik, G.F.: Astron. Zhur., Vol. 42, p. 59, 1965.
12. Vitense, E.: Z. Astrophys., Vol. 28, p. 81, 1951.
13. deYager, K.: Stroyeniye i dinamika atmosfery Solntsa (Structure and Dynamics of the Solar Atmosphere). Foreign Languages Publishing House, 1962.
14. Polonskiy, V.V.: Atron, Zhur., Vol. 42, No. 4, 1965.
15. Rosa, S.: Z. Astrophys., Vol. 25, p. 1, 1948.
16. Allen, K.U.: Astrofizicheskiye velichiny (Astrophysical Magnitudes). Foreign Languages Publishing House, 1960.
17. Pikel'ner, S.B.: Astron. Zhur., Vol. 37, p. 616, 1960.

THE AREA VARIATION CURVE AND THE LIFETIME OF CHROMOSPHERIC FLARES

S.O. Obashev

ABSTRACT: The paper discusses certain characteristic peculiarities of the photometric curves for the brightness of a chromospheric flare. Ratios are obtained between the area and the duration, as well as the relaxation time, of a chromospheric flare.

Chromospheric flares are powerful energetic phenomena. Depending on their intensity, the energy emitted during their existence on the hydrogen H_α line is 10^{27} - 10^{32} erg. This energy is expended in the relatively short period of time of $(3\text{-}100)\cdot 10^2$ sec. /87*

The curve for the development of chromospheric flares has a characteristic appearance: at first, the luminosity grows abruptly against the background up to a maximum value during the course of one minute or several minutes, and then it increases, but much less rapidly. Such an appearance for the curves of the luminosity variation is the most characteristic property of all chromospheric flares without exception. The area in which the chromospheric flares develop also have the same type of curves.

Figure 1 shows graphs for the changes of $\log(I/I_{max})$ with time for a decreasing branch of the development of chromospheric flares, where I changes from I_{max}, and t is read off from the point I_{max}.

As can be seen from the graph, the subsidence of the luminosity of chromospheric flares can be characterized in first approximation by a linear function of the following type:

$$-\log\frac{I}{I_{max}} = kt. \qquad (1)$$

The value of $k \leq 0.025$ [1] also changes in dependence on the power of the phenomenon.

The change in the luminosity of chromospheric flares on the hydrogen line [2] can be the result of the following: (a) processes of intensified recombinations linked with increased hydrogen ionization; (b) processes of excited atoms caused by a possible increase in electron temperature.

---

* Numbers in the margin indicate pagination in the foreign text.

Let us assume that the principal sources of emission in the H_α line is recombination. The emission in the decreasing branch for the development of chromospheric flares will thus weaken because of the decrease in the density of gas ionization, i.e.,

$$dn_e/dt = -c(T)\,n_e^2.$$

Having integrated this expression, we have the following:

$$\frac{n_0}{n} = \left[1 + \frac{t}{n_0 c(T)}\right]$$

Assuming that $I \propto n_e^2$, we find that

$$-\log\frac{I}{I_{\max}} = 2\lg\left[1 + \frac{t}{n_0 c(T)}\right], \qquad (2)$$

where $n_0 c$ (T) is the recombination time for the initial density of the ionized substance. This time is on the order of several seconds /88

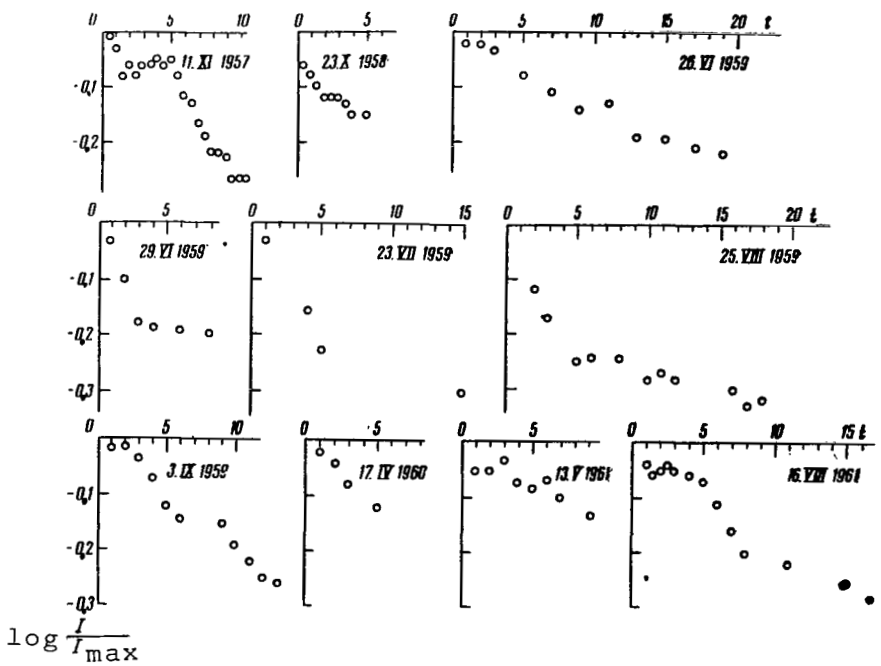

Fig. 1. Change in log I/I_{max} with Time for the Decreasing Branch of Development of Chromospheric Flares.

for the conditions which govern in chromospheric flares ($T \sim 10^4$ °K, $n_e \sim 10^{13}$ cm^{-3}).

The inclinations of the lines depicted by functions (1) and (2) do not coincide. The decrease in emission intensity due to the recombination mechanism takes place e times during the course of 1 sec, while the observed decrease in brightness takes place during the course of several minutes. The gas is cooled as a result of non-elastic collisions, which brings about a decrease in the energy of the electrons. The time for cooling (or decrease in energy by a factor of e) is hundredths of a second for the flare parameters mentioned above [2].

The decrease in emission intensity of the flares should have taken place almost instantaneously, while the actual duration of the decending developmental branch of the chromospheric flares is several minutes or several tens of minutes. This indicates that there is a certain energy source in the region of the flare which sustains the luminosity, not only in the rising branch but also in the decending one.

A constant influx of energy is therefore necessary for the formation and further development of the chromospheric flares. This energy is generated in the volume of the chromospheric flares, or is supplied from some outer source. It is hard to say anything definite about this, since the general problem of the arisal of chromospheric flares has still remained unsolved. However, disregarding the nature of the phenomenon, we can obtain certain qualitative evaluations of the parameters of chromospheric flares and clarify the nature of the statistical link between them. Energy can be accumulated in the region of the flare before its beginning, or it can be supplied in a relatively short period of time.

We will not try to explain here where and how this energy arises and what its nature is. It is sufficient for us to know that a chromospheric flare transforms some part of the energy into an emission derived in the given region or supplied to it. /89

The energy can be consumed, first of all, in a change of the volume of the chromospheric flares. It is proportional to the following:

$$\varepsilon_1 = u_1 \frac{dv}{dt} \text{ erg/sec}. \qquad (3)$$

Second of all, a certain amount of energy is needed for the existence of a chromospheric flare occupying a volume of v (de-excitation, or outflow of energy, takes place constantly). This is proportional to the volume of the flare at each given moment, i.e.,

$$\varepsilon_2 = u_2 v \text{ erg/sec}. \qquad (4)$$

Consequently, the total energy is the following sum:

$$\varepsilon_1 + \varepsilon_2 = \varepsilon(t). \tag{5}$$

This energy changes during the course of development of a chromospheric flare, and it is a function of the time, i.e.,

$$u_1 \frac{dv}{dt} + u_2 \dot{v} = \varepsilon(t). \tag{6}$$

The chromospheric flare is a spatial phenomenon. However, its geometric depth cannot be ascertained from observations. Therefore, let us turn to the parameter of a solar flare which is determined directly from observations. The expression in (6) is then transformed, if we assume that

$$\varepsilon(t) = {}^3/_2 u_1 S^{1/2} \frac{dS}{dt} + u_2 S^{3/2}$$

or

$$\frac{dS}{dt} + \frac{2}{3}\frac{u_2}{u_1} S = \frac{2}{3}\frac{\varepsilon(t)}{u_1 S^{1/2}}. \tag{7}$$

The development of chromospheric flares with time arises not only in a change of the luminosity, but also in a change of the area. The area usually increases with an increase in the luminosity, i.e., a flare increase in volume when inflamed, and it decreases when dying down [3]. Figure 2 shows curves for the development of the area of flares. These graphs give us a basis on which we can consider that the areas of flares on the decending developmental branch decrease almost linearly. In such a case,

$$\frac{dS}{dt} = \text{const}. \tag{8}$$

The expression in (7) then gives the following:

$$\frac{dS}{dt} + \frac{1}{\tau} S = A - Bt. \tag{9}$$

Having solved this equation, we find that

$$S = (1 - e^{-\frac{t}{\tau}})(\tau A + \tau^2 B) - \tau B t, \tag{10}$$

where $\tau = \frac{3}{2}\frac{u_1}{u_2}$ is a constant value for the given flare, and designates the energy relaxation time.

Let us assume that a chromospheric flare has the following characteristic points: (1) at t = 0 it has an area of S = 0; (2) at t = T (total lifetime of chromospheric flares) S=0; (3) at t = t_{max} (time in which the area reaches its maximum value) S = S_{max}. /90

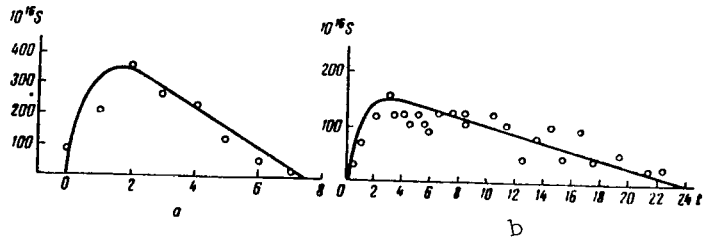

Fig. 2. Curves for the Area Variation of Chromospheric Flares of April 17, 1960 (a) and May 13, 1961 (b). The Points Designate Observational Data, and the Solid Curves Designate Theoretical Values.

We can find these characteristic points from the equation for the developmental curves of the area of chromospheric flares in (10):

(a) t = 0, S = 0;

(b) t = T, S = 0 or $(1 - e^{-\frac{t}{\tau}})(\tau A + \tau^2 B) - \tau B t = 0$.

We have the following expression for the total lifetime of chromospheric flares from condition "b":

$$T = \tau + \frac{A}{B} \tag{11}$$

for $e^{-t/\tau} \ll 1$. This is fulfilled with great accuracy.

Expressing (10) in terms of the total lifetime of chromospheric flares, we can finally obtain the formula for the area determined by (11):

$$S = \tau B T \left(1 - \frac{t}{T} - e^{-\frac{t}{\tau}}\right). \tag{12}$$

This is the basic formula which will be used for further investigations. We will show below to what extent this formula reflects the actual situation.

The area of chromospheric flares reaches its maximum value in the following time:

$$t_{max} = \tau \ln\left(\frac{T}{\tau}\right). \tag{13}$$

Using (11) and (12), we can find the connection between the maximum area and the total lifetime of chromospheric flares, i.e.,

$$S_{max} = T\left\{\tau B\left[1 - \frac{\ln\left(\frac{T}{\tau}\right)}{\left(\frac{T}{\tau}\right)} - e^{-\ln\left(\frac{T}{\tau}\right)}\right]\right\}. \tag{14}$$

We have the following from (11):

$$B = A/\tau\left(\frac{T}{\tau} - 1\right).$$

Substituting the value of B into (14), we find that /91

$$S_{max} = T\left\{\frac{A}{\frac{T}{\tau} - 1}\left[1 - \frac{\ln\left(\frac{T}{\tau}\right)}{\left(\frac{T}{\tau}\right)} - e^{-\ln\left(\frac{T}{\tau}\right)}\right]\right\}, \tag{15}$$

or

$$S_{max} = kT,$$

where

$$k = \left\{\frac{A}{\frac{T}{\tau} - 1}\left[1 - \frac{\ln\left(\frac{T}{\tau}\right)}{\left(\frac{T}{\tau}\right)} - e^{-\ln\left(\frac{T}{\tau}\right)}\right]\right\} = \text{const},$$

since

$$\left(\frac{T}{\tau}\right) = \text{const}. \tag{16}$$

Thus, there is a definite dependence between the maximum area and the total lifetime of chromospheric flares. This dependence is characterized by a linear law.

There is also a definite dependence between S_{max} and t_{max}. It is characterized by the following expression:

$$S_{max} = t_{max} \left\{ \frac{A}{\ln\left(\frac{T}{\tau}\right)} \left[1 - \frac{\ln\left(\frac{T}{\tau}\right)}{\left(\frac{T}{\tau}\right)} - e^{-\ln\left(\frac{T}{\tau}\right)} \right] \right\} \qquad (17)$$

or

$$S_{max} = ct_{max}$$

where

$$c = \left\{ \frac{A}{\ln\left(\frac{T}{\tau}\right)} \left[1 - \frac{\ln\left(\frac{T}{\tau}\right)}{\left(\frac{T}{\tau}\right)} - e^{-\ln\left(\frac{T}{\tau}\right)} \right] \right\} = \text{const.} \qquad (18)$$

Our study materials were motion-picture observations of the chromosphere on the hydrogen H_α line carried out according to the IGY Program on the AFR-2 Telescope of the Astrophysical Institute of the Academy of Sciences of the Kazakh SSR with the aid of a narrow-band polarizing interference filter with band width of 0.5 Å. The table gives a list of chromospheric flares we analyzed, as well as their parameters.

The values of S_{max}, t_{max} and T are determined directly from the observations, with a certain error. These data permit us to evaluate A, B and τ, as well as the dependence of T/τ on T, $\sqrt{B}$ on T, A on T, and S_{max} on T. The ratio T/τ in dependence on T is shown in Fig. 3.

The energy relaxation time changes in the same way as does the total lifetime of chromospheric flares, while the ratio remains constant, i.e.,

$$\frac{T}{\tau} = 15. \qquad (19)$$

Thus, τ increases with an increase of T.

The numerical value of (19) confirms the assumption we used in deriving (11).

The parameter A, which has dimensionality of cm^2/sec, does not change with a variation in the lifetime of chromospheric flares. The dependence of A on the total lifetime is shown in Fig. 4. The parameter A remains constant for all flares, regardless of the value

of T, and is equal on the average to the following: /92

$$A = 6 \cdot 10^{16} \text{cm}^2/\text{sec} \quad (20)$$

Date	Coordinate of flares	Beginning of flare	End of flare	T, min	t_{max}, min	τ, min	$10^{-16} A$, cm^2/sec	$10^{-6} \sqrt{E}$, cm/sec	Smax, millionths of hemisphere
		h m	h m						
07.XI 1956*				180.0	37.0	15.0	3.2	1.8	736.0
02.XI 1957	20°S, 16°W	09 04	09 43	34.0	8.0	3.54	2.16	3.43	112.0
02.XII 1957	18 S, 31 W	07 52	08 00	6.5	1.5	0.64	5.64	12.70	54.4
29.IX 1958	09 S, 10 E	05 16	05 54	28.0	3.0	0.86	5.20	5.63	79.2
23.X 1958	15 S, 11 W	06 24	06 36	10.0	1.5	0.5	5.70	10.0	46.0
27.II 1959	24 N, 10 W	06 57	07 18	13.0	2.5	0.96	1.75	4.90	75.2
29.VI 1959	09 N, 50 W	05 08	05 20	10.5	2.5	1.10	3.90	8.30	62.8
23.VI 1959	18 N, 03 W	03 25	04 26	60.0	12.0	4.72	3.45	3.22	248.0
26.VI 1959	10 N, 06 W	04 11	04 44	36.0	10.0	5.12	3.10	4.10	214.0
23.VII 1959	21 S, 51 E	03 31	03 54	24.0	5.0	2.00	5.95	6.70	181.0
30.VII 1959	10 N, 19 E	05 12	05 21	7.5	1.8	0.82	4.70	10.7	54.4
30.XI 1959	11 N, 10 E	07 19	07 26	6.0	0.5	0.43	6.1	32.2	86.0
17.IV 1960	14 N, 33 E	05 52	05 59	7.5	1.5	0.59	12.40	17.5	115.0
17.V 1960	09 S, 34 E	04 18	04 46	28.0	4.0	1.33	3.25	4.50	72.4
11.VIII 1960	22 N, 37 E	02 42	03 39	58.0	12.0	4.75	4.46	3.74	330.0
11.X 1960	16 S, 37 E	05 45	07 00	50.0	7.0	2.26	8.6	5.50	330.0
22.X 1960	20 N, 11 W	05 42	05 55	12.0	2.0	0.70	2.92	6.55	33.0
13.V 1961	04 N, 16 W	05 51	06 09	14.0	3.0	1.24	4.21	7.44	79.2
13.V 1961	04 N, 14 W	04 41	05 03	24.0	2.5	0.71	3.92	5.30	49.6
24.V 1961	16 S, 18 E	04 23	05 26	46.0	12.0	5.68	2.59	3.26	214.0
12.VII 1961*				150.0	20.0	8.35	6.45	2.77	880.0
18.VII 1961*				150.0	30.0	12.0	4.60	2.36	840.0
22.VII 1961	10 S, 45 E	03 14	03 19	45.0	1.0	0.42	9.25	19.4	57.6
24.VII 1961	13 N, 18 E	04 10	06 12	110.0	36.0	23.6	1.56	1.73	454.0
16.VIII 1961	13 N, 24 W	03 01	03 46	22.0	4.0	1.48	6.26	7.15	132.0
16.VIII 1961	18 N, 27 W	04 55	05 27	16.0	4.0	1.85	1.87	4.7	49.5
20.IX 1961	17 N, 60 W	04 10	04 21	8.0	1.5	0.57	8.45	13.8	76.0
17.X 1961	13 N, 61 W	05 21	05 26	4.5	0.8	0.30	18.9	27.4	89.0
21.XI 1961	19 N, 56 W	06 03	06 15	9.0	2.0	0.85	12.4	10.4	67.0

Note: The beginning and end of the flares are given according to Universal Time.

* Flare of Nov. 7, 1956 according to [3], flares of July 12 and 18, 1961 according to [4].

The dependence of log $\sqrt{B}$ cm/sec on the relaxation time (or total lifetime of the flare) is shown in Fig. 5. The characteristic peculiarity of this graph is seen in the fact that the value of $\sqrt{B}$ decreases as the relaxation time increases (or as the total lifetime of the chromospheric flares increases). Flares with short lifetimes have a large value of $\sqrt{B}$, and the curve decreases repidly at first; as T increases, it changes by a very substantial value.

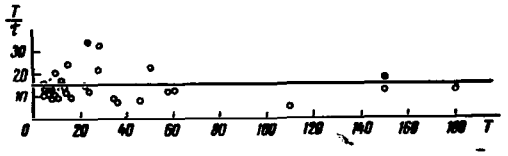

Fig. 3. Change of T/τ in Dependence on the Total Lifetime of Flares.

Consequently, we can assume that chromospheric flares in the initial stage of their development are similar to an outburst, since /93

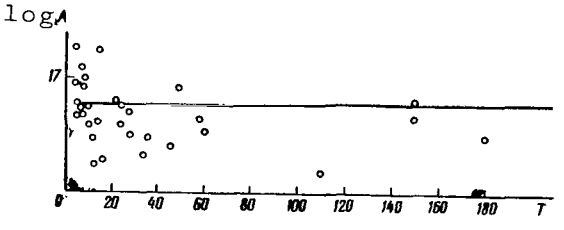

Fig. 4. Observed Change of Parameter A(T).

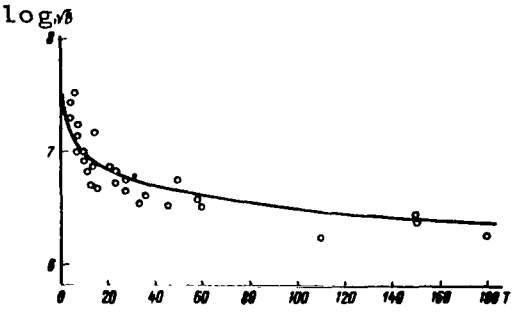

Fig. 5. Dependence of log $\sqrt{B}$ on Lifetime of Flares. The Points Designate Experimental Data; the Solid Curve is Given by the Expression $B = 0.0715 \frac{A}{\tau} = \frac{A}{T}$

$\sqrt{B}$ has a large value for a small value of T. This point of view does not contradict the observational data of [4].

We derived a formula above (15) which links the maximum area with the total lifetime of chromospheric flares. Substituting numerical values into (15), we have the following:

$$k = 0{,}32 \cdot 10^{16} \text{ cm}^2/\text{sec}. \tag{21}$$

Thus,

$$S_{\max} = 0{,}32 \cdot 10^{16} \cdot T \text{ cm}^2 . \tag{22}$$

where T is the total lifetime of chromospheric flares, expressed in seconds.

If S_{max} is expressed in terms of millionths of a hemisphere of the Sun, and T in minutes, then

$$S_{max} = 6{,}35\,T. \tag{23}$$

It can be seen from Fig. 6 that the dependence between the lifetime and the maximum area is represented satisfactorily by the latter formula.

The dependence between S_{max} and t_{max} is determined by (18).

After substituting the numerical values, we have the following:

$$c = 1{,}66 \cdot 10^{16}\ \mathrm{cm}^2/\mathrm{sec}.$$

Consequently,

$$S_{max} = 1{,}66 \cdot 10^{16}\, t_{max}. \tag{24}$$

In normal units,

$$S_{max} = 32{,}7\, t_{max.}, \tag{25}$$

where t_{max} is expressed in minutes, and S_{max} in millionths of the visible hemisphere of the Sun. /94

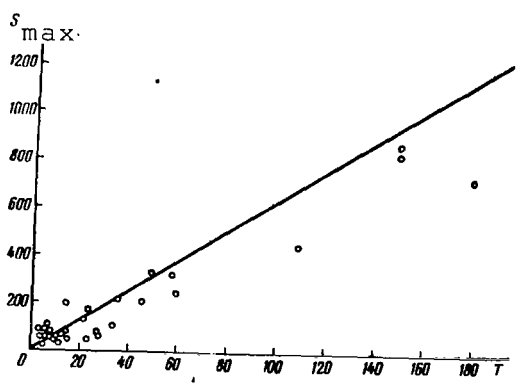

Fig. 6. Dependence of S_{max} on T.

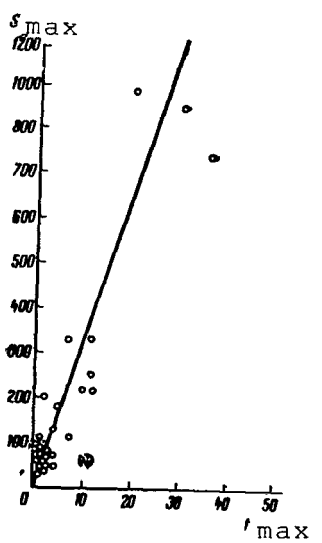

Fig. 7. Dependence of S_{max} on t_{max}.

Figure 7 shows the observed dependence of S_{max} and t_{max}, as well as the theoretical one obtained according to (25). As can be seen from the graphs, the convergence is satisfactory.

Conclusions

1. A relationship is obtained which links the area with the total lifetime of chromospheric flares, and which agrees with observational data (Fig. 2).

2. There is a linear dependence between S_{max} and T. The coefficient of proportionality is equal to $0.32 \cdot 10^{16}$ (Fig. 6).

3. There is also a linear dependence between S_{max} and t_{max}, (Fig. 7).

4. The total lifetime of chromospheric flares (T) is determined by the energy relaxation time and the ratio between parameters A and B.

5. The ratio between the total duration of chromospheric flares and the energy relaxation time is a constant value equal to 15 (Fig. 3).

6. The time during which the area of chromospheric flares reaches its maximum value is determined by the energy relaxation time, i.e., $t_{max} = 2.8\ \tau$.

REFERENCES

1. deYager, K.: Stroyeniye i dinamika atmosfery Solntsa (Structure and Dymanics of the Solar Atmosphere). Foreigh Languages Publishing House, 1962.
2. Severnyy, A.B.: Izv. Krymskoy Astrofiz. Obs., Vol. 19, 1958.
3. Severnyy, A.B. and Ye.F. Shaposhnikova: Izv. Krymskoy Astrofiz. Obs., Vol. 12, 1954.
4. Obashev, S.O.: Astron. Zhur., Vol. 42, No. 5, 1965.

TOTAL ENERGY OF CHROMOSPHERIC FLARES

S.O. Obashev

ABSTRACT: An evaluation is made of the total energy of a chromospheric layer. The total energy is found to be proportional to the total period of the flare, to the power 5/2.

The energy of flares is evolved in the form of the wave emission of high-energy particles and movement of the solar plasma. In the visible range the most intensive form is the H_α line emission. Evaluations of the emission energy of flares are usually carried out by different methods: /95*

(a) in the case of the polarizing interference filter [1],

$$\varepsilon = I_\odot \left(\frac{I_f}{I_b} - 1\right) S \int r_\lambda k_\lambda \alpha_\lambda \text{ erg/sec}, \tag{1}$$

where I_f/I_b is the intensity ratio between the flare and the background, and $\int r\lambda k\lambda \alpha\lambda$ is the energy within the band limit of the polarizing interference filter;

(b) in the case of using the spectral method in [2], we have

$$\varepsilon = \Delta\lambda I_\odot S \text{ erg/sec}, \tag{2}$$

where $\Delta\lambda$ is the equivalent width of the $H\alpha$ line, $I_\odot$ is the emission intensity of the sun, and S is the area of the flare.

Thus, the wave energy of flares is determined mainly by two parameters - $\Delta\lambda$ and S, which change within a wide range.

We are presenting another method of evaluating the energy of chromospheric flares here. An expression of the following type was obtained for the energy of a flare in [3] on the basis of simple physical assumptions:

$$\varepsilon = U_1 S^{1/2} B \left(\frac{A}{B} - t\right) \text{erg/sec}, \tag{3}$$

* Numbers in the margin indicate pagination in the foreign text.

where U_1 is the energy per unit volume of the flare, A and B are parameters characterizing the flares [3, see table], and t is the time.

The area is determined by the following function:

$$S = \tau b T \left(1 - \frac{t}{T} - e^{-t/\tau}\right), \tag{4}$$

where τ is the relaxation time, T is the total lifetime of chromospheric flares, i.e.,

$$T = \frac{A}{B} + \tau. \tag{5}$$

Substituting the value of the area from (4) into (3), we have the following:

$$\varepsilon(t) = U_1 (\tau T)^{1/3} B^{2/3} \left(1 - \frac{t}{T} - e^{-\frac{t}{\tau}}\right)^{1/3} \left(\frac{A}{B} - t\right). \tag{6}$$

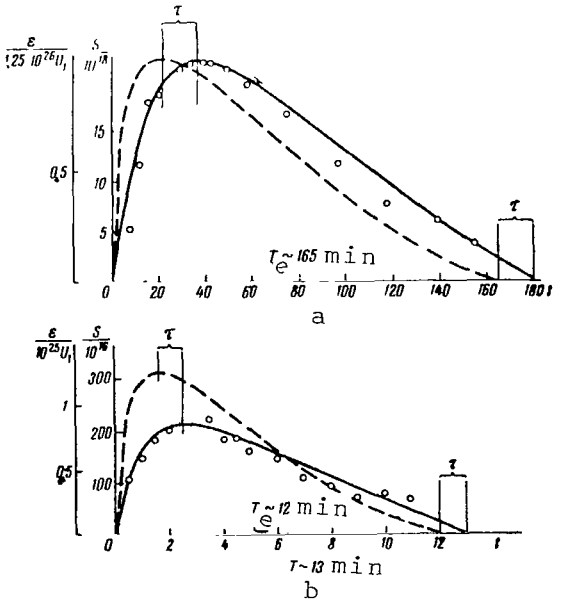

Fig. 1. Energy Change in Correspondence with the Expressions in (4), and (6) (dashed curve) and Area Variation (solid curve) for January 27, 1959, (a) and for November 7, 1956, (b). The Points Designate Observational Data. $T - T_e = \tau$ is the Energy Relaxation Time of the Flare. /96

It follows from the latter expression for the energy and (5) that

$$\frac{A}{B} = T - \tau \approx T_e, \tag{7}$$

i.e., the total duration of a flare which is determined according to the area is not equal to the duration of a flare which is determined according to the energy.

Figure 1 shows the change in energy and area of chromospheric flares in correspondence with (6) and (4) for a flare on January 27, 1959 and November 7, 1956 [3]. It can be seen from the figure that

the maximum of the energy curve is displaced along the time axis by a value of τ in relation to the maximum of the curve for the area change. This fact agrees with observations. In most of the cases, the values of I_{max} and S_{max} are not attained simultaneously, but one lags behind another. As a rule, I_{max} comes somewhat in advance of S_{max}.

Let us evaluate the total energy of a flare, using (6). In order to find the total energy of chromospheric flares, we will assume that $T_e \sim T$. This assumption does not involve a substantial error in the final results. Before integrating, let us find the value of U_1 and substitute it into (6):

$$U_1 \sim \tau U_2$$

or

$$U_1 \simeq 0{,}066\, U_2 T \text{ from [3]}, \tag{8}$$

where U_2 is the isolated energy from an area of the flare with unit volume per unit time. We can consider this energy to be constant in first approximation. The total energy is now

$$E = \int_0^T \varepsilon(t)\, dt = 0{,}066 U_2 \int_0^T T (\tau T)^{1/2} B^{3/2} \left(1 - \frac{t}{T} - e^{-t/\tau}\right)^{1/2} (T - t)\, dt. \tag{9}$$

If the function $e^{-t/\tau} \approx 1 - \frac{t}{\tau}$, then

$$E = 0{,}066\, U_2 \tau^{1/2} (TB)^{3/2} \left(\frac{1}{\tau} - \frac{1}{T}\right)^{1/2} \int_0^T t^{1/2} (T - t)\, dt. \tag{10}$$

Since the ratio $T/c \gg 1$, then we can obtain the following expression for the total energy after integration and elementary transformations: /97

$$E = 0{,}017\, U_2 B^{3/2} T^4 \text{ erg}, \tag{11}$$

where T is expressed in seconds.

The observed values of S_{max} and t_{max} (time during which the flare acquires the maximum area) and T permit us to determine the value of the total energy for each flare.

Figure 2 shows the change in total energy in units of $\left(\frac{E}{0.25\cdot10^{24}U_2}\right)$ with the change in the total lifetime of the chromospheric flares.

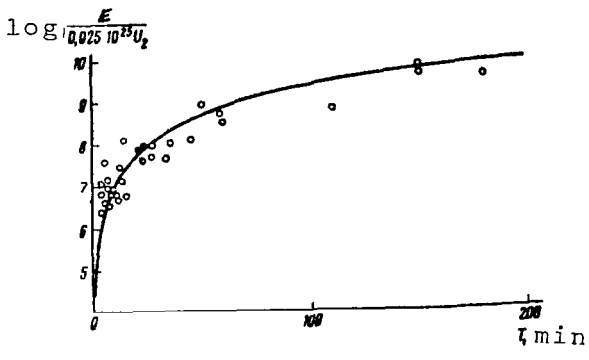

Fig. 2. Dependence of Energy on Duration of Chromospheric Flares.

The latter expression for the energy can be written in another way by using (7), i.e.,

$$E = 0{,}017\, U_2 A^{1/2} T^{5/2} \text{ erg}, \tag{12}$$

or, having substituted the value of $A = 6\cdot10^{16}$ cm^2/sec, we have

$$E = 0{,}25\cdot10^{24}\, U_2 T^{5/2} \text{ erg}. \tag{13}$$

Thus, the total energy of chromospheric flares is directly proportional to the total lifetime of chromospheric flares, to the power of 5/2.

The energy change in correspondence with (13) is shown by the solid line in Figure 2. It can be seen that the similarity is satisfactory. The scattering of the points could be due to an error in measuring the values of S_{max}, t_{max} and T.

REFERENCES

1. Severnyy, A.B.: Izv. Krymskoy Astrofiz. Obs., Vol. 9, 1952.
2. deYager, K.: Stroyeniye i dinamika atmosfery Solntsa (Structure and Dynamics of the Solar Atmosphere). Foreign Languages Publishing House, 1962.
3. Obashev, S.O.: This Collection, p. 107.

ENERGY CLASSIFICATION OF CHROMOSPHERIC FLARES

C.O. Obashev

ABSTRACT: An empirical evaluation is made of the total energy of chromospheric flares of different intensities.

It was shown in [1] that the total energy of chromospheric flares is expressed by the following relationship: /98*

$$E = 0{,}25 \cdot 10^{24} \alpha U_2 T^{3/2} \text{ erg}, \quad (1)$$

where U_2 is the energy derived from a region of the flare with unit volume per unit time, T is the total duration of the chromospheric flares, expressed in seconds, and α is the transformation ratio.

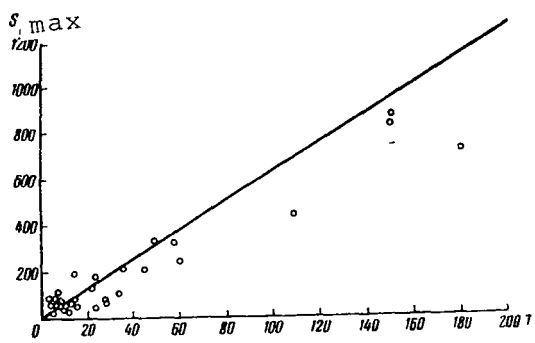

Fig. 1. Dependence of S_{max} on T. The Points Designate Observational Data and The Solid Line Designates Theoretical Data.

The following question naturally arises: Does all this energy go into the H_α emission, or is there a certain transformation ratio $\alpha \lesssim 1$? For the sake of definiteness, we will assume that $\alpha \sim 1$ (observations show that the H_α emission plays the principal role in the energy flow of chromospheric flares [2]).

The surface brightness of a chromospheric flare on the H_α hydrogen line changes from flare to flare. We would assume that its average value is equal to $2 \cdot 10^7$ erg/cm^2·sec. The total energy is then equal to the following:

$$E = 5 \cdot 10^{21} T^{3/2} \text{ erg} \quad (2)$$

for U_2 = 0.02 erg/cm^3·sec.

On the other hand, there is a definite dependence between the maximum area and the total duration of chromospheric flares [3], i.e.,

* Numbers in the margin indicate pagination in the foreign text.

$$S_{max} = 6{,}35\,T. \qquad (3)$$

Figure 1 shows the dependence of S_{max} on T, where S_{max} is expressed in millionths of a solar hemisphere, and T is expressed in minutes. /99

Using (2) and (3), we can evaluate the total energy (within the limits of the above-presented assumption) of chromospheric flares of different intensities.

The existing classification of chromospheric flares is based mainly on the value of the area. The principal scale numbers (1, 2, 3) of the classification are characterized by the limiting values of the area presented below (the areas are expressed in terms of millionths of a solar hemisphere).

Scale Number	S_{max}	E, erg
1	100-250	$10^{29} - 10^{30}$
2	250-600	$10^{30}-8\cdot10^{30}$
3	600-1200	$8\cdot10^{30}-7\cdot10^{31}$

Figure 2 shows the dependence of the total energy of chromospheric flares on their area. Let us find the limiting values of the total energy of chromospheric flares on the basis of this graph and the limiting values for the area of flares of different scale numbers. The value of this energy is given in the last column of the table. It can be seen from the table that the limiting energy values increase roughly by one order during a transition to the following class, while the area nearly doubles.

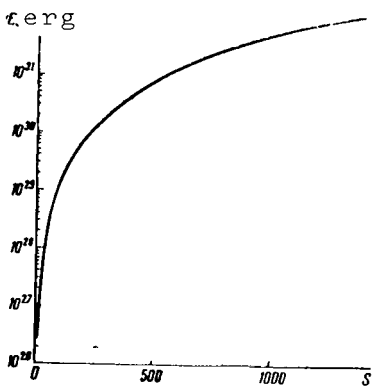

Fig. 2. Dependence of Energy Derived from Chromospheric Flares on Area.

These estimates of the energy which were obtained from certain simple physical assumptions [1, 3] agree well with direct observational data. According to [4, 5] and others, the total energy for chromospheric flares of scale numbers 3 and 3^+ is on the order of 10^{32} erg, while that of scale 2 is $(1\text{-}10)\cdot10^{31}$ erg on the H_α line. A powerful flare on February 23, 1956 of scale 3^+ emitted energy on the order of 10^{32} erg on the H_α line [6].

We should mention that the point of view developed in [1, 3] and in this article can explain in quantitative terms the developmental curves of the area and the statistical laws of different parameters, and it can give a correct dimension for the

energy of chromospheric flares. The expressions obtained should be considered merely as empirical relationships which will be of significance in studying the physics of chromospheric flares.

REFERENCES

1. Obashev, S.O.: This Collection, p. 118.
2. Dubov, E.Ye.: Izv. Krymskoy Astrofiz. Obs., Vol. 29, 1963.
3. Obashev, S.O.: This Collection, p. 107.
4. deYager, K.: Stroyeniye i dinamika atmosfery Solntsa (Structure and Dynamics of the Solar Atmosphere). Foreign Languages Publishing House, 1962.
5. Ellison, M.A.: Quart. J. Roy. Astron. Soc., Vol. 4, 1963.
6. Sb.: Issledovaniya verkhney atmosfery s pomoshch'yu raket i sputnikov (Collection: Investigations of the Upper Atmosphere with the Aid of Rockets and Satellites), ed. G.S. Ivanov-Kholodnyy. Foreign Languages Publishing House, 1961.

CONTOURS OF THE Mg I b_1 - b_4 AND Sr II 4216 AND 4078 Å LINES IN THE CHROMOSPHERE

N.S. Shilova

ABSTRACT: The mechanism responsible for the shapes of the contours of the chromospheric lines of neutral magnesium (5184 and 5173 Å) are analyzed. It is shown that the shape of optically thick lines of the chromosphere is not determined by photospheric radiation scattering. The intrinsic radiation of the chromosphere must be known in order to explain the observed shape.

The high-intensity neutral magnesium (5184 and 5173 Å) and ionized strontium (4078 and 4216 Å) lines can be isolated from among the lines of metals in the chromosphere. They were obtained on the coronagraph of the IZMIRAN (Institute of Terrestrial Magnitism, The Ionosphere and Radio Wave Propagation of the Academy of Sciences, USSR) in the summer of 1963 and 1964. The Mg I b_1 - b_4 lines were observed in the second order of the diffraction grid with dispersion of 2 Å/mm, and the Sr II lines in the third order with dispersion of 1.3 A/mm. The half-width of the instrumental contour in the second and third orders were 0.13 and 0.08 Å, respectively. The instrumental contour was not eliminated because of the qualitative nature of the investigation. Figure 1 (a) shows the characteristic appearance of the b_1 - b_2 contours which were constructed according to photographs for August 1, 1963, and Figure 1, (b) shows contours constructed according to photographs for July 26, 1963. In all, 13 b_1 contours were constructed, 14 b_2 contours, and 4 b_4 contours. The shape of the contours depicted in Figure 1 (b) was not often found (in two out of 13 cases for b_1 and 4 out of 14

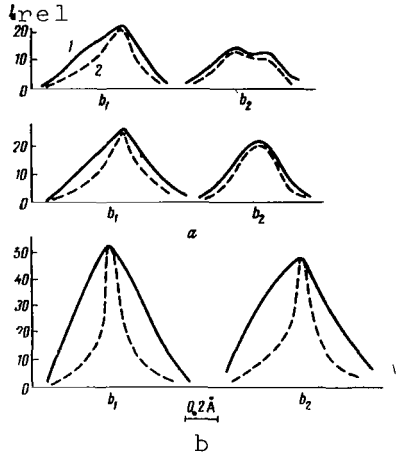

Fig. 1. Contours of b_1 and b_2 Lines According to Photographs of August 1, 1963 (a) and July 26, 1963 (b). (1) Profiles of the Change After Subtracting the Scattered Light of the Photosphere; (2) Reduced Profiles.

/100*

* Numbers in the margin indicate pagination in the foreign text.

cases for b_2). Obviously, the photographs for July 26, relate to a greater height than those of observations for August 1; a precise determination of the altitude in observations of the coronagraph of the IZMIRAN was difficult. The similarity of the contours of the lines for July 26 to a Gaussian contour indicates this. We constructed reduced contours for all the lines under investigation by the method proposed in [1]. The reduced profiles in all the figures are designated by the dashed line, while the contours obtained only after subtracting the scattered light of the photosphere are designated by the solid line.

Let us examine the reduced b_1 and b_2 contours in Figure 1 (a). /101
The reduced b_2 contour has the shape of a Gaussian contour which is distorted by self-absorption. The contour of the b_4 line is not presented on the figures, since this line is a blend in which the Mg I (5167.34 Å) and Fe I (5167.49 Å) lines are mixed (intensity ratio, 3:1 [2]). Although the 5167.34 Å line yields the principal contribution and the equivalent width of the observed lines can be taken as the equivalent width of b_4, the profile of the line is doubtlessly greatly distorted. The two-peak contour of b_4 is seen very clearly after reduction. The appearance of the b_1 contour is similar to a line in which collisions play the determinant role in splitting. However, in addition to the hardly-probably difference in mechanisms of line expansion of one multiplex (b_1 and b_2), we should note the following strange facts: after reduction, $\Delta\lambda_{b_1} < \Delta\lambda_{b_2}$, although the optical thickness decreases with the number of the line.

Let us examine the effect of collisions of neutral magnesium atoms with electrons (Stark quadratic effect) and neutral hydrogen atoms (van der Walls forces) on the contour of the b_1 line. We will examine rather removed wings of the line ($\Delta\lambda \geq 1.5\ \Delta\lambda_D$), where it ceases to be optically thick ($\tau_{b_1} = 13.6$ [3]) and thus the dependence $I(\lambda)$ can be considered as similar to the dependence $\alpha(\nu)/\alpha(\nu_D)$. In order to determine the change in the absorption coefficient with distance from the center of the line, we must determine the constant of attenuation due to the van der Walls forces γ_c, the constant of attenuation due to the Stark quadratic effect γ_s, and the constant of attenuation due to radiation γ_e, and we must find the relationship $\frac{\gamma_c + \gamma_s + \gamma_e}{4\pi\Delta\nu_D}$. We will then use the tables presented in [4]. In calculating γ_c, there is uncertainty in the estimate of the mean square radius of orbit for the upper excited state of the transition under investigation $\bar{R}_k^2$:

$$\gamma_c = \left[\sqrt{\frac{8RT}{\pi}\left(\frac{1}{\mu_1}+\frac{1}{\mu_2}\right)}\right]^{3/5}\left[\frac{e^2}{h}6{,}63\cdot10^{-25}\bar{R}_k^2\right]^{2/5}\cdot17\cdot n_H,$$

where μ_1, and μ_2 are the atomic weights of hydrogen and the radiating element. The value of $\bar{R}_k^2$ for the given transition of Mg I is unknown. For the sodium D-lines, $\bar{R}_k^2 = 41a_0^2$ [5]. If we use the formula for the upper levels of light metals [5] in order to determine $\bar{R}_k^2$, then $\bar{R}_k^2 = 18\ a_0^2$. In view of the estimating nature of our calculations, we will assume that $\bar{R}_k^2 = 30a_0^2$ for the b_1 line. Then $\gamma_c = 8 \cdot 10^{-8} n_H$. If we assume that the b_1 line arises in the vicinity of the base of the chromosphere, then $n_H = 2.5 \cdot 10^{13}$ [6] and $\gamma_c/4\pi = 1.5 \cdot 10^5$. Let us calculate the value of γ_s, which was previously an exaggerated value of the Stark constant C. For the metal line $\lambda = 4000$ Å, which is relatively sensitive to the Stark effect, thisa value is equal to $9.3 \cdot 10^{-13}$. $\gamma_s = 38.8\ C^{2/3} \sqrt{\frac{8RT}{\pi} \frac{1}{\mu_e}}$ [7], where $\mu_e = 1/1847$ for collision with electrons of $\gamma_s = 1.3 \cdot 10^{-4} n_e$. At the base of the chromosphere, $n_e = 2.6 \cdot 10^{11}$ [8] and $\gamma_s/4\pi = 2.45 \cdot 10^6$. The constant of attenuation due to radiation $\frac{\gamma_B}{4\pi} = \frac{\sum^A}{4\pi} = 4.4 \cdot 10^6$. The Doppler half-width in frequency units at T = 5500° K and v_t = 3 km/sec is equal to $6.9 \cdot 10^9$ cm^{-1}.

Thus, under the conditions of the lower coronosphere, collisions with neutral hydrogen atoms and with electrons cannot expand the line more greatly than it is expanded because of attenuation in radiation. Naturally, we cannot preliminarily exclude the possibility that distant wings of b_1 are formed in the photosphere. However, we can examine the extreme case: the wings are formed at a depth of h = -300 km. According to [9], $n_H = 1 \cdot 10^{17}$ cm^{-3} at this depth, and $n_e = 3.2 \cdot 10^{13}$ cm^{-3}. For such densities, $\gamma_s/4\pi = 3.4 \cdot 10^8$ and $\gamma_e/4\pi = 6.3 \cdot 10^8$. However, the extremely wide wings of the reduced contour cannot be explained in this case. /102

Figure 2 shows the reduced b_1 contour in units of central intensity for August 1, 1963, as well as a profile calculated according to the tables in [4] for $n_H = 10^{17}$ cm^{-3} and $n_e = 3.2 \cdot 10^{13}$ cm^{-3}. It can be seen that the effects of attenuation cannot explain the shape of the reduced b_1 contour according to the photographs of August 1. In this case, the contours for August 1 were corrected before reduction only for the effect of oscillation of the image and scattered light, and they had the shape of a Gaussian contour greatly distorted by self-absorption, sometimes even with a marked dip. For the photographs of July 26, the contour was close to Gaussian even before reduction, and its nature did not change after reduction (if we disregard the extended wings for $I < 0.1\ I_0$). In this regard, the strange relationship $\Delta\lambda_{b_1} < \Delta\lambda_{b_2}$ was not observed in any case for the non-reduced contours; rather, it can be said that these half-widths were identical within the limits of error. In the case of July 26, they corresponded to $\Delta\lambda_D = 0.104$ Å and, most frequently, were determined by the value of the instrumental contour, inasmuch as $\Delta\lambda_i = 0.13$ Å.

V.A. Krat and V.M. Sobolev [10] also obtained the strange half-width ratio after reduction for the H_δ and H_ε lines, for which $\Delta\lambda_{H_\delta} < \Delta\lambda_{H_\varepsilon}$. Having compared their equivalent widths, V.A. Krat

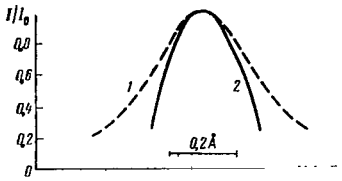

Fig. 2. Reduced (1) and Theoretical (2) b_1 Contours.

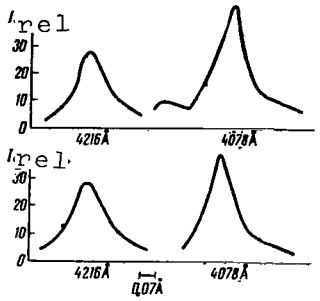

Fig. 3. Reduced Contours of 4216 and 4078 Å Lines.

drew the conclustion that the population of the upper H_δ level was determined by roughly 50%, not by the excited photospheric radiation, but by the electron impact and recombination. Obviously, the inherent radiation of the chromosphere also plays a substantial role in the emission of the b_1 and b_2 lines. The b_1 line has a greater optical thickness, and this effect is more strongly pronounced in it, while it is possible that the excitation of photospheric radiation also plays a great role for b_2, together with the inherent radiation. At rather high altitudes (photographs of July 26), when the optical thickness in both lines is close to 1, the excitation of photospheric radiation predominates. Therefore, there are no anomously wide wings in the contours for July 26 after reduction, and the contours are close to Gaussian, while $\Delta\lambda$ acquires a reasonable value. In this case, the penetration of photospheric radiation in an unchanged form at an altitude of h > 1000 km in optically thick lines possibly indicates that there is porosity.

Figure 3 shows reduced contours of Sr II lines (4216 and 4078 Å). The digreasion for a Doppler shape begins on the reduced contours at $I \approx 0.35\ I_0$. It is difficult to see how the developed wings are determined, since the theory of the expansion of spark lines by the Stark effect, for example, has still not been completely developed. The ratio of equivalent widths of the 4216 and 4078 Å lines, which is equal to 1.9, is close to the theoretical value. Since the initial levels of these lines are sublevels of one term, the ratio of their population is determined with the aid of the Boltzmann formula, and corresponds to an intensity ratio of 1.85 for T = 6000° K and 1.82 for 5500° K. Thus, they are not optically /103 thick for the altitude of these lines. According to our observations $I_{4078} = 8.7 \cdot 10^{-3}$ Å, and $I_{4216} = 4.6 \cdot 10^{-3}$ Å. A change of τ_{tang} with the altitude in these lines was found in [11]. According to the calculations of J. Kawaguchi, these lines are actually optically thick, beginning with h > 1200 km, for a substantial range of altitudes.

Thus, the dispersion of photospheric radiation obviously determines in full the illumination of only optically thick lines of the chromosphere. For optical thicknesses at the center of the line $\gtrsim 10$, we must consider the inherent radiation of the chromosphere.

1. Krat, V.A. and T.V. Krat: Izv. GAO, Vol. 20, No. 155, p. 1, 1956.
2. Mitchell, S.A.: Astrophys. J., Vol. 105, No. 1, 1947.
3. Shilova, N.S.: Astron. Zhur., Vol. 42, p. 757, 1965.
4. Aller, L.H.: Astrofizika (Astrophysics). Foreign Languages Publishing House, 1955.
5. Mustel', E.R.: Zvezdnyye atmosfery (Stellar Atmospheres). "Fizmatgiz", 1960.
6. van der Holst: Sb.: Solntse (Collection: The Sun), ed. D. Koyper. Foreign Languages Publishing House, 1957.
7. Unsold, A.: Sovremennyye problemy astrofiziki i fiziki Solntsa (Modern Problems of Astrophysics and the Physics of the Sun). Foreign Languages Publishing House, 1951.
8. Gulyayev, R.A., K.I. Nikol'skaya and G.M. Nikol'skiy: Astron. Zhur., Vol. 40, p. 443, 1963.
9. Minnart, M.: Sb.: Solntse (Collection: The Sun), ed. D. Koyper. Foreign Languages Publishing House, 1957.
10. Krat, V.A. and V.M. Sobolev: Izv. GAO, Vol. 21, No. 160, p. 116, 1957.
11. Kawaguchi, J.: Publ. Astron. Soc. Japan, Vol. 11, p. 138, 1959.

HELIUM IONIZATION AND THE EXCITATION OF ORTHOHELIUM IN THE SOLAR ATMOSPHERE

R.A. Gulyayev

ABSTRACT: The concentration of He I, He II and He III in the solar atmosphere is calculated, as is the population of the lower levels of orthohelium as a function of kinetic temperature and electron density. The calculation is based on available experimental data for the effective cross sections of elementary processes not considered by previous authors. Particular attention is given to the two limiting cases where (1) the ionizing radiation field (504 Å) is absent and helium ionization is accomplished only by electron impact, and (2) the helium atoms are ionized by the coronal emission.

The helium lines are of particular interest in solar spectroscopy. Since it is difficult to excite (excitation potentials of 20 eV and more), helium, which is the most abundant element after hydrogen, is represented in the Fraunhofer spectrum of the undisturbed Sun only by a weak quasi-resonance λ10830 line of 2^3 S-2^3 P. The λ10830 absorption line in faculae is a factor of 5-6 more intensified, compared to undisturbed regions, i.e., it is a sensitive indicator of the activity on the Sun. In the emission spectrum of the chromosphere, the helium lines are very intensive. Since a high temperature is necessary for helium excitation, (no lower than ~ 20,000°) or a rather powerful emission field with λ < 504 Å, the luminescence of the helium lines in the chromosphere obviously indicates that there are regions with particular physical conditions in the "cold" chromosphere. It is clear that a study of the fine structure of the chromosphere is unthinkable without a detailed investigation of the helium line. /104*

Many authors have carried out calculations of the ionization and excitation of helium under the conditions of the solar atmosphere For example, V.A. Krat and B.M. Sovelev [1] calculated the populations of the upper He I levels for a number of values of the kinetic temperature T and electron density n_e. Based on the most reliable experimental data concerning active cross sections of elementary processes, we again calculated the concentration of He I, He II, and He III and the populations of the lower levels of orthohelium independent of T and n_e. In this case, we considered ele-

* Numbers in the margin indicate pagination in the foreign text.

mentary processes which had not been examined by the other authors. The calculations were carried out for two limiting cases: (1) the field of ionizing radiation ($\lambda < 504$ Å) was absent, i.e., the ionization of helium took place only in an electron impact; (2) the helium atoms were in the field of hard coronal radiation.

Figure 1 shows a schematic diagram of the energy levels of a helium atom. Optical intercombination transitions between triplet and singlet levels in helium are strictly forbidden. Therefore, the 2^3S level is highly metastable. The 2^1S level is also metastable, but it has an optical link with the principal level under the conditions of the solar atmosphere through the 2^1P level: the 2^1S - 2^1P transition is carried out in quantum absorption of photospheric radiation with λ20582 Å, and the 2^1P - 1^1S transition takes place spontaneously. Because of the lack of an optical link, the triplet and singlet systems are practically independent and, as a result, the helium seems to consist of two types of atoms: parahelium atoms with ionization potential of 24.6 eV and orthohelium with ionization potential of 4.8 eV.

Evaluations have shown that transitions between levels of orthohelium take place much more frequently (several orders) under the conditions of the solar atmosphere than do transitions of orthohelium-parahelium and orthohelium-He II. It is obvious that /105 in such a case the relative distribution of populations over orthohelium levels should be determined solely by transitions between triplet levels ("internal" transitions in the triplet system). The transitions which are linked with a change in multiplicity or ionization state ("external" transitions) determine the total concentration of orthohelium (sum of the populations of all levels). Therefore, a calculation of the absolute values of the orthohelium population levels is conveniently carried out in two stages: (1) calculation of the relative populations (for example, in relation to the sum of populations and of the levels under investigation); (2) calculation of the total orthohelium concentration by means of a solution to the equations of ionization equilibrium.[1]

Together with T.L. Vinnikova [3], I constructed a program for calculating the relative populations of atomic levels on an electron computer "Ural-2" which considered only the "internal" transitions. Elementary processes were examined: spontaneous transitions, excitation and quenching by radiation, excitation and quenching

[1] The populations of the higher levels are determined to a great extent by the exchange processes with the continuum: ionization from excited states by electron impact and triple recombination [2]. However, the contribution of the higher levels to the total concentration is insignificantly small.

by electron impact. The following data were fed into the machine for calculations according to the program constructed: excitation potentials and statistical weights of the levels, oscillator forces, kinetic temperature and electron density of the medium, Planck emission temperature or emission intensity at the corresponding wavelength, and emission dilution factor. The program allowed us to calculate the populations of any number of levels from 2 to 30. The populations of the levels were calculated in relation to the sum of populations of all the levels under investigation.

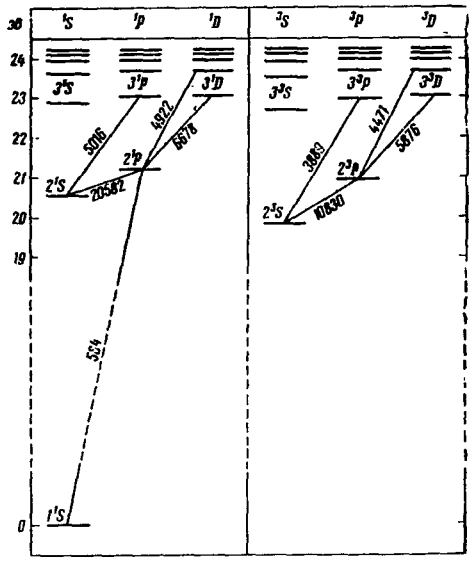

Fig. 1. Schematic Diagram of He I Energy Levels.

The relative populations of eight levels of orthohelium in a field of photospheric radiation (dilution factor of 1/2) were calculated for various values of T and n_e as an example in [3]. Some of the results obtained for the 2^3S and 2^3P levels are presented in Table 1. It can be seen that the relative populations of the lower orthohelium levels at $n_e \leq 10^{12}$ do not depend on n_e or T, and therefore are determined solely according to the field of photospheric radiation. The effect of an electron impact on the population distribution is substantial for $n_e > 10^{12}$. V.A. Krat and V.M. Sobolev [1] came to this same conclusion earlier. It can also be seen from the table that practically all the orthohelium atoms at $n_e \leq 10^{13}$ are on levels with a principal quantum number of 2. This circumstance greatly alleviates calculations of the orthohelium concentrations.

In comparing the steady-state equations, which link the orthohelium concentration to the He I and He II concentrations, we must consider the following elementary processes: excitation of triplet/106 levels from the principal He I state by an electron impact, quenching of the 2^3S level by an electron impact of the second type, ionization by radiation and electron impact, recombination into singlet and triplet levels. We must also consider the transitions between metastable 2^3S and 2^1S levels by the effect of electron impacts, since, because they are so near, the transitions between them should take place rather frequently. Let us turn to an investigation of the enumerated processes.

1. Ionization By Electron Impact. Based on experimental data concerning cross sections of ionization of neutral atoms of different elements (including helium), a formula for the probability

of ionization by electron impact was obtained in [4] (number of ionization acts per sec, in relation to one atom in the initial state and one free electron) for Maxwellian distribution of electron velocities:

TABLE 1
RELATIVE POPULATIONS OF THE 2^3S AND 2^3P LEVELS

Level	T	n_e 10^9	10^{10}	10^{11}	10^{12}	10^{13}	10^{14}	10^{15}
2^3S	$1\cdot10^4$	0,844	0,844	0,844	0,843	0,835	0,774	0,580
	$3\cdot10^4$	0,844	0,844	0,844	0,840	0,804	0,561	0,141
	$1\cdot10^5$	0,844	0,844	0,844	0,837	0,775	0,395	0,049
	$3\cdot10^5$	0,844	0,844	0,844	0,837	0,772	0,362	0,036
2^3P	$1\cdot10^4$	0,146	0,146	0,146	0,147	0,153	0,203	0,325
	$3\cdot10^4$	0,146	0,146	0,146	0,150	0,177	0,310	0,204
	$1\cdot10^5$	0,146	0,146	0,147	0,152	0,196	0,306	0,095
	$3\cdot10^5$	0,146	0,146	0,147	0,152	0,196	0,288	0,074

$$I = 1{,}8bNT^{-\frac{3}{2}} e^{-x}x^{-2}\left(1 - \frac{1+5x}{1+12x}e^{-4x}\right); \quad (1)$$

$$x = \chi/kT, \quad (2)$$

where χ is the ionization potential, k is the Boltzmann constant, and N is the number of equivalent electrons in the outer shell of the atom (for the principal He I state N = 2), b is a coefficient close to 1; for He I, b = 0.70. At $x > 0.5$, i.e., $T < 2\cdot10^4\ \chi$ (χ is expressed in electron volts), (1) is substantially simplified:

$$I = 1{,}8bNT^{-\frac{3}{2}} e^{-x}x^{-2}. \quad (3)$$

There are no experimental data on the cross sections of helium ionization (or atoms of other elements) from excited states. However, the fact that (1) is valid for atoms with different electron configurations of the principal levels (see [4]) gives us a basis on which we can assume that it can be used in calculating the ionization from excited levels. We will consider that b = 0.70 for excited He I levels, as for the principal state. It is obvious that N = 1 for the excited levels.

Cross sections of He II ionization were measured in [5]. The data of [5] agree with (1), which was obtained for neutral atoms,

while b (He II) = 0.90. It is obvious that N(He II) = 1.

2. Photoionization. The number of photoionization acts per /107
sec per atom is determined by the following expression:

$$\Phi = \int_{\nu_0}^{\infty} \frac{\alpha_\nu \, d\nu}{h\nu} \int_{\Omega} I_\nu(\vartheta, \varphi) \, d\omega, \qquad (4)$$

where $I_\nu(\vartheta, \phi)$ is the intensity of emission of frequency ν in the direction ϑ, ϕ; the radiation covers a solid angle Ω, α_ν is the atomic coefficient of continuous absorbtion, ν_0 is the frequency of the limit of the corresponding spectral series, and h is the Planck constant. The value and dependence of the absorption coefficient for the 1^1S, 2^1S, and 2^3S He I levels and for the principle He II states on ν are found in [6]. Since the absorption coefficients are unknown for the other He I levels, we will use the same values of $\alpha(\nu/\nu_0)$ as for the 2^3S level in calculating the ionization from excited orthohelium levels.

TABLE 2.
HELIUM PHOTOIONIZATION

Level	λ_0, A	α_ν, cm^2	Φ, sec^{-1}
He I 1^1S	504	$7.6 \cdot 10^{-18} (\nu_0/\nu)^2$	$1 \cdot 10^{-8}$
2^3S	2598	$2.8 \cdot 10^{-18} (\nu_0/\nu)$	$1.1 \cdot 10^{3}$
2^3P	3430	$2.8 \cdot 10^{-18} (\nu_0/\nu)$	$1.7 \cdot 10^{3}$
3^3D	8200	$2.8 \cdot 10^{-18} (\nu_0/\nu)$	$4.3 \cdot 10^{4}$
He II 1^2S	228	$1.8 \cdot 10^{-18} (\nu_0/\nu)^3$	$3 \cdot 10^{-5}$

The photoionization of orthohelium in the solar chromosphere is accomplished mainly by photospheric radiation ($\lambda \gtrsim 1800$ Å for 2^3S, $\lambda \gtrsim 2500$ Å for 2^3P, $\lambda \gtrsim 3000$ Å for 3^3D, etc.); consequently, $\Omega \approx 2\pi$ and $\int_{\Omega} I_\nu dw = 2\pi J_\nu \approx 2E_\nu$ (⊙), where J is the radiation intensity averaged over the disk, E is the flux of radiation on the solar surface. The energy distribution in the spectrum of the Sun in the 1600-2600 Å range (radiation flux E_λ(⊕) at the boundary of the Earth's atmosphere) is given in [7,8]. It is obvious that $E(\odot) = (A/R)^2 E(\oplus) = 4.6 \cdot 10^4 E(\oplus)$, where R is the radius of the Sun and A is the radius of the Earth's orbit. For $\lambda > 2600$ Å, the values of J_λ are found in [6].

The photoionization of He I and He II from the principal levels is accomplished by means of hard coronal radiation. It is easy to show that $E < \int_{2\pi} I d\omega < 2E$ both at the outer and inner boundaries of the radiating layer, while the flux going outside, i.e., E(⊙) is somewhat greater than the flux going into the chromosphere. Because of the lack of more precise information, we will consider that $\int I d\omega = E(\odot)$ and in disregarding the errors linked

with inaccuracy in the assumed relationship between $\int Id\omega$ and $E(\odot)$, it will not exceed the errors in the determination of $E(\oplus)$. The energy distribution in the λ 60-1100 Å range was obtained by G.S. Ivanov-Kholoclnyy and G.M. Nikol'skiy [9,10] on the basis of a prognosis of the intensities of short-wave lines and an analysis of rocket measurements. The measurements were carried out in 1959-1961, when the active regions in the far ultraviolet spectral range occupied 0.2-0.3 of the area of the solar disk, while the brightness exceeded that of the undisturbed regions by a factor of ~ 30 [11].

The probability of photoionization was calculated by means of a numerical integration of (4) with the aid of the spectral energy distribution according to [6, 7, 10], and with a consideration of the above-mentioned brightness ratio and the ratio of the areas of active and undisturbed regions (for $\lambda \leq 500$ Å). The values of /108 Φ, which were obtained for the undisturbed chromosphere (for regions transmittive to radiation beyond the limits of the corresponding series), are shown in Table 2.

3. Photorecombination. An expression for the sum of recombinations at all levels of the hydrogen atom was obtained in [2] on the basis of the famous Menzel formula [12]:

$$\Sigma R_n = 3{,}26 \cdot 10^{-6} T^{-\frac{3}{2}} \left[e^x Ei(x) + \frac{1}{2x} e^{\frac{4x}{9}} Ei\left(\frac{4x}{9}\right) + \frac{1{,}15}{x} \lg(0{,}79x) \right]; \qquad (5)$$

$$x = \chi_1 / kT.$$

The sum of recombinations into triplet and singlet He I levels was calculated in [13] with the aid of (5):

$$\left.\begin{aligned} R^{(1)} &= \Sigma R_n^{(1)} = R_1 + 0{,}25\,(\Sigma R_n - R_1), \\ R^{(3)} &= \Sigma R_n^{(3)} = 0{,}75\,(\Sigma R_n - R_1), \end{aligned}\right\} \qquad (6)$$

where R_1 is the number of recombinations on the 1^1S level, i.e.,

$$R_1 = 3{,}26 \cdot 10^{-6} T^{-\frac{3}{2}} e^x Ei(x).$$

The results obtained for He I according to (5) and (6) agree rather well with the more precise calculations of Burgess and Seaton [14]. The He III - He II recombination is calculated according to (5) with the supplementary coefficient $Z^2 = 4$ (Z is the charge of the He III ion).

4. Excitation of Triplet Levels From the Principal State by Electron Impact. The first reliable measurements of the cross section of excitation of the 2^3S level in the vicinity of the excitation threshold were carried out by Maier-Leibnitz [15], who

found the existence of an extremely sharp maximum near the excitation threshold (at a distance of $\sim$ 0.2 eV). The results of [15] were confirmed later by experiments of other authors [16,17] and by theoretical calculations [18].

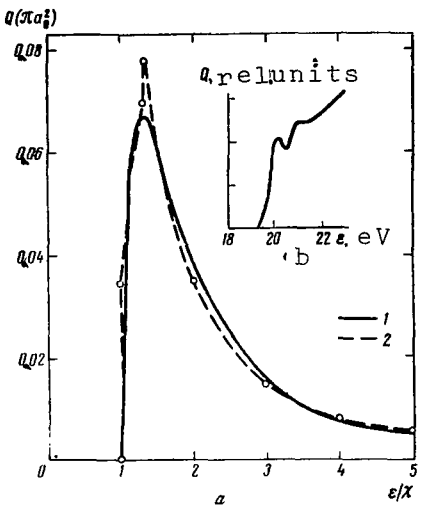

Fig. 2. Cross Section of Orthohelium Excitation From the Principal He I State by Electron Impact. (a) Experimental Curves (1), Approximation (2); (b) Course of the Luminescence in the Vicinity of the Excitation Threshold.

According to the measurements of Dorrestein [19] and Woudenberg and Milatz [20], the excitation cross section of the 2^3S level reaches a maximum at a distance of $\sim$ 6 eV from the threshold. However, these authors actually measured the rate of settlement of the 2^3S level, and not the frequency of 1^1S-2^3S transitions. Since the effect of cascade transitions from over-lying levels was not considered in this regard, the results they obtained are the sum of excitation cross sections of all the triplet levels from the principal state (see also [21] for this topic). We should mention that traces of the Maier-Leibnitz peak are clearly found on Dorrestein's curve at a distance of $\sim$ 0.2 eV from the excitation threshold of the 2^3S level (see Fig. 2).

Since we are interested in the total orthohelium concentration, let us use Dorrestein's data [19], normalized to the results of more contemporary absolute measurements of the cross section at the Maier-Leibnitz peak [17] ($Q = 2.8\cdot10^{-18}$ cm^2 at $\varepsilon-\chi = 0.2$ eV, ε is the kinetic energy of the incident electron). The experimental curve is approximated by the following function: /109

$$\Sigma Q^{(3)} = \begin{cases} 0{,}15\,\pi a_0^2\left(1{,}23 - \dfrac{\chi}{\varepsilon}\right); & 1 \leqslant \dfrac{\varepsilon}{\chi} \leqslant 1{,}3, \\ 0{,}14\pi a_0^2\left(\dfrac{\chi}{\varepsilon}\right)^2; & \dfrac{\varepsilon}{\chi} \geqslant 1{,}3, \end{cases} \tag{7}$$

where πa_0^2 is the area inside the first Bohr orbit. Having integrated (7) over the Maxwellian energy distribution, we can find the expression for the probability of excitation of the triplet levels:

$$W = \Sigma W^{(3)} = 0{,}54T^{-\frac{3}{2}}\left\{\frac{1}{x}\left[\left(0{,}187 + \frac{1}{x}\right)e^{-x} - \left(0{,}488 + \frac{1}{x}\right)e^{-1{,}3x}\right] + 0{,}74Ei\,(1{,}3x)\right\}; \tag{8}$$

$$x = \chi_{2^3S}/kT = 2{,}30\cdot10^5/T,$$

where $\chi_2{}^3s$ is the excitation potential of the 2^3S level.

We obtained a different expression for the probability of excitation of the triplet levels in [13] as a result of the use of another, less accurate approximation of the experimental curve:

$$W = 0{,}1T^{-\frac{3}{2}}[2{,}4e^{-x}x^{-1} - Ei(x)]. \tag{9}$$

The values of W, which were calculated according to (8) and (9), differed by no more than 20% at $x > 0.5$. The deviation becomes substantial only at $x < 0.5$, i.e., at $T > 5 \cdot 10^5$. It is clear that the simple expression in (9) is completely suitable for the conditions of the solar chromosphere and the transition layer between the chromosphere and the corona. At $x > 5$, it acquires an even simpler form:

$$W = 0{,}14T^{-\frac{3}{2}}e^{-x}x^{-1}. \tag{10}$$

For calculations of the probability of G-transitions at the principal level by the effect of collisions of the second type (quenching), we will use the famous relationship obtained from the condition of detail equilibrium:

$$\frac{G_{21}}{W_{12}} = \frac{g_1}{g_2}e^x, \tag{11}$$

where g is the statistical weight.

5. 2^3S-2^1S Transitions By the Effect of Electron Impact. It is completely obvious that transitions between the close metastable 2^3S and 2^1S levels (energy difference of 0.79 eV) by the effect of electron impacts should take place rather frequently. In order to calculate the probability of a G' transition of 2^1S - 2^3S, let us use the results of Phelps' measurements [22] and the theoretical calculations of Marriott [23]. There are still no other data in the literature. The effective cross sections of the 2^1S - 2^3S transitions were calculated in [23] for several values of the energy of the incident electron. The results of [23] can be approximated by the following function:

$$Q = C\chi\varepsilon^{-1}[1 - 0{,}83\exp(-2{,}9\,\varepsilon/\chi)], \tag{12}$$

where C is the coefficient of proportionality, for the determination of which we will use the experimental data. The probability of a /110 2^1S - 2^3S transition at T = 300° was measured in [22] in a calcula-

tion per one atom in the 2^1S state and one free electron: $G' = 3.5 \cdot 10^{-7}$ sec^{-1}. The expressions for the probability of a 2^1S - 2^3S transition which was obtained by integration of (12) over the Maxwellian energy distribution should now be normalized to the measured value of G' at T = 300°. As a result, we find that $C = 51\ \pi\ a_0^2$ and

$$G' = 0{,}23\, T^{-\frac{3}{2}} \left(\frac{1}{x} - \frac{0{,}83}{x + 2{,}9}\right), \qquad x = \chi_{2^1s-2^3s}/kT = 9{,}05 \cdot 10^3/T. \tag{13}$$

We can obtain the probability formula W' for the inverse 2^3S - 2^1S transition from (13) and (11):

$$W' = 0{,}077\, T^{-\frac{3}{2}} e^{-x} \left(\frac{1}{x} - \frac{0{,}83}{x + 2{,}9}\right). \tag{14}$$

Let us evaluate the relative frequency of direct and reverse transitions between metastable helium levels. The population ratio of the 2^1S and 2^3S levels can obviously be determined by a comparison of the intensities of the singlet and triplet lines observed simultaneously at the same point on the chromosphere. An evaluation we carried out on the basis of the results of significant observations in [24] (the pairs of lines 3P - 2S (3889-5016), 3D-2P (5876-6678) and 4D=2P (4471-4922) were used) showed that the population of the 2^1S level was two orders lower than the population of 2^3S level. It follows from (11) that $G' \approx 3W'$ at $T > 10^4$. Consequently, the 2^3S-2^1S transitions take place in a unit volume roughly 30 times more often than do the 2^1S-2^3S transitions. Since the total number of all "external" drifts from the 2^3S levels per unit time should be equal to the total number of all "external" advances onto this level under stationary conditions, then it follows from the relationship $n_2 1_S G' \leq n_2 3_S W'$ that the role of the 2^1S-2^3S transitions in the settlement of orthohelium is not great in comparison to other "population" processes (excitation from the principal state and recombinations). Therefore, we will consider only the 2^3S-2^1S transition in the future.

The probabilities of the elementary processes under investigation are shown in Table 3 for a number of values of the kinetic temperature.

Let us turn to the cross section of the steady-state equations. We will carry out the calculations for $n_e \leq 10^{13}$, and we will assume that the orthohelium atom has only one level (see Table 1). In such a case, the steady-state equations which link the concentration of He I (principal state), orthohelium and He II have the following form:

$$\left.\begin{aligned} n_I^{(1)}(I + \Phi/n_e + W) &= n_{II} R^{(1)} + n_I^{(3)}(G + W'), \\ n_I^{(3)}(I' + \Phi'/n_e + W' + G) &= n_{II} R^{(3)} + n_I^{(1)} W, \end{aligned}\right\} \tag{15a}$$

where $n_I^{(1)}$, n_{II} and $n_I^{(3)}$ are the concentration of He I, He II and orthohelium, respectively. The right hand part of the second equation takes into account all the "populating" processes in orthohelium--transitions from the principal He I state and recombination through all the triplet levels. If in the lefthand part of the equation we consider that $n_I^{(3)} = n_{2^3S}$, then the ionization from the overlying triplet levels will not be taken into account. At the same time, the number of ionizations from the 2^3P and 3^3D levels per unit volume is found to be comparable to, and sometimes exceeding, the number of ionizations from the 2^3S level, since a decrease in the population of the overlying levels is compensated by an increase in the probability of the process. For ionization by electron impact, this is connected with a decrease in the bonding energy of the overlying levels, and for photoionization it is connected with an increase in the energy of the ionizing radiation during transition from the ultraviolet to the visible spectral range. In such a case the terms I' and Φ' should have the following form: /111

$$\left.\begin{aligned} I' &= \frac{n_{2^3s}}{n_I^{(3)}} I_{2^3s} + \frac{n_{2^3P}}{n_I^{(3)}} I_{2^3P} + \frac{n_{3^3D}}{n_I^{(3)}} I_{3^3D} + \dots \\ \Phi' &= \frac{n_{2^3s}}{n_I^{(3)}} \Phi_{2^3s} + \frac{n_{2^3P}}{n_I^{(3)}} \Phi_{2^3P} + \frac{n_{3^3D}}{n_I^{(3)}} \Phi_{3^3D} + \dots \end{aligned}\right\} \qquad (16)$$

TABLE 3
PROBABILITIES OF ELEMENTARY PROCESSES

T	$I(1^1S)$	$I(2^1S)$	$I(2^1P)$	$I(3^1D)$	I (He II)	$R^{(1)}$
$5\cdot10^3$	$3{,}6\cdot10^{-34}$	$4{,}3\cdot10^{-13}$	$1{,}2\cdot10^{-11}$	$8{,}3\cdot10^{-9}$	0	$2{,}3\cdot10^{-13}$
$1\cdot10^4$	$1{,}3\cdot10^{-21}$	$1{,}7\cdot10^{-10}$	$1{,}1\cdot10^{-9}$	$6{,}9\cdot10^{-8}$	$1{,}6\cdot10^{-37}$	$1{,}6\cdot10^{-13}$
$2\cdot10^4$	$2{,}8\cdot10^{-15}$	$3{,}7\cdot10^{-9}$	$1{,}3\cdot10^{-8}$	$2{,}3\cdot10^{-7}$	$1{,}2\cdot10^{-23}$	$1{,}0\cdot10^{-13}$
$3\cdot10^4$	$3{,}9\cdot10^{-13}$	$1{,}2\cdot10^{-8}$	$3{,}1\cdot10^{-8}$	$3{,}9\cdot10^{-7}$	$5{,}0\cdot10^{-19}$	$7{,}8\cdot10^{-14}$
$5\cdot10^4$	$2{,}3\cdot10^{-11}$	$3{,}1\cdot10^{-8}$	$7{,}1\cdot10^{-8}$	$5{,}2\cdot10^{-7}$	$2{,}9\cdot10^{-15}$	$5{,}5\cdot10^{-14}$
$1\cdot10^5$	$5{,}8\cdot10^{-10}$	$7{,}4\cdot10^{-8}$	$1{,}3\cdot10^{-7}$	$7{,}2\cdot10^{-7}$	$2{,}3\cdot10^{-12}$	$3{,}3\cdot10^{-14}$
$3\cdot10^5$	$6{,}6\cdot10^{-9}$	$1{,}3\cdot10^{-7}$	$2{,}1\cdot10^{-7}$	$8{,}0\cdot10^{-7}$	$2{,}7\cdot10^{-10}$	$1{,}4\cdot10^{-14}$

T	$R^{(3)}$	R (He II)	W	G	W'
$5\cdot10^3$	$2{,}3\cdot10^{-13}$	$9{,}8\cdot10^{-13}$	$9{,}0\cdot10^{-29}$	$2{,}6\cdot10^{-9}$	$1{,}3\cdot10^{-8}$
$1\cdot10^4$	$1{,}3\cdot10^{-13}$	$6{,}0\cdot10^{-13}$	$6{,}1\cdot10^{-19}$	$1{,}9\cdot10^{-9}$	$2{,}8\cdot10^{-8}$
$2\cdot10^4$	$7{,}6\cdot10^{-14}$	$3{,}9\cdot10^{-13}$	$4{,}2\cdot10^{-14}$	$1{,}4\cdot10^{-9}$	$3{,}4\cdot10^{-8}$
$3\cdot10^4$	$5{,}4\cdot10^{-14}$	$2{,}8\cdot10^{-13}$	$1{,}7\cdot10^{-12}$	$1{,}2\cdot10^{-9}$	$3{,}4\cdot10^{-8}$
$5\cdot10^4$	$3{,}4\cdot10^{-14}$	$2{,}0\cdot10^{-13}$	$2{,}9\cdot10^{-11}$	$9{,}6\cdot10^{-10}$	$3{,}0\cdot10^{-8}$
$1\cdot10^5$	$1{,}8\cdot10^{-14}$	$1{,}2\cdot10^{-13}$	$2{,}2\cdot10^{-10}$	$6{,}9\cdot10^{-10}$	$2{,}4\cdot10^{-8}$
$3\cdot10^5$	$5{,}7\cdot10^{-15}$	$4{,}8\cdot10^{-14}$	$6{,}8\cdot10^{-10}$	$4{,}1\cdot10^{-10}$	$1{,}5\cdot10^{-8}$

It is easy to show that at $n_e \leq 10^{13}$ it is sufficient to consider only the levels with principal quantum numbers of 2 and 3. The relative populations of these levels and the probabilities of ionization from them are already known. As for the terms W' and G, they should be approximately identical for all the orthohelium levels. For G, this is linked with the fact that the excitation potentials of the triplet levels differ insignificantly, while it can be seen from Table 3 that a change in the value of χ/kT by a factor of 60 brings about a change in G merely by a factor of 6. The minimum value of W' differs from the maximum one in the temperature range of $5 \cdot 10^3$-$3 \cdot 10^5$ by a factor of 2.5. This can be explained by the fact that the position of the maximum for the cross section of the 2^3S-2^1S transition within the temperature range under investigation coincides approximately with the position of the maximum of the Maxwellian distribution of electron energy. Thus, we can consider for the processes G and W' that the orthohelium atom has only one level with population of n_I^3.

The equations in (15a) are also equations for He I-He II ionization equilibrium. In contrast to the regular equation of ionization balance, the system in (15a) takes into account the mechanism of helium ionization, which consists of excitation by electron impact of the metastable 2^3S level with subsequent ionization from this or other triplet levels. I.S. Shklovskiy [25] and M.I. Yamoto [26] were the first to examine such a mechanism of He I ionization. We could wonder what the role of the metastable 2^1S level is in helium ionization. Since the bonding energies of the 2^1S and 2^3S levels are rather close, the probability of ionization by impact or radiation should be roughly identical for both levels (the same holds for the levels 2^1P and 2^3P, 3^1D and 3^3D, etc.). However, the population of the 2^1S level under the conditions of the solar chromosphere is two orders lower than that of the 2^3S level. Therefore, the contribution of the 2^1S level (and, obviously, of the overlying parahelium levels) in helium ionization is incomparably less than the contribution of the triplet levels. We therefore will not consider the ionization from excited parahelium levels in (15a). /112

The equation for He II - He III ionization equilibrium is the following:

$$\frac{n_{II}}{n_{III}} = \frac{\Sigma R}{I + \Phi/n_e}, \qquad (15b)$$

where n_{III} is the concentration of He III.

We will calculate the helium concentration at different stages of ionization according to its relationship to the total concentration of all helium. Therefore, the fourth equation of the system

TABLE 4a

RELATIVE CONCENTRATION OF He I, He II, He III AND ORTHOHELIUM INDEPENDENCE ON n_e AND T (THERE IS NO RADIATION FIELD WITH $\lambda < 504$ Å).

Ionization Stage	T	n_e 10^8	10^9	10^{10}	10^{11}	10^{12}	10^{13}
He I	$5\cdot10^3$	1,00	1,00	1,00	1,00	1,00	1,00
	$1\cdot10^4$	1,00	1,00	1,00	1,00	1,00	1,00
	$2\cdot10^4$	0,692	0,713	0,816	0,924	0,945	0,935
	$3\cdot10^4$	$3,6\cdot10^{-2}$	$3,9\cdot10^{-2}$	$6,0\cdot10^{-2}$	$9,7\cdot10^{-2}$	0,106	$9,4\cdot10^{-2}$
	$5\cdot10^4$	$1,0\cdot10^{-3}$	$1,1\cdot10^{-3}$	$1,4\cdot10^{-3}$	$1,7\cdot10^{-3}$	$1,7\cdot10^{-3}$	$1,6\cdot10^{-3}$
	$1\cdot10^5$	$2,0\cdot10^{-5}$	$2,1\cdot10^{-5}$	$2,3\cdot10^{-5}$	$2,4\cdot10^{-5}$	$2,4\cdot10^{-5}$	$2,4\cdot10^{-5}$
	$3\cdot10^5$	$3,4\cdot10^{-10}$	$3,4\cdot10^{-10}$	$3,5\cdot10^{-10}$	$3,6\cdot10^{-10}$	$3,6\cdot10^{-10}$	$3,6\cdot10^{-10}$
He II	$5\cdot10^3$	$3,9\cdot10^{-16}$	$3,7\cdot10^{-16}$	$2,4\cdot10^{-16}$	$5,5\cdot10^{-17}$	$6,9\cdot10^{-18}$	$1,4\cdot10^{-18}$
	$1\cdot10^4$	$3,8\cdot10^{-6}$	$3,4\cdot10^{-6}$	$1,9\cdot10^{-6}$	$3,7\cdot10^{-7}$	$7,9\cdot10^{-8}$	$5,7\cdot10^{-8}$
	$2\cdot10^4$	0,308	0,287	0,184	$7,6\cdot10^{-2}$	$5,5\cdot10^{-2}$	$6,6\cdot10^{-2}$
	$3\cdot10^4$	0,964	0,961	0,940	0,902	0,895	0,905
	$5\cdot10^4$	0,985	0,985	0,985	0,985	0,985	0,983
	$1\cdot10^5$	$5,0\cdot10^{-2}$	$5,0\cdot10^{-2}$	$5,0\cdot10^{-2}$	$5,0\cdot10^{-2}$	$5,0\cdot10^{-2}$	$5,0\cdot10^{-2}$
	$3\cdot10^5$	$1,8\cdot10^{-4}$	$1,8\cdot10^{-4}$	$1,8\cdot10^{-4}$	$1,8\cdot10^{-4}$	$1,8\cdot10^{-4}$	$1,8\cdot10^{-4}$
He III	$5\cdot10^3$	0,00	0,00	0,00	0,00	0,00	0,00
	$1\cdot10^4$	$1,0\cdot10^{-30}$	$9,2\cdot10^{-31}$	$5,0\cdot10^{-31}$	$9,8\cdot10^{-32}$	$2,2\cdot10^{-32}$	$1,5\cdot10^{-32}$
	$2\cdot10^4$	$9,5\cdot10^{-12}$	$8,9\cdot10^{-12}$	$5,6\cdot10^{-12}$	$2,3\cdot10^{-12}$	$1,7\cdot10^{-12}$	$2,0\cdot10^{-12}$
	$3\cdot10^4$	$1,7\cdot10^{-6}$	$1,7\cdot10^{-6}$	$1,7\cdot10^{-6}$	$1,6\cdot10^{-6}$	$1,6\cdot10^{-6}$	$1,6\cdot10^{-6}$
	$5\cdot10^4$	$1,4\cdot10^{-2}$	$1,4\cdot10^{-2}$	$1,4\cdot10^{-2}$	$1,4\cdot10^{-2}$	$1,4\cdot10^{-2}$	$1,4\cdot10^{-2}$
	$1\cdot10^5$	0,952	0,950	0,950	0,952	0,951	0,951
	$3\cdot10^5$	1,00	1,00	1,00	1,00	1,00	1,00
Ortho-helium	$5\cdot10^3$	$3,5\cdot10^{-23}$	$3,3\cdot10^{-22}$	$2,2\cdot10^{-21}$	$5,0\cdot10^{-21}$	$5,7\cdot10^{-21}$	$5,8\cdot10^{-21}$
	$1\cdot10^4$	$2,2\cdot10^{-13}$	$2,0\cdot10^{-12}$	$1,0\cdot10^{-11}$	$1,8\cdot10^{-11}$	$2,0\cdot10^{-11}$	$2,0\cdot10^{-11}$
	$2\cdot10^4$	$1,0\cdot10^{-8}$	$9,4\cdot10^{-8}$	$5,3\cdot10^{-7}$	$9,6\cdot10^{-7}$	$1,0\cdot10^{-6}$	$1,0\cdot10^{-6}$
	$3\cdot10^4$	$2,2\cdot10^{-8}$	$2,1\cdot10^{-7}$	$1,5\cdot10^{-6}$	$3,8\cdot10^{-6}$	$4,3\cdot10^{-6}$	$3,6\cdot10^{-6}$
	$5\cdot10^4$	$1,2\cdot10^{-8}$	$1,1\cdot10^{-7}$	$6,2\cdot10^{-7}$	$1,1\cdot10^{-6}$	$1,2\cdot10^{-6}$	$1,0\cdot10^{-6}$
	$1\cdot10^5$	$2,6\cdot10^{-10}$	$2,2\cdot10^{-9}$	$8,7\cdot10^{-9}$	$1,2\cdot10^{-8}$	$1,3\cdot10^{-8}$	$1,2\cdot10^{-8}$
	$3\cdot10^5$	$2,4\cdot10^{-13}$	$1,8\cdot10^{-12}$	$6,0\cdot10^{-12}$	$7,6\cdot10^{-12}$	$7,7\cdot10^{-12}$	$8,3\cdot10^{-12}$

TABLE 4b

RELATIVE CONCENTRATION OF He, I, He II, He III AND ORTHOHELIUM /113
INDEPENDENCE ON n_e AND T (IN THE FIELD OF CORONAL RADIATION WITH $\lambda < 504$ Å)

Ionization Stage	T	n_e					
		10^8	10^9	10^{10}	10^{11}	10^{12}	10^{13}
He I	$5\cdot10^3$	$1.7\cdot10^{-2}$	0.187	0.740	0.975	1.00	1.00
	$1\cdot10^4$	$1.1\cdot10^{-2}$	0.137	0.675	0.965	1.00	1.00
	$2\cdot10^4$	$5.6\cdot10^{-3}$	$8.6\cdot10^{-2}$	0.497	0.873	0.940	0.935
	$3\cdot10^4$	$3.1\cdot10^{-3}$	$2.4\cdot10^{-2}$	$5.6\cdot10^{-2}$	$9.5\cdot10^{-2}$	0.106	$9.4\cdot10^{-2}$
	$5\cdot10^4$	$3.6\cdot10^{-4}$	$9.5\cdot10^{-4}$	$1.4\cdot10^{-3}$	$1.7\cdot10^{-3}$	$1.7\cdot10^{-3}$	$1.6\cdot10^{-3}$
	$1\cdot10^5$	$1.8\cdot10^{-6}$	$2.1\cdot10^{-6}$	$2.3\cdot10^{-6}$	$2.4\cdot10^{-6}$	$2.4\cdot10^{-6}$	$2.4\cdot10^{-6}$
	$3\cdot10^5$	$3.4\cdot10^{-10}$	$3.4\cdot10^{-10}$	$3.5\cdot10^{-10}$	$3.6\cdot10^{-10}$	$3.6\cdot10^{-10}$	$3.6\cdot10^{-10}$
He II	$5\cdot10^3$	0.753	0.790	0.260	$2.4\cdot10^{-2}$	$2.2\cdot10^{-3}$	$2.2\cdot10^{-4}$
	$1\cdot10^4$	0.660	0.821	0.325	$3.6\cdot10^{-2}$	$3.5\cdot10^{-3}$	$3.5\cdot10^{-4}$
	$2\cdot10^4$	0.562	0.849	0.503	0.127	$6.1\cdot10^{-2}$	$6.6\cdot10^{-2}$
	$3\cdot10^4$	0.482	0.884	0.932	0.902	0.895	0.906
	$5\cdot10^4$	0.397	0.857	0.970	0.984	0.985	0.984
	$1\cdot10^5$	$4.3\cdot10^{-2}$	$4.9\cdot10^{-2}$	$5.0\cdot10^{-2}$	$5.0\cdot10^{-2}$	$5.0\cdot10^{-2}$	$5.0\cdot10^{-2}$
	$3\cdot10^5$	$1.8\cdot10^{-4}$	$1.8\cdot10^{-4}$	$1.8\cdot10^{-4}$	$1.8\cdot10^{-4}$	$1.8\cdot10^{-4}$	$1.8\cdot10^{-4}$
He III	$5\cdot10^3$	0.230	$2.4\cdot10^{-3}$	$8.0\cdot10^{-4}$	$7.4\cdot10^{-6}$	$6.8\cdot10^{-8}$	$6.7\cdot10^{-10}$
	$1\cdot10^4$	0.330	$4.1\cdot10^{-3}$	$1.6\cdot10^{-3}$	$1.8\cdot10^{-5}$	$1.8\cdot10^{-7}$	$1.7\cdot10^{-9}$
	$2\cdot10^4$	0.433	$8.5\cdot10^{-3}$	$3.9\cdot10^{-3}$	$9.8\cdot10^{-5}$	$4.7\cdot10^{-6}$	$5.0\cdot10^{-7}$
	$3\cdot10^4$	0.516	$9.4\cdot10^{-2}$	$1.0\cdot10^{-2}$	$9.7\cdot10^{-4}$	$9.8\cdot10^{-5}$	$1.1\cdot10^{-5}$
	$5\cdot10^4$	0.603	0.141	$2.9\cdot10^{-2}$	$1.6\cdot10^{-2}$	$1.4\cdot10^{-3}$	$1.4\cdot10^{-2}$
	$1\cdot10^5$	0.965	0.950	0.950	0.952	0.952	0.952
	$3\cdot10^5$	1.00	1.00	1.00	1.00	1.00	1.00
Ortho-helium	$5\cdot10^3$	$3.4\cdot10^{-8}$	$3.4\cdot10^{-7}$	$9.0\cdot10^{-7}$	$2.3\cdot10^{-7}$	$3.2\cdot10^{-8}$	$3.2\cdot10^{-9}$
	$1\cdot10^4$	$1.7\cdot10^{-8}$	$2.0\cdot10^{-7}$	$5.2\cdot10^{-7}$	$1.3\cdot10^{-7}$	$1.5\cdot10^{-8}$	$1.5\cdot10^{-9}$
	$2\cdot10^4$	$8.8\cdot10^{-9}$	$1.2\cdot10^{-7}$	$6.4\cdot10^{-7}$	$9.9\cdot10^{-7}$	$1.0\cdot10^{-6}$	$1.0\cdot10^{-6}$
	$3\cdot10^4$	$6.1\cdot10^{-9}$	$1.6\cdot10^{-7}$	$1.4\cdot10^{-6}$	$3.7\cdot10^{-6}$	$4.3\cdot10^{-6}$	$3.6\cdot10^{-6}$
	$5\cdot10^4$	$4.6\cdot10^{-9}$	$9.8\cdot10^{-8}$	$6.0\cdot10^{-7}$	$1.1\cdot10^{-6}$	$1.2\cdot10^{-6}$	$1.0\cdot10^{-6}$
	$1\cdot10^5$	$2.3\cdot10^{-10}$	$2.2\cdot10^{-9}$	$8.6\cdot10^{-9}$	$1.2\cdot10^{-8}$	$1.3\cdot10^{-8}$	$1.2\cdot10^{-8}$
	$3\cdot10^5$	$2.4\cdot10^{-13}$	$1.9\cdot10^{-12}$	$6.0\cdot10^{-12}$	$7.6\cdot10^{-12}$	$7.7\cdot10^{-12}$	$8.2\cdot10^{-12}$

in (15) is written out in the following way:

$$n_{\mathrm{I}} + n_{\mathrm{II}} + n_{\mathrm{III}} = 1. \tag{15c}$$

Let us remember that the calculations are being carried out for two limiting cases: (1) Φ (1^1S He I) = Φ (He II) = 0; (2) the values of Φ (1^1S He I) and Φ (He II) are equal to the values in Table 2. The results of the calculation are given in Tables 4(a) and (b).

In order to calculate the absolute orthohelium concentration, we must know ratio the between $n_{\Sigma He}$ and n_e. According to the modern concepts [6],

(17)

$$n_{\Sigma He} = 0{,}1 n_{\Sigma H}.$$

TABLE 5a /114

ABSOLUTE CONCENTRATIONS OF LOWER ORTHOHELIUM LEVELS (RADIATION FIELD WITH $\lambda < 504$ Å IS ABSENT).

Level	T	n_e 10^9	10^{10}	10^{11}	10^{12}	10^{13}
2^3S	$1\cdot10^4$	$1{,}3\cdot10^{-3}$	$1{,}2\cdot10^{-1}$	6,4	$1{,}1\cdot10^2$	$1{,}2\cdot10^3$	$1{,}1\cdot10^4$
	$2\cdot10^4$	$8{,}6\cdot10^{-3}$	8,0	$4{,}4\cdot10^2$	$8{,}1\cdot10^3$	$8{,}6\cdot10^4$	$6{,}4\cdot10^5$
	$3\cdot10^4$	$1{,}9\cdot10^{-1}$	$1{,}8\cdot10^1$	$1{,}3\cdot10^3$	$3{,}2\cdot10^4$	$3{,}5\cdot10^5$	$2{,}0\cdot10^6$
	$5\cdot10^4$	$1{,}0\cdot10^{-1}$	9,5	$5{,}2\cdot10^3$	$9{,}2\cdot10^3$	$9{,}1\cdot10^4$	$4{,}9\cdot10^5$
	$1\cdot10^5$	$2{,}2\cdot10^{-3}$	$1{,}8\cdot10^{-1}$	7,4	$1{,}0\cdot10^2$	$9{,}8\cdot10^2$	$4{,}8\cdot10^3$
	$3\cdot10^5$	$2{,}0\cdot10^{-6}$	$1{,}6\cdot10^{-4}$	$5{,}0\cdot10^{-3}$	$6{,}4\cdot10^{-2}$	$6{,}0\cdot10^{-1}$	3,0
2^3P	$1\cdot10^4$	$2{,}3\cdot10^{-4}$	$2{,}1\cdot10^{-2}$	1,1	$2{,}0\cdot10^1$	$2{,}2\cdot10^2$	$3{,}0\cdot10^3$
	$2\cdot10^4$	$1{,}5\cdot10^{-2}$	1,4	$7{,}7\cdot10^1$	$1{,}4\cdot10^3$	$1{,}8\cdot10^4$	$2{,}8\cdot10^5$
	$3\cdot10^4$	$3{,}2\cdot10^{-2}$	3,1	$2{,}2\cdot10^2$	$5{,}6\cdot10^3$	$7{,}6\cdot10^4$	$1{,}1\cdot10^6$
	$5\cdot10^4$	$1{,}8\cdot10^{-2}$	1,6	$9{,}0\cdot10^1$	$1{,}7\cdot10^3$	$2{,}2\cdot10^4$	$3{,}3\cdot10^5$
	$1\cdot10^5$	$3{,}7\cdot10^{-4}$	$3{,}2\cdot10^{-2}$	1,3	$1{,}8\cdot10^1$	$2{,}5\cdot10^2$	$3{,}7\cdot10^3$
	$3\cdot10^5$	$3{,}4\cdot10^{-7}$	$2{,}7\cdot10^{-5}$	$8{,}8\cdot10^{-4}$	$1{,}2\cdot10^{-2}$	$1{,}5\cdot10^{-1}$	2,4
3^3D	$1\cdot10^4$	$3{,}4\cdot10^{-6}$	$3{,}1\cdot10^{-4}$	$1{,}6\cdot10^{-2}$	$2{,}9\cdot10^{-1}$	3,3	$4{,}5\cdot10^1$
	$2\cdot10^4$	$2{,}2\cdot10^{-4}$	$2{,}0\cdot10^{-2}$	1,1	$2{,}1\cdot10^1$	$2{,}7\cdot10^2$	$6{,}5\cdot10^3$
	$3\cdot10^4$	$4{,}8\cdot10^{-4}$	$4{,}6\cdot10^{-2}$	3,3	$8{,}3\cdot10^1$	$1{,}2\cdot10^3$	$3{,}3\cdot10^4$
	$5\cdot10^4$	$2{,}5\cdot10^{-4}$	$2{,}4\cdot10^{-2}$	1,3	$2{,}5\cdot10^1$	$3{,}8\cdot10^2$	$1{,}3\cdot10^4$
	$1\cdot10^5$	$5{,}6\cdot10^{-6}$	$4{,}7\cdot10^{-4}$	$1{,}9\cdot10^{-2}$	$2{,}8\cdot10^{-1}$	4,8	$2{,}0\cdot10^2$
	$3\cdot10^5$	$5{,}1\cdot10^{-9}$	$4{,}0\cdot10^{-7}$	$1{,}3\cdot10^{-5}$	$1{,}8\cdot10^{-4}$	$3{,}2\cdot10^{-3}$	$1{,}6\cdot10^{-1}$

From the equation of hydrogen ionization equilibrium of $n_e/n_{HI} = I/\Sigma R$ and (17), we find that $n_{\Sigma He} = 72\, n_e$ for $T = 10^4$, and $n_{\Sigma He} = 0.1\, n_e$ for $T \geq 2\cdot10^4$. At $T < 10^4$, the concentration of free electrons is produced mainly by ionization of the metals, and a determination of the ratio between $n_{\Sigma He}$ and n_e becomes much more complicated. Therefore, we will calculate the absolute concentration of orthohelium for $T \geq 10^4$ when there is no radiation field with $\lambda < 504$ Å. It is easy to show that $n_{\Sigma He} = 0.1\, n_e$ in the regions which are transmitted to radiation with $\lambda < 504$ Å at $n_e \leq 10^9$, even if $T < 10^4$. For $n_e > 10^9$, coronal radiation with $\lambda < 504$ Å is insufficient for a total hydrogen ionization (for $T \leq 10^4$). However, at $n_e = 10^{10}$ the total hydrogen ioniza-

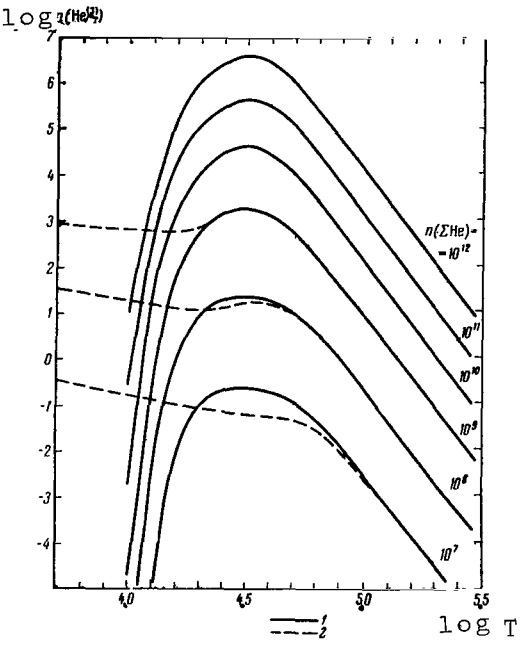

tion can still be accomplished by radiation in the λ 500-912 Å region.

Fig. 3. Dependence of Orthohelium Concentration on Temperature and Density. (1) External Radiation with λ < 504 Å is Absent; (2) He Atoms Are in the Field of Coronal Radiation with λ < 504 Å.

For higher values of n_e, hydrogen ionization by coronal radiation is only partial. Because we do not know the ratio between $n_{\Sigma He}$ (or $n_{\Sigma H}$) and n_e for $n_e > 10^{10}$ and $T < 2 \cdot 10^4$, we will carry out the calculations for the absolute

TABLE 5b
ABSOLUTE POPULATIONS OF LOWER ORTHOHELIUM LEVELS (IN FIELD OF CORONAL RADIATION WITH λ < 504 Å). /115

Level	T	n_e		
		10^8	10^9	10^{10}
2^3S	$5 \cdot 10^3$	$2{,}8 \cdot 10^{-1}$	$2{,}9 \cdot 10^1$	$7{,}6 \cdot 10^2$
	$1 \cdot 10^4$	$1{,}4 \cdot 10^{-1}$	$1{,}7 \cdot 10^1$	$4{,}4 \cdot 10^2$
	$2 \cdot 10^4$	$7{,}4 \cdot 10^{-2}$	$1{,}0 \cdot 10^1$	$5{,}4 \cdot 10^2$
	$3 \cdot 10^4$	$5{,}2 \cdot 10^{-2}$	$1{,}4 \cdot 10^1$	$1{,}2 \cdot 10^3$
	$5 \cdot 10^4$	$3{,}9 \cdot 10^{-2}$	$8{,}2$	$5{,}1 \cdot 10^2$
	$1 \cdot 10^5$	$1{,}9 \cdot 10^{-3}$	$1{,}8 \cdot 10^{-1}$	$7{,}3$
	$3 \cdot 10^5$	$2{,}0 \cdot 10^{-5}$	$1{,}6 \cdot 10^{-4}$	$6{,}4 \cdot 10^{-3}$
2^3P	$5 \cdot 10^3$	$4{,}9 \cdot 10^{-2}$	$5{,}0$	$1{,}3 \cdot 10^2$
	$1 \cdot 10^4$	$2{,}4 \cdot 10^{-2}$	$2{,}9$	$7{,}7 \cdot 10^1$
	$2 \cdot 10^4$	$1{,}3 \cdot 10^{-2}$	$1{,}8$	$9{,}4 \cdot 10^1$
	$3 \cdot 10^4$	$8{,}9 \cdot 10^{-3}$	$2{,}4$	$2{,}1 \cdot 10^2$
	$5 \cdot 10^4$	$6{,}7 \cdot 10^{-3}$	$1{,}4$	$8{,}9 \cdot 10^1$
	$1 \cdot 10^5$	$3{,}4 \cdot 10^{-4}$	$3{,}2 \cdot 10^{-2}$	$1{,}3$
	$3 \cdot 10^5$	$3{,}4 \cdot 10^{-7}$	$2{,}7 \cdot 10^{-5}$	$8{,}8 \cdot 10^{-4}$
3^3D	$5 \cdot 10^3$	$7{,}3 \cdot 10^{-4}$	$7{,}4 \cdot 10^{-2}$	$2{,}0$
	$1 \cdot 10^4$	$3{,}6 \cdot 10^{-4}$	$4{,}3 \cdot 10^{-2}$	$1{,}1$
	$2 \cdot 10^4$	$1{,}9 \cdot 10^{-4}$	$2{,}7 \cdot 10^{-2}$	$1{,}4$
	$3 \cdot 10^4$	$1{,}3 \cdot 10^{-4}$	$3{,}5 \cdot 10^{-2}$	$3{,}1$
	$5 \cdot 10^4$	$9{,}9 \cdot 10^{-5}$	$2{,}1 \cdot 10^{-2}$	$1{,}3$
	$1 \cdot 10^5$	$5{,}0 \cdot 10^{-6}$	$4{,}7 \cdot 10^{-4}$	$1{,}9 \cdot 10^{-2}$
	$3 \cdot 10^5$	$5{,}1 \cdot 10^{-9}$	$4{,}0 \cdot 10^{-7}$	$1{,}3 \cdot 10^{-5}$

orthohelium concentration in a field of coronal radiation with $\lambda < 504$ Å only for $n_e \leq 10^{10}$. The results are shown in Fig. 3. Each curve represents the dependence of the total orthohelium concentration on the temperature for a given total concentration of all helium. The absolute populations of the 2^3S, 2^3P and 3^3D levels as a function of n_e and T were calculated on the basis of these results as well as the relative populations of the lower orthohelium levels obtained earlier. The results of these calculations are shown in Table 5 (a) and (b). We can see that the temperature range of 20,000-50,000° is optimum for excitation of orthohelium. The orthohelium concentration observed in the chromosphere [27] for reasonable values of n_e is guaranteed only at $T \geq 20{,}000°$. On the other hand, it can be seen from Fig. 3 and Table 5 that, if they are transmitted to coronal radiation with $\lambda \leq 504$ Å in the "cold" regions ($T \leq 10^4$), then the requisite (i.e., that known from observations) concentration of orthohelium can be produced by means of He I photoionization with subsequent recombination at the triplet levels. I.S. Shklovskiy [28] pointed out the possibility of such a mechanism for helium excitation in 1945. At the present, A.I. Nikol'skaya [29] is now developing a concept concerning the determinant role of coronal radiation with $\lambda < 504$ Å in the population of the metastable 2^3S level in "cold" spicules.

TABLE 6
INTENSITY RATIO FOR λ 10830 AND λ 5876 LINES /116

T	n_e						Boltzmann
	1[illegible]	10^{10}	10^{11}	10^{12}	10^{13}	10^{14}	
$5 \cdot 10^3$	5,35	5,35	5,35	5,35	5,35	5,38	6,37
$1 \cdot 10^4$	5,35	5,35	5,35	5,32	4,75	2,96	0,55
$2 \cdot 10^4$	5,35	5,35	5,33	5,07	3,40	1,02	0,16
$3 \cdot 10^4$	5,35	5,35	5,31	4,86	2,71	0,59	0,11
$5 \cdot 10^4$	5,35	5,35	5,25	4,55	2,03	0,38	0,08
$1 \cdot 10^5$	5,35	5,35	5,19	4,10	1,50	0,28	0,06
$3 \cdot 10^5$	5,35	5,35	5,16	3,73	1,20	0,22	0,05

Finally, we see in Table 6 the intensity ratio for the λ 10830 and λ 5876 (D_3) lines as a function of n_e and T. It is obvious that this ratio does not depend on the presence or absence of a field of coronal radiation. The intensity ratio I (λ 10830)/I (λ 5876), which corresponds to the Boltzmann population distribution, is given in the last column of Table 6 for the indicated values of kinetic temperature. It can be seen that the intensity ratio approaches the "Boltzmann" one with an increase in the density of the substance (it becomes equal to the "Boltzmann" one at $n_e = 10^{16}$ [3]).

REFERENCES

1. Krat, V.A. and V.M. Sobolev: Izv. GAO, Vol. 21, No. 163, p. 2, 1960.
2. Ivanov-Kholodnyy, G.S., G.M. Nikol'skiy and R.A. Gulyayev: Astron Zhur., Vol. 37, p. 799, 1960.
3. Gulyayev, R.A. and T.L. Vinnikova: Astron. Zhur., Vol. 42, p. 509, 1965.
4. Gulyayev, R.A.: Astron. Zhur., Vol. 43, p. 948, 1966.
5. Dolder, K.T., M.F.A. Harrison and P.C. Thonemann: Proc. Roy. Soc., Series A, Vol. 264, p. 367, 1961.
6. Allen, K.W.: Astrofizicheskiye velichiny (Astrophysical Magnitudes). Foreign Languages Publishing House, 1960.
7. Detwiler, C.R., D.L. Garrett, J.D. Purcell, R. Tousey: Ann. Geophys., Vol. 17, p. 263, 1961.
8. Hinteregger, H.E.: J. Geophys. Res., Vol. 66, p. 2367, 1961.
9. Ivanov-Kholodnyy, G.S. and G.M. Nikol'skiy: Geomagnetizm i Aeronomiya, Vol. 2, p. 425, 1962.
10. Nikol'skiy, G.M.: Geomagnetizm i Aeronomiya, Vol. 3, p. 793, 1963.
11. Ivanov-Kholodnyy, G.S. and G.M. Nikol'skiy: Astron. Zhur., Vol. 39, p. 777, 1962.
12. Menzel, D.H.: Astrophys. J., Vol. 85, p. 330, 1937; Russian Translation in the Collection: Fizicheskiye protsessy v gazovykh tumannostyakh (Physical Processes in Gaseous Fogs). Foreign Languages Publishing House, 1948.
13. Gulyayev, R.A., K.I. Nikol'skaya and G.M. Nikol'skiy: Astron. Zhur., Vol. 40, p. 433, 1963. /117
14. Burgess, A., and M.J. Seaton: Month Notices Roy. Astron. Soc., Vol. 121, p. 471, 1960.
15. Maier-Leibnitz, H.: Z. Phys., Vol. 95, p. 499, 1935.
16. Schulz, G.J. and R.E. Fox: Phys. Rev., Vol. 106, p. 1179, 1957.
17. Fleming, R.J. and G.S. Higginson: Proc. Phys. Soc., Vol. 84, p. 531, 1964.
18. Massey, N.S. and B. L. Moiseiwitsch: Proc. Roy. Soc., A, Vol. 227, p. 38, 1954.
19. Dorrestein, R.: Physica, Vol. 9, p. 447, 1942.
20. Woudenberg, J.P.M. and J.M.W. Milatz: Physica, Vol. 8, p. 871, 1941.
21. Bates, D.R., A. Fundaminsky, J.W. Zeech and H.S.W. Massey: Philos. Trans, A, Vol. 243, p. 93, 1950.
22. Phelps, A.V.: Phys. Rev., Vol. 99, p. 1307, 1955.
23. Marriott, R.: Proc. Phys. Soc. A, Vol. 70, p. 288, 1957.
24. Tomas, R. and R. Atey: Fizika solnechnoy khromosfery (Physics of the Solar Chromosphere). "Mir", 1965.
25. Shklovskiy, I.S.: Trudy GAISh, Vol. 20, p. 5, 1951.
26. Miyamoto, S.: Publ. Astron. Soc. Japan, Vol. 2, p. 113, 1951.
27. Gulyayev, R.A.: Astron. Zhur., Vol. 41, p. 313, 1964.
28. Shklovskiy, I.S.: Astron. Zhur., Vol. 22, p. 249, 1945.
29. Nikol'skaya, K.I.: Astron. Zhur., Vol. 43, p. 936, 1966.

SHAPE OF THE CONTOURS OF THE Hα LINE IN PROMINENCES

M.Yu. Zel'dina

ABSTRACT: The dependence of the contour of the Hα emission line on the height of the solar prominence over the limb and on its orientation relative to the line of sight and to the normal to the solar surface is determined. A thin homogeneous sheet perpendicular to the solar surface is assumed as a model of the prominence. An integral equation is solved for the radiation diffusion for the total energy redistribution with respect to frequency in an elementary scattering event. Contours of the Hα line emitted by prominences and filaments are obtained under the assumption that Hα glow is caused by scattering of the photospheric radiation.

It was shown in [1] that the luminescence of quiet prominences /118* in the Hα line is due to the scattering of photospheric radiation. This conclusion was based on a solution to an integral equation of radiation diffusion on the assumption that there was complete energy redistribution by frequencies in an elementary scattering event. A thin sheet perpendicular to the Sun's surface was used as a model of the prominence. For optically thick prominences on the Hα line ($\tau_0 \geq 10$), we obtained saddle-shaped contours whose shape and total energy corresponded to the observations. However, the observations showed that the Hα line often had a plane-peak contour. Contours with little horns and bell-shaped curves were also found. This article examines the dependence of the contour of the Hα emission line on the height of the prominence over the limb and on its orientation relative to the line of sight and the surface of the Sun. As before, a plane homogeneous sheet was used for a model of the prominence. The sole source of energy was the radiation of the Sun on the Hα line which was scattered by the prominence. As before it was assumed that there is a total redistribution by frequencies. The Doppler half-width of the Hα line was taken as equal to 0.33 Å (in certain cases $\Delta\lambda_D$ = 0.66 Å and 1 Å) and calculated according to the thickness constants of the prominence. The problem was solved by the methods described in [1].

Let a prominence be perpendicular to the surface of the Sun. In order to find the function of the source, we will solve the

---

* Numbers in the margin indicate pagination in the foreign text.

following integral equation:

$$B(\tau) = \int_0^{\tau_0} B(t) K(|t-\tau|)\, dt + g(\tau), \qquad (1)$$

where τ_0 is the optical thickness of the prominence on the H_α line. The independent term of the equation $g(\tau)$ is determined by the direct solar radiation. The value of $4\pi\sqrt{\pi}\, I_\odot\, g(\tau)\, d\tau$ is the energy of the direct solar radiation absorbed by the layer $g(\tau)$. Since the prominence is illuminated by the Sun from both sides in an identical manner, the function $g(\tau)$ is symmetrical in relation to the plane $\tau = \tau_0/2$ and equal to $g(\tau) = g_1(\tau) + g_1(\tau_0 - \tau)$.

The calculations of $g_1(\tau)$ were carried out according to the following formula:

$$g_1(\tau) = \frac{1}{\sqrt{\pi}} \int_{-\infty}^{+\infty} r_v e^{-v^2} E_w(\tau e^{-v^2})\, dv,$$

where E_w is the intensity of direct solar radiation at a depth τ, averaged over the angle 4π. It is determined by the following expression:

$$E_w(x) = \frac{1}{4\sqrt{\pi}} \int_{\pi/2-\chi_0}^{\pi/2} e^{-x\sec\vartheta} \sin\vartheta \int_{-\beta(\vartheta,\chi_0)}^{\beta(\vartheta,\chi_0)} (1 - u + u\cos\theta)\, d\beta\, d\vartheta.$$

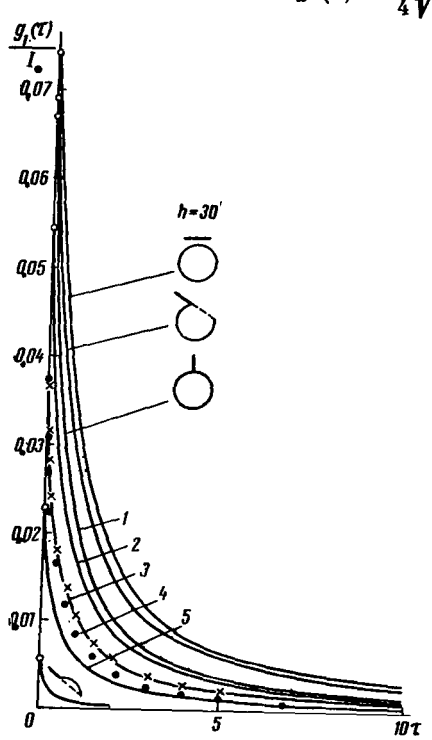

Fig. 1. Direct Solar Radiation Absorbed by Level $d\tau$ (With Accuracy to the Coefficient $4\pi\sqrt{\pi} i_\odot\, d\tau$) for Unidirectional Illumination of Prominences Arranged Horizontally, Obliquely and Vertically Relative to the Surface of the Sun. (1) $\Delta\lambda_D$ = 1 Å; (2) $\Delta\lambda_D$ = 0.66 Å; (3) $\Delta\lambda_D$ = 0.33 Å; (4) g B = const; (5) h = 3', $\Delta\lambda_D$ = 0.33 Å. The Points Designate the Values of $g_1(\tau)$, and the Crosses Designate the Value of $g_1(\tau)$ According to (2).

/119

Angles ν and β show the direction of radiation, which comes from the solar surface at an angle of θ [1]. The central intensity of Fraunhofer H_α line was taken as equal to the average value over the disk $r_c = 0.21$. We examined cases when the line of sight intersected the prominence at heights of h = 30" and 3' (corresponding values of the dilution factor equal to 0.30 and 0.186).

The darkening of the disk can be considered more precisely by using the data of [2], from which it follows that the contour of the Fraunhoffer H_α line in the spectrum of the edge becomes less deep and more narrow. The central intensity of H_α at the center of the disk is equal to 0.17, and that at the edge is 0.32. If we consider that the intensity of the continuous spectrum from the center to the edge decreases roughly by a factor of 2, then, as calculations show, the darkening of the disk on the H_α line is very little. Actually, the value $B_0=\frac{W}{\sqrt{\pi}}\int_{-\infty}^{+\infty} r_v e^{-v^2} dv$ decreases by 8% during the transition from the center to the edge. The values of $g(\tau)$ for a vertical prominence which were calculated with these data do not differ from results obtained with $r_c = 0.21$, with a consideration of the darkening of the disk in the continuous spectrum.

The functions of $g_1(\tau)$ are represented on Figure 1. They are expressed in terms of the intensity of the continuous spectrum of the center of the solar disk. The optical depths τ are plotted along the abscissa axis. The values of $g_1(\tau)$ calculated according to [2] are designated by the crosses. It can be seen from the figure that the function $g_1(\tau)$ decreases by a factor of 1.5-2 with a change in the height over the limb from 30" to 3'.

The distribution of energy sources in resonance scattering also depends on the assumed value for the Doppler width of the H_α line. Figure 1 shows $g_1(\tau)$ for a prominence which is a height of 30" in the case of $\Delta\lambda_D$ = 0.33, 0.66 and 1 Å. The function $g_1(\tau)$ increases with an increase of the Doppler width.

With the indicated values of the independent term, (1) was replaced by a system of linear algebraic equations solved by the method of successive approximations.

Figure 2 gives values of the function of the source for a vertical prominence (h = 30" and 3', $\Delta\lambda_D$ = 0.33 Å) which had an optical thickness of τ_0 = 1, 10 and 100 on the H_α line. They are expressed in terms of unit intensity of the continuous spectrum for the center of the solar disk. The value of τ_0 is taken each time for a unit of the abscissa axis. The arrows point out the values of B_0 (functions of the source for a prominence of zero optical thickness). The boundary values of $B(\tau)$ are determined as in [1], according to the following formula:

$$B(0)\approx B_1 - B_1\int_0^{\Delta\tau/2} K\left(\left|\tau-\frac{\Delta\tau}{2}\right|\right)dt - g_1 + g(0), \qquad (2)$$

/120

where B_1 and g_1 are the value of the source function and the independent term for the middle of the first layer.

The ratio B_{max}/B_0 characterizes the effect of accumulation of quanta inside the prominence. For $\tau_0 = 100$, this ratio is equal to 2.2 for h = 30", and 1.7 for h = 3', i.e., the effect of accumulation decreases with a removal of the prominence from the Sun. This decrease takes place somewhat more slowly than does the decrease in the dilution factor.

The contours of the H_α emission line were calculated according to the following formula:

$$I_v(\vartheta) = \int_0^{\tau_0} B(t)\, e^{-t\sec\vartheta}\, e^{-v^2} \sec\vartheta e^{-v^2}\, dt,$$

where ϑ is the angle between the normal to the plane of the prominence and the direction toward the observer. Figure 3 shows contours of the H_α line emitted by prominences which were a height of 30" and 3' in the direction ϑ = 0°, 60° and 89°. The values

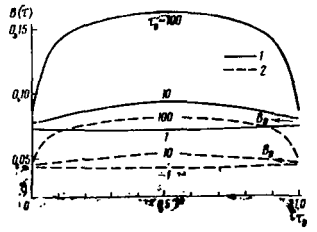

Fig. 2. Dependence of the Source Function on the Optical Depth for Different Values of τ_0 and h for a Vertical Prominence. (1) Case When the Line of Sight Intersects the Prominence at a Height of 30"; (2) At a Height of 3'.

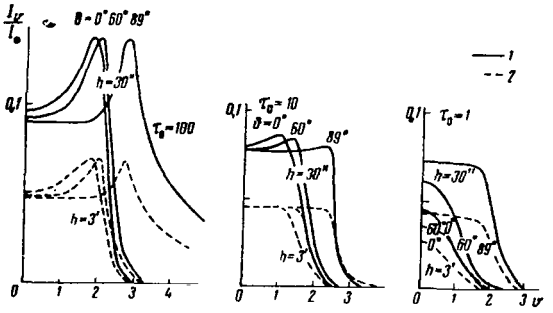

Fig. 3. Theoretical Contours of the H_α Line in the Case of a Vertical Prominence for Different Values of τ_0, h and v; The Intensities are Plotted in Relation to the Center of the Disk of the Sun.

of v, or the distances from the center of the line expressed in terms of Doppler widths, are plotted along the abscissa axis; the intensities related to the continuous spectrum of the solar disk are plotted along the ordinate axis. It can be seen from the figure that the contour acquires a saddle-shaped appearance for great optical thickness ($\tau_0 \geq 10$) at any value of g. The ratio I_{max}/I_{center} remains almost unchanged with a change of the height h for any τ_0. An increase of the angle ϑ brings about an increase of the half-width and an increase of the distance of the "little

horns" from the center of the lines. The central intensities and I_{max} remain roughly identical. For $\tau_0 = 1$, the central intensities increase with an increase of ϑ .

The parameters of the H_α contour also depend on the value of $\Delta\lambda_D$. Figure 4 shows profiles emitted by a vertical prominence at a height of 30" for optical thickness of $\tau_0 = 10$. All the contours have a saddle-shaped appearance. The central intensities increase with an increase of $\Delta\lambda_D$, and the half-width remains constant in this respect.

Let us examine a prominence inclined to the surface of the Sun at an angle of 30°. The function $g(\tau)$ in this case is determined mainly by the radiations entering the prominence through the boundary surface turned toward the Sun. This is very clear in Fig. 1, where the values of $g_1(\tau)$ and $g_2(\tau_0 - \tau)$ are shown in relation to an oblique prominence. The values of $g_1(\tau)$ are due to radiation coming from the part of the surface of the Sun which is intersected by the plane of the prominence. /121

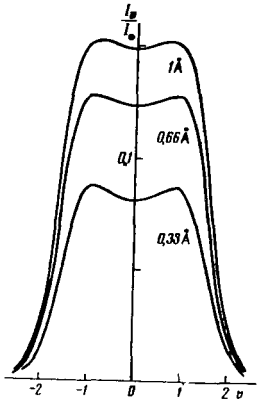

Fig. 4. Theoretical Contours of the H_α Line in the Case of a Vertical Prominence for $\tau_0 = 10$ and Various Values of $\Delta\lambda_D$; The Intensities Are Related to the Center of the Disk of the Sun.

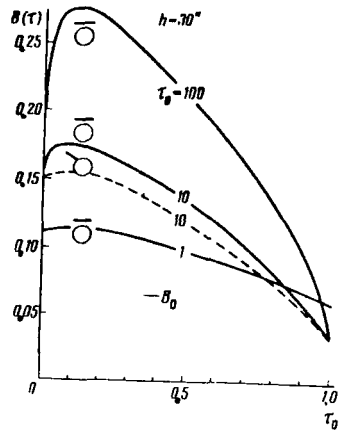

Fig. 5. Dependence of the Source Function on the Optical Depth for Various τ_0 for Prominences Arranged Horizontally and Obliquely Relative to the Surface of the Sun.

The graph of the source function for $\tau_0 = 10$ is given in Fig. 5. As before, the values of $B(\tau)$ are plotted in relation to the intensity of the continuous spectrum of the center of the solar disk. The source function for the oblique protuberance has a maximum near the surface turned toward the Sun ($\tau = 0.1\ \tau_0$), and it decreases rapidly with an increase of the optical thickness.

The H_α contours were calculated for the case when a prominence was a height of 30" over the limb, and the line of sight made an angle of $\vartheta = 60°$ with the normal to the plane of the prominence. Figure 6 shows theoretical contours of the H_α line emitted in the direction toward the Sun and away from the Sun. The difference in these contours is linked with the fact that the source function changes in different ways with the depths in relation to the boundary surfaces.

The plane of the prominence is "parallel" to the surface of the Sun. In this case, the value of $g(\tau)$ is greater than for any other orientation of a prominence (see Fig. 1). The source function has a maximum at a distance of $0.1\ \tau_0$ from the boundary turned toward the Sun (Fig. 5).

A somewhat different development of the source function with the optical depth was obtained in [4] in relation to an inaccuracy in solving [1].

The contours of the H_α line emitted by a prominence-filament in the direction $\vartheta = 89°$ to the Sun and away from the Sun for $\tau_0 = 1$, 10, and 100 are shown on Fig. 7. This prominence reflects toward the Sun a substantial part of the H_α radiation and, illuminating the chromosphere, produces a bright border around itself [5]. It follows from our calculations that the surface brightness of the plane turned toward the Sun is very great. For example, for $\tau_0 = 100$ and $\vartheta = 89°$ the Maxwellian intensity of the H_α line reaches 1/4 of the intensity of the continuous spectrum for the center of the solar disk.

For $\vartheta = 0°$, we have the case when the filament is projected onto the center of the disk of the Sun. The contours of the diffuse photospheric radiation on the H_α line as well as the radiation going through the filament are shown in Fig. 8 (a) for the cases when $\tau_0 = 1$, 10 and 100. The assumed profile of the Fraunhofer H_α line is also presented here. The contours representing the sum of diffuse photospheric radiations coming from the filament are given in Fig. 8 (b).

The contours obtained for these H_α lines are rather varied. Their shape is determined by the dependence of the source function on the optical thickness. If $B(\tau)$ increases from the surface turned toward the observer toward the center of the prominence, the contour has a saddle-shaped form. A further change in the source function with τ does not have a substantial effect on the spectral part of the line contour, since the radiation coming from the remote layers determines only the wings of the contours. For a constant value of $B(\tau)$, the contour has a plane apex.

The change of the source function with the depth is determined by the independent term in (1). The values of $B(\tau)$ depend to a

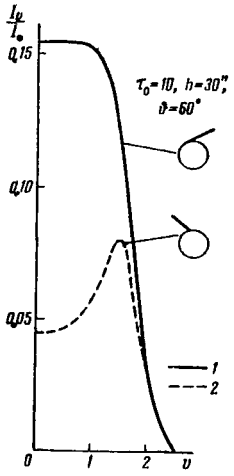

Fig. 6. Theoretical Contours of the H_α Line Emitted by a Prominence Inclined in the Direction Toward the Sun (1) and Away from the Sun (2).

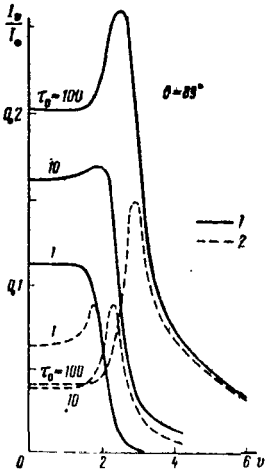

Fig. 7. Theoretical Contours of the H_α Line Emitted by a Prominence-Filament Inclined in the Direction Toward the Sun (1) and Away from the Sun (2).

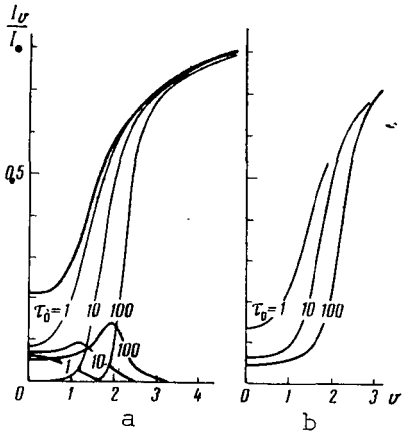

Fig. 8. Contours of the H_α Line in Filaments. (a) Contours of the Lines of Diffuse Radiation and Radiation Coming Through the Filament of the Photosphere for H_α. The Darkened Line Represents the Profile of the Fraunhofer H_α Line; (b) Total Contour of Diffuse and Photospheric Radiations on the H_α Line for Filaments of Different Optical Thicknesses.

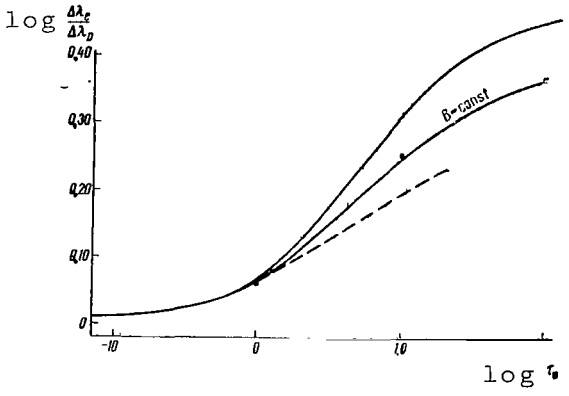

Fig. 9. "Saturation" Curve According to [7], for Different Dependences of the Source Function on τ (Formula (3) and Case of B = const). The Points Indicate the Widths of the Contours (Fig. 10) at a Height of e^{-1} I_{max}; The Dashed Line Represents the Curve of the Source Function Which Acquires a Zero Value at the Center of the Prominence.

rather great extent on $g(\tau)$. Figure 1 gives values of $g(\tau)$ for which the source function for a vertical prominence (h = 30") becomes constant in thickness. As we can see, these values are close to those obtained above. /123

A comparison of the contours obtained (see Fig. 3,4,6 and 7) with those corresponding to a constant value of the source function in terms of the line of sight showed that their wings coincide. There is particularly good agreement for $\tau_0 \sec\vartheta \leq 50$. The optical thicknesses and half-widths of the contours also coincide, if we draw a plane apex through the maxima of the intensity for the profile of (2). The optical thicknesses $\tau_0 \sec\vartheta$ and half-widths $v_{1/2}$ of the contours for (2) obtained from our calculations are given in the table below. The values of $\tau_0 \sec\vartheta$ and $v_{1/2}$ which were determined for these contours by the method of six sections [6] are also given here. In this regard the plane apex was extended to points corresponding to the maximum and the central intensities. It can be seen from the table that these parameters are close to ours in the first case. For optical thicknesses on the order of one, the contours of (2) practically coincide with those for which B = const.

		$\tau_0 = 1$			$\tau_0 = 10$			$\tau_0 = 100$	
		$\vartheta°$							
		0	60	89	0	60	89	0	60
Given From Calculations	$\tau_0 \sec\vartheta$	1,0	2,0	57	10	20	573	100	200
	$v_{1/2}$	1,0	1,1	2,1	1,6	1,8	2,5	2,3	2,4
Plane Apex Extended Through I_{max}	$\tau_0 \sec\vartheta$	1,0	2,0	25	10	20	500	125	170
	$v_{1/2}$	1,0	1,1	1,9	1,6	1,8	2,5	2,3	2,4
Plane Apex Extended Through I_{centr}	$\tau_0 \sec\vartheta$	1,0	2,0	25	16	20	500	400	630
	$v_{1/2}$	1,0	2,1	1,9	1,7	1,8	2,5	2,5	2,6

We should mention that the "saturation" curves examined in [7] for the source function given by the following conditions

$$B(\tau) = \frac{2A}{\tau_0}\tau \qquad (0 \leqslant \tau \leqslant \tau_0/2),$$
$$B(\tau) = \frac{2A}{\tau_0}(\tau_0 - \tau) \qquad (\tau_0/2 \leqslant \tau \leqslant \tau_0) \qquad (3)$$

and $B(\tau)$ = const also coincide if we extend a plane apex through the maxima of the intensities of the contours. These curves are shown on Figure 9, which was taken from [7]. For the case of (3) and B = const, we supplemented the figure by including the range of $10 \leq \tau_0 \leq 100$. The optical thicknesses at the center of the line were plotted along the abscissa axis, and the widths of the contours expressed in terms of $\Delta\lambda_D$ for a height of 1/e from the *central* intensity of the line were plotted along the ordinate axis.

The widths measured at a height equal to 1/e from the *maximum* intensity are pointed out by the dots. They lie on the curve corresponding to a constant value of the source function. The contours calculated according to (3) are represented in Figure 10.

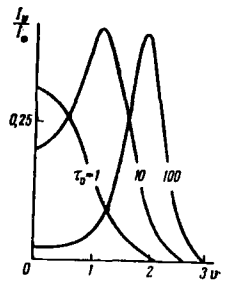

Fig. 10. Theoretical Contours of H_α Corresponding to Source Functions According to (3).

Thus, $\tau_0 \sec \vartheta$ and $\Delta\lambda_D$ can be determined by the same methods as in the case of the source function which is constant in thickness. However, the contour for this must be approximated by a plane-apex curve extended through the intensity maxima. Having analyzed the shapes of the contour, we could have separated τ_0 and $\sec \vartheta$; however, the model of the prominence selected is not the only one which can be used for this. /124

Conclusions

We solved an integral equation of radiation diffusion for total energy redistribution by frequencies in an elementary scattering act. A plane sheet was used for the model of the prominence. The contours of the H_α line emitted by the prominences (see Figs. 3,4,6 and 7) and a filament (see Fig. 8) were obtained on the assumption that the luminescence was due to scattering of photospheric radiation. The difference in the orientation of the prominence relative to the surface of the Sun and to the observer results in the following:

1. For prominences which are inclined or parallel to the surface of the Sun, the function of the source has a maximum near the boundary turned toward the Sun, while it has a maximum in its central region for a vertical prominence. The calculated contours of the H_α line are found to be saddle-shaped or plane-peaked. A bell-shaped form appears if the line of sight intersects a thin prominence at a small angle to its plane (Fig. 3, τ_0 = 1 and 10, ϑ = 89°). For $\tau_0 \sec \vartheta \sim 1$, the contours are described by a Gaussian curve.

2. The equivalent widths of the line increase roughly in proportion to the value of the Doppler width (Fig. 4).

3. The protuberance which is parallel to the surface of the Sun is brightest if it is observed from the photosphere.

4. It is shown that the existing methods can be used for determining the optical thickness and Doppler widths. In this regard, the half-widths of the contours for the line under observation should be measured at a height corresponding to half the maximum intensity.

REFERENCES

1. Yakovkin, N.A. and M.Yu. Zel'dina: Astron. Zhur., Vol. 41, p. 914, 1964.
2. Kuli-Zade, D.M.: Astron. Zhur., Vol. 41, p. 920, 1964.
3. Yakovkin, N.A. and M.Yu. Zeldina: Solnechnyye dannyye, No. 9, p. 62, 1964.
4. Kostik, R.I. and T.V. Orlova: Solnechnyye dannyye, No. 3, p. 51, 1964.
5. Kostik, R.I. and T.V. Orlova: (Unpublished).
6. Yakovkin, N.A. and M. Yu. Zel'dina: Solnechnyye dannyye, No. 12, p. 67, 1961.
7. Jefferies, J.T. and F.Q. Orrall: Astrophys. J., Vol. 127, p. 714, 1958.

SPECTRAL PHOTOMETRY OF THE CHROMOSPHERIC FLARE OF JULY 12, 1961

P.N. POLUPAN

ABSTRACT: A table is compiled according to the results of a photometric analysis of the spectrum of a flare on July 12, 1961. The table contains the central intensities and equivalent widths of 918 spectral emission lines.

To the present, the lines of metals in flares have been studied to a very small extent. This article presents the results of a photometric analysis of a large chromospheric flare, in the spectrum of which there were observed several hundreds of emission lines of Fe, Cr, Ni, Co, Mn, V and other elements. The spectra were photographed on a mirror diffraction spectrograph for dispersion of $\sim$ 1 Å/mm. The spectrograms were scanned photometrically with the aid of an electronic attachment on the microphotometer and were recorded immediately in units of intensity. Because of this, the number of emission lines found was on the average four times greater than that found in visual evaluations in the same spectral regions [1]. /125*

Data of Chromospheric-Photospheric Observations

The flare arose at 1003, reached a maximum of development around 1030, and disappeared at 1206 UT. During the chromospheric observations, its power was evaluated as scale-number 3^+ [2,3]. This flare existed in a large group consisting of 23 spots [Fig. 1(a)]. It was not very far from the center of the solar disk (ϕ = -7°, l = -25°) and it occupied a very large area extending 15° in longitude and 3.3° in latitude. At a distance of 5.2° from the flare, there was an arch-shaped filament [Fig. 1(d)]. The film obtained at the Ukrainian Academy of Sciences with the aid of a chromospheric telescope permitted us to study the development of the flare. In Figure 1, this flare is depicted on the H_α line before, during and after its maximum. We should mention that it appeared at the moment when the group of spots acquired the maximum area. This can be seen from the following data of the photospheric observations:

Date . . .	11.VII	12.VII	13.VII	14.VII	15.VII	16.VII	17.VII
Sp.	1426	1531	1400	1410	1150	1150	974

Sp is given in millionths of a solar hemisphere.

* Numbers in the margin indicate pagination in the foreign text.

Spectral Observations

A number of photographs in the following spectral regions were obtained in the solar telescope of Kiev University: (1) 3260-3340 Å, (2) 3340-3420, (3) 3420-3500, (4) 3500-3580, (5) 3580-3660, (6) 3660-3740, (7) 3730-3810, (8) 3790-3870, (9) 3850-3930, (10) 3905-3985, (11) 4060-4140, (12) 4300-4380, (13) 4430-4510, (14) 4670-4750, (15) 4820-4900, (16) 4880-4960, (17) 5130-5210, (18) 5825-5905, (19) 6520-6600 Å. These segments were photographed in sequence on a Rot Rapid plate with average exposure of 0.5 sec in the second and third spectral orders (dispersion of 1.3 and 0.8 Å/mm). The times of the exposures were recorded on a chronographic tape. During the time from 1035 to 1115, there were repeated photographs on three plates. Clouds prevented further observations. Although the spectral regions on the two subsequent plates contained much fewer emission lines, they could serve as study materials for /126

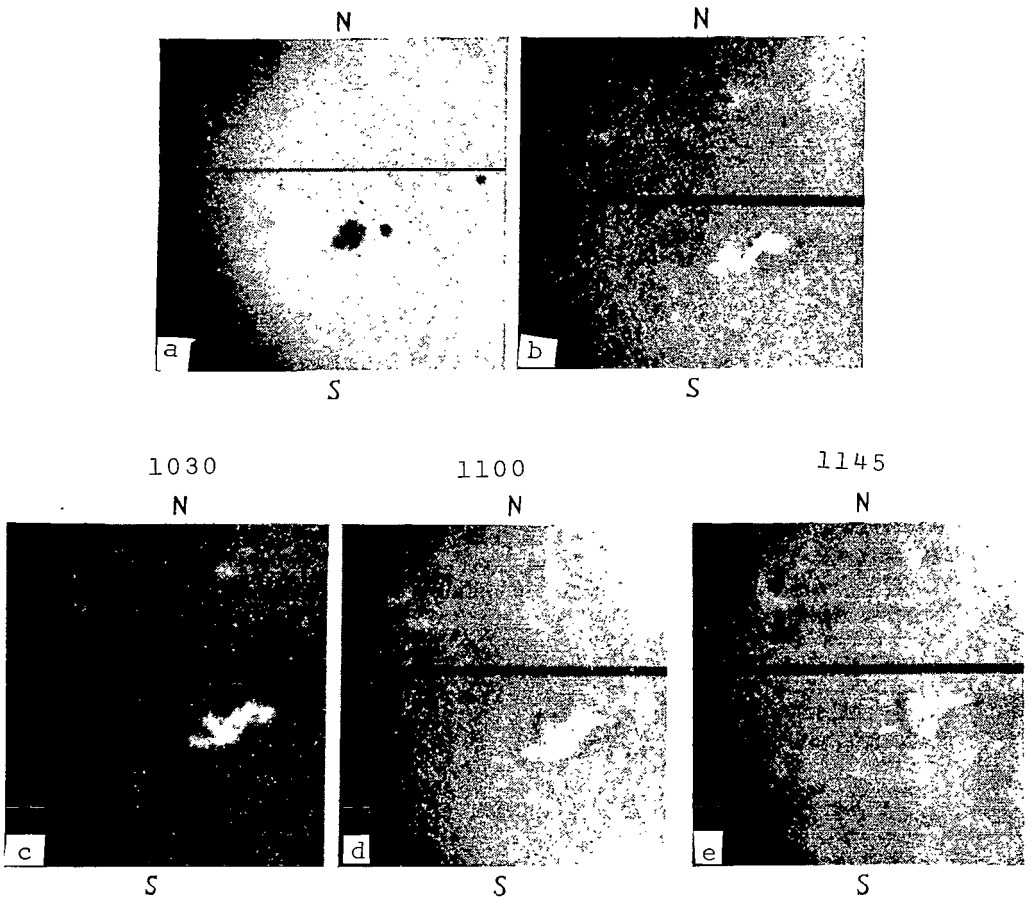

Fig. 1. Group of Sunspots on July 12, 1961 (a) in Which the Flare Was Observed; Images of This Flare on the H_α at various times (b-e).

evaluating the measurements of the processes at the stage of extinguishment of the flare. Nevertheless, we are examining spectrographs of the richest emission lines which were obtained 5 minutes after the maximum of the flare. These spectrograms were photographed during the course of a 2-minute interval. The first, second and sixteenth spectral regions on this plate were not analyzed because of a superposition of another order of the spectrum.

Results of Spectral Photometric Analysis

The photometric analysis of the spectrum was carried out with the aid of a microphotometer equipped with an electronic attachment and an automatic recorder, so that the data were written down immediately in units of intensity. Figure 2 shows an example of the emission spectrum of this flare in the region of the Balmer H_9 hydrogen lines. The photometric sections were carried out along a /127 dispersion through the bright part of the flare. Since this part of the flare was projected onto the half-shadow of a spot, the spectrum for the half-shadow of another spot found on the spectrograms was taken as a comparative spectrum (Fig. 2). In this regard, the point on the half-shadow of this spot was selected so that the levels of the continuous spectra were identical. The photometric sections were repeated 2-3 times for each region, and the best records of the comparative spectra were used in each individual case.

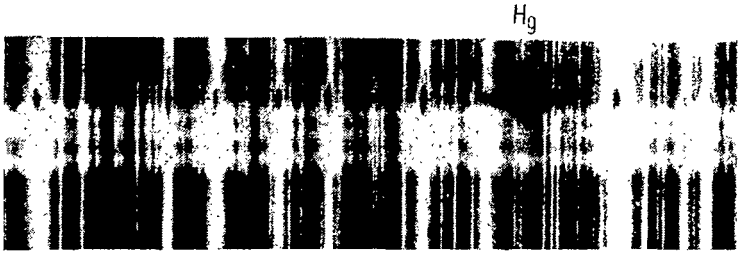

Fig. 2. Region of a Spectrum of the Flare Around the H_9 Line.

The records were analyzed by means of a careful superposition of the spectra of half-shadows of both spots and a measurement of the central residual intensities and equivalent widths. The central residual intensities were expressed in units of the continuous spectrum for the center of the solar disk, while the equivalent widths were expressed in terms of angstroms. The entire scattered light in the instrument was 1.5%, and it was not taken into special account [4].

The instrumental contour whose total half-width was 0.056 Å in the second spectral order was also disregarded. The errors in the intensities due to the instrumental distortion were not very great. Actually, since most of the relatively intensive lines have a total half-width on the order of 0.1 Å, then according to the approximative formula $\Delta\lambda^2_{1/2}$ (real) = $\Delta\lambda^2_{1/2}$ (obs.) - $\Delta\lambda^2_{1/2}$ (instr.), the real total half-width of such a contour was 0.083 Å. In this

regard the central intensity increased roughly by 10%. Instrumental distortions did not effect the equivalent widths.

The lines were identified with the aid of the Utrecht Atlas of the Solar Spectrum [7], the Rowland table, and the Moor catalog [5,6].

A table of 918 spectral emission lines was composed as a result of the spectral analysis. The numbers of the lines, wavelengths, designations of the elements, numbers of the multiplex, central residual intensities and equivalent line widths in relation to the continuous spectrum of the center of the solar disk are indicated in the table. The wavelengths and multiplet numbers are given according to Moor [6]. The asterisks mark data on λ according to Rowland.

Finally, we should mention that all the lines belong to neutral and ionized atoms of 41 elements. The principal mass of the lines was concentrated in the ultraviolet regions. The ionized calcium K line was most intensive; its intensity exceeded the level of the continuous spectrum by a factor of 4.8.

A more detailed investigation of these spectral materials will be carried out at a later date.

No.	λ, element	multiplet	$I_{\lambda_0} \cdot 10^{-3}$	$E_\lambda \cdot 10^{-3}$	No.	λ, element	multiplet	$I_\lambda, 10^{-3}$	$E_\lambda \cdot 10^{-3}$
1	3418,528 Sc	21	17	10	42	57,047 Gd+	—	8,4	9,2
2	21,20 Cr+	3	33	35		57,088 Y+	77		
	21,22 Ni	105			43	57,62 Cr+	135	11	7,7
3	22,739 Cr+	3	49	64	44	58,474 Ni	19	25	14
4	23,711 Ni	20	15	26	45	59,429 Fe	297	9,3	12
5	20,582 Fe+	5	12	16	46	60,03 Cr+	60	9,3	16
6	26,383 Fe	25	25	19		60,039 Mn+	1		
		82			47	60,312 Mn+	3	7,5	7,7
7	26,637 Fe	81	22	13	48	3461,496 Ti+	6	8,9	160
8	27,002 Fe	26	15	13	49	61,652 Ni	17	20	19
9	27,121 Fe	81	25	22	50	62,33 ?	—	12	12
10	28,192 Fe	81	20	16	51	62,804 Co	23	13	28
11	31,582 CO	6	7,4	10		62,808 Fe	373		
	31,59 Cr	53			52	63,330 Mn+	12	8,9	11
12	31,815 Fe	376	7,4	9,6	53	64,02 Cr+	2	11	13
		676			54	64,043 Mn+	12	4,7	3,0
13	31,995 Cr	53	9,8	12	55	64,914 Fe	241	11	3,0
14	32,318 CO	102	9,8	16	56	65,863 Fe	6	66	92
	32,32 Cr+	8			57	66,59 V+	58	10	9,2
15	33,045 Co	23	7,9	13	58	66,952 Gd+	23	7,0	3,0
16	33,30 Cr+	3	40	60	59	67,502 Ni	3	15	21
17	33,558 Ni	19	25	32	60	67,715 Cr	110	11	6,1
18	36,045 Fe	614	9,8	19	61	68,476 Ca	10	12	7,7
	36,112 Fe+	91	4,9		62	68,849 Fe	242	15	30
19	37,280 Ni	3	20	26	63	68,973 Co	159	10	15
20	38,27 ?	—	3,9	9,6	64	68,012 Fe	614	8,9	15
21	38,978 Mn+	1	59	54	65	69,486 Ni	8	8,4	20
22	40,610 Fe	6	83	83	66	69,834 Fe	242	8,9	6,1
23	40,989 Fe	6	74	73	67	70,549 Cr	77	8,0	18
24	3441,983 Mn+	3	110	110	68	71,35 Ni+	4	11	55
25	43,083 Fe+	16	83	64		71,350 Fe	130		
26	44,251 Ni	122	97	96	69	72,545 Ni	20	19	52
	44,306 Ti+	6			70	73,32 ?	—	6,1	6,1
27	45,151 Fe	81	12	26	71	73,67 ?	—	17	12
28	46,263 Ni	20	21	26	72	74,037 Mn+	3	107	166
29	47,278 Fe	82	5,4	9,6		74,124 Mn+	3		
	47,281 CO	161			73	74,41 Fe++	27	11	6,1
30	49,170 CO	22	7,4	11	74	75,13 Cr+	2	29	30
31	50,328 Fe	82	5,9	13	75	3475,450 Fe	6	86	92
32	51,628 Fe	139	4,9	12	76	75,74 Fe+	4	61	49
33	51,915 Fe	81	7,9	25	77	76,704 Fe	6	87	70
34	52,273 Fe	25	6,8	18	78	76,982 Ti+	6	39	30
35	52,47 Ti+	99	11	6,1	79	77,181 Ti+	6	83	98
36	52,96 ?	—	20	34	80	77,864 Ni	124	13	3,1
37	53,514 Co	22	11	40	81	78,74 P+	2,18	7,5	9,2
38	53,10 A	44	11	30	82	78,744 Co	67	9,3	3,0
39	55,237 Co	6	7,5	21	83	79,29 Hf+	2	13	4,6
40	56,390 Ti+	99	13	15	84	80,012 Co	67	27	21
41	56,924 Co	5	23	21	85	80,28 Cr	141	8,0	3,0
	56,928 Fe+	76			86	80,31 ?	—	8,0	9,2

No.	λ, element	multiplet	$I_{\lambda_0} \cdot 10^{-3}$	$E_\lambda \cdot 10^{-3}$
87	80,897 Ti^+	22	18	12
88	81,126 Ti	271	9,4	7,7
89	82,18 ?	—	9,9	6,1
90	82,905 Mn^+	3	85	100
91	83,774 Ni	6	23	12
92	84,15 Cr^+	2	19	21
	84,16 Cr^+	185		
93	85,368 Co	161	13	18
94	85,976 V^+	6	6,7	15
95	86,556 Fe	79	4,7	3,0
96	87,990 Fe^+	4	32	15
97	89,673 Mn^+	3	91	86
98	89,399 Co	36	15	7,7
99	89,739 Ti^+	6	16	10
100	90,575 Fe	6	91	86
101	91,053 Ti^+	6	64	61
102	92,956 Ni	18	23	21
103	93,468 Fe^+	114	5,6	4,6
104	3494,672 Fe^+	16	28	26
105	95,37 Cr^+	2	10	37
106	95,831 Mn^+	3	89	70
107	96,27 O^+	7	13	21
108	96,814 Mn^+	3	70	50
109	97,137 Fe	78	13	19
110	97,536 Mn^+	3	89	61
111	97,843 Fe	6	89	99
112	3502,278 Co	21	23	23
113	03,474 Fe^+	4	69	57
114	04,890 Ti^+	88	23	23
115	06,310 Co	21	16	23
116	06,54 ?	—	24	26
117	06,843 V	81	6,8	4,2
118	07,14 Fe	835	6,8	9,4
119	07,387 Fe^+	16	11	17
120	07,694 Ni	3	4,2	3,8
121	08,213 Fe^+	4	5,1	3,4
122	08,52 Fe	239	4,7	2,8
123	09,843 Co	22	21	26
	09,844 Ti^+	88		
124	10,338 Ni	18	23	37
125	11,84 Cr^+	2	11	11
126	12,219 Gd^+	38	5,5	4,2
127	12,640 Co	21	4,2	4,2
128	13,03 Cr^+	107	4,2	4,2
129	13,478 Co	5	12	8,1
130	15,054 Ni	19	33	54
131	17,298 V^+	6	5,1	4,2
132	18,23 Fe	575	5,9	8,5
133	18,632 Gd^+	7	4,6	5,6
	18,634 Ni	124		

No.	λ, element	multiplet	$I_{\lambda_0} \cdot 10^{-3}$	$E_\lambda \cdot 10^{-3}$
134	3518,860 Fe	78	4,6	4,7
135	19,766 Ni	5	17	24
136	21,264 Fe	24	34	47
137	21,567 Co	20	19	20
138	21,833 Fe	78	4,2	7,1
	21,836 V^+	57		
139	23,423 Co	21	15	28
140	24,075 Fe	239	4,2	5,7
141	24,236 Fe	130	10	13
142	24,54 Cr^+	107	37	67
	24,541 Ni	18		
143	26,039 Fe	6	38	66
	26,167 Fe	24	39	
144	26,465 Fe	131	28	42
145	26,847 Co	4	16	18
146	27,867 V^+	117	6,8	9,9
147	27,982 Ni	6	8,5	8,5
148	29,032 Co	5	8,0	8,5
149	29,816 Co	22	15	15
	29,818 Fe	326		
150	30,385 Fe	326	6,8	7,1
151	30,580 Ti	22	5,1	5,7
152	32,121 Mn	18	4,2	6,7
153	32,60 ?	—	6,8	5,7
154	33,008 Fe	326	4,2	5,7
155	33,201 Fe	326	7,6	7,0
156	34,914 Fe	48	5,1	5,7
157	45,408 Ti^+	98	8,5	9,4
158	36,556 Fe	326	15	23
159	37,491 Fe	239	4,2	2,8
160	37,707 Co	68	4,2	4,2
161	3537,896 Fe	327	4,2	4,2
162	38,86 Mg^+	12	4,2	3,8
163	40,121 Fe	329	4,2	3,8
164	41,083 Fe	326	16	23
165	42,076 Fe	326	8,5	8,8
166	43,669 Fe	734	6,3	5,7
167	44,631 Fe	239	5,9	5,9
168	45,190 V^+	5	7,2	6,5
169	45,639 Fe	321	6,9	8,5
170	47,802 Mn	18	5,1	4,2
171	48,029 Mn	18	5,1	5,7
	48,037 Fe	496		
172	48,185 Ni	3,20	14	14
	48,202 Mn	18		
173	48,51 A^+	56	5,1	5,7
174	49,02 Y^+	9	5,1	5,1
	49,030 V^+	103		
175	49,868 Fe	48	8,5	7,0
176	50,592 Co	4	6,8	5,7

No.	λ, element		multiplet	$I_\lambda \cdot 10^{-3}$	$E_\lambda \cdot 10^{-3}$
177	51,11	Fe	321	5,9	5,7
178	51,666	Co	67	9,3	6,0
179	51,94	Zr^+	1	8,0	7,0
180	52,85	Ti^+	15	7,6	6,7
181	53,483	Ni	16	8,5	13
182	54,122	Fe	23	13	20
183	54,95	?	—	22	28
184	56,877	Fe	327	19	20
185	58,518	Fe	24	37	54
	58,538	Sc^+	3		
186	60,594	V^+	4	9,3	8,5
				9,3	8,5
187	3560,855	Os	6	9,7	8,5
188	61,575	Ti^+	15	6,3	7,0
189	61,751	Ni	2	8,5	11
190	61,910	Ti^+	42	4,2	4,2
191	64,11	Fe^+	48	8,5	10
192	64,51	Fe	183	7,6	8,5
193	65,02	A^+	57	7,2	10
194	65,381	Fe	24	39	57
195	66,37	Cr^+	76	25	41
	67,372	Ni	36		
196	67,045	Fe	325	7,6	8,5
197	67,36	Fe	183	7,2	6,7
198	67,701	Sc^+	3	4,2	3,8
199	68,423	Fe	321	4,2	3,8
200	68,828	Fe	673	6,3	7,0
201	68,97	Fe^+	113	8,0	8,5
	68,977	Fe	294		
202	69,370	Co	35	8,0	12
	69,493	Mn	18		
203	70,100	Fe	24	38	102
	70,243	Fe	326	35	
204	71,228	Fe	46	6,3	5,7
205	71,869	Ni	5	21	42
	71,933	Gd	4	17	
206	72,523	Sc^+	3	37	47
207	73,403	Fe	673	4,2	4,2
208	73,737	Ti^+	15	17	37
	73,896	Fe	611	10	
209	74,967	Co	21	3,4	2,8
210	75,11	Fe	321	4,2	8,5
211	3575,249	Fe	322	6,3	28
	75,361	Co	4	8,0	
	75,374	Fe	496	4,7	
212	77,880	Mn	8	4,2	5,7
213	78,380	Fe	321	4,2	5,7
214	78,687	Cr	4	34	57
	78,903	Co	41		
215	82,101	Fe	612	14	14
216	82,69	Fe	328	8,7	14
217	83,337	Fe	574	7,9	8,6
218	83,704	V	45	4,0	2,9
219	83,912	CN •	—	5,2	4,4
220	84,663	Fe	294	11	14
221	84,790	Fe	322	7,9	8,6
222	84,960	Fe	395	7,9	8,6
			611		
223	85,31	Cr^+	13	48	63
	85,320	Fe	23		
224	85,708	Fe	23	36	51
225	86,10	Fe	497	10	23
	86,114	Fe	611		
226	86,543	Mn	8	5,2	3,9
	86,557	Al^+	7		
227	86,811	Al^+	7	7,1	3,9
228	86,985	Fe	23	36	48
	87,068	Ar^+	7		
229	87,130	Ti^+	15	18	37
230	87,309	Al^+	7	7,9	11
231	87,75	V?	—	5,9	5,7
	87,752	Fe	—		
232	3587,931	Ni	16	8,6	8,6
233	88,615	Fe	325	7,1	8,6
234	88,918,	Fe, CN	322	7,9	8,6
235	89,107	Fe	23	12	19
236	89,456	Fe	295	9,9	8,6
237	89,635	Sc^+	3	9,9	26
	89,745	V^+	4	9,1	
238	90,08	Fe	440	4,8	4,3
239	90,468	Gd^+	22	9,9	19
	90,47	Ne^+	32		
	90,475	Sc^+	3		
240	90,99	Fe	573	4,8	3,9
241	91,345	Fe	321	7,9	6,7
242	91,485	Fe	568	4,8	3,9
243	92,012	V^+	4	5,9	7,2
244	92,603	Sm	39	4,0	6,4
245	93,488	Cr	4	16	43
246	94,632	Fe	322	4,8	10
247	94,870	Co	4	4,0	6,6
248	95,294	Fe	322	4,0	4,3
249	95,66	Fe	322	5,4	4,3
250	96,048	Ti	15	17	23
251	97,705	Ni	18	14	23
252	98,26	?	—	5,8	3,9
253	98,71	Fe	674	8,9	5,4
254	98,98	Fe	322	4,9	3,9
255	99,395	Cr	89	4,2	2,6
256	99,624	Fe	809	8,9	8,0

No.	λ, element	multiplet	$r_{\lambda_0}\cdot10^{-3}$	$E_\lambda\cdot10^{-3}$
257	99,974 Ce+	219	4,5	2,7
258	3600,74 V+	9	6,7	8,5
259	3601,93 V+	9	8,0	3,6
260	02,079 Co	4	8,9	11
261	02,281 Ni	3	12	17
262	02,534 Fe	324, 391	8,9	14
263	03,205 Fe	295	8,5	14
264	03,61 Cr+	13	18	23
265	03,745 Cr	74	15	19
266	03,91 A+	43,68	7,6	4,3
267	04,284 Ti+ / 04,285 Sm+	21, 47	8,9	17
268	05,41 Cr	49	31	63
269	06,38 Fe	233	4,5	4,3
270	06,679 Fe	294	15	34
271	07,537 Mn	8	3,5	2,3
272	08,146 Fe	325, 438	8,9	8,6
273	08,58 Cr	140	7,6	7,1
274	08,89 Ti+	76	36	34
275	09,314 Ni	16	11	17
276	10,154 Ti / 10,159 Fe	58, 321	12	12
277	11,06 V+	9	10	6,3
278	12,068 Fe	325	10	17
279	12,741 Ni	6	14	23
280	12,940 Fe	46,77	6,7	7,1
281	13,15 Fe	324	8,8	11
282	13,43 Zr+	8,45	7,6	3,4
283	13,641 He	6	10	5,7
284	13,80 Mg+	2	15	35
285	3614,550 Fe	—	8,9	7,1
286	14,73 ?	—	4,5	5,1
287	15,19 Fe	569	8,0	4,3
288	15,387 Co	66	5,8	2,6
289	15,66 Fe	46	12	8,6
290	16,15 Fe	569	8,0	10
	16,152 Eu+	28		
291	17,09 Fe / 17,164 Gd+	535, 89	7,1, 4,5	11
292	17,317 Fe / 17,32 Cr+	—, 147	7,6	8,6
293	17,788 Fe	496	5,8	8,6
294	18,769 Fe	23	27	57
295	23,51 Fe	393	4,5	4,1
296	24,111 Ca	9	5,5	5,4
297	24,72 Ni / 24,733 Ni	121, 2	5,1	16
298	30,03 Zr+	10	4,3	6,8
299	30,353 Fe	323	8,5	14
300	30,740 Sc+ / 30,748 Ca	2, 9	10	41
301	31,464 Fe	23	42	46
302	31,72 Cr+	12	18	14
303	32,558 Fe	437	2,0	2,0
304	34,235 He	28	13	8,5
305	34,373 He	28	8,5	11
306	34,713 Co	146	11	8,0
307	37,05 Fe / 37,05 A+	438, —	6,1	4,2
308	39,024 V	83	8,0	6,0
309	3640,388 Fe	295	6,1	5,6
310	41,01 Cr	47	5,5	3,0
311	41,330 Ti+ / 41,470 Cr	52, 47	14	13
312	41,830 Cr	47	6,0	4,2
313	42,785 Sc+ / 42,798 F+	2, 11	4,0	22
314	43,181 Co	99	4,1	4,0
315	43,627 Fe / 43,716 Fe / 43,80 Fe	385, 233, 670	4,0	11
316	45,090 Fe	323, 495	5,0	17
317	47,84 Fe / 47,844 Fe	569, 23	45	114
318	49,329 Co	146	19	28
319	59,508 Fe	291	9,3	9,0
320	50,031 Fe	394	8,1	8,4
321	50,280 Fe	180	5,0	8,4
322	51,065 Al+ / 51,096 Al+	12, 12	5,0	11
323	51,469 Fe	295	6,0	14
324	52,541 Co	4	11	3,0
325	53,763 Fe	180	6,5	3,0
326	54,995 Al+	12	8,1	5,6
327	55,465 Fe	369	8,1	6,0
328	55,63 ?	—	11	8,4
329	68,489 V+	46	9,3	4,4
330	68,893 Fe / 68,965 Ti	229, 18	3,7	2,2
331	3639,151 Fe / 69,241 Ni	437, 2	7,3	6,7
332	69,523 Fe	291	7,3	8,9
333	70,035 Fe / 70,041 Co / 70,071 Fe	369, 64, 435	7,3	9,0

No.	λ, element	multiplet	$I_\lambda \cdot 10^{-3}$	$E_\lambda \cdot 10^{-3}$
334	71,672 Ti	19	5,0	6,7
335	72,69 Fe	180	4,4	4,4
336	73,90 ?	—	4,3	3,3
337	74,06 Ni	15	7,3	13
	76,15 Ni	32		
338	74,766 Fe	369	3,3	4,4
339	76,314 Fe	228	7,5	16
340	77,309 Fe	773	5,0	6,7
341	77,630 Fe	291	13	26
342	77,86 Cr^+	12	11	26
343	78,91 Zr^+	101	6,0	11
344	79,915 Fe	5	37	60
345	82,226 Fe	772	10	14
346	83,047 Co	99	19	35
	83,054 Fe	5		
347	84,108 Fe	292	10	12
348	85,192 Ti^+	14	30	43
349	85,998 Fe	385	30	29
350	87,100 Fe	75	43	4,4
351	87,458 Fe	21	23	30
352	87,656 Fe	291	4,3	6,7
353	88,44 Cl^+	56	6,0	6,7
354	89,457 Fe	369, 386	7,3	9,0
355	3690,70 V^+	190	6,0	6,7
356	93,989 Sm^+	2	7,0	8,0
	94,005 Fe	394		
357	95,054 Fe	229, 534a	7,3	6,9
358	97,426 Fe	389	9,0	12
359	3701,086 Fe	385	7,3	8,5
360	02,033 Fe	369	8,6	6,7
361	02,237 Co	145	4,3	2,2
362	02,500 Fe	46,75	7,0	4,4
363	03,556 Fe	291	10	29
	03,697 Fe	389	10	
	03,824 Fe	369	10	
364	04,060 Co	35	11	8,9
365	04,463 Fe	290	10	8,9
366	04,73 O^{++}	21	13	13
367	0,567 Fe	5	44	62
368	06,026 Ca^+	3	77	120
	06,035 V	104		
	06,219 Ti^+	73		
369	07,048 Fe	385, 392	6,3	4,0
370	07,828 Fe	5	20	47
	07,918 Fe	76	17	
371	09,246 Fe	21	26	35
	09,25 Cr^+	6		
372	11,225 Fe	228	8,7	8,7
373	11,411 Fe	494	6,8	5,5
374	11,974 Fe^+	192	9,0	7,0
375	12,109 Sm^+	—	8,5	4,4
376	15,911 Fe	124	6,7	8,5
377	3719,935 Fe	5	60	60
378	21,278 Fe	75, 705	3,7	3,2
379	22,568 Ti	17	50	50
	22,601 V	91		
380	23,631 Ti^+	72	6,7	8,8
381	24,106 Ti^+	73	2,6	2,2
382	24,380 Fe	124	7,0	18
383	26,926 Rn	2	7,0	3,3
	26,927 Fe	385		
	26,931 Mn	24		
384	27,03 Fe	668	6,5	3,3
	27,04 Fe^+	192		
385	30,386 Fe	533	5,0	4,2
	30,46 Fe	389		
	30,476 Co	62		
386	30,807 Cr	2	6,7	4,2
	30,81 Tm^+	11		
387	30,945 Fe	228	9,3	4,4
388	31,374 Fe	225	7,3	6,7
389	32,032 Cr	2	66	2,2
390	32,390 Co	62	12	22
	32,399 Fe	76		
391	32,760 V^+	15	6,5	3,3
392	33,319 Fe	5	47	80
393	34,370 H_{13}	3	15	220
394	34,867 Fe	21	47	58
395	35,325 Fe	388	13	3,3
396	36,813 Ni	30	73	135
	36,901 Ca^+	3		
397	28,308 Fe	609	5,0	4,4
398	3739,229 Ni	2	6,0	11
399	39,527 Fe	—	4,3	13
400	40,241 V	98	3,3	2,2
	40,247 Fe	667		
401	41,059 Ti	17	4,0	2,2
402	41,504 V	124	3,1	26
	41,633 Ti^+	72	10	
403	42,621 Fe	387	3,1	8,7
404	43,364 Fe	21	22	41
	43,468 Fe	806		
	43,578 Cr	43		
405	43,884 Cr	43	3,1	4,3
406	44,105 Fe	385	4,3	11
407	45,561 Fe	5	68	80

No.	λ, element	multiplet	$I_\lambda \cdot 10^{-3}$	$E_\lambda \cdot 10^{-3}$
408	45,901 Fe	5	45	73
409	46,486 Fe	73	6,2	3,6
410	46,931 Fe	386	5,6	11
411	47,55 Y^+	8	4,0	4,3
412	48,264 Fe	5	56	84
413	48,998 Cr	43	6,2	17
414	49,487 Fe	21	28	50
415	50,154 H_{12}	2	25	280
416	52,420 Fe	385, 392	4,6	3,0
417	52,860 Ti	17	6,2	4,3
418	53,154 Fe	177	6,2	4,3
419	53,610 Fe	73	11	15
420	54,506 Fe	386	8,4	6,5
421	56,069 Fe	74	4,6	3,2
422	56,934 Fe	805	3,1	2,1
423	3757,662 Cr 57,684 Ti^+	43 72	12	13
424	58,22 V^+ 58,235 Fe	100 21	34	50
425	59,291 Ti^+	13	56	54
426	60,052 Fe	177	10	8,6
427	60,534 Fe	76	9,0	6,5
428	61,320 Ti^+	13	30	52
429	61,72 Ca	8	6,2	2,1
430	61,90 Cr^+	11	5,0	3,2
431	62,205 Fe	705	6,8	4,3
432	62,588 Sm^+	25	3,7	2,1
433	63,00 Gd^+	1	3,1	2,1
434	63,57 Fe	128	3,1	3,2
435	63,790 Fe	21	31	52
436	64,21 Fe	74	3,1	2,1
437	66,542 Fe	608	8,7	7,6
438	66,092 Fe	226	3,6	3,2
439	66,665 Fe	366	3,1	2,1
440	67,18 Cr^+ 67,194 Fe	20 21	27	37
441	68,030 Fe	73	8,7	6,3
442	69,45 Gd^+ 69,455 Ni^+	37 4	19	19
443	70,632 H_{11}	2	25	300
444	72,530 Ni	15	6,2	5,0
445	74,3 Al^+	33	4,6	4,0
446	75,572 Ni	33	11	16
447	76,454 Fe	74	3,5	3,0
448	77,448 Fe	223	3,5	3,0
449	3778,063 Ni	15	5,8	4,0
450	78,320 Fe	367	4,0	2,0
451	78,69 Cr^+ 78,697 Fe	— 73	5,8	6,0
452	79,444 Fe	665	3,5	6,0
453	81,23 Cl^+	72	4,5	6,0
454	81,620 Ce^+ CN	163 —	2,9	5,0
455	81,938 Fe	917	2,9	4,0
456	82,139 Ti	82	3,2	5,0
457	82,450 Fe	388	3,0	5,0
458	83,347 Fe^+	14	7,0	8,0
459	83,530 N	30	9,0	10
460	84,506 CN *	—	3,0	5,0
461	85,950 Fe	177	5,8	8,0
462	87,883 Fe 87,89 Cr^+	21 6	17	26
463	90,095 Fe	22	12	14
464	95,004 Fe	21	14	26
465	97,900 H_{10}	2	32	320
466	99,549 Fe	21	21	36
467	3807,144 N	33	6,0	16
468	07,534 Fe	73	11	19
469	07,926 Cr	139	10	8,0
470	08,772 Nd^+	—	6,2	3,9
471	09,592 Mn	6	5,6	5,8
472	10,759 Fe	665	5,5	3,9
473	11,05 Fe	223 287	8,5	9,7
474	11,32 Ni	15	7,0	5,8
475	11,80 Fe	701	3,7	5,8
476	3812,964 Fe	22	31	39
477	13,059 Fe 13,390 Ti^+ 13,45 V	222 12 28	15	29
478	13,638 Fe	283	5,6	5,8
479	13,891 Fe 13,94 Fe	854 174	7,9	21
480	14,580 Ti^+, CN	12	14	41
481	14,855 Ti^+	180	3,1	3,1
482	15,842 Fe	45	25	54
483	16,340 Fe	73	7,3	17
484	16,92 Fe	387	2,8	3,9
485	17,639 Ti	189	6,0	13
486	18,34 Y^+	7	2,8	2,9
487	18,64 ?	—	11	7,7
488	19,04 A^+	129	7,6	8,7
489	19,25 He	23	6,5	9,7
490	19,67 Eu^+	1	22	46
491	20,428 Fe	20	59	89
492	21,181 Fe	608	7,9	7,7
493	21,834 Fe	222	4,2	3,9
494	22,987 Mo	8	3,7	2,9
495	23,513 Mn	6	5,6	3,9

No.	λ, element	multiplet	$I_{\lambda_0} \cdot 10^{-3}$	$E_\lambda \cdot 10^{-3}$
496	24,074 Fe	224	4,5	5,8
497	24,306 Fe	607	68	81
	24,444 Fe	4		
498	24,882 Nb	2	10	14
499	25,884 Fe	29	42	82
500	26,836 Fe	283	6,5	7,7
501	27,825 Fe	45	45	68
502	29,355 Mg	3	56	109
503	3830,757 Fe	224	58	58
504	31,84 Nb^+	10	7,9	3,6
505	31,75 Fe^{++}	109	10	25
506	32,300 Mg	3	59	45
	32,304 Mg	3		
507	35,386 H_δ	2	79	900
508	38,292 Mg	3	62	152
	38,294 Mg	3		
509	39,259 Fe	529	6,5	13
510	39,64 Gd^+	20	9,0	9,7
511	40,439 Fe	20	28	54
	40,44 V	44		
512	41,051 Fe	45	28	39
	41,082 Mn	6		
513	42,03 Cr	70	6,5	5,8
514	42,90 Fe	222	4,2	14
	42,975 Fe	221		
515	43,259 Fe	528	7,9	7,7
516	43,72 Fe	703	4,5	3,0
517	43,983 Mn	6	5,6	5,8
518	44,25 ?	—	4,8	4,0
519	44,438 V	7	3,5	3,5
520	45,170 Fe	124	7,5	9,7
	45,18 Fe^+	127		
521	45,692 Fe	771	8,5	7,8
522	45,974 V	—	20	29
523	47,89 O^+	12	4,0	7,8
524	48,29 Fe	224	7,3	9,7
525	48,86 ?	—	6,5	7,8
526	49,02 La^+, CN	12	6,5	7,5
		—		
527	3849,365 Cr	138	5,6	4,0
528	49,52 Hf^+	61	4,0	4,0
529	49,969 Fe	20	28	37
530	50,820 Fe	22	21	35
531	51,58 Fe	—	17	21
532	51,848 Co	128	4,2	3,9
533	52,218 Cr	24	5,6	2,9
534	52,574 Fe	73	14	24
535	53,176 Cr	69	6,5	4,0
536	53,462 Fe	429	4,0	2,0
537	54,375 Fe	567	4,0	2,0
538	56,021 Si^+	1	19	21
539	56,373 Fe	4	59	70
540	57,18 O^+, CN	13	8,5	5,8
541	57,631 Cr	69	5,1	3,9
542	57,912 Sm	28	7,6	6,0
543	58,301 Ni	32	16	43
544	59,214 Fe	175	14	12
545	59,913 Fe	4	75	110
546	61,164 Co	33	6,6	3,9
547	63,056 Nb^+	9	6,8	3,1
548	63,70 Fe	565	7,8	6,2
549	64,30 Fe	565	7,2	4,5
550	64,49 La^+	141	6,9	6,2
551	64,862 V	7	9,0	6,2
552	65,153 CN •	—	9,0	12
553	65,526 Fe	20	23	52
554	66,01 Cr^+	130	8,4	6,2
555	71,750 Fe	429	12	10
556	72,504 Fe	20	34	38
557	72,923 Fe	284	12	10
558	3873,120 Co	18	11	6,4
559	73,577 CN •	—	9,0	7,3
560	73,953 Co	18	10	8,4
	74,053 Fe	120		
561	75,26 A^+	2	4,5	6,2
	75,262 Ti	15,175		
562	78,021 Fe	20	42	65
	CN	—		
563	80,74 ?	—	5,5	2,6
564	81,36 ?	—	4,5	6,3
565	82,28 Ti^+	34	4,9	9,3
566	84,359 Fe	282	7,4	19
567	85,190 Pr^+	18	6,7	7,0
568	85,512 Fe	124	7,4	4,6
569	86,284 Fe, La^+	4	5,8	7,7
		—		
570	87,051 Fe	20	37	51
571	89,051 H_δ	2	78	880
572	90,844 Fe	280	4,0	8,0
573	93,316 Fe	364	7,5	18
	93,376 Mg	47		
574	93,924 Fe	175	3,7	12
	94,005 Fe	663	6,7	
575	95,658 Fe	4	35	51
576	97,896 Fe	280	7,4	16
	98,012 Fe	20		
577	99,709 Fe	4	41	53
578	3900,546 Ti^+	34	26	42
579	02,948 Fe	45	24	49
	02,968 Mo	1		

No.	λ, element	multiplet	$I_{\lambda_0} \cdot 10^{-3}$	$E_\lambda \cdot 10^{-3}$
580	03,902 Fe	429	9,3	9,3
581	3904,785 Ti	56		
	04,79 P++	9	3,7	2,3
	04,790 Co	171		
582	05,527 Si	3	80	100
583	06,482 Fe	4	24	22
584	07,937 Fe	280	5,1	3,5
585	13,464 Ti+	34	24	31
586	14,635 Fe	120	5,9	11
587	14,333 V+	33	3,9	2,6
	14,334 Ti	15		
588	17,185 Fe	20	14	26
589	18,418 Fe	364	5,1	3,6
590	18,644 Fe	430	7,8	5,2
591	19,069 Fe	430	5,1	3,9
	19,15 Cr	136		
592	20,260 Fe	4	42	52
593	21,80 Zr	8	6,0	4,0
594	22,914 Fe	4	43	59
595	25,201 Fe	567	5,1	7,7
596	25,646 Fe	364	5,5	7,7
597	25,946 Fe	364	5,1	7,7
	25,001 Fe	562		
598	27,922 Fe	4		
	27,926 V	90	104	111
	27,93 Fe	361		
599	30,299 Fe	4	105	105
	30,31 Fe+	3		
600	32,007 Ti+	34	27	30
601	33,664 Ca+	1	484	2200
602	37,329 Fe	278	7,0	13
603	3940,882 Fe	20	16	17
	40,887 Co	18		
604	42,40 ?	—	5,8	6,5
605	44,009 Al	1	61	84
606	47,533 Fe	361,	7,0	17
		426		
607	48,105 Fe	562	8,0	10
	48,113 Sm+	9		
608	48,779 Fe	604	11	23
609	49,96 Cl+	36	14	17
610	51,164 Fe	661	6,9	13
611	52,606 Fe	278	11	17
	52,704 Fe	362		
612	52,917 Co	28	6,9	4,0
613	53,156 Fe	430	8,0	5,5
	53,163 Cr	136		
614	53,863 Fe	362	8,0	4,4
615	55,352 Fe	562	9,6	13
616	55,956 Fe	488	10	10
617	56,681 Fe	278	12	20
618	58,206 Ti	13	5,3	10
619	61,523 Al	1	53	116
620	63,690 Cr	38	8,1	10
621	66,066 Fe	45	19	24
622	68,470 Ca+	1	425	1750
623	70,074 H_7	1	149	1980
624	73,562 Ni	31	8,0	10
625	76,615 Fe	729	9,6	10
626	77,743 Fe	72	11	20
627	79,479 Nd+	57	6,0	5,1
	79,518 Co	3		
628	3981,761 Ti	12	9,6	14
	81,775 Fe	278		
629	83,237 Cr	213	9,5	6,7
630	83,960 Fe	277	5,3	2,7
631	86,176 Fe	655	11	14
632	86,753 Mg	17	11	17
633	87,090 Ni	137		
	87,098 Mn	33	5,3	20
	87,117 Co	16		
634	87,63 Ti+	11	5,3	6,7
635	4062,446 Fe	359	3,5	2,0
636	63,286 Fe	698	3,2	2,0
637	63,597 Fe	43	27	39
638	68,003 Mn	5	4,9	5,4
639	70,766 Fe	558	6,8	11
640	71,52 Fe	218		
	71,541 F	96	20	41
	71,740 Fe	43		
641	73,759 Gd+	44	4,9	5,4
	73,760 Fe	558		
642	74,794 Fe	524	4,6	18
643	76,498 Fe	218	7,2	18
	76,636 Fe	558	8,3	
644	76,810 Fe	557	3,9	3,6
645	77,714 Sr+	1	3,6	9,1
646	78,365 Fe	217	9,0	12
	78,471 Ti	80		
647	81,221 Cr	66		
	81,226 Fe	558	4,9	5,2
	80,227 Nd+	18		
648	82,125 Fe	698	4,6	2,7
649	4082,944 Mn	5	5,2	2,7
650	84,498 Fe	698	4,9	3,4
651	85,312 Fe	559	5,4	8,4
652	86,300 Co	58	7,2	17
653	94,930 Ca	25	4,0	17

No.	λ, element		multiplet	$I_\lambda \cdot 10^{-3}$	$E_\lambda \cdot 10^{-3}$
654	95,486	V	41	5,2	5,1
655	95,975	Fe	217	5,4	3,4
656	96,118	Fe	911	7,0	3,4
657	98,18	Ce	97	5,2	3,4
	98,183	Fe	558		
658	99,77	Mg	46	5,2	5,1
659	4101,737	H_δ	1	157	1720
660	07,492	Fe	354	6,1	3,2
661	14,95	Na^+	20	4,6	4,9
	14,957	Fe	695		
662	15,185	V	27	5,6	7,5
663	16,470	V	47	7,9	9,0
664	18,549	Fe	801	2,8	4,5
	18,551	Sm^+	54		
665	21,318	Co	28	3,2	6,0
666	21,806	Fe	356	2,8	3,0
	21,817	Cr	108		
667	22,162	Cr	65	2,3	2,3
668	22,638	Fe^+	28	2,8	4,5
669	23,387	Cr	108	2,9	7,7
670	23,748	Fe	217	3,3	6,2
			422		
671	25,622	Fe	1103	3,1	3,1
672	26,521	Cr	35	4,3	2,8
673	28,071	V	27	6,6	11
674	4128,858	V	112	3,3	1,4
675	29,166	Ti	—	3,3	2,1
676	31,099	Ce^+	112	5,0	3,1
677	32,060	Fe	43	23	34
678	4301,928	Ti^+	41	13	26
679	03,166	Fe^+	27	24	40
680	05,474	Ti	147	4,0	6,5
681	06,87	?	—	3,2	17
682	07,900	Ti^+	41	5,4	
	07,906	Fe	42	29	101
		CH	—	—	
683	09,11	A^+	36	4,0	14
684	09,46	Fe	478	5,9	21
685	12,861	Ti	41	15	31
686	14,084	Sc^+	15	13	23
		CH	—		
687	14,979	Ti^+	41	13	30
	15,087	Fe	71		
688	18,652	Ca	5	5,3	10
	18,68	S^+	49		
689	20,745	Sc^+	15	6,1	6,9
690	20,965	Ti^+	41	7,7	14
691	24,961	Fe	70	6,1	9,0
692	27,04	Fe^+	20	4,0	5,2
	27,100	Fe	761		
693	27,89	O^+	41	4,0	5,2
	27,92	Fe	597		
694	37,049	Fe	41	16	29
695	37,566	Cr	22	10	12
696	40,468	H_5	1	160	1730
697	4344,921	Ti^+	20	6,9	11
698	51,051	Cr	22	6,4	13
699	51,764	Fe^+	27	63	260
	51,770	Cr	22		
		CH	—		
	51,894	Mg	14	15	
	51,906	Mg	14		
700	52,68	Cr^+	37	11	18
701	58,169	Nd^+	10	2,0	1,6
702	59,585	Ni	83	7,3	9,6
703	60,31	?	—	5,0	6,4
704	62,55	?	—	4,9	4,8
705	66,67	CH	—	5,0	8,0
706	67,581	Fe	414	5,0	21
707	69,774	Fe	518	8,3	11
		CH	—		
708	71,00	Fe	69	3,7	3,2
	71,069	Hd^+	57		
709	71,279	Cr	22	8,0	8,0
	71,28	Cr	304		
710	72,254	Cr	22	4,9	4,2
	73,232	Sm^+	42		
711	74,455	Sc^+	14	11	11
712	4430,197	Fe	472	8,5	12
713	30,618	Fe	68	9,2	12
714	31,82	Ni^+	55	5,0	5,9
715	32,572	Fe	797	4,7	5,4
716	33,223	Fe	830	5,8	4,1
717	33,793	Fe	825	8,0	6,2
718	34,960	Ca	4	13	23
719	4435,151	Fe	2	10	21
720	35,688	Ca	4	5,0	4,0
721	36,138	V	21	6,0	8,3
722	36,352	Mn	22	3,0	3,0
723	36,981	Ni	86	5,0	6,2
724	37,549	He	50	5,8	2,0
725	37,837	V	21	5,8	8,2
726	38,353	Fe	828	4,2	3,1
727	40,479	Fe	829	7,2	14
728	41,73	Ti^+	40	3,0	4,0
729	42,343	Fe	68	18	25
730	43,197	Fe	350	6,7	7,0
731	43,802	Ti^+	19	27	43
732	44,559	Ti^+	31	9,2	14
	44,563	Fe^+	201		

No.	λ, element	multiplet	$I_{\lambda_0} \cdot 10^{-3}$	$E_\lambda \cdot 10^{-3}$	No.	λ, element	multiplet	$I_{\lambda_0} \cdot 10^{-3}$	$E_\lambda \cdot 10^{-3}$
733	45,48 Fe	2	6,7	8,2	773	80,570 Ni	211	11	4,9
734	46,842 Fe	828	17	10	774	80,85 Ar^+	104	5,0	4,9
735	47,722 Fe	68	15	25	775	81,129 Mg^+	4	15	20
736	49,143 Fe	160	5,0	5,4		81,261 Ti	146	16	
737	50,320 Fe	476	12	5,2	776	81,621 Fe	827	4,2	2,0
738	51,586 Mn	22	5,0	4,2	777	84,257 Fe	68	17	42
739	53,35 V^+	199	10	10	778	84,227 Fe	828	6,7	3,9
740	53,708 Ti	160	10	8,5	779	85,64 ?	—	8,4	11
741	54,382 Pr^+	5	12	13	780	88,140 Fe	818	5,0	2,1
	54,383 Fe	350			781	89,185 Fe^+	37	14	14
742	54,781 Ca	4	15	23	782	89,741 Fe	2	13	12
	54,80 Zr^+	40			783	90,081 Mn	22	8,0	4,2
743	55,012 Mn	28	5,0	5,2	784	90,773 Fe	974	7,5	3,5
	55,032 Fe	974			785	91,401 Fe^+	37	33	28
744	55,318 Mn	28	5,0	6,2	786	94,568 Fe	68	22	32
	55,321 Ti	113			787	95,95 ?	—	5,0	2,0
745	4455,887 Ca	4	13	25	788	96,146 Ti	146	7,2	4,1
746	56,331 Fe	516	6,7	10	789	98,897 Mn	22	2,5	2,1
747	56,63 Fe	973	6,7	6,2	790	4501,270 Ti^+	31	28	36
748	57,045 Mn	28	6,5	5,2	791	01,788 Cr	81	13	21
749	57,42 Zr^+	79	5,8	10	792	4672,31 ?	—	7,8	7,0
	57,428 Ti	113			793	73,169 Fe	820	6,2	7,5
	57,549 Mn	28	3,3		794	79,118 Ti	77	8,9	12
750	58,101 Fe	992	5,0	3,2	795	78,160 Cd	2	2,4	2,0
751	58,262 Mn	28	6,7	7,3	796	78,852 Fe	821	5,0	7,0
752	58,538 Cr	127	5,5	6,5	797	79,229 Fe	688	2,4	3,0
753	59,121 Fe	68	12	29	798	4680,297 Fe	39	3,8	4,0
754	59,34 Cr	63	7,5	7,2	799	81,908 Ti	16	3,0	3,0
755	60,292 V	21	2,5	2,5	800	82,12 La^+	37	8,1	6,7
756	61,205 Fe	471	4,2	6,2	801	83,565 Fe	346	6,5	4,4
	61,22 Zr^+	67			802	85,265 Ca	51	6,2	6,9
757	61,654 Fe	2	2,5	3,1	803	86,218 Ni	98	8,1	7,8
758	62,022 Mn	28	4,0	4,0	804	91,414 Fe	409	8,1	12
759	64,458 Ti^+	40	9,7	10	805	99,38 ?	—	6,5	9,6
760	64,747 V	110	4,0	18	806	4701,536 Ni	235	3,8	3,9
	64,773 Fe	472			807	02,983 Mg	11	18	34
761	65,357 Cr	127	3,7	5,2		02,991 Mg	11		
762	65,807 Ti	146	7,0	8,2	808	04,958 Fe	821	10	8,6
763	66,554 Fe	350	12	25	809	06,542 Nd^+	3	5,7	5,8
764	68,493 Ti^+	31	28	47		06,574 V	119		
765	69,160 Ti^+	18	17	10	810	07,281 Fe	554	7,2	9,1
766	69,381 Fe	830	10	10	812	07,487 Fe	346	9,0	9,9
767	70,138 Mn	22	8,4	9,3	813	08,663 Ti^+	49	4,3	3,8
768	71,477 He	14	33	94	814	08,972 Fe	889	4,3	6,7
	71,688 He	14				08,976 Ti	203		
769	72,792 Mn	22	5,5	2,5	815	09,092 Fe	821	4,3	4,2
770	4472,921 Fe^+	37	5,0	5,2	816	09,715 Mn	21	2,5	4,2
771	76,082 Fe	830	13	24	817	10,286 Fe	409	10	5,8
772	79,612 Fe	828	5,8	5,0	818	14,421 N	98	8,7	7,6
		848			819	15,778 Ni	98	4,4	3,3

No.	λ, element	multi. plet	$I_{\lambda_0} \cdot 10^{-3}$	$E_\lambda \cdot 10^{-3}$
820	18,429 Cr	188	6,6	6,3
821	27,476 Mn	21	6,0	7,8
822	30,711 Cr	145	4,5	2,6
823	31,439 Fe^+	43	9,0	17
824	36,780 Fe	554	4,6	6,0
825	37,350 Cr	145	3,4	3,0
826	4741,533 Fe	346	2,3	2,0
827	4823,516 Mn	16	9,0	20
828	24,162 Fe	888	14	24
829	29,028 Ni	131	2,1	4,1
830	29,376 Cr	31	4,4	4,1
831	31,183 Ni	111	3,5	6,1
832	32,704 N	146		
	32,734 Fe	888	5,2	6,1
		1098		
833	34,511 Fe	115	5,2	8,0
834	35,862 Fe	1068	7,8	8,2
835	36,22 Cr^+	30	4,0	4,1
836	38,519 Fe	687	4,0	6,1
837	38,651 N	260	3,7	3,1
838	39,549 Fe	588	7,0	8,2
839	40,329 Fe	1068	3,5	3,1
840	41,80 Fe	1070	2,6	3,1
841	43,155 Fe	687	5,2	6,1
	43,165 Ni	50		
842	44,016 Fe	750	3,5	1,0
843	45,656 Fe	588	3,0	3,1
		888		
844	47,296 Ca	50	2,1	1,0
845	48,24 Cr^+	30	7,5	7,2
846	48,898 Fe	114	10	6,2
847	49,18 Ti^+	29	7,3	8,2
848	51,483 V	3	7,3	7,2
849	52,560 Ni	130	5,2	4,1
850	54,87 V^+	23	4,8	5,1
	54,89 Fe	1043		
851	4855,414 Ni	130	7,5	9,2
852	55,683 Fe	687	10	8,5
853	56,012 Ti	231	5,6	2,0
854	57,382 Ni	111	4,0	2,0
855	61,332 H_α	1	165	3040
856	66,267 Ni	111	4,3	2,0
857	67,870 Co	158	1,7	1,0
858	68,264 Ti	231	5,2	2,0
859	69,45 Fe	751	3,8	3,3
860	70,845 Ni	131	4,9	3,1
861	71,323 Fe	318	20	38
862	71,94 Fe	630	14	21
863	72,144 Fe	318	19	28
864	73,27 Ni	112	6,9	5,0
865	73,437 Ni	111	6,4	5,0
866	74,35 Fe	467	5,0	4,4
867	74,651 Cr	167	5,2	3,3
868	75,462 V	3	10	10
869	75,89 Fe	687	2,1	2,0
870	78,132 Ca	35	14	26
871	81,554 V	3	6,9	8,0
872	81,726 Fe	588, 1041	6,9	8,0
873	85,082 Ti	157	2,8	2,0
874	85,435 Fe	966	5,0	3,0
875	86,335 Fe	1066	3,5	2,0
876	87,189 Fe	1064	7,0	5,4
877	88,651 Fe	1066	7,8	7,0
878	89,069 Fe	67,749	3,5	6,0
	89,113 Fe	985	4,5	
879	4890,762 Fe	318	17	19
880	5137,075 Ni	48	4,8	4,1
	37,09 Cr	201		
881	37,388 Fe	1090	2,4	1,2
882	39,260 Fe	383	7,7	7,9
883	39,468 Fe	383	12	9,7
884	41,750 Fe	114	2,4	1,0
885	42,541 Fe	1092	2,9	2,1
886	42,98 Ni	113	5,6	5,3
887	50,890 Mn	32	8,2	6,4
	50,93 Fe^+	35		
888	53,235 Cu	7	12	39
	53,402 Na	8	22	
889	54,061 Ti	70	7,2	3,0
890	62,288 Fe	1089	4,8	5,9
891	65,422 Fe	1089	2,5	3,5
892	67,322 Mg	2	80	190
	67,491 Fe	37		
893	69,030 Fe^+	42	130	250
894	71,599 Fe	36	22	54
895	72,684 Mg	2	88	210
896	73,742 Ti^+	4	3,2	3,0
897	77,230 Fe	930	11	21
898	83,604 Mg	2	85	200
899	85,90 Ti^+	86	8,0	10
900	87,922 Fe	1032	2,4	3,0
901	88,700 Ti^+	70	15	26
	88,848 Ca	49	4,0	
902	91,448 Nd^+	45	11	12
	91,46 Cr^+	24		
	91,460 Fe	383		
903	5192,350 Fe	383	13	17

No.	λ, element	multiplet	$I_{\lambda_0} \cdot 10^{-3}$	$E_\lambda \cdot 10^{-3}$	No.	λ, element	multiplet	$I_{\lambda_0} \cdot 10^{-3}$	$E_\lambda \cdot 10^{-3}$
904	92.971 Ti	4	7.4	11	912	5875.618 He	11		
905	94.943 Fe	36	20	15		75.650 He	11	100	540
906	95.471 Fe	1092	5.6	5.9		75.989 He	11		
907	97.569 Fe+	49	63	70	913	89.953 Na	1	69	168
908	98.714 Fe	66	11	18	914	92.878 Ni	68	3.9	2.7
909	5856.084 Fe	1128	3.9	2.7	915	95.923 Na	1	73	184
910	57.454 Ca	47	8.4	24	916	5905.673 Fe	1181	5.9	5.4
911	62.357 Fe	1180	10	11	917	6562.817 H_α	1	172	4280
					918	75.022 Fe	206	5.0	6.0

REFERENCES

1. Severnyy, A.B., N.V. Steshenkoand and V.L. Khokhlova: Astron. Zhur., Vol. 37, p. 23, 1960.
2. Alikayeva, K.V. and T.V. Orlova: Solnechnyye dannyye, No. 7, p. 68, 1961.
3. Hrebik, F., J. Koicala, L. Kriosky and J. Olmr: Bull. Astron. Czechoslovakia, Vol. 13, p. 199, 196a.
4. Polipan, P.N.: Publ. Kiyevskoy Astron. Obs., No. 11, p. 24, 1962.
5. Revision of Rowland's Preliminary Table of Solar Spectrum Wavelengths. Washington, 1928.
6. Moor, Ch.E.: Contrib. Princeton Univ. Observ., No. 20, 1945.
7. Minnaert, M., J.F.W. Mulders, and J. Houtgast: Photometric Atlas of the Solar Spectrum. Amsterdam, 1940.

THE SYNCHRONISM OF ACTIVE FLUCTUATIONS OF THE OLD AND NEW CYCLES IN THE INTERMEDIATE EPOCH

V.S. Chistyakov

ABSTRACT: An analysis of the solar activity in the intermediate epoch shows that the monthly activity fluctuations develop synchronously at high latitudes (old cycles) and low latitudes (new cycles). The strict synchronization of the fluctuation peaks before the minimum and the appearance of the high-latitude groups of the new cycle are maintained only on the condition that the heliographic latitude of these groups of spots is close to 24.3. During an increase of the heliographic latitude of groups of the new cycle, this synchronization is observed in the activity of the high and low latitudes. The results obtained suggest that the Sun has a special mechanism of short-period oscillations, i.e., "the mechanism of monthly oscillation", which act continually and independently in the 11-year cycle phase.

The neighboring 11-year cycles of solar activity develop in close relation to one another in such a way that the characteristics of development of a preceeding cycle predetermine the characteristics of the development of the following cycle. The internal rules of the 22-year cycles indicate this: (1) the Gnevyshev-Olya rule, which states that a less powerful cycle with an even number is followed by a more powerful cycle with an odd number [1, 2]; (2) the close interrelationships between the total power of the 11-year cycles comprising a given 22-year cycle and its duration [3,4]; (3) the facts of the interaction of neighboring 22-year cycles [5,6]. However, the subsequent cycle can be considered as a completely independent object. The effect of the interaction of neighboring 11-year cycles speaks in favor of this. This takes place in the neighbothood of the activity minima, during the so-called intermediate epoch, when the sunspot-formation processes of the old cycle (at low attitudes) and those of the new-cycle (at high latitudes) develop simultaneously. Consequently, the intermediate epoch is very suitable for studying the nature of interrelationships between neighboring cycles. /140*

It is well known that shorter oscillations, or the so-called monthly activity fluctuations, which last from 2-6 months are super-

* Numbers in the margin indicate pagination in the foreign text.

imposed on the curves of the 11-year cycle. According to Yu.I. Vitinskiy and R.N. Ikhsanov [7,8] the development of monthly fluctuations does not depend on the phase of the 11-year cycle, but has a random nature. Since monthly fluctuations and the intermediate epoch develop at the same time at high and low latitudes, their synchronism should be questioned. Under the condition of the independence of the fluctuations in relation to the phase of the 11-year cycles, the synchronism of development of fluctuations at high and low latitudes would mean that there is a continuously-acting mechanism of short oscillations on the Sun--the mechanism of "monthly fluctuations"--which oscillations would seem to produce a unique noise background against which longer oscillations or cycles are superposed.

Before turning to an investigation of these factual data, let us examine some characteristics of the cyclic activity in the neighborhood of the minima.

1. The effect of the overlapping of neighboring 11-year cycles depends to a great extent on the phase of the 90-year cycle [8] and is most pronounced at the junction of powerful 11-year cycles. Therefore, certain weak cycles for which there is almost no overlapping give relatively small amounts of factual data.

2. In the neighborhood of the minimum, the total activity level is very low, in view of which a high random coincidence element is introduced into the determination of the monthly fluctuation. For the sake of comparison, we will show that the monthly /141
activity fluctuations determined at a certain average level when the values of the Wolf numbers W change from 50 to 100 is calculated according to the daily arisal of from 5 to 10 groups of spots on the Sun, which are found rather reliably. On the other hand, the random coincidence element increases in the neighborhood of the minimum when W = 5-10. Having mentioned this non-coincidence, we can base our discussions only on factual materials, or we can assume, for example, that the arisal of individual groups of sunspots in the vicinity of a minimum could be the sign of a rather strong fluctuation.

3. The daily indices of solar activity are usually derived for the entire Sun without a limitation in terms of whether they belong to the old or new cycles. Therefore, the monthly fluctuations before the minimum preferably characterize the activity of the old cycle, while those after the minimum characterize the activity of the new cycle. We can discuss the activity fluctuations of the new cycle before the minimum or the old cycle after the minimum only according to observations of individual groups of sunspots appearing at high latitudes before the minimum or at low latitudes after it. Therefore, the moment of the minimum is the moment of balance between the activities of the old and new cycles. If the moment of the minimum relates to the first months when predominance of spots of the new cycles is first observed, then there is good

correspondence with the moment of the minimum usually found along the smoothed curve of the average monthly values for the relative numbers of spots. The degree of correspondence between both methods can be determined according to Table 1, where Δt characterize the accuracy in determining the moment of the minimum on the basis of the relationship between the numbers of groups at high and low latitudes, compared to the generally-accepted method.

TABLE 1

Cycle No.	Moments of Min. Along W Curve	Δt(Unit Measment = 1 Year	Cycle No.	Moments of Min. Along W Curve	Δt(Unit Measment = 1 Year
11	1867.2	0	16	1923.6	+0.1
12	1879.1	0	17	1937.8	+0.3
13	1889.7	+0.1	18	1944.5	0
14	1901.7	+0.5	19	1954.6	+0.2
15	1913.6	+0.2			
Average					+0.15 ± 0.13

In this study we used the moments of the minima determined according to a new method which is more suitable for analyzing the materials.

For the original materials, we used catalogs of sunspots, from which we recorded the values of the heliographic coordinates of the spots (ϕ and L) and the moments they were first observed. For reference, we took the Greenwich catalog [10], supplemented by the data of other shorter catalogs [11-18] and individual articles [19-21]. For cycle No. 20, we used the results of current observations of sunspots obtained at the Ussuriysk Solar Observatory. With the aid of these catalogs we composed lists of high-latitude groups of sunspots of the new cycle observed before the minimum (list A) and low-latitude groups of spots observed after the minimum (list B). For ten subsequent cycles (Nos. 11-20), 60 groups of spots were put in list A and 87 groups in the list B. Both lists are shown in Table 2, where $\Delta\tau$ is the time difference between the moment the group was first observed and the moment of the greatest development of the monthly fluctuations.

TABLE 2

No.	Observation Date	$\varphi°$	$L°$	$\Delta\tau$, days	Source
	List A. High-latitude groups of new cycle observed before minimum.				
1	14—19.III 1867	34.1		1	[11]
2	30.III 1867	—32.0		15	[11]
3	8.IV 1876	35.0	151.5	23	[12]
4	7.IX 1876	43.2	286.5	—33	[12]
5	30.IV 1877	28.6	207.8	—16	[10, 12]
6	17.VIII 1878	34.4	253.0	—28	[12]
7	14.II 1879	—36.9	302.0	30	[12]
8	28.VI 1889	—40.3	249.5	—47	[10, 13]
9	26.VII 1889	—23.5	342.9	—21	[10, 13]
10	1.VIII 1889	—20.3	165.4	—15	[10, 13]
11	27.VIII 1889	—19.0	301.0	12	[13]
12	24.I 1900	38.4	43.0	—22	[10]
13	28.I 1900	—34.7	88.5	—18	[10]
14	3.IX 1900	—21.1	107.0	—12	[10]
15	22.VI 1901	—20.0	164.5	37	[10]
16	12.IX 1901	36.4	129.5	—33	[10]
17	18.XII 1911	22.7	295.5	33	[10]
18	16.XII 1912	20.1	228.0	1	[10]
19	29.XII 1912	26.0	58.0	14	[10]
20	19.VI 1922	33.0	114.5	—26	[10]
21	24.VI 1922	31.4	35.5	—21	[10]
22	22.VII 1922	—22.0	61.0	7	[10]
23	21.VIII 1922	21.1	39.5	36	[10]
24	24.XI 1922	—41.5	278.5	—31	[10]
25	17.III 1923	—30.5	127.0	—28	[10]
26	10.IV 1923	23.2	122.0	—4	[10]
27	21.VI 1923	29.9	10.5	6	[10]
28	27.IV 1923	26.5	327.5	—19	[10]
29	15.I 1932	48.0	22.5	30	[10]
30	3.II 1932	—34.6	131.5	48	[10]
31	10.X 1933	27.2	308.0	25	[10]
32	29.X 1933	—31.2	31.5	44	[10]
33	20.XII 1942	31.0	264.0	35	[10]
34	16.V 1943	—40.5	166.5	31	[10, 15]
35	9.X 1943	—26.2	16.5	54	[10, 15]
36	14.XII 1943	—22.5	136.0	—1	[10]
37	24.I 1944	—24.0	141.0	36	[10]
38	14.III 1944	—28.0	16.5	—1	[10, 15]
39	18.III 1944	—25.3	309.0	3	[10, 15]
40	13.VIII 1953	52.0	42.0	58	[21]
41	18.I 1954	—37.8	82.0	33	[10]
42	9.II 1954	31.3	236.0	—36	[10, 17]
43	1.III 1954	—24.1	341.5	—14	[10]
44	9.V 1954	33.3	180.5	54	[10]
45	4.VI 1954	28.5	180.0	—41	[10]
46	1.VII 1963	24.0	269.0	15	
47	8.X 1963	34.5	28.0	21	
48	12.X 1963	24.0	308.0	0	
49	10.XI 1963	30.5	254.0	25	

Table 2 (continued)

No.	Observation Date	φ°	L°	$\Delta\tau$, days	Source
50	18.XI 1963	28.0	255.0	33	
51	24.I 1964	23.5	47.0	—30	
52	7.III 1964	28.0	278.5	0	
53	10.IV 1964	18.0	140.5	0	
54	9.VI 1964	25.5	10.5	0	
55	13—18.VI 1964	28.0	317.0	0	
56	17—18.VI 1964	28.0	303.0	2	
57	5—6.VII 1964	31.0	51.0	20	
58	14—15.VII 1964	28.5	297.5	29	
59	2—3.III 1964	19.0	151.0	—13	
60	12—17.VIII 1964	23.0	339.0	—3	

List B. Low latitude groups observed after minimum.

1	8—21.IX 1867	10.0		—37	[11]
2	2—8.X 1867	—16.0	251.0	—13	[11]
3	7—8.X 1867	9.5	326.0	—8	[11]
4	4—10.XII 1867	9.0	317.0	—11	[11]
5	26—28.XII 1867	6.0	235.0	11	[11]
6	8—18.VII 1879	5.0	170.0	—41	[12]
7	12—13.VIII 1879	9.5	94.0	—3	[10, 12]
8	25—28.XI 1879	—12.1	28.4	10	[10]
9	12—13.XII 1889	—7.1	334.5	—3	[10]
10	27.XII—1.I 1890	—9.0	113.6	0	[13]
11	3.IV 1890	1.0	248.0	18	[13]
12	20—21.V 1890	—9.8	357.7	5	[10, 13]
13	23—31.VII 1890	—6.6	137.0	8	[13]
14	6.X 1890	—10.6	233.0	21	[13]
15	21—25.X 1890	—5.2	25.4	36	[10, 13]
16	5—15.I 1902	—8.3	8.7	—10	[10]
17	1.II 1902	—8.4	238.3	16	[10]
18	5—7.IV 1913	—1.2	230.7	—10	[10]
19	7—9.IX 1913	5.6	359.1	—38	[10]
20	3.I 1914	0.9	175.8	18	[10]
21	9.I 1914	—5.0	88.0	24	[10]
22	18.IX 1923	8.9	228.2	3	[10]
23	16.X 1923	7.2	215.3	0	[10]
24	22.X 1923	—5.3	95.3	0	[10]
25	23.I 1924	—4.3	354.3	—22	[10]
26	21.III 1924	—9.0	297.0	—25	[10]
27	22.V 1924	8.6	164.0	0	[10]
28	1.IV 1924	2.0	72.5	0	[10]
29	2.VI 1924	3.8	69.7	0	[10]
30	9.VII 1924	5.3	251.2	0	[10]
31	1.VIII 1924	5.5	261.9	15	[10]
32	28.VIII 1924	4.8	263.5	—18	[10]
33	24.IX 1924	6.0	264.8	0	[10]
34	9.II 1934	7.6	60.7	—6	[10]
35	4.III 1934	—0.6	180.6	18	[10]
36	7.III 1934	—3.7	125.7	21	[10]
37	27.IV 1934	—1.3	216.5	—18	[10]
38	8.V 1934	6.3	28.4	—7	[10]

Table 2 (continued)

No.	Observation Date	φ°	L°	$\Delta\tau$, days	Source
39	39.V 1934	—0,6	213,2	13	[10]
40	15.VI 1934	2,9	204,0	30	[10]
41	13.VII 1934	1,4	211,9	—2	[10]
42	12.III 1934	4,1	194,4	0	[10]
43	12.IX 1934	7,1	196,5	27	[10]
44	25.X 1934	4,9	249,5	—14	[10]
45	14.II 1935	3,0	238,0	—29	[10]
46	1.VII 1944	—4,0	41,1	—45	[10]
47	4.VII 1944	—8,3	63,4	—41	[10]
48	11.VII 1944	—5,9	310,9	—34	[10]
49	6.VIII 1944	—10,4	306,3	—9	[10]
50	14.VIII 1944	8,0	155,6	—1	[10]
51	16.VIII 1944	—8,1	215,8	1	[10]
52	17.VIII 1944	—2,3	191,3	2	[10]
53	23.VIII 1944	7,2	163,6	8	[10]
54	25.IX 1944	9,1	64,4	0	[10]
55	29.IX 1944	—7,1	349,0	0	[10]
56	30.IX 1944	—4,9	285,0	0	[10]
57	9.X 1944	—10,5	261,1	0	[10]
58	28.X 1944	—5,4	245,3	13	[10]
59	29.X 1944	—5,5	225,0	14	[10]
60	30.XI 1944	—9,4	217,9	—15	[10]
61	20.XII 1944	—6,0	267,7	5	[10]
62	11.I 1945	10,1	110,7	27	[10, 15]
63	16.I 1945	—4,5	318,1	32	[10]
64	26.I 1945	—7,4	214,0	42	[10, 15]
65	14.IV 1945	—6,7	234,5	—1	[10, 15]
66	5.VI 1945	—6,5	295,0	0	[15]
67	12.VII 1945	—2,5	169,0	0	[15]
68	27.VII 1954	—4,8	57,8	—18	[10]
69	14.X 1954	11,9	144,3	—31	[10]
70	11.XI 1954	6,3	104,0	—4	[10]
71	16.II 1954	—2,0	308,0	2	[10, 17]
72	22.II 1954	—8,5	288,0	8	[17]
73	27.V 1954	—3,0	79,0	0	[17]
74	1.IX 1964	5,0	340,5	17	
75	13—14.IX 1964	6,0	297,5	29	
76	2.X 1964	—8,0	38,0	48	
77	1—4.XI 1964	—7,5	319,0	—75	
78	11—15.XII 1964	—6,0	98,0	—35	
79	18—21.XII 1964	—9,0	27,0	—28	
80	20.XII 1964	7,0	97,5	—26	
81	27—29.XII 1964	0	256,5	—19	
82	29.I—9.II 1965	7,5	162,0	14	
83	25—1.1965	—3,0	182,5	41	
84	25—1.03.1965	9,0	165,0	41	
85	28.II 1965	—2,0	180,0	43	
86	12—18.IV 1965	6,5	278,0	—18	
87	26—28.IV 1965	—2,5	198,0	—4	

TABLE 3

Interval, days	n(number of turns)	$\overline{\Delta\tau}$	$\lvert\overline{\varphi}\rvert$	Interval, days	n(number of turns)	$\overline{\Delta\tau}$	$\lvert\overline{\varphi}\rvert$
—(45—55)	1	—47	40,3	+(05—15)	6	+11,5	25,5—3,8
—(35—45)	3	—38,3	34,5—5,6	+(15—25)	5	+22,8	31,6—2,5
—(25—35)	6	—29,3	33,2—4,2	+(25—35)	8	+31,7	34,1—6,7
—(15—25)	6	—19,5	30,5—4,3	+(35—45)	4	+38,2	25,4—3,6
—(05—15)	4	—13,5	21,1—1,5	+(45—55)	4	+55,3	36,5—7,7
+(05—05)	13	—0,1	25,2—3,1				

We used the following rules in determining the value of $\Delta\tau$: (1) all the fluctuations of W were conditionally divided into two classes--those with a sharp peak ("triangular") and those with a plane one ("trapezoid"). We read off the values of $\Delta\tau$ for the first class from the apex of a triangle, and those for the second class of $\Delta\tau$ from one of the end of the upper base of a trapezoid; (2) the average monthly values of the relative numbers of W spots was taken for the 15th day of each month; (3) since the moments the groups of spots appeared always fell during an interval between two fluctuation peaks, we took the least of the two values of $\Delta\tau$, as shown in Table 2. An exception was made for group No. 40 in list A, where $\Delta\tau$ was read off from the farthest fluctuation peak. The particular method used in reading off $\Delta\tau$ for group No. 40 was due to the presence of the particular interaction between ϕ and $\Delta\tau$, which we will discuss below.

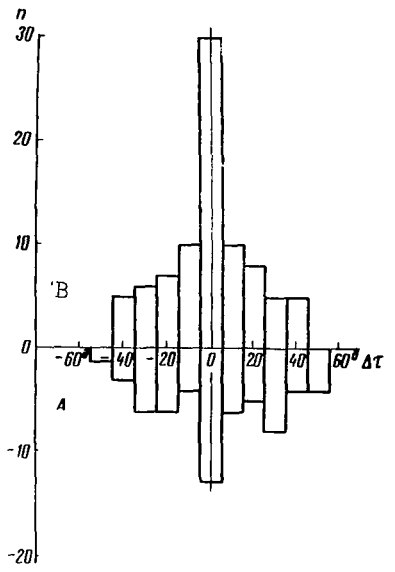

Fig. 1. Histograms of the Values $\Delta\tau$ for Lists A and B, Table 2.

The results of an analysis of list A are shown in Table 3 and Figures 1-3. Figure 1 shows a histogram of different values of $\Delta\tau$. It can be seen that synchronous groups ($\Delta\tau = 0$) are found most frequently, but the corresponding peak is narrow and isolated. To the right and the left of this, there are two other maxima, for $\Delta\tau = 25^d$ and $\Delta\tau = -30^d$. It seems that the central peak is, to some extent, the result of superposition of two bell-shaped curves arranged to the right and left of the origin of the coordinates. It is possible that this is not coincidental, since $\Delta\tau$ and ϕ are linked together by a dependence, and the maxima for $\Delta\tau$ $25\text{-}30^d$ corresponds to a heliographic latitude of $\phi \approx 30°$,

i.e., the latitude at which spots of the new cycle are usually observed.

Figure 2 depicts the dependence between the latitude of groups of spots of the new cycle and the values of $\Delta\tau$. In view of the small amount of materials, the data for the northern and southern hemispheres of the Sun were usually combined. It follows from the figure that, despite the substantial deviation of the points on the diagram, the absolute value of $\Delta\tau$ generally increases with an increase of ϕ. The average values of $\Delta\tau$ and ϕ for various intervals of time are shown in Table 3, while Figure 3 gives the correlation between absolute values of $\Delta\tau$ and ϕ. It can be seen from Figure 3 that most of the points are arranged closely along a straight line, while two points (for $\Delta\tau = -13^d$, 5 and $\Delta\tau = -33.2^d$) gives a substantial deviation. If we disregard these anomalous points, then

TABLE 4

/146

Interval, days	n(number of turns)	$\overline{\Delta\tau}$	$\lvert\overline{\varphi}\rvert$	Interval, days	n(number of days)	$\overline{\Delta\tau}$	$\lvert\overline{\varphi}\rvert$
—(35—45)	5	—40,0	6,6—2,1	+(05—15)	10	+11,4	6,5—1,9
—(35—35)	6	—30,5	6,8—2,4	+(15—25)	8	+19,1	4,4—2,5
—(15—25)	7	—19,7	4,4—2,1	+(25—35)	5	+29,0	6,1—2,0
—(05—15)	10	—10,4	8,3—2,6	+(35—45)	5	+40,2	5,3—1,9
—(05—05)	29	—0	6,0—1,2	+(45—55)	1	+48,0	8,0

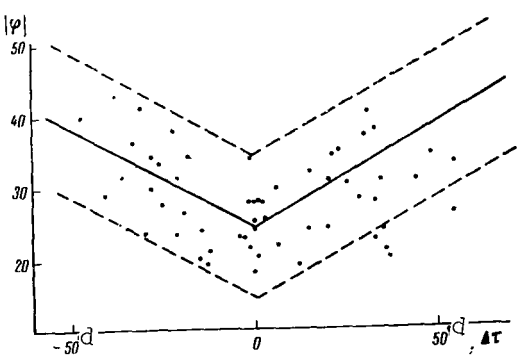

Fig. 2. Dependence Between Latitudes of Groups of Sunspots of a New Cycle and Values of $\Delta\tau$.

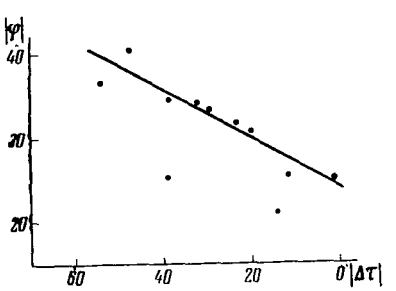

Fig. 3. Correlation Between Absolute Values of $\Delta\tau$ and ϕ.

for the remaining nine points the dependence between $\bar{\phi}$ and $\Delta\bar{\tau}$ has a high correlation factor, equal to r = +0.937, and is described by the following regression equation:

$$|\bar{\varphi}| = 0{,}289\,|\overline{\Delta\tau}| + 24{,}34.$$

It follows from the equation that the first high-latitude groups of sunspots of the new cycle arise at the same time as the peaks of the monthly fluctuations of W for the lower latitudes only for a latitude equal to $\bar{\phi}$ = 24.3°. During an increase of the heliographic latitudes of the high-latitude group in the new cycle, the advance or delay of the moment when these groups appear in relation to the moment of the maximum for the nearest monthly fluctuation of W at lower latitudes increases.

The results of an analysis of list B are shown in Table 4, which was constructed according to the same principle as was Table 3. A histogram of different values of $\Delta\tau$ (according to the data of the second column of Table 4) is presented in Figure 2, which shows that the last low-latitude spots of the old cycle tend to appear at the same time as fluctuations of the W numbers due to spot-formation processes of the new cycle at high latitudes. Out of the 87 groups of spots listed in B, $\Delta\tau < 15^d$ in 49 groups (56%). This means that the value for the average deviation on the histogram does not go beyond the limits of accuracy in determining the moments of a peak fluctuation equal to 15^d (see above).

A comparison of the values for $\Delta\bar{\tau}$ and $\bar{\phi}$ in Table 4 shows that these indices are not interconnected by any dependence, despite the variance of the values, and that all the last low latitude spots are grouped around a center which lies at a heliographic latitude of $\bar{\phi}$ = 6.2°. It is well known [22-24] that the spot-formation /147 processes of the old cycle begin to die out at this latitude.

REFERENCES

1. Gnevyshev, M.N. and A.I. Ol': Astron. Zhur., No. 1, 1948.
2. Ol', A.I.: Priroda, No. 8, 1948.
3. Chernosky, E.J.: Publ. Astron. Soc. Pacif., Vol. 66, No. 392, 1954.
4. Chistyakov, V.F.: Byull. VAGO, No. 25, p. 32, 1959.
5. Bezrukova, A.N.: Solnechnyye dannyye, No. 2, 1957.
6. Chistyakov, V.F.: Solnechnyye dannyye, No. 2, 1959.
7. Vitinskiy, Yu.I. and R.N. Ikhsanov: Solnechnyye dannyye, No. 1, 1960.
8. Vitinskiy, Yu.I.: Prognozy solnechnoy aktivnosti (Predictions of Solar Activity). "Nauka", 1963.
9. Chistyakov, V.F.: Solnechnyye dannyye, No. 7, 1961.
10. Greenwich Photoheliograph results, 1874-1955.
11. Peters, C.H.: Heliographic Positions of Sunspots Observed at Hamilton College from 1860-1870.

12. Spörer, G.: Publ. Astrophys. Observ. Potsdam, 1880, 2, N 5.
13. Spörer, G.: Publ. Astrophys. Observ. Potsdam, 1894, 10, N 32.
14. Gnevyshev, M.N. and B.M. Rubashev: Katalog solnechnoy aktivnosti za 1932-1927 gg. Trudy GAO, Vol. 54, 1941.
15. Gnevysheva, R.S.: Katalog solnechnoy aktivnosti za 1940-1945 gg. Trudy GAO, Vol. 62, 1949.
16. Gnevysheva, R.S.: Katalog solnechnoy aktivnosti za 1952-1953 gg. Trudy GAO, 1955.
17. Gnevysheva, R.S.: Katalog solnechnoy aktivnosti za 1954-1955 gg. Trudy GAO, 1957.
18. Kosmicheskiye dannyye (Cosmic Data), Nos. 1-12, 1944. "Gidrometeoizdat", 1944.
19. Nicholson, S.B.: Publ. Astron. Soc. Pacif., 1957, 69, N 406.
20. Kopecky, M.: Bull. Astron. Inst. Czeckosl., 1958, 9, N 1.
21. Dodson, H.E.: Publ. Astron. Soc. Pacif., 1953, 65, N 386.
22. Gnevyshev, M.N. and R.S. Gnevysheva: Byull. KISO, No. 1, p. 15, 1949.
23. Rubashev, B.M.: Problemy solnechnoy aktivnosti (Problems of Solar Activity). "Nauka", 1964.
24. Chistyakov, V.F.: Nekotoryye voprosy proiskhozhdeniya i stroyeniya solnechnykh pyaten (Certain Problems of the Origin and Structure of Sunspots). Author's Abstract of Dissertation. Leningrad, 1964.

Translated for the National Aeronautics and Space Administration by:
Aztec School of Languages, Inc.,
Research Translation Division (173)
Maynard, Massachusetts.
NASw-1692

NASA-Langley, 1969 —— 29 F-581

NATIONAL AERONAUTICS AND SPACE ADMINISTRATION
WASHINGTON, D. C. 20546
OFFICIAL BUSINESS

FIRST CLASS MAIL

POSTAGE AND FEES PAID
NATIONAL AERONAUTICS AND
SPACE ADMINISTRATION

POSTMASTER: If Undeliverable (Section 158 Postal Manual) Do Not Return

"The aeronautical and space activities of the United States shall be conducted so as to contribute . . . to the expansion of human knowledge of phenomena in the atmosphere and space. The Administration shall provide for the widest practicable and appropriate dissemination of information concerning its activities and the results thereof."

—NATIONAL AERONAUTICS AND SPACE ACT OF 1958

NASA SCIENTIFIC AND TECHNICAL PUBLICATIONS

TECHNICAL REPORTS: Scientific and technical information considered important, complete, and a lasting contribution to existing knowledge.

TECHNICAL NOTES: Information less broad in scope but nevertheless of importance as a contribution to existing knowledge.

TECHNICAL MEMORANDUMS: Information receiving limited distribution because of preliminary data, security classification, or other reasons.

CONTRACTOR REPORTS: Scientific and technical information generated under a NASA contract or grant and considered an important contribution to existing knowledge.

TECHNICAL TRANSLATIONS: Information published in a foreign language considered to merit NASA distribution in English.

SPECIAL PUBLICATIONS: Information derived from or of value to NASA activities. Publications include conference proceedings, monographs, data compilations, handbooks, sourcebooks, and special bibliographies.

TECHNOLOGY UTILIZATION PUBLICATIONS: Information on technology used by NASA that may be of particular interest in commercial and other non-aerospace applications. Publications include Tech Briefs, Technology Utilization Reports and Notes, and Technology Surveys.

Details on the availability of these publications may be obtained from:

SCIENTIFIC AND TECHNICAL INFORMATION DIVISION

NATIONAL AERONAUTICS AND SPACE ADMINISTRATION

Washington, D.C. 20546